

Investigating the Roles of Wnt Signaling in Mature Adipocyte Function

by

Devika Priya Bagchi

A dissertation submitted in partial fulfillment
of the requirements for the degree of
Doctor of Philosophy
(Molecular and Integrative Physiology)
in the University of Michigan
2020

Doctoral Committee:

Professor Ormond A. MacDougald, Chair
Professor Charles Burant
Professor Christin Carter-Su
Professor Jiandie Lin
Associate Professor Carey N. Lumeng



By Devika Priya Bagchi

Devika Priya Bagchi
dpbagchi@med.umich.edu
ORCID iD: 0000-0002-2258-2289

© Devika Priya Bagchi
All rights reserved

DEDICATION

For my parents, Drs. Milan and Indrani Bagchi, who instilled in me the virtues of perseverance and commitment, and whose unfaltering support and love encourage me to strive for excellence always.

This accomplishment is as much yours as it is mine.

ACKNOWLEDGEMENTS

The successful completion of a doctorate comes at the end of a long, winding and sometimes bumpy road, and it is certainly not done singlehandedly. I am so grateful to all of the special people who have crossed my path and challenged, supported, and cheered me on along the way.

First and foremost, this doctoral thesis would not be possible without the invaluable guidance, advice, and patience of my supervisor, Dr. Ormond MacDougald. Ormond, your unflinching support, encouragement, constructive criticism, and confidence in me has inspired and enriched my growth as a scientist, leader, and individual. Your mentorship has truly shaped the foundation of my research career, but more importantly, the wisdom and life lessons you shared will stay with me always. To Annie, thank you for so warmly welcoming me into the fold and making me feel like one of your own. Of course, I would be remiss if I did not mention Eloise, Liam and Maisie – getting to spend time with you and watch you grow up over the past few years has been a true joy.

A sincere thank you to my doctoral committee: Dr. Chuck Burant, Dr. Christy Carter-Su, Dr. Carey Lumeng, and Dr. Jiandie Lin. Thank you for always making time for me despite your exceedingly busy schedules. Your insights and guidance were invaluable for the successful completion of my projects and this thesis.

To the MacLab family, both past and present – this experience would not have been the same without you all. I could not have hoped for a better group of people to learn from and work alongside. Thank you for the enduring friendships, endless laughs, and for truly being a dream team. A special thank you to Zlru Li, Callie Corsa, Julie Hardij, and Brian Learman, who taught me so much in the lab and without whose help the

experiments outlined in this thesis would not have been possible. When I look back, I can't remember exactly how I ended up in the MacLab, but I know that it is exactly where I was meant to be. As I move on to the next adventure, I am comforted by the knowledge that the MacLab will always be my family. Go team!

Thank you to my academic community, particularly the Medical Scientist Training Program (MSTP) and the Department of Molecular & Integrative Physiology (MIP). Within the MSTP, I'd like to specifically acknowledge Dr. Ron Koenig, Justine Hein, Ellen Elkin, Hilkka Ketola, Laurie Koivupalo, Gretchen Aland, and Liz Bowman – thank you for supporting me and helping me grow over the past seven years, and for solving any and all administrative issues at the drop of a hat. Within MIP, a special thank you to Dr. Sue Moenter, Dr. Bishr Omary, Dr. Santiago Schnell, Dr. Dan Michele, Dr. Beth Rust and Michele Boggs for your unwavering support and help in all my endeavors, academic and otherwise. Thank you for helping me to grow as a student, teacher, and leader, and for believing in my vision for SEEK.

My doctoral work would not have been possible without support from my funding sources, including the Center for Organogenesis Training Grant Predoctoral Fellowship (T32HD007505), Michigan Medical Scientist Training Program (T32GM007863), Rackham Merit Fellowship, and Tylenol Future Care Scholarship.

To my MSTP cohort, it has been quite the adventure. An inherent part of this program is watching friends graduate and move on while we work toward what sometimes feels like an unattainable goal. It has been a comfort to have your camaraderie over the past few years, and I cannot wait to see what the next chapter holds for us all.

My deep and sincere gratitude to my amazing circle of friends, both near and far, without whom this journey would have been more difficult and certainly much less fun. Thank you for always lending an ear to listen and sharing sound advice, comforting me in my failures and sharing enthusiastically in my successes. You all inspire me with your own passion and dedication to life and I am so honored to call you my tribe.

To my baby brother, Vikram – you are my best friend and adventure buddy. Thank you for truly always being there, even when you didn't have a choice in the matter. Mostly, thank you for always understanding.

Above all, thank you to my parents, who instilled in me a love of learning, filled me with the spirit of ambition, commitment and creativity, and who have always believed in me, even when I didn't believe in myself – this dissertation would not be possible without your wisdom, encouragement, and unconditional love. Whatever I am, it is because of you.

To all those who remain unnamed but who nonetheless have a hand in the successful realization of this goal of mine, thank you from the bottom of my heart – it truly takes a village.

TABLE OF CONTENTS

DEDICATION	ii
ACKNOWLEDGEMENTS	iii
LIST OF FIGURES	viii
ABBREVIATIONS	xxiii
ABSTRACT	xxiv
CHAPTER I: Introduction	1
Adipose tissues have important roles in metabolic health and disease.....	1
Adipocytes located in discrete depots and niches have specialized characteristics and functions	2
Wnts play fundamental and diverse roles in tissue development and maintenance	4
Wntless is a dedicated chaperone protein required for Wnt secretion	6
Signal transduction through the canonical Wnt pathway	7
Canonical Wnt signaling is an important endogenous inhibitor of adipogenesis ...	9
Recent genetic studies in humans and mice suggest fundamental roles for Wnt signaling in mature adipocyte metabolism	12
Figures and legends	14
References	22
CHAPTER II: Methodology for Dissection of Diverse Murine Adipose Depots	35
Abstract.....	35
Introduction	36
Protocol.....	38
Discussion	47
Figures and legends	49
References	52

CHAPTER III: Wntless Regulates Lipogenic Gene Expression in Adipocytes and Protects Against Diet-Induced Metabolic Dysfunction 55

Abstract..... 55
Introduction 57
Results 60
Discussion 70
Materials and methods 76
Figures and legends 86
References 108

CHAPTER IV: Wnt/ β -catenin Signaling Regulates Adipose Tissue Lipogenesis and Adipocyte-Specific Loss is Rigorously Defended by Surrounding Stromal-Vascular Cells..... 115

Abstract..... 115
Introduction 117
Results 120
Discussion 133
Materials and methods 139
Figures and legends 148
References 175

CHAPTER V: Discussion and Future Perspectives 182

Does Wnt signaling directly regulate lipogenic gene transcription or are the effects mediated indirectly by *Srebf1* and *Mlxipl* activity? 183
Are other adipocyte functions regulated by Wnt signaling? 185
What is the compensatory mechanism by which stromal-vascular cells sense and respond to loss of adipocyte-specific Wnt signaling? 186
Is β -catenin delivered back to deficient adipocytes from stromal-vascular cells by extracellular vesicles?..... 188
How does adipocyte-specific loss of Wnt signaling provide functional protection from diet-induced obesity?..... 190
Why does ablation of Wnt signaling confer resistance to diet-induced obesity and metabolic dysfunction? 192
References 195

LIST OF FIGURES

CHAPTER I: Introduction

Figure 1.1 Adipocytes serve protective roles and safely store circulating lipids
..... 14

When circulating energy exceeds the storage capacity of WAT, such as in obesity or lipodystrophy, lipids accumulate in ectopic locations, including liver and muscle. Ectopic storage of lipids causes metabolic dysfunction, including insulin resistance and hepatosteatosis.

Figure 1.2 Adipocytes located in discrete depots and niches have specialized characteristics and functions..... 15

The intrinsic cellular and metabolic properties of different adipocytes are shaped by the specific niches in which they reside. Important regional differences in the developmental, molecular, and functional profiles of four major types of adipocytes (subcutaneous, visceral, brown, marrow) are depicted.

Figure 1.3 Lipidation of Wnt ligands are required for binding to Wntless and subsequent intracellular trafficking, secretion, and functional activity
..... 17

(A) Wnts are lipid-modified secreted glycoproteins (~30-40 kDa) characterized by a signal peptide sequence (yellow), varying numbers of N-glycosylation sites (N-glyc; purple), and two conserved lipid modifications: palmitic acid (C16:0) at Cys77 and palmitoleic acid (C16:1) at Ser209. Palmitoleoylation (C16:1) at Ser209 is required for the interaction between Wnts and their dedicated chaperone protein, Wntless; palmitoylation (C16:0) at Cys77 is required for functionality of secreted Wnts. (B) Wntless is an evolutionarily conserved transmembrane protein required for intracellular trafficking and secretion of lipidated Wnts. Wntless (~62 kDa) is predicted to have seven transmembrane domains (TMD; red), a signal peptide sequence (yellow), an endocytosis motif (green), and a hydrophobic lipocalin domain (teal) thought to be the site of interaction with Wnts.

Figure 1.4 Wntless is an evolutionarily conserved chaperone protein dedicated to trafficking lipidated Wnts through the intracellular secretory compartment..... 18

After Wnt proteins are synthesized in the endoplasmic reticulum (ER), they undergo significant post-translational modifications, including N-glycosylation and lipidation. The ER acyltransferase Porcupine catalyzes addition of palmitic (C16:0) and palmitoleic (C16:1) acid moieties at conserved Cys77 and Ser209 residues, respectively. Palmitoleoylation (addition of C16:1) is required for interaction of Wnts with their chaperone protein, Wntless. Wntless binds to and chaperones Wnt proteins from the ER through the trans-Golgi network, and to the plasma membrane in secretory vesicles. Once Wnts are secreted, Wntless is transported back via the retromer complex to the Golgi for reuse or to lysosomes for degradation.

Figure 1.5 Structural composition of β -catenin provides insights into its dual roles in cell mechanics and Wnt signaling 19

(A) β -catenin is comprised of a central 12-unit Armadillo repeat domain (ARM) flanked on either side by distinct N- and C-terminal domains. The N-terminal region consists of conserved serine and threonine residues that are sequentially phosphorylated by CK1 α and GSK3 β ; phosphorylation of these sites promotes binding to β -TrCP, subsequent ubiquitination, and proteasomal degradation. (B) The ARM region forms a superhelix featuring a positively charged groove that serves as a platform for interactions with various β -catenin binding partners, including E-cadherin, Axin, APC, and TCF/LEF proteins. These partners share overlapping binding sites in the ARM groove, and thus typically cannot bind simultaneously.

Figure 1.6 Activation of the canonical Wnt signaling pathway promotes β -catenin-mediated transcription of Wnt target genes 20

In the absence of extracellular Wnts (inactive; left panel), β -catenin is bound by a destruction complex comprised of Axin, APC, GSK3 β , CK1 α , and PP2A. CK1 α and GSK3 β sequentially phosphorylate free cytosolic β -catenin, targeting it for ubiquitination by β TrCP and subsequent proteasomal degradation. When canonical Wnts bind to their frizzled receptors and LRP co-receptors (active; right panel), they trigger an intracellular signaling cascade that leads to hypo-phosphorylation, stabilization, and accumulation of cytosolic β -catenin. β -catenin can then translocate to the nucleus, displace Groucho/TLE repressors, and coactivate TCF/LEF transcription factors to mediate Wnt target gene expression.

Figure 1.7 The canonical Wnt signaling pathway is an important endogenous regulator of cell fate determination 21

Activation of canonical Wnt/ β -catenin signaling in mesenchymal stem cells suppresses adipogenesis and promotes osteoblastogenesis. Wnt signaling suppresses adipocyte differentiation by inhibiting expression of PPAR γ and C/EBP α , the central regulators of adipogenesis.

CHAPTER II: Methodology for Dissection of Diverse Murine Adipose Depots

Figure 2.1 Schematic depiction of dissected mouse adipose depots..... 49

Adipocytes are located throughout the body in discrete depots, as well as singly and in small clusters associated with vascular and lymphatic structures. Although adipocytes throughout the body have overlapping molecular and metabolic characteristics, the degree to which these properties are realized will undoubtedly depend on the specific niches in which these cells reside.

Figure 2.2 Gross anatomical locations of mouse adipose depots 50

Gross anatomy of (A) anterior subcutaneous; (B) brown; (C) epididymal (b, bladder); (D) ovarian (u, uterine horns); (E) posterior subcutaneous (dorsolumbar (d), inguinal (i), gluteal (g)); (F) inguinal; (G) mesenteric; (H) perirenal (k, kidney); (I) retroperitoneal (k, kidney); (J) pericardial (h, heart); and (K) popliteal adipose depots in C57BL/6J adult mice. Arrows point to specific depots if multiple depots are depicted. Relevant organs are designated by appropriate letters.

Figure 2.3 Histological evaluation of discrete mouse adipose depots 51

Histology of (A) anterior subcutaneous; (B) dorsolumbar; (C) inguinal; (D) gluteal; (E) brown; (F) gonadal; (G) perirenal; (H) retroperitoneal; (I) omental; (J) mesenteric; (K) pericardial; (L) popliteal; (M) constitutive and (N) regulated bone marrow adipose; (O) intermuscular; and (P) infrapatellar depots in C57BL/6J adult mice. Tissues were isolated according to the presented protocol, fixed overnight in 10% neutral buffered formalin, processed, and embedded in paraffin. 5 μ m sections were stained with H&E. Most images were taken at 100x magnification; scale bar = 100 μ m.

Chapter III: Wntless Regulates Lipogenic Gene Expression in Adipocytes and Protects Against Diet-Induced Metabolic Dysfunction

Figure 3.1 Canonical Wnt signaling is active in cultured adipocytes and Wntless is up-regulated by diet-induced obesity 86

(A-B) MSCs isolated from C57BL/6J mice were cultured under standard conditions and induced to differentiate. Wntless gene (n = 6) and protein expression at indicated days of differentiation. (C) Wntless gene expression in the stromal-vascular (SVF) and adipocyte (Ads) fractions isolated from epididymal (eWAT) and inguinal (iWAT) white adipose tissues of C57BL/6J mice (males; n = 6). (D) Representative immunoblot of Wntless protein expression across C57BL/6J mouse tissues (asWAT, anterior subcutaneous WAT; pWAT, perirenal WAT; BAT, brown adipose tissue); Adiponectin, Laminin, and Ponceau S included as controls. (E-F) Regulation of Wntless gene and protein expression in eWAT and iWAT of 16-week-old wildtype mice fed with normal chow diet (NCD) or 8 weeks of high fat diet (HFD) (males; n = 6). (G) Wnt-related genes found to be significantly up- or down-regulated by RNA-seq analyses of day 12 adipocytes vs. day 0 cultured MSCs (n = 4). (H) Select Wnt-related genes found to be significantly up- or down-regulated by RNA-seq analyses of day 12 cultured adipocytes treated with recombinant Wnt3a (20 ng/ml) for 4 h (n = 4). RNA expression normalized to PPIA. Data presented as mean \pm S.D. * indicates significance at $p < 0.05$.

Supplemental Figure 3.1 88

(A) Wntless gene expression in the stromal-vascular (SVF) and adipocyte (Ads) fractions isolated from eWAT and inguinal iWAT of 16-week-old wildtype mice fed with NCD or 8 weeks of HFD (males; n = 6). (B) Regulation of Wntless gene expression in eWAT and iWAT by nutritional and environmental conditions: fast: 18 h; refed: 6 h after 18 h fast; 30% calorie restriction (CR): 6 wks; 4°C cold exposure: 6 hr. Each condition normalized to its individual experimental control set to 1 (indicated by grey dashed line). (C) Wntless gene expression in male and female human tissues; data obtained from the GTEx-RNA-Seq dataset. (D) Wnt-related genes found by RNA-seq analyses to be expressed at similar levels in both day 12 adipocytes and confluent day 0 cultured MSCs (n = 4). RNA expression normalized to PPIA. Data presented as mean \pm S.D. * indicates significance at $p < 0.05$.

Figure 3.2 Wntless is required for canonical Wnt signaling in differentiated primary adipocytes..... 90

(A) Schematic model for deletion of Wntless in cultured adipocytes using adenoviral Cre recombinase. (B) Genetic recombination of Wntless in *Wls^{fl/fl}* and *Wls^{-/-}* adipocytes using a 3-primer PCR system (n = 3). (C-D) Wntless RNA and protein expression in adipocytes following adenoviral GFP or Cre infection (n = 3). (E) Representative brightfield and Oil Red-O images, and (F) triacylglycerol accumulation in *Wls^{fl/fl}* and *Wls^{-/-}* adipocytes (n = 4). (G) Expression of known Wnt target genes in *Wls^{fl/fl}* and *Wls^{-/-}* adipocytes (n = 3). (H) Free cytosolic and membrane β -catenin protein expression in *Wls^{fl/fl}* and *Wls^{-/-}* confluent MSCs under basal conditions (n = 6) and after 20 ng/ml Wnt3a treatment for 4 h (n = 2); GAPDH and laminin shown as cytosolic and membrane loading controls, respectively. RNA expression normalized to PPIA. Data presented as mean \pm S.D. * indicates significance at p < 0.05.

Supplemental Figure 3.2..... 91

(A) Densitometry quantification of cytosolic and membranous β -catenin protein expression in *Wls^{fl/fl}* and *Wls^{-/-}* day 0 MSCs under basal conditions and after 20 ng/ml Wnt3a treatment for 4 h (n = 6). (B) Proteins found by untargeted proteomics analysis to be increased over 200% or decreased more than 50% in cultured day 12 *Wls^{-/-}* adipocytes (n = 1). Data presented as mean \pm S.D. * indicates significance at p < 0.05.

Figure 3.3 Adipocyte Wntless regulates expression of a network of lipogenic genes and influences triacylglycerol fatty acid composition and *de novo* lipogenesis 92

(A-B) Lipogenic gene and protein expression in *Wls^{fl/fl}* and *Wls^{-/-}* adipocytes (n = 3). RNA expression normalized to PPIA. (C) Proportion of total saturated (solid) versus unsaturated fatty acids (hatched) in lipids extracted from *Wls^{fl/fl}* and *Wls^{-/-}* adipocytes (n = 6). Relative proportions of (D) myristic (C14:0) versus myristoleic acid (C14:1), (E) palmitic (C16:0) versus palmitoleic acid (C16:1), and (F) stearic (C18:0) versus vaccenic (C18:1, n-7) or oleic acid (C18:1, n-9). *De novo* lipogenesis was evaluated in cultured *Wls^{fl/fl}* and *Wls^{-/-}* adipocytes using [¹⁴C]-acetate for 1, 2, 4 and 8 h. [¹⁴C]-radiolabel in (G) conditioned media versus (H) whole cell lysates after indicated incubation times was measured by scintillation counting (n = 3). (I) Representative thin-layer chromatography analysis of [¹⁴C]-acetate incorporation into lipid species over indicated incubation times; TAG, triacylglycerol; DAG, diacylglycerol; PL, phospholipid. (J) Radiolabel incorporation into TAG fractions extracted from *Wls^{fl/fl}* and *Wls^{-/-}* adipocytes was quantified by scintillation counting (n = 3). Data presented as mean \pm S.D. * indicates significance at p < 0.05.

Supplemental Figure 3.3..... 94

(A) Lipogenic proteins quantified by densitometry (n = 3). (B) *De novo* lipogenesis was evaluated in cultured *Wls^{fl/fl}* and *Wls^{-/-}* adipocytes using [¹⁴C]-acetate for 1, 2, 4 and 8 h. Radiolabel incorporation into PL and DAG fractions extracted from *Wls^{fl/fl}* and *Wls^{-/-}* adipocytes was quantified by scintillation counting (n = 3). (C) Basal and induced glycerol release from *Wls^{fl/fl}* and *Wls^{-/-}* adipocytes using 1 μM isoproterenol (Iso), 5 μM forskolin (Forsk), or 1 μM CL-316,243 (CL-316) for 3 h (n = 3). (D) β-oxidation of [³H]-palmitic acid; 100 μM etomoxir used as negative control (n = 3). (E) Expression of proteins related to lipolysis or β-oxidation (n = 3). Data presented as mean ± S.D. * indicates significance at p < 0.05.

Figure 3.4 Wntless is required for expression of *Srebf1* and *Mlxipl*, transcriptional regulators of lipogenesis..... 95

(A-B) Gene and protein expression of indicated transcription factors (n = 3); I: immature, insoluble form of SREBP1c at relative mobility of 100 kDa; M: mature, soluble form of SREBP1c at 50 kDa. (C) Mature versus immature forms of SREBP1c quantified by densitometry. (D) Basal and insulin-stimulated glucose uptake into *Wls^{fl/fl}* and *Wls^{-/-}* adipocytes (n = 3). (E) Representative immunoblot of AKT phosphorylation in *Wls^{fl/fl}* and *Wls^{-/-}* adipocytes following treatment with indicated insulin concentrations for 10 min. (F) Expression of *Srebf1* or *Mlxipl* mRNAs in *Wls^{fl/fl}* and *Wls^{-/-}* adipocytes following treatment with indicated insulin concentrations for 24 h (n = 3). (G) Expression of *Scap* mRNA in *Wls^{fl/fl}* and *Wls^{-/-}* adipocytes following treatment with indicated insulin concentrations for 24 h (n = 3). (H) Representative immunoblot of SCAP protein expression in *Wls^{fl/fl}* and *Wls^{-/-}* adipocytes following treatment with indicated insulin concentrations for 10 min; pAKT(thr308) shown as a control for insulin response. RNA expression normalized to PPIA. Data presented as mean ± S.D. * indicates significance at p < 0.05.

Supplemental Figure 3.4..... 96

(A) Growth curve of 20-week-old female *Wls^{fl/fl}* and *Wls^{-/-}* mice on NCD. (B) Glucose tolerance test in 16-week-old *Wls^{fl/fl}* and *Wls^{-/-}* mice. (C) Insulin tolerance test in 18-week-old mice. (D) Body composition of 16-week-old *Wls^{fl/fl}* and *Wls^{-/-}* mice. (E) Blood glucose concentrations in random-fed and 16 h fasted mice. Serum concentrations of (F) insulin, (G) adiponectin, and (H) triacylglycerols in 20-week-old mice. (I) Tissue weights at time of sacrifice. *Wls^{fl/fl}*: n = 7; *Wls^{-/-}*: n = 9. Data presented as mean ± S.D. * indicates significance at p < 0.05.

Figure 3.5 Adipose-specific Wntless deletion does not influence whole-body metabolism on a normal chow diet..... 97

(A) Genetic recombination of Wntless in tissues isolated from *Wntless*^{-/-} mice. (B-C) Wntless mRNA and protein expression in iWAT and eWAT of *Wntless*^{fl/fl} and *Wntless*^{-/-} mice. (D) Wntless mRNA expression in SVF and adipocytes isolated from iWAT and eWAT of *Wntless*^{fl/fl} and *Wntless*^{-/-} mice (n = 3). (E) Body composition of 16-week-old *Wntless*^{fl/fl} and *Wntless*^{-/-} mice on NCD. (F) Growth curve of 20-week-old *Wntless*^{fl/fl} and *Wntless*^{-/-} mice. (G) Glucose tolerance test in 16-week-old *Wntless*^{fl/fl} and *Wntless*^{-/-} mice. (H) Insulin tolerance test in 18-week-old mice. (I) Blood glucose concentrations in random-fed and 16 h fasted mice. Serum concentrations of (J) insulin, (K) adiponectin, and (L) triacylglycerols in 20-week-old mice. (M) Tissue weights at time of sacrifice. RNA expression normalized to PPIA. Data shown in E-M from male mice, n = 5 per group. Data presented as mean ± S.D. * indicates significance at p < 0.05.

Supplemental Figure 3.5..... 99

(A) Representative histological images of H&E-stained distal and proximal tibia of male and female *Wntless*^{fl/fl} and *Wntless*^{-/-} mice fed NCD for 20 weeks; 100x magnification; scale bar, 50 μm. μCT analyses of (B) tibial length measured by distance from growth plate (GP) to tibia/fibula junction (T/F J), (C) mid-tibia cortical bone area (Ct. BA/TA), (D) bone mineral density (Ct. BMD), (E) tibial trabecular bone volume fraction (Tb. BV/TV), (F) trabecular number (Tb. N), (G) trabecular bone mineral density (Tb. BMD), (H) trabecular separation (Tb. Sp) and (I) trabecular thickness (Tb. Th). Data presented as mean ± S.D. * indicates significance at p < 0.05.

Figure 3.6 Adipose tissues compensate for adipocyte-specific Wntless deficiency by increasing Wnt signaling in stromal-vascular cells .. 100

(A) Representative histological images of H&E-stained tissues from *Wntless*^{fl/fl} and *Wntless*^{-/-} mice fed normal chow diet for 20 weeks; 200x magnification; scale bar, 100 μm. (B) Lipogenic gene expression in eWAT and iWAT isolated from *Wntless*^{fl/fl} and *Wntless*^{-/-} mice. (C) Lipogenic gene expression in isolated eWAT adipocytes (n = 7). (D) Wnt target gene expression in isolated eWAT adipocytes and SVF of *Wntless*^{fl/fl} and *Wntless*^{-/-} mice (n = 5). (E) Expression of Wnt mRNAs in SVF isolated from eWAT of *Wntless*^{fl/fl} and *Wntless*^{-/-} mice (n = 6). Data shown from male mice. RNA expression normalized to PPIA. Data presented as mean ± S.D. * indicates significance at p < 0.05.

Supplemental Figure 3.6..... 102

(A) Lipogenic gene expression in livers isolated from male *Wls^{fl/fl}* and *Wls^{-/-}* mice on NCD. (B) Representative plots of flow cytometric analyses of eWAT SVF isolated from male *Wls^{fl/fl}* and *Wls^{-/-}* mice, stained with CD31-APC (endothelial cells) and CD45-PE (immune cells). (C) Quantification of SVF cell populations based on flow cytometric analyses (n = 6). RNA expression normalized to PPIA. Data presented as mean ± S.D. * indicates significance at p < 0.05.

Figure 3.7 *Wls^{-/-}* mice on HFD have decreased eWAT and improved glucose tolerance..... 103

(A) Growth curve over time of 32-week-old *Wls^{fl/fl}* and *Wls^{-/-}* mice fed 60% HFD for 24 weeks. (B) Body composition analysis of 28-week-old mice. (C) Glucose tolerance test in 28-week-old mice. (D) Serum insulin concentrations in fed and 16 h fasted mice. (E) Serum insulin concentrations in 16 h fasted mice at indicated times after intraperitoneal glucose injection (1 mg/kg body weight). (F) Insulin tolerance test in 30-week-old mice. (G) Blood glucose concentrations in random-fed and 16 h fasted mice. Circulating concentrations of (H) leptin, (I) adiponectin, (J) triacylglycerols, and (K) total and free cholesterol in 32-week-old mice. (L) Tissue weights of mice at time of sacrifice. Data shown from male mice; *Wls^{fl/fl}*: n = 8; *Wls^{-/-}*: n = 7. Data presented as mean ± S.D. * indicates significance at p < 0.05.

Supplemental Figure 3.7..... 105

(A) Daily food intake of male *Wls^{fl/fl}* and *Wls^{-/-}* mice fed HFD for 24 weeks. (B) Adipocyte size quantification of iWAT (400-500 adipocytes/mouse; n = 8, 7). (C) Representative H&E-stained images and UCP1 protein expression in BAT of male *Wls^{fl/fl}* and *Wls^{-/-}* mice fed HFD for 24 weeks; 200x magnification; scale bar, 100 µm. (D) Expression of Wnt mRNAs in SVF isolated from eWAT of HFD-fed male *Wls^{fl/fl}* and *Wls^{-/-}* mice (n = 10). (E) Lipogenic gene expression in livers isolated from male *Wls^{fl/fl}* and *Wls^{-/-}* mice on HFD. RNA expression normalized to PPIA. Data presented as mean ± S.D. * indicates significance at p < 0.05.

Figure 3.8 *Wls*^{-/-} mice on HFD have reduced epididymal adipocyte size and decreased DNL gene expression 106

(A) Representative histological images of H&E-stained tissues from *Wls*^{fl/fl} and *Wls*^{-/-} mice fed 60% HFD for 24 weeks; 200x magnification; scale bar, 100 μ m. (B) Adipocyte size quantification of eWAT (400-500 adipocytes/mouse, n = 8, 7). (C) Wnt target gene expression in adipocytes and SVF isolated from eWAT. (D-E) Lipogenic mRNA and protein expression in isolated eWAT adipocytes. (F) Lipogenic gene expression in eWAT and iWAT from *Wls*^{fl/fl} and *Wls*^{-/-} mice. Data shown from male mice. RNA expression normalized to PPIA. Data presented as mean \pm S.D. * indicates significance at p < 0.05.

Figure 3.9 Schematic depicting the consequences of adipocyte-specific deletion of *Wntless* 107

Adipocyte-derived Wnts are required for expression of a network of lipogenic genes and loss of secreted Wnts in *Wls*^{-/-} adipocytes is sensed and compensated for by surrounding stromal-vascular cells to maintain tissue-wide Wnt signaling homeostasis.

CHAPTER IV: Wnt/ β -catenin Signaling Regulates Adipose Tissue Lipogenesis and Adipocyte-Specific Loss is Rigorously Defended by Surrounding Stromal-Vascular Cells.

Figure 4.1 β -catenin is expressed in cultured and primary adipocytes and up-regulated by diet-induced obesity 148

(A-B) Mesenchymal stem cells (MSC) isolated from C57BL/6J mice were cultured under standard conditions and induced to differentiate. *Ctnnb1* gene (n = 6) and protein (n = 2) expression at indicated days of adipogenesis. (C) *Ctnnb1* gene expression in stromal-vascular (SVF) and adipocyte (Ads) fractions isolated from epididymal (eWAT) and inguinal (iWAT) white adipose tissues (WAT) of C57BL/6J mice (males; n = 5). (D) Expression of *Ctnnb1* in eWAT and iWAT of mice fed normal chow diet (NCD) or high fat diet (HFD) for 10 weeks. (E) *Ctnnb1* expression in SVF and Ads of eWAT and iWAT isolated from NCD- and HFD-fed mice (males; n = 6). (F) *Ctnnb1* allele structure and genetic recombination in β -cat^{fl/fl} and β -cat^{-/-} adipocytes using a 3-primer PCR system (n = 3). (G-H) *Ctnnb1* RNA (n = 6) and protein (n = 3) expression in adipocytes following adenoviral GFP or Cre infection. (I) Representative brightfield and Oil Red-O images, and (J) triacylglycerol (TAG) accumulation in β -cat^{fl/fl} and β -cat^{-/-} adipocytes (n = 6). (K) Expression of *Ctnnb1* and downstream Wnt target genes in β -cat^{fl/fl} and β -cat^{-/-} adipocytes treated with vehicle or 3

μM CHIR99021 for 4 h (n = 6). RNA expression normalized to PPIA. Data presented as mean \pm S.D. * indicates significance at $p < 0.05$.

Supplemental Figure 4.1..... 150

(A) Representative immunoblot of β -catenin protein expression across C57BL/6J mouse tissues (BAT, brown adipose tissue; pWAT, perirenal WAT); adiponectin and laminin included as controls. (B) *Dlk1* and *Adipoq* gene expression in SVF and adipocyte fractions isolated from eWAT and iWAT of C57BL/6J mice (males; n = 5). (C-D) *Lep* and *Nkd1* mRNA expression in SVF and adipocytes isolated from eWAT and iWAT of mice fed NCD or 10 weeks of HFD (males; n = 5). (E) Regulation of *Ctnnb1* gene expression in eWAT and iWAT by nutritional and environmental conditions: fast: 18 h; refed: 6 h after 18 h fast; 30% calorie restriction (CR): 6 weeks; 4°C cold exposure: 6 h. Each condition normalized to its individual experimental control set to 1 (indicated by dashed line; n = 6). (F) *Ctnnb1* gene expression in male and female human tissues; data obtained from the GTEx-RNA-Seq dataset. (G) Schematic model for deletion of β -catenin in cultured preadipocytes or adipocytes using adenoviral Cre recombinase. (H) *Ctnnb1* gene recombination (n = 2) and β -catenin protein expression (n = 4) in preadipocytes treated with adenoviral GFP or Cre. (I) Expression of downstream Wnt target genes in β -cat^{fl/fl} and β -cat^{-/-} adipocytes treated with vehicle or 3 μM CHIR99021 for 4 h (n = 6). RNA expression normalized to PPIA. Data presented as mean \pm S.D. * indicates significance at $p < 0.05$.

Figure 4.2 β -catenin regulates metabolic pathways in adipocytes and exclusively mediates effects of canonical Wnt3a signaling..... 152

RNA-seq analyses were performed on β -cat^{fl/fl} and β -cat^{-/-} adipocytes under basal conditions or after 4 h treatment with recombinant Wnt3a (20 ng/ml; n = 4 per group). (A) Heat maps of differential gene expression changes in β -cat^{fl/fl} and β -cat^{-/-} adipocytes under basal conditions (left panel) and β -cat^{fl/fl} cells treated with vehicle or Wnt3a (right panel). (B) Gene Set Enrichment Analyses (GSEA) of genes expressed in β -cat^{fl/fl} and β -cat^{-/-} adipocytes under basal conditions (top panel) and β -cat^{fl/fl} cells treated with vehicle or Wnt3a (bottom panel). (C-D) MA plots of gene expression changes following Wnt3a treatment of β -cat^{fl/fl} or β -cat^{-/-} adipocytes. (E) Venn diagram depicting meta-analysis of gene expression changes in β -cat^{fl/fl} or β -cat^{-/-} adipocytes treated with vehicle or Wnt3a for 4 h. (F) Expression of *Ctnnb1* and downstream Wnt target genes in β -cat^{fl/fl} and β -cat^{-/-} adipocytes treated with vehicle or 20 ng/ml recombinant Wnt3a for 4, 12 or 24 h (n = 6). RNA expression normalized to PPIA. Data presented as mean \pm S.D. * indicates significance at $p < 0.05$.

RNA-seq analyses were performed on β -cat^{fl/fl} and β -cat^{-/-} preadipocytes under basal conditions or after 4 h treatment with recombinant Wnt3a (20 ng/ml; n = 4 per group). **(A)** Heat maps of differential gene expression changes in β -cat^{fl/fl} and β -cat^{-/-} preadipocytes under basal conditions (left panel) and β -cat^{fl/fl} cells treated with vehicle or Wnt3a (right panel). **(B)** Gene Set Enrichment Analyses (GSEA) of genes in β -cat^{fl/fl} and β -cat^{-/-} preadipocytes under basal conditions (top panel) and β -cat^{fl/fl} cells treated with vehicle or Wnt3a (bottom panel). **(C-D)** MA plots of gene expression changes following Wnt3a treatment of β -cat^{fl/fl} or β -cat^{-/-} preadipocytes. **(E)** Venn diagram depicting meta-analysis of gene expression changes in β -cat^{fl/fl} or β -cat^{-/-} preadipocytes treated with vehicle or Wnt3a for 4 h. **(F)** Expression of *Ctnnb1* and downstream Wnt target genes in β -cat^{fl/fl} and β -cat^{-/-} preadipocytes treated with vehicle or 20 ng/ml recombinant Wnt3a for 4, 12 or 24 h (n = 6). RNA expression normalized to PPIA. Data presented as mean \pm S.D. * indicates significance at p < 0.05.

Figure 4.3 β -catenin-dependent Wnt signaling regulates lipogenesis and fatty acid desaturation in adipocytes..... 156

(A-B) Heat map and MA plot showing differentially expressed genes related to fatty acid, cholesterol, and bile acid metabolism in cultured β -cat^{fl/fl} and β -cat^{-/-} adipocytes (n = 4). **(C-D)** Lipogenic gene (n = 6) and protein (n = 3) expression in β -cat^{fl/fl} and β -cat^{-/-} adipocytes. **(E)** Proportion of total saturated versus unsaturated fatty acids in lipids extracted from β -cat^{fl/fl} and β -cat^{-/-} adipocytes (n = 3). **(F)** Relative proportions of myristic (C14:0) and palmitic (C16:0) versus myristoleic (C14:1, n-5) and palmitoleic (C16:1, n-7) acids (n = 3). **(G)** *De novo* lipogenesis (DNL) was evaluated in cultured β -cat^{fl/fl} and β -cat^{-/-} adipocytes using [¹⁴C]-acetate for 2, 4 and 8 h. Incorporation of [¹⁴C]-radiolabel into TAG fractions extracted from β -cat^{fl/fl} and β -cat^{-/-} adipocytes was quantified by scintillation counting (n = 6). **(H-I)** Gene (n = 6) and protein (n = 3) expression of indicated transcription factors in β -cat^{fl/fl} and β -cat^{-/-} adipocytes. **(J)** Protein expression in β -cat^{fl/fl} and β -cat^{-/-} adipocytes treated for 72 h with adenovirus expressing GFP, ChREBP, or SREBP1c (1 x 10⁵ viral particles/ml). **(K)** Integrative Genomics Viewer capture showing Tcf7l2 peaks (indicating binding occupancy) in the regions \pm 3 kb from transcription start sites (black arrows) of indicated genes in cultured *Tcf7l2*^{fl/fl} and *Tcf7l2*^{-/-} adipocytes. RNA expression normalized to PPIA. Data presented as mean \pm S.D. * indicates significance at p < 0.05.

Supplemental Figure 4.3..... 158

(A) Lipogenic proteins quantified by densitometry (n = 3). (B) Relative proportions of stearic (C18:0) versus vaccenic (C18:1, n-7) and oleic (C18:1, n-9) acids in β -cat^{fl/fl} and β -cat^{-/-} adipocytes (n = 3). [¹⁴C]-radiolabel in (C) conditioned media versus (D) whole cell lysates after indicated incubation times measured by scintillation counting (n = 6). (E) Expression of genes related to acetate uptake and activation (n = 6). (F-G) Radiolabel incorporation into DAG and PL fractions extracted from β -cat^{fl/fl} and β -cat^{-/-} adipocytes quantified by scintillation counting (n = 6). (H) Linear regression analyses comparing slopes of acetate uptake over time from conditioned media into β -cat^{fl/fl} and β -cat^{-/-} adipocytes. (I) Linear regression analyses comparing slopes of radiolabel incorporation over time into TAG fractions of β -cat^{fl/fl} and β -cat^{-/-} adipocytes. (J) Gene expression in β -cat^{fl/fl} and β -cat^{-/-} adipocytes treated with adenovirus expressing GFP, ChREBP, or SREBP1c for 72 h (1 x 10⁵ viral particles/ml; n = 4). RNA expression normalized to PPIA. Data presented as mean ± S.D. * indicates significance at p < 0.05.

Figure 4.4 Adipocyte-specific β -catenin deletion does not influence global metabolism on a normal chow diet..... 160

(A) Genetic recombination in tissues isolated from β -cat^{-/-} mice. (B) Growth curve of 28-week-old β -cat^{fl/fl} and β -cat^{-/-} mice. (C) Body composition of 16-week-old β -cat^{fl/fl} and β -cat^{-/-} mice on NCD. (D) Glucose tolerance tests in 16-week-old β -cat^{fl/fl} and β -cat^{-/-} mice. (E) Insulin tolerance test in 19-week-old mice. (F) Blood glucose concentrations in random-fed and 16 h fasted mice. Serum concentrations of (G) random-fed and fasted insulin and (H) adiponectin levels in 28-week-old mice. (I) Basal and stimulated lipolysis in 22-week-old mice (iso, isoproterenol: 10 mg/kg body weight). (J) Serum TAG in 28-week-old mice. (K) Tissue weights at time of sacrifice. (L) Representative histological images of H&E-stained tissues from β -cat^{fl/fl} and β -cat^{-/-} mice fed NCD for 28 weeks; 200x magnification; scale bar, 100 μ m. Data in B-L from male mice, n = 8 per group. Data presented as mean ± S.D. * indicates significance at p < 0.05.

Supplemental Figure 4.4..... 162

(A) Representative traces and quantification of daily running distance in chow-fed male 23-week-old β -cat^{fl/fl} and β -cat^{-/-} mice given access to voluntary exercise wheels for six weeks. (B) Growth curve of 28-week-old female β -cat^{fl/fl} and β -cat^{-/-} mice. (C) Body composition of 16-week-old β -cat^{fl/fl} and β -cat^{-/-} mice on NCD. (D) Glucose and insulin tolerance tests in 16- and 19-week-old β -cat^{fl/fl} and β -cat^{-/-} mice, respectively. (E) Blood

glucose concentrations in random-fed and 16 h fasted mice. Serum concentrations of (F) insulin, (G) adiponectin, and (H) TAG in 28-week-old mice. (I) Tissue weights at time of sacrifice. (J) Representative histological images of H&E-stained tissues from female β -cat^{fl/fl} and β -cat^{-/-} mice fed NCD for 28 weeks; 200x magnification; scale bar, 100 μ m. Data in B-J from female mice, n = 6 per group. Data presented as mean \pm S.D. * indicates significance at p < 0.05.

Figure 4.5 β -catenin is up-regulated in the stromal-vascular fraction of adipose tissues from knockout mice 164

(A) Genetic recombination in tissues isolated from β -cat^{fl/fl} and β -cat^{-/-} mice (n = 3). (B-C) *Ctnnb1* mRNA (n = 3) and protein (n = 6) expression in eWAT and iWAT of β -cat^{fl/fl} and β -cat^{-/-} mice. (D) Genomic recombination of β -catenin in adipocytes and SVF isolated from eWAT and iWAT of β -cat^{fl/fl} and β -cat^{-/-} mice. (E) *Ctnnb1* mRNA expression in isolated eWAT adipocytes and SVF of β -cat^{fl/fl} and β -cat^{-/-} mice (n = 6). (F) β -catenin protein expression in isolated eWAT adipocytes and SVF of β -cat^{fl/fl} and β -cat^{-/-} mice; adiponectin and laminin shown as protein loading controls. (G-H) Wnt target gene expression in adipocytes and SVF isolated from eWAT of β -cat^{fl/fl} and β -cat^{-/-} mice (n = 8). (I) Representative plots showing flow cytometry analysis of SVF isolated from β -cat^{fl/fl} and β -cat^{-/-} mice (3 mice per sample; n = 3 samples). (J) Quantification of SVF cell proportions evaluated by flow cytometry analysis (3 mice per sample; n = 3 samples). (K) *Ctnnb1* mRNA expression normalized to PPIA in cellular fractions isolated by FACS analysis (3 mice per sample; n = 3 samples). Data presented as mean \pm S.D. * indicates significance at p < 0.05.

Supplemental Figure 4.5..... 166

(A) Representative histological images of H&E-stained proximal tibia (regulated bone marrow adipose tissue) of male and female β -cat^{fl/fl} and β -cat^{-/-} mice fed NCD for 28 weeks (male: n = 8; female: n = 6). (B) μ CT analyses of tibial trabecular bone volume fraction (Tb. BV/TV) and trabecular bone mineral density (Tb. BMD). (C) Representative histological images of H&E-stained distal tibia (constitutive bone marrow adipose tissue) of male and female β -cat^{fl/fl} and β -cat^{-/-} mice. (D) μ CT analyses of mid-tibial cortical bone area (Ct. BA/TA) and cortical bone mineral density (Ct. BMD). Histological images shown at 100x magnification; scale bar, 50 μ m. Data presented as mean \pm S.D. * indicates significance at p < 0.05.

Figure 4.6 *β-cat*^{-/-} mice are protected from diet-induced obesity and metabolic dysfunction 167

(A) Growth curve over time of 32-week-old *β-cat*^{fl/fl} and *β-cat*^{-/-} mice fed 60% HFD for 24 weeks. (B) Body composition analysis of 28-week-old mice. (C-D) Glucose tolerance test and area under the curve analysis in 28-week-old mice. (E) Blood glucose concentrations in random-fed and 16 h fasted mice. (F) Insulin tolerance test in 30-week-old mice. (G) Serum insulin concentrations in random-fed mice or in 16 h fasted mice at indicated times after intraperitoneal glucose injection (1 mg/kg body weight). Serum (H) TAG, (I) total cholesterol, and (J) adiponectin in 32-week-old mice. (K) Tissue weights at time of sacrifice. (L) Representative histological images of H&E-stained tissues from *β-cat*^{fl/fl} and *β-cat*^{-/-} mice fed HFD for 24 weeks; 200x magnification; scale bar, 100 μm. (M) Quantification of liver TAG in 32-week-old mice. Data shown from male mice; *β-cat*^{fl/fl}: n = 5, *β-cat*^{-/-}: n = 11. Data presented as mean ± S.D. * indicates significance at p < 0.05.

Supplemental Figure 4.6..... 169

(A-D) Lipogenic gene expression in whole eWAT, iWAT, liver, or isolated eWAT adipocytes of *β-cat*^{fl/fl} and *β-cat*^{-/-} mice (n = 8). (E) Expression of immune, endothelial, and stromal cell markers in SVF isolated from eWAT of *β-cat*^{fl/fl} and *β-cat*^{-/-} mice (n = 6). (F) Expression of inflammatory markers in whole eWAT of *β-cat*^{fl/fl} and *β-cat*^{-/-} mice (n = 6; n = 10). (G-H) Expression of cell markers and Wnt target genes in SVF sub-populations isolated by FACS analysis (3 mice per sample; n = 3 samples). RNA expression normalized to PPIA. Data presented as mean ± S.D. * indicates significance at p < 0.05.

Figure 4.7 **Diet-induced obesity overcomes compensatory up-regulation of β-catenin in SVF from knockout mice**..... 171

(A) *Ctnnb1* mRNA expression in eWAT and iWAT of *β-cat*^{fl/fl} and *β-cat*^{-/-} mice fed HFD for 28 weeks (n = 5). (B) *Ctnnb1* mRNA expression in isolated eWAT adipocytes and SVF of HFD-fed *β-cat*^{fl/fl} and *β-cat*^{-/-} mice (n = 5). (C) β-catenin protein expression in isolated eWAT adipocytes and SVF of *β-cat*^{fl/fl} and *β-cat*^{-/-} mice fed HFD; adiponectin and laminin shown as controls. (D-E) Wnt target gene expression in SVF and adipocytes isolated from eWAT of obese *β-cat*^{fl/fl} and *β-cat*^{-/-} mice (n = 5). (F) Lipogenic gene expression in eWAT adipocytes isolated from HFD-fed *β-cat*^{fl/fl} and *β-cat*^{-/-} mice (n = 8). (G) Expression of immune, endothelial, and stromal cell markers in SVF isolated from eWAT of obese *β-cat*^{fl/fl} and *β-cat*^{-/-} mice (n = 8). (H-I) Expression of inflammatory markers in whole eWAT and iWAT of *β-cat*^{fl/fl} and *β-cat*^{-/-} mice fed HFD (n = 8). RNA

expression normalized to PPIA. Data presented as mean \pm S.D. * indicates significance at $p < 0.05$.

Supplemental Figure 4.7..... 173

(A) Daily food intake of male β -cat^{fl/fl} and β -cat^{-/-} mice fed HFD for 24 weeks. (B) ITT area under the curve analysis of male β -cat^{fl/fl} and β -cat^{-/-} HFD-fed mice. (C) Pancreas weights at time of sacrifice of HFD-fed mice (n = 5, n = 11). (D-E) mRNA expression of adipokines in eWAT and iWAT of HFD-fed mice (n = 8). (F) Immunoblot and densitometry quantification of UCP1 and β -catenin protein expression in BAT isolated from HFD-fed β -cat^{fl/fl} and β -cat^{-/-} mice (n = 4). Data presented as mean \pm S.D. * indicates significance at $p < 0.05$.

Figure 4.8 Schematic depicting the consequences of adipocyte-specific deletion of β -catenin..... 174

Canonical Wnt/ β -catenin signaling is required for coordinate regulation of adipocyte lipogenesis and fatty acid desaturation. In chow-fed mice, loss of adipocyte β -catenin is sensed and compensated for by neighboring stromal cells to defend tissue-wide canonical Wnt signaling homeostasis. Chronic overnutrition overrides this compensatory mechanism, revealing that adipocyte-specific β -catenin knockout mice are protected from diet-induced obesity and metabolic dysfunction.

LIST OF ABBREVIATIONS

β -cat^{-/-}: adipocyte-specific β -catenin knockout
BAT: brown adipose tissue
DNL: *de novo* lipogenesis
ER: endoplasmic reticulum
eWAT: epididymal white adipose tissue
Fzd: frizzled
HFD: high fat diet
iWAT: inguinal white adipose tissue
LRP: low-density lipoprotein receptor-related protein
MSC: mesenchymal stem cell
NCD: normal chow diet
pWAT: perirenal white adipose tissue
sEV: small extracellular vesicle
SVC: stromal-vascular cell
SVF: stromal-vascular fraction
TAG: triacylglycerol
TCF/LEF: T-cell factor/lymphoid enhancer-binding factor
WAT: white adipose tissue
Wnt1^{-/-}: adipocyte-specific Wntless knockout

ABSTRACT

Obesity is a key risk factor for many secondary chronic illnesses, including type 2 diabetes and cardiovascular disease. Canonical Wnt/ β -catenin signaling is well-established as an important regulator of mesenchymal cell fate determination and differentiation, inhibiting adipogenesis and promoting osteoblastogenesis. Emerging genetic evidence in humans has linked various Wnt pathway members to body fat distribution, obesity, and metabolic dysfunction, suggesting that this pathway is also operative in terminally-differentiated adipocytes. Indeed, recent studies in mice have uncovered compelling evidence suggesting that the Wnt pathway plays important roles in adipocyte metabolism, particularly under obesogenic conditions. However, the exact functional roles of the Wnt pathway and its underlying molecular mechanisms in this context remain unclear due to complexities of Wnt signaling and differences in experimental models, approaches, and results.

My dissertation work endeavored to unravel the unique contributions of Wnt pathway members to adipocyte metabolism. To this end, I generated novel cultured cell and mouse models to functionally characterize the differential roles of two key pathway members, Wntless and β -catenin, in terminally-differentiated adipocytes. Deletion of Wntless, a dedicated intracellular chaperone for Wnt proteins, allowed me to investigate the functional roles of both canonical and non-canonical Wnts secreted from adipocytes, whereas loss of β -catenin allowed me to specifically interrogate the contribution of canonical Wnt signaling to adipocyte function.

These studies revealed for the first time that loss of adipocyte-derived Wnts or canonical Wnt/ β -catenin signaling in adipocytes coordinately down-regulates a wide network of lipogenic genes, resulting in impaired *de novo* lipogenesis and fatty acid desaturation. Further, these effects on lipid metabolism are mediated by repression of

Srebf1 and *Mlxipl*, known master transcriptional regulators of lipogenic enzyme expression. At first glance, Wntless and β -catenin do not appear to influence global metabolism in mice maintained on chow diet. However, my studies revealed a striking phenomenon by which adipose tissues defend adipocyte-specific loss of Wntless or β -catenin through compensatory up-regulation of Wnt signaling in neighboring stromal-vascular cells. Finally, long-term overnutrition overrides this compensatory mechanism, revealing that both adipocyte-specific Wntless and β -catenin knockout mice are resistant to diet-induced obesity, adipocyte hypertrophy, and metabolic dysfunction.

Taken together, my doctoral findings demonstrate that Wnt signaling in adipocytes is required for fatty acid and glucose metabolism. In addition, adipose tissues rigorously defend Wnt signaling homeostasis under standard nutritional conditions, underscoring the critical importance of this pathway in mature adipocyte metabolism and adipose tissue function. Finally, given the evolutionary conservation and ubiquitous nature of this pathway, it is likely that the findings herein, including compelling evidence of Wnt-mediated cross-talk between diverse cell types, will be widely applicable to the biology of other tissues.

CHAPTER I

Introduction

Adipose tissues have important roles in metabolic health and disease.

Historically, adipose tissue was considered to be an inert organ primarily responsible for storage of excess energy. The ability to store nutrients that can be mobilized during periods when energy demands exceed caloric intake is an evolutionarily preserved function; indeed, the ability to store energy in the form of cytoplasmic triacylglycerol is conserved from *Saccharomyces cerevisiae* to *Drosophila melanogaster* to *Homo sapiens*¹⁻³. Over the past two decades, however, tremendous strides in understanding the molecular underpinnings of adipocyte development and physiology have replaced this simplistic view of adipose tissue function. We now know that adipose tissues have fundamental and complex roles not only in whole-body homeostasis, including storage and release of energy in response to local and global needs, but also in thermoregulation, mechanical support, and secretion of adipokines to regulate energy balance, metabolism and immune responses^{4,5}.

In 1949, researchers at Jackson Laboratory discovered a strain of mice harboring an autosomal recessive allele that caused them to weigh three times as much as normal mice⁶. These mice were fittingly designated *obese* (*ob*) and their profound phenotype suggested for the first time the existence of a single gene critical for feeding behavior, body weight, and global metabolism. Over 40 years later, the mouse *ob* allele and its corresponding human homolog were successfully positionally cloned in 1994⁷. The *ob* gene was found to encode a novel adipocyte hormone that was named leptin, after the Greek root *leptos* meaning “thin”, based on the notion that leptin functions to keep mice from becoming obese⁸. Similar to *ob/ob* mice, humans lacking leptin due to genetic mutations are characterized by profound hyperphagic obesity, decreased energy expenditure and insulin insensitivity; these effects can be rescued in both humans and mice with recombinant leptin therapy^{9,10}. Thus, the break-through

discovery of leptin revealed the central role of adipocytes in global energy homeostasis and initiated a decades-long explosion of interest in adipose tissue biology.

Of course, interest has also surged in recent years due to the dramatic increase in global prevalence of obesity¹¹⁻¹³. Indeed, nearly a third of the world's population is now classified as overweight or obese, and the epidemic has significantly impacted all age groups and both sexes, irrespective of ethnicity, geography, and socioeconomic status¹². Obesity, defined as excess accumulation of white adipose tissue (WAT), has far-reaching consequences: it is correlated with elevated risk for many secondary chronic illnesses, including type 2 diabetes, dyslipidemia, and cardiovascular disease, reduced quality of life, increased medical care costs, and premature mortality¹³⁻¹⁵.

Given the association between obesity and metabolic dysfunction, it is easy to assign the role of villain to WAT and overlook its beneficial functions. However, adipocytes provide a safe location for lipid storage, and expansion of WAT with obesity is the result, rather than the cause, of energy imbalance¹⁶⁻¹⁸. When circulating energy exceeds the storage capacity of WAT, lipids accumulate in ectopic locations, including muscle and liver; this ectopic storage is believed to cause metabolic dysfunction, including insulin resistance and hepatosteatosis^{17,18}. Interestingly, lipodystrophy, a disorder characterized by WAT loss and redistribution, is associated with many of the same metabolic complications observed with obesity^{19,20}, providing further support for the protective role of adipocytes (**Figure 1.1**).

Adipocytes located in discrete depots and niches have specialized characteristics and functions.

Adipocytes are distributed throughout the body in discrete depots, and in some cases serve specialized roles within their microenvironments²¹⁻²⁵ (**Figure 1.2**). Most unilocular white adipocytes are distributed throughout the body in subcutaneous and visceral WAT depots^{26,27} and the characteristics of these depots are important for differential susceptibility to metabolic diseases^{3,18,26,28}. Indeed, subcutaneous white adipocytes, located beneath the skin, have been associated with protective metabolic effects^{18,25,26}, whereas visceral white adipocytes, which surround the vital organs and are contained within the gonadal, perirenal, retroperitoneal, omental and pericardial depots, are

commonly linked to metabolic disorders, including type 2 diabetes and cardiovascular disease^{5,18,26}.

First identified as thermogenic cells in 1961, classical multilocular brown adipocytes are contained in the interscapular brown adipose tissue (BAT) depot^{21,29,30}. Additionally, clusters of brown adipocytes are also found in other locations throughout the body, including in supraclavicular, infra/subscapular, cervical, paravertebral and periaortic depots³⁰⁻³². Brown and brown-like adipocytes are rich in mitochondria, express uncoupling protein 1 (UCP1), and play important roles in adaptive thermogenesis and glucose homeostasis³³⁻³⁵. When activated, UCP1 uncouples the electrochemical gradient driving ATP synthesis, thereby stimulating the respiratory chain to generate heat^{36,37}. In response to various stimuli, including cold exposure, clusters of UCP1-expressing adipocytes, termed beige or “brite” (brown in white), also develop within WAT³⁸⁻⁴¹. Although brown and beige/brite adipocytes share key features, like the ability to undergo thermogenesis, emerging evidence suggests that these cell populations are distinct in their development, molecular characteristics, and regulation^{39,42-44}.

Since fluorodeoxyglucose positron emission tomography (FDG-PET) studies identified the presence and functionality of BAT in adult humans ten years ago⁴⁵⁻⁴⁹, this tissue has been considered an attractive target for weight loss and has thus enjoyed the spotlight in AT research over the last decade. Considerable efforts have been put forth to harness BAT biology as a therapeutic target for the treatment of obesity, including recruitment of new brown adipocytes or stimulation of thermogenesis in existing brown adipocytes to increase energy expenditure^{41,50,51}. Although the question of whether BAT can feasibly be targeted in humans remains unanswered, the wider field of adipose biology has undoubtedly benefitted from a deeper understanding of brown adipocyte development and function.

In addition to their location in major WAT and BAT depots, adipocytes also exist in specialized niches throughout the body^{22,23}. These depots are typically small in size, closely associated with other anatomic structures, and are thought to perform unique functions within their microenvironments⁵². Although recognition of their importance is growing, the underlying biology of these distinct groups of adipocytes remains, for the

most part, incompletely understood. For example, bone marrow adipose tissue (BMAT) serves as a lipid reservoir, is a major source of circulating adiponectin, and closely interacts with osteoblasts, osteoclasts, and hematopoietic cells⁵³⁻⁵⁵. Dermal adipocytes contribute to widespread processes, including wound healing, immune response, thermoregulation, and hair follicle growth⁵⁶⁻⁵⁹. Further, epicardial adipocytes may produce several adipokines and chemokines that exert local and systemic effects on the development and progression of coronary artery disease^{60,61}. Expansion of inter/intramuscular WAT has been positively correlated with increased adiposity, systemic insulin resistance, and decreased muscular strength and mobility⁶². In addition, popliteal adipocytes serve as a lipid reservoir for lymphatic expansion during infection^{63,64}. While the specific roles of different articular depots are generally unknown, the Hoffa (infrapatellar) depot within the knee is now thought to contribute to pathologies, including anterior knee pain and osteoarthritis⁶⁵.

Thus, although adipocytes throughout the body have overlapping molecular and metabolic characteristics, the degree to which these properties are realized may depend on the specific niches in which these cells reside. The developmental and functional differences between depots are currently under intense study. Investigation of discrete adipose depots will undoubtedly allow further definition of critical differences in their development, gene expression, and function.

Wnts play fundamental and diverse roles in tissue development and maintenance.

The first mammalian *Wnt* gene, originally named *Integration 1 (Int1)* and now known as *Wnt1*, was initially discovered in 1982 as a gene activated by integration of mouse mammary tumor virus (MMTV) pro-viral DNA in virally-induced mammary carcinomas⁶⁶. During this time, independent studies in *Drosophila* larval development identified the fly *Wingless (Wg)* gene as a pivotal regulator of segment polarity and wing formation⁶⁷. In 1987, *Int1* and *Wg* were found to be homologous genes⁶⁸. Thus, the *Wnt* nomenclature was derived from the combination of both gene names to yield a consistent classification system across species; today, most homologs of *Int1* and *Wg*, from *Drosophila* to humans, share the *Wnt* name.

Since the initial discovery of *Wnt1*, interest in Wnt signaling and its fundamental functions in organismal biology has grown steadily. Wnt signaling is an ancient pathway used by all multicellular animals, from the earliest metazoans to mice to humans⁶⁹⁻⁷². The mammalian Wnt signaling pathway is complex: the 19 different *Wnt* genes, 10 *Frizzled* genes and two *Lrp* co-receptor genes are accompanied by an intricate network of intracellular components, giving rise to promiscuous interactions on the cell surface and innumerable downstream molecular responses^{71,73-78}.

In 1991, mutation in the *Apc* gene, which encodes adenomatous polyposis coli (APC), was identified as the genetic cause of familial adenomatous polyposis, a hereditary cancer syndrome⁷⁹⁻⁸¹. Shortly thereafter, APC was found to interact directly with central Wnt pathway protein β -catenin^{82,83}, providing the first direct connection between Wnt signaling and human disease. Since then, aberrant Wnt signaling has been implicated in diverse pathologic processes, including developmental disorders, cancers, and degenerative diseases^{70,72,74,84,85}.

Wnt ligands are evolutionarily conserved secreted, lipid-modified glycoproteins with well-established and diverse roles in cell proliferation, fate determination, and differentiation^{70,72,75,86}. Analyses of Wnt primary amino acid sequences reveal that Wnt proteins share a conserved pattern of 23 cysteine residues and an N-terminal signal sequence for endoplasmic reticulum (ER) targeting and subsequent secretion^{71,87,88}. During synthesis, Wnt proteins, which are ~30-40 kDa in size, undergo extensive post-translational processing to ensure proper secretion and function.

In addition to variable N-glycosylation by the oligosaccharyl transferase (OST) complex^{88,89}, all 19 Wnts are predicted to be lipid-modified by the O-acyltransferase enzyme Porcupine (*Porcn*)⁹⁰⁻⁹³: Wnt proteins undergo palmitoylation (addition of palmitic acid; C16:0) at conserved Cys77⁹⁴ and palmitoleoylation (addition of palmitoleic acid; C16:1) at conserved Ser209^{95,96} (**Figure 1.3 A**). *Porcn* is a dedicated and highly conserved component of Wnt signaling; indeed, it is only active in Wnt-producing cells. Mutations in the *Porcn* gene lead to impaired Wnt lipidation, retention at the ER, and defective release from cells^{92,96-98}. Whereas the functional necessity of N-glycosylation remains unclear^{99,100}, lipid modifications are critically coupled to the secretion and function of Wnts: Ser209 acylation is required for intracellular targeting and secretion⁹⁵,

whereas Cys77 acylation is required for proper extracellular signaling^{94,101,102}. Indeed, mutation of Ser209 to Ala disrupts Wnt3a secretion and promotes accumulation at the ER; in contrast, mutation of Cys77 to Ala does not impact secretion but impairs downstream signaling activity.

Wntless is a dedicated chaperone protein required for Wnt secretion.

Wntless (Wls; also known as GPR177, Sprinter, or Evenness interrupted) is an evolutionarily conserved, multipass, transmembrane protein dedicated to trafficking of Wnts to the plasma membrane for secretion¹⁰³⁻¹⁰⁵. First discovered in *Drosophila* in 2006, the structure of Wls provides important clues for its intracellular function¹⁰³. Analysis of its primary amino acid sequence predicts that Wls contains a long N-terminal region, seven to eight transmembrane domains, and an intracellular C-terminus (**Figure 1.3 B**). Similar to most membrane-associated proteins, Wls is modified with N-linked oligosaccharides; indeed, SDS-PAGE analysis of N-glycosidase-treated Wls protein yields a collapsed fast-migrating band^{106,107}. Further, a lipocalin-like domain in the N-terminal region is essential for the association between Wls and Wnt1, Wnt3, and Wnt5a¹⁰⁸. Thus, this lipocalin-like domain affords Wls the ability to bind to hydrophobic regions of Wnt proteins, such as the post-translational lipid modifications. Finally, Wls contains a conserved endocytosis signal motif that is recognized by clathrin adapter protein 2 and is critical for internalization and recycling of Wls from the plasma membrane; mutations in this motif result in accumulation of Wls at the cell surface¹⁰⁹⁻¹¹¹.

After Wnts are produced, the covalent addition of acyl moieties at the ER renders Wnt proteins hydrophobic and limits their mobility through the secretory pathway⁷¹. Wls is localized throughout the Wnt secretory route, including the ER, Golgi apparatus, intracellular vesicles, and plasma membrane¹¹². Thus, Wls binds modified Wnts at the ER and Golgi apparatus and facilitates their movement throughout the cell to the plasma membrane for extracellular release^{103-105,113} (**Figure 1.4**). Importantly, palmitoleoylation at conserved Ser209 on Wnt proteins is thought to be required for binding to Wls; mutants lacking this lipid modification are unable to interact with Wls and are thus retained at the ER^{95,114,115}. In contrast, Wnt proteins with defective N-glycosylation bind appropriately to Wls and are secreted normally. Following secretion

of Wnts, Wls undergoes clathrin-mediated endocytosis^{112,116}. Wls then has two distinct fates: it is either transported back to the ER and Golgi for reuse or is targeted for lysosomal degradation¹¹⁶⁻¹¹⁸.

Two *Wls* knockout mouse models generated by distinct gene targeting strategies demonstrated that global homozygous *Wls* deletion is embryonic lethal^{108,119}. Both models exhibit phenotypes observed with global deletion of *Wnt1*, *Wnt3*, *Wnt1* and *Wnt3* together, or *Ctnnb1* (β -catenin)¹²⁰⁻¹²⁴, providing *in vivo* support for the role of *Wls* in Wnt secretion and function. Generation of a mouse harboring a floxed *Wls* allele has allowed the study of conditional tissue-specific *Wls* deletion¹¹⁹. Thus, ablation of *Wls* in various vertebrate and invertebrate animal models and tissues results in phenotypes consistent with loss of Wnt function, supporting the notion that *Wls* regulates signaling at the level of Wnt transport and secretion in signal-producing cells^{103,119,125-130}.

Signal transduction through the canonical Wnt pathway

Several pathways can be activated by binding of Wnt proteins to their receptors on receiving cells, including the canonical, non-canonical Wnt/calcium, and non-canonical planar cell polarity pathways¹³¹⁻¹³³. Of these, the best studied is the canonical pathway, which regulates activation of Wnt target genes through stabilization of the central protein β -catenin^{72,84,134}.

In the late 1980s, two independent groups simultaneously identified β -catenin, based on its different functions in cell structure and signaling^{135,136}. Studies of proteins associated with E-cadherin, a pivotal player in cell adhesion, identified α -catenin, β -catenin, and γ -catenin; collectively, these proteins were called catenins, based on the Latin word *catena* meaning chain, to reflect their roles in anchoring E-cadherin to the cytoskeleton^{135,137}. Studies of its *Drosophila* ortholog Armadillo first uncovered the potential function of β -catenin in Wnt signaling: *armadillo* mutant flies exhibit developmental abnormalities in segment polarity, similar to *wg* mutants^{136,138}. Subsequent studies demonstrated that *Drosophila* segmentation dysfunction in *armadillo* mutants is due to impaired *Wg* signaling¹³⁹. These initial studies were pivotal for the ensuing characterization of the Wnt/ β -catenin (*Wg*/Armadillo) signaling cascade.

The protein structure of β -catenin makes it uniquely suited for roles in both cell mechanics and signaling (**Figure 1.5 A**). β -catenin is comprised of a central region containing 12 Armadillo repeats and flanked on either side by distinct N- and C-terminal domains^{140,141}. The Armadillo repeats form a superhelix featuring a positively charged groove that serves as a platform for interactions with various β -catenin binding partners in the adherens junctions, cytosol, and nucleus. Structural analyses have revealed that many β -catenin binding partners, including E-cadherin, APC, and T-cell factor/lymphoid enhancer-binding factor (TCF/LEF) proteins, share overlapping binding sites in this groove; thus, partners typically cannot bind simultaneously (**Figure 1.5 B**). All of these β -catenin interactors bind to a core binding site comprised of Armadillo repeats 3 through 9, forming salt bridges with two key amino acid residues, Lys 312 and Lys 435¹⁴⁰⁻¹⁴³.

The majority of endogenous intracellular β -catenin is bound to E-cadherin and α -catenin at adherens junctions, whereas a small pool exists as free cytosolic β -catenin^{134,144,145}. Association of β -catenin with E-cadherin protects it from binding to a multi-unit destruction complex comprised of Axin, APC, protein phosphatase 2A (PP2A), protein kinases casein kinase 1 α (CK1 α) and glycogen synthase 3 β (GSK3 β), and the E3 ligase β -TrCP^{72,134,141,146}. In the absence of Wnt signaling, this destruction complex triggers rapid CK1 α and GSK3 β -mediated phosphorylation of N-terminal serine and threonine residues on free cytosolic β -catenin^{147,148}, thereby promoting its binding to and ubiquitination by β -TrCP. Phosphorylated and ubiquitinated β -catenin is subsequently targeted for proteasomal degradation to prevent activation of Wnt target genes^{84,148-150} (**Figure 1.6**). The half-life of free cytosolic β -catenin is on the order of minutes, whereas the pool associated with adherens junctions is stable; thus, free cytosolic β -catenin is the Wnt-responsive signaling pool^{134,151-153}.

Once secreted, hydrophobic Wnt proteins have limited abilities to diffuse in the aqueous extracellular environment and thus act in an autocrine/paracrine manner. When Wnts bind to their membrane-spanning frizzled (Fzd) receptors and low-density lipoprotein receptor-related protein (LRP) co-receptors, they trigger an intracellular signaling cascade that disrupts the destruction complex and prevents phosphorylation

of free cytosolic β -catenin, thereby promoting its stabilization^{72,84,134,146,154}. Accumulated β -catenin then translocates to the nucleus, where it associates with DNA-binding TCF/LEF proteins, which act as transcriptional switches. In the absence of Wnt signals, TCF/LEF factors form complexes with Groucho/transducin-like enhancer of split (TLE) to act as transcriptional repressors. Binding of β -catenin physically displaces Groucho/TLE, forming bipartite TCF/ β -catenin co-activators that then mediate transcription of downstream Wnt target genes^{134,153,155-159} (**Figure 1.6**).

Canonical Wnt signaling is an important endogenous inhibitor of adipogenesis.

Mesenchymal stem cells (MSC) arising from the mesoderm are multipotent and have the potential to differentiate into adipocytes, osteocytes, chondrocytes, or myocytes¹⁶⁰; adipogenesis is the process by which MSCs differentiate into mature lipid-laden adipocytes. The transcriptional programming of adipogenesis has been studied extensively and is comprised of two phases: determination and terminal differentiation¹⁶¹⁻¹⁶⁴. During determination, MSCs are committed to the adipogenic lineage and are converted to preadipocytes. Terminal differentiation is the process whereby preadipocytes then acquire characteristics of the mature adipocyte, including expression of cellular machinery required for lipid synthesis and storage, insulin sensitivity, and adipokine secretion. Studies have shown that induction of differentiation in precursors results in rapid activation of transcription factors, leading to dramatic changes in the epigenome^{165,166}. These events culminate in the temporal induction of the master regulator of adipogenesis, peroxisome proliferator activated receptor γ (PPAR γ), and other key adipogenic transcription factors, including CCAAT-enhancer binding protein α (C/EBP α) and C/EBP β , which together drive the adipocyte gene program^{162,167-169}.

Canonical Wnt/ β -catenin signaling has well-established roles in MSC fate determination and terminal differentiation. Although studies have explored Wnt-mediated regulation of myogenesis and chondrogenesis¹⁷⁰⁻¹⁷², the differential roles of this pathway in osteogenesis versus adipogenesis have been particularly well-characterized (**Figure 1.7**). Indeed, enforced expression of canonical Wnt3a, Wnt6, Wnt10a, Wnt10b, or a β -catenin stable mutant, in multipotent progenitor cells stabilizes

Wnt/ β -catenin signaling, which promotes osteoblastogenesis and inhibits adipogenesis¹⁷³⁻¹⁷⁹.

Further, canonical Wnt signaling activation in committed preadipocytes through pharmacological inhibition of GSK3 with lithium or CHIR99021, or enforced expression of Wnt1, Wnt6, Wnt10a, Wnt10b, or a dominant-stable form of β -catenin, suppresses induction of PPAR γ and C/EBP α and thus blocks adipogenesis^{151,152,180-182}. Similarly, overexpression of Pygo2, a nuclear promoter of β -catenin/TCF/LEF transcription, in preadipocytes mediates β -catenin signaling to inhibit differentiation, whereas Pygo2 deletion induces spontaneous differentiation¹⁸³. Although β -catenin is often considered to function exclusively as a canonical Wnt effector, it can also signal through unrelated pathways in certain contexts. In response to testosterone, for example, β -catenin binds to the androgen receptor and is subsequently shuttled to the nucleus to coactivate TCF/LEFs to inhibit adipocyte differentiation¹⁸⁴. Additionally, tumor necrosis factor α (TNF α) treatment blocks differentiation of preadipocytes by stabilizing β -catenin and enhancing TCF7L2-dependent transcription, suggesting that β -catenin mediates effects of inflammatory cytokines on adipogenesis¹⁸⁵.

Conversely, inhibition of Wnt signaling in precursor cells promotes adipogenic differentiation. Indeed, treatment of preadipocytes with soluble Wnt inhibitors such as secreted frizzled-related protein 1 (SFRP1) or SFRP2, or overexpression of negative pathway regulators, such as Axin or dominant-negative TCF4, results in spontaneous differentiation into adipocytes^{151,152}. Enforced expression of nuclear β -catenin antagonist Chibby induces spontaneous adipogenesis by binding to β -catenin and blocking activation of TCF/LEF, thus repressing β -catenin-mediated transcription^{186,187}. In contrast, loss of Chibby up-regulates β -catenin transcriptional activity and blocks differentiation^{186,187}.

In mice, conditional deletion of β -catenin in uterine mesenchymal cells impairs smooth muscle myogenesis and stimulates conversion of these progenitors into adipocytes¹⁸⁸. This report provided the first *in vivo* evidence linking Wnt signaling and MSC fate determination. Since then, studies have shown that AT-specific overexpression of canonical Wnt10b results in dramatically reduced WAT mass and

resistance to genetic and diet-induced obesity, absence of BAT development, and increased trabecular bone thickness and strength, whereas loss of *Wnt10b* causes reduction of trabecular bone mass¹⁸⁹⁻¹⁹¹. Additionally, deletion of Wnt signaling activator *Pygo2* in progenitor cells promotes accumulation of visceral WAT, glucose intolerance, and insulin insensitivity in diet-induced obese mice¹⁸³.

A robust literature has also emerged to highlight the role of canonical Wnt/ β -catenin signaling in bone development and homeostasis *in vivo*. Interest in Wnt signaling within the bone was first sparked by identification of *LRP5* loss-of-function mutations in human patients diagnosed with osteoporosis pseudoglioma¹⁹². Since then, mutations in many members of the Wnt signaling pathway, including *LRP4*, *LRP5*, *LRP6*, *LGR4*, *WNT1*, *WNT16*, and *SOST* have been associated with altered bone mass in humans¹⁹³⁻²⁰⁰. Of particular interest, genome-wide studies across various human populations have also identified single-nucleotide polymorphism (SNP) in *CTNNB1* and *WLS* that are correlated with reduced bone mineral density and osteoporosis^{201,202}.

Thus, various mouse models manipulating Wnt components in bone development and function have been generated and characterized to date²⁰⁰. Deletion of either *Wls* or *Ctnnb1* in progenitor cells blocks osteoblast commitment and differentiation, resulting in severe osteopenia^{203,204}, whereas overexpression of β -catenin promotes bone formation²⁰⁵. Osteoblast-specific *Wls* knockout mice are characterized by severe impairment in bone formation, dramatic reductions in both cortical and trabecular bone mass, increased fracture risk, and premature lethality¹²⁸. Further, *Ctnnb1* deletion in osteoblasts results in severe osteopenia due to increased osteoclastogenesis; in contrast, constitutive activation of β -catenin in osteoblasts impairs formation of osteoclasts^{206,207}. Indeed, FABP4- and OCN-*Wnt10b* mice exhibit increased osteoblastogenesis and extensive trabeculation throughout the entire endocortical compartment, whereas *Wnt10b*^{-/-} mice are characterized by decreased trabecular bone volume and bone mineral density^{191,208}.

Finally, investigations into the role of sclerostin, a glycoprotein secreted predominantly by osteocytes, have opened a new avenue of inquiry into endocrine-mediated communication between WAT and bone. Sclerostin, encoded by *Sost*, interacts with *LRP5* and *LRP6* co-receptors, thereby preventing downstream

intracellular propagation of Wnt signaling²⁰⁹⁻²¹¹. In humans, elevated serum sclerostin levels are associated with increased body mass index, adiposity, fasting glucose concentrations, and insulin resistance^{212,213}. Global deletion of *Sost* in mice profoundly influences both WAT and bone: *Sost*^{-/-} mice exhibit dramatically increased bone formation, decreased adiposity, and improved insulin sensitivity, whereas overproduction of sclerostin causes adipocyte hypertrophy and insulin insensitivity²¹⁴. Taken together, these studies and many others illustrate the fundamental roles of Wnt signaling in directing MSC fate determination and the development of adipose tissue and bone.

Recent genetic studies in humans and mice suggest fundamental roles for Wnt signaling in mature adipocyte metabolism.

Whereas the critical role of Wnt signaling in regulation of adipogenesis has been well-studied, its function in terminally-differentiated adipocytes remains unclear. However, increasing genetic evidence is linking various Wnt signaling pathway members to body fat distribution, obesity, and metabolic dysfunction in humans. Indeed, missense *WNT10B* variants and certain *WNT5B* SNPs are associated with increased risk of obesity and type 2 diabetes, respectively^{215,216}, whereas polymorphisms in the Wnt inhibitor *SFRP5* locus have been linked to decreased adiposity in men²¹⁷. Further, common variants in Wnt signaling inhibitor *ZNRF3* and Wnt signaling activator *RSPO3* are associated with increased waist-to-hip ratio²¹⁸⁻²²⁰. Patients harboring loss-of-function mutations in Wnt co-receptors *LRP5* and *LRP6* are predisposed to develop impaired glucose homeostasis, coronary disease, and osteoporosis^{221,222}, whereas gain-of-function *LRP5* mutations are correlated with altered body fat distribution, increased adiposity, and osteosclerosis²²³. Nonsense mutations in *LGR4*, which encodes a protein that stabilizes Wnt receptors, are associated with reduced adiposity and impaired bone formation and remodeling²²⁵; in contrast, gain-of-function mutations in *LGR4* are correlated with increased visceral adiposity²²⁴. Strikingly, genome-wide association studies across a broad range of human populations have found that polymorphisms in the canonical Wnt effector *TCF7L2* are perhaps the strongest genetic risk factors associated with development of type 2 diabetes risk²²⁶⁻²²⁸. Finally, rare gain-of-function

mutations in *CTNNB1* (β -catenin) have recently been linked to altered body fat distribution and increased obesity risk²²⁹. Together, these studies provide compelling genetic evidence for critical roles of canonical Wnt/ β -catenin signaling in regulation of adiposity, body composition, and metabolic health.

Recent studies in mice have also found that Wnt signaling is operative and important in adipocyte metabolism, but its exact functional roles in this context remain unclear^{189,190,229-231}. For example, stabilization of Wnt signaling through global deletion of secreted frizzled-related protein 5 (SFRP5) – an adipocyte protein highly induced by obesity that binds to and sequesters Wnts – provides protection from diet-induced obesity²³⁰. Whereas total adipocyte numbers are unaffected, adipocytes in SFRP5-deficient mice have increased mitochondrial number and are smaller in size compared to those of control mice, resulting in reduced WAT and improved glucose tolerance. Adipocyte-specific deletion of *Ctnnb1* has recently been reported to cause decreased subcutaneous WAT mass and improved glycemic control in diet-induced obese mice²²⁹. In contrast, adipocyte-specific deletion of the Wnt target *Tcf7l2* results in adipocyte hypertrophy and impaired glucose homeostasis with high fat diet feeding²³¹.

These reports provide the first evidence that canonical Wnt signaling plays an important role in the ability of existing adipocytes to accommodate excess energy, but additional studies are required to unravel the complex mechanisms underlying this regulation. Thus, my doctoral work described in the following chapters endeavors to provide novel insights into the specific and differential contributions of various Wnt pathway members, including WIs and β -catenin, to mature adipocyte metabolism.

Figure 1.1

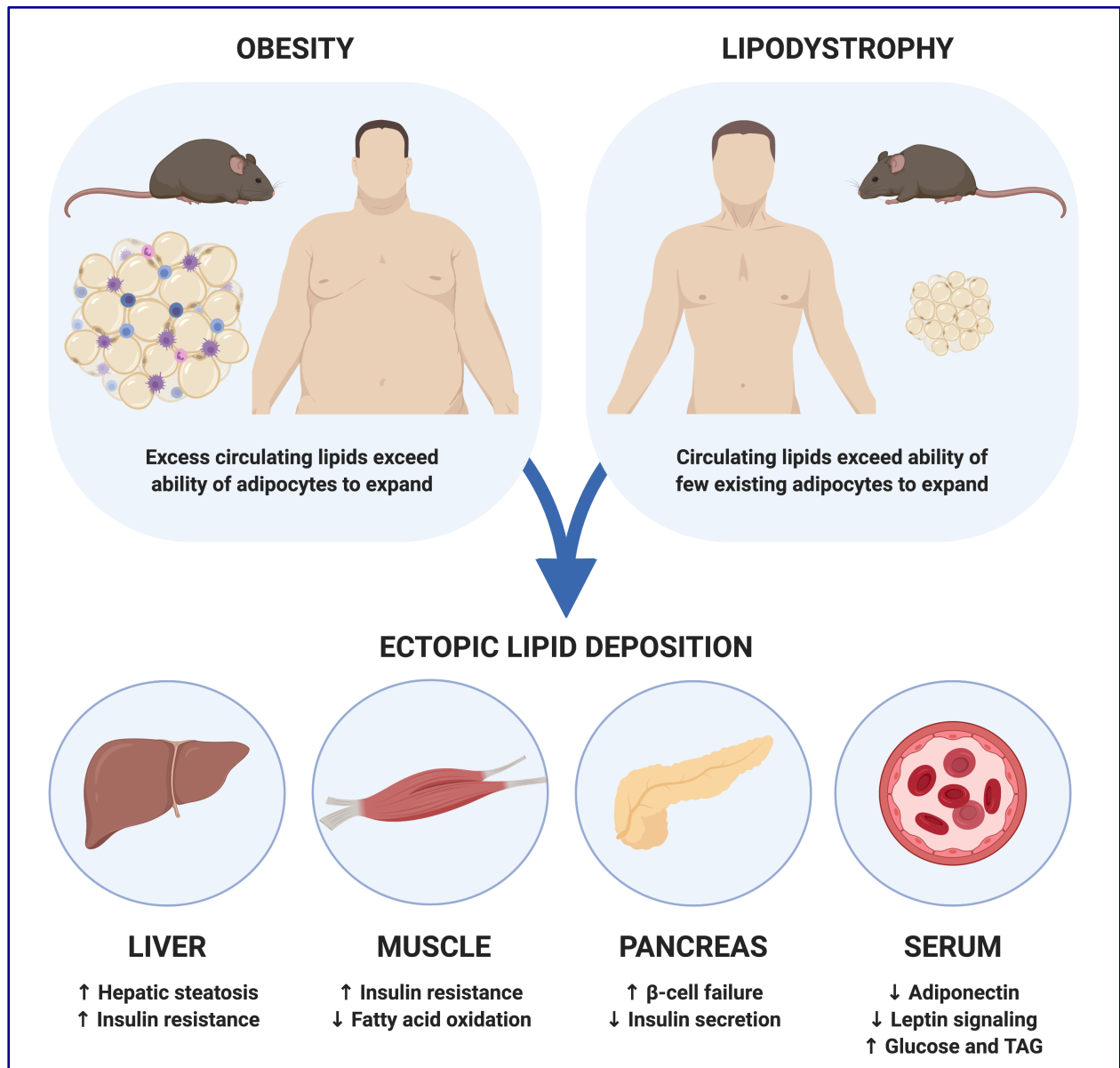


Figure 1.1. Adipocytes serve protective roles and safely store circulating lipids. When circulating energy exceeds the storage capacity of WAT, such as in obesity or lipodystrophy, lipids accumulate in ectopic locations, including liver and muscle. Ectopic storage of lipids causes metabolic dysfunction, including insulin resistance and hepatosteatosis. Adapted from Savage, 2009²³²; Rochford, 2014²³³.

Figure 1.2








	Subcutaneous	Visceral	Brown	Marrow
				
ANATOMY				
Murine depots	Anterior subcutaneous: interscapular, subscapular, axillary, cervical Posterior subcutaneous: dorsolumbar, inguinal, gluteal	Perigonadal (epididyma/parametrial), perirenal, mesenteric, omental, retroperitoneal	Interscapular (characteristics below have been studied in interscapular brown fat; other brown and brown-like depots are not addressed here)	Constitutive: distal tibia, tail vertebrae Regulated: mid-to-proximal tibia, femur, lumbar vertebrae
Developmental origin	Lateral mesoderm Mesodermal precursor	Lateral mesoderm Mesodermal precursor	Paraxial mesoderm Dermomyotomal precursor	? Mesodermal precursor
Metabolic risk with expansion	+	+++	-	?
CELLULAR CHARACTERISTICS				
Adipocyte size (diameter)	+++ 70 µm	++++ 100 µm	+ 20 µm	++ cMAT: 40 µm rMAT: 30 µm
Expansion with obesity	Hypertrophy Hyperplasia	Hypertrophy	-	cMAT: none rMAT: hyperplasia
Mitochondrial respiration	+	+	++	?
Adiponectin secretion	++	+++	+	++++ (rabbit)
Leptin secretion	+++	++	+	?
Pro-inflammatory cytokine secretion	++	+++	?	?
METABOLIC CHARACTERISTICS				
Insulin-stimulated glucose uptake	+	+	+++	?
Cold-stimulated glucose uptake	+	+	+++	?
β₃AR-mediated lipolysis	++	+++	+++	?
Triacylglycerol turnover rate	+	++	?	?
Note: unless noted, all characteristics above have been defined in rodents housed in standard conditions on normal chow.				
Diet-induced obesity		Calorie restriction		Cold exposure
				
Subcutaneous: ↑ depot size, ↑ inflammation, ↑ metabolic dysfunction Visceral: ↑ depot size, ↑ inflammation, ↑ metabolic dysfunction Regulated marrow: ↑ depot size, ↓ bone mass		Subcutaneous: ↓ depot size, ↑ browning, ↑ metabolic function Visceral: ↓ depot size, ↑ metabolic function Brown: ↑ thermogenic activity Regulated marrow: ↑ depot size, ↓ bone mass		Subcutaneous: ↓ depot size, ↑ browning, ↑ metabolic function Visceral: ↓ depot size, ↑ browning, ↑ metabolic function Brown: ↑ thermogenic activity Regulated marrow: ↑ depot size

Figure 1.2. Adipocytes located in discrete depots and niches have specialized characteristics and functions. The intrinsic cellular and metabolic properties of different adipocytes are shaped by the specific niches in which they reside. Important regional differences in the developmental, molecular, and functional profiles of four major types of adipocytes (subcutaneous, visceral, brown, marrow) are depicted. *Adapted from Bagchi et al., 2018²³.*

Figure 1.3

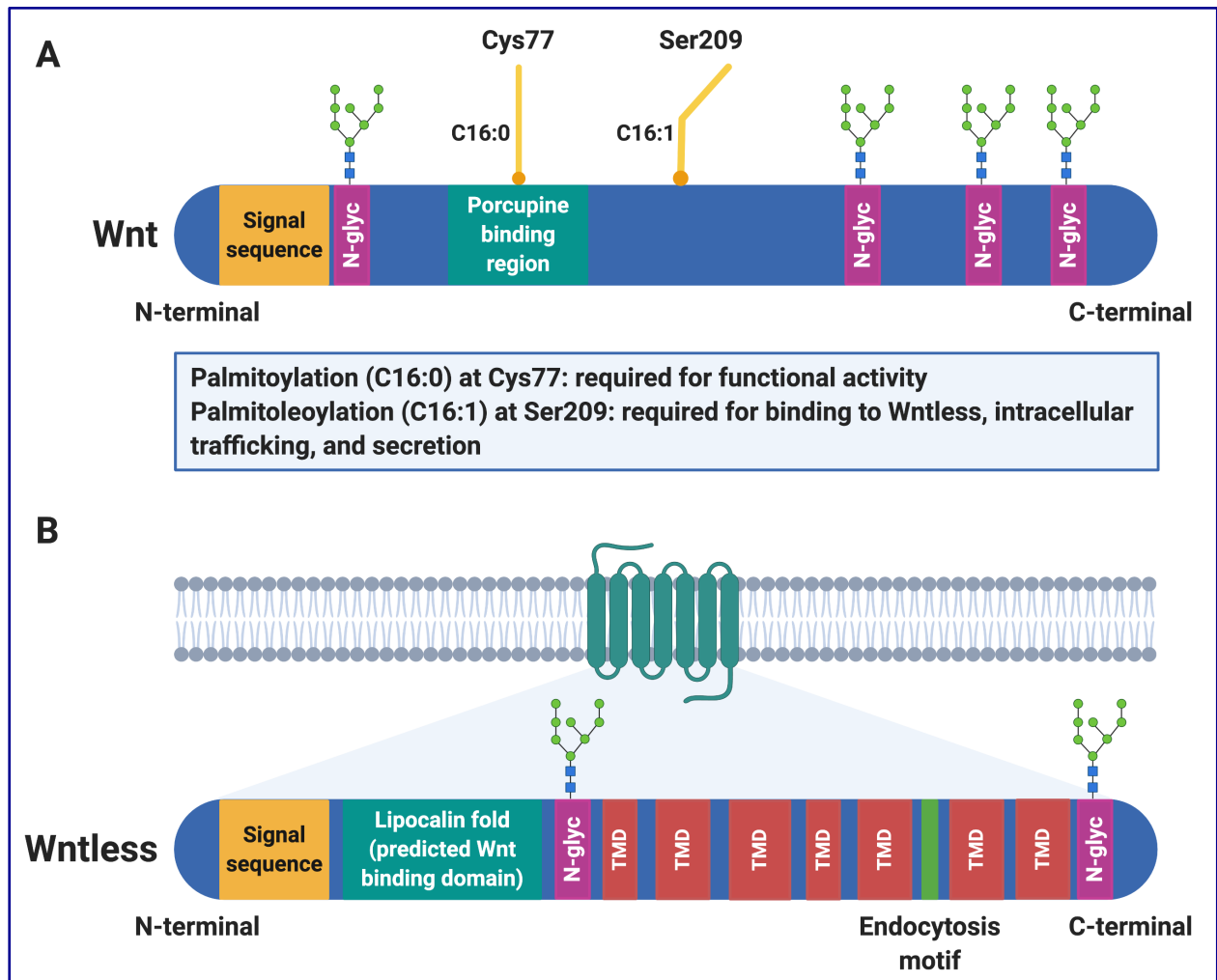


Figure 1.3. Lipidation of Wnt ligands are required for binding to Wntless and subsequent intracellular trafficking, secretion, and functional activity. (A) Wnts are lipid-modified secreted glycoproteins (~30-40 kDa) characterized by a signal peptide sequence (yellow), varying numbers of N-glycosylation sites (N-glyc; purple), and two conserved lipid modifications: palmitic acid (C16:0) at Cys77 and palmitoleic acid (C16:1) at Ser209. Palmitoleoylation (C16:1) at Ser209 is required for the interaction between Wnts and their dedicated chaperone protein, Wntless; palmitoylation (C16:0) at Cys77 is required for functionality of secreted Wnts. (B) Wntless is an evolutionarily conserved transmembrane protein required for intracellular trafficking and secretion of lipidated Wnts. Wntless (~62 kDa) is predicted to have seven transmembrane domains (TMD; red), a signal peptide sequence (yellow), an endocytosis motif (green), and a hydrophobic lipocalin domain (teal) thought to be the site of interaction with Wnts. Adapted from Das et al., 2012²³⁴; Herr et al., 2012¹¹⁵.

Figure 1.4

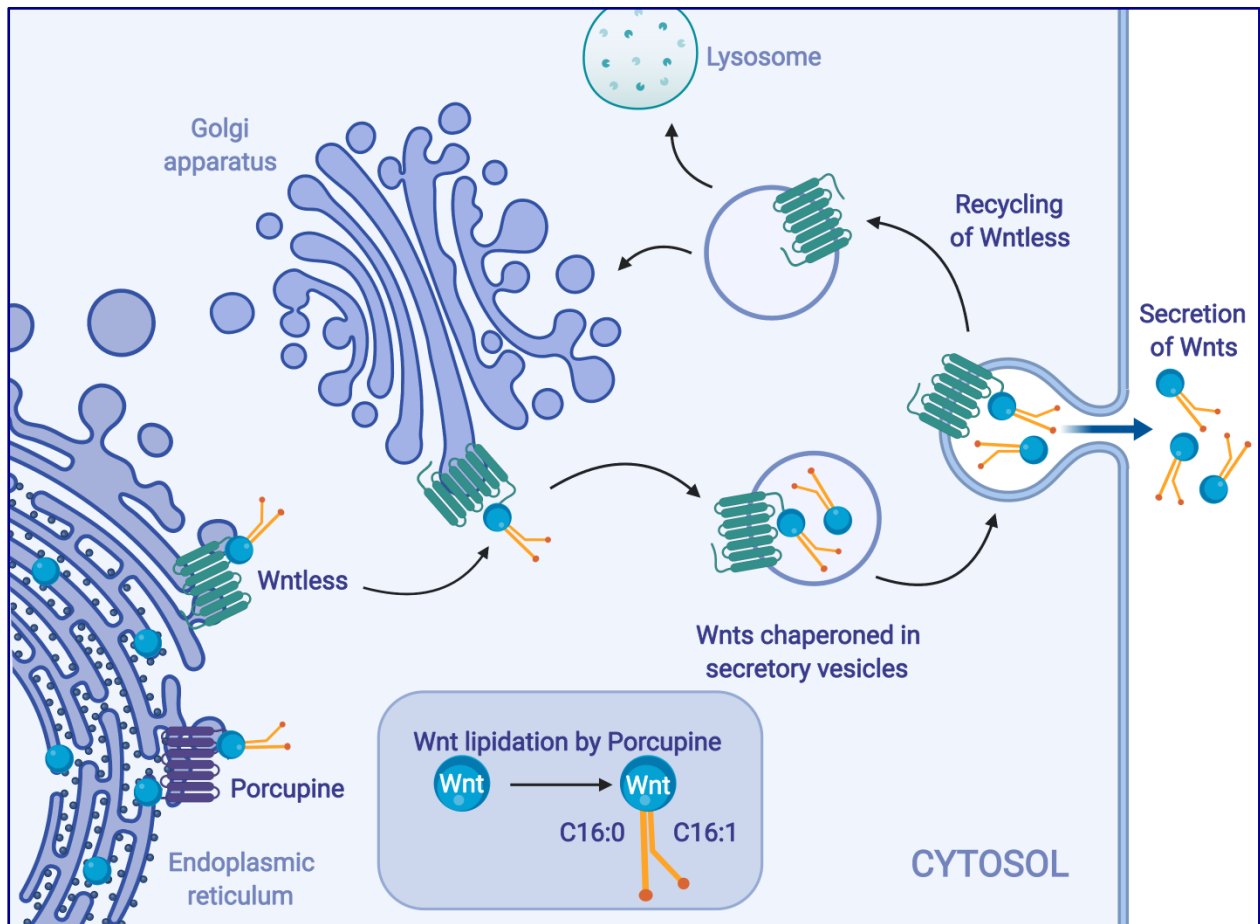


Figure 1.4. Wntless is an evolutionarily conserved chaperone protein dedicated to trafficking lipidated Wnts through the intracellular secretory compartment. After Wnt proteins are synthesized in the endoplasmic reticulum (ER), they undergo significant post-translational modifications, including N-glycosylation and lipidation. The ER acyltransferase Porcupine catalyzes addition of palmitic (C16:0) and palmitoleic (C16:1) acid moieties at conserved Cys77 and Ser209 residues, respectively. Palmitoleoylation (addition of C16:1) is required for interaction of Wnts with their chaperone protein, Wntless. Wntless binds to and chaperones Wnt proteins from the ER through the trans-Golgi network, and to the plasma membrane in secretory vesicles. Once Wnts are secreted, Wntless is transported back via the retromer complex to the Golgi for reuse or to lysosomes for degradation. *Adapted from Herr et al., 2012¹¹⁵.*

Figure 1.5

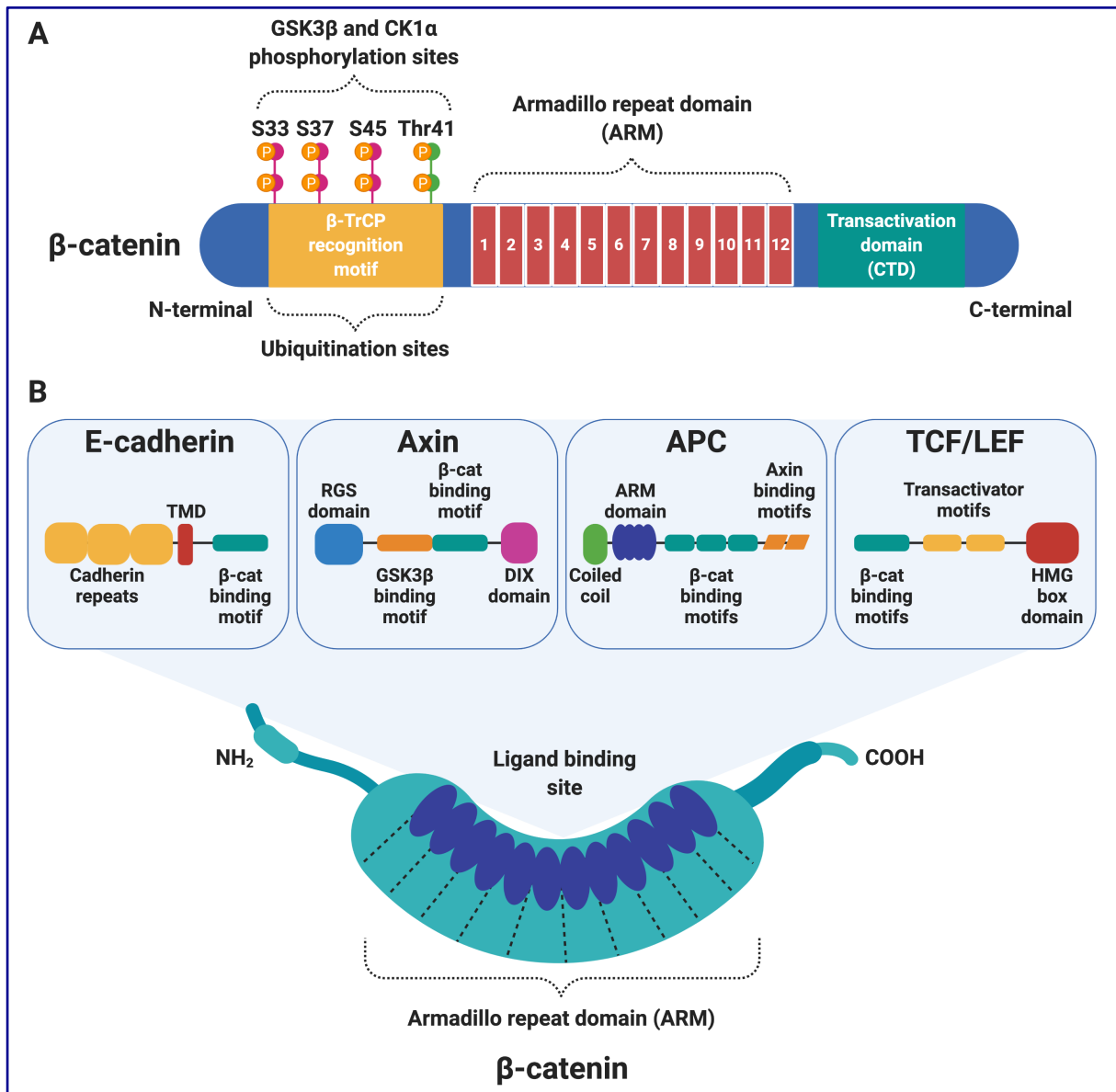


Figure 1.5. Structural composition of β -catenin provides insights into its dual roles in cell mechanics and Wnt signaling. (A) β -catenin is comprised of a central 12-unit Armadillo repeat domain (ARM) flanked on either side by distinct N- and C-terminal domains. The N-terminal region consists of conserved serine and threonine residues that are sequentially phosphorylated by CK1 α and GSK3 β ; phosphorylation of these sites promotes binding to β -TrCP, subsequent ubiquitination, and proteasomal degradation. (B) The ARM region forms a superhelix featuring a positively charged groove that serves as a platform for interactions with various β -catenin binding partners, including E-cadherin, Axin, APC, and TCF/LEF proteins. These partners share overlapping binding sites in the ARM groove, and thus typically cannot bind simultaneously. Adapted from Xu et al., 2007²³⁵; Graham et al., 2000¹⁴⁰.

Figure 1.6

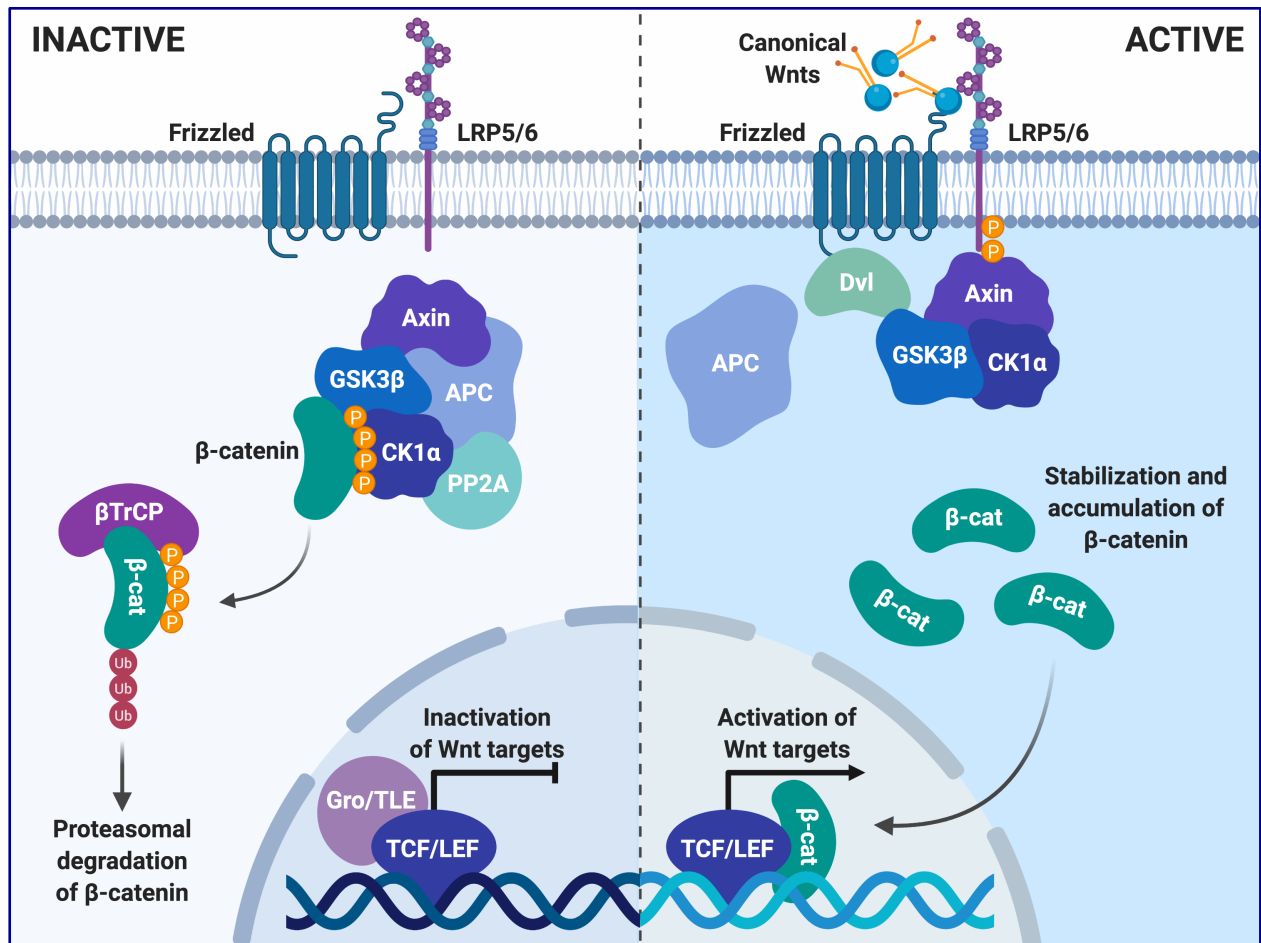


Figure 1.6. Activation of the canonical Wnt signaling pathway promotes β -catenin-mediated transcription of Wnt target genes. In the absence of extracellular Wnts (inactive; left panel), β -catenin is bound by a destruction complex comprised of Axin, APC, GSK3 β , CK1 α , and PP2A. CK1 α and GSK3 β sequentially phosphorylate free cytosolic β -catenin, targeting it for ubiquitination by β TrCP and subsequent proteasomal degradation. When canonical Wnts bind to their frizzled receptors and LRP co-receptors (active; right panel), they trigger an intracellular signaling cascade that leads to hypophosphorylation, stabilization, and accumulation of cytosolic β -catenin. β -catenin can then translocate to the nucleus, displace Groucho/TLE repressors, and coactivate TCF/LEF transcription factors to mediate Wnt target gene expression. *Adapted from Palomer et al., 2019²³⁶.*

Figure 1.7

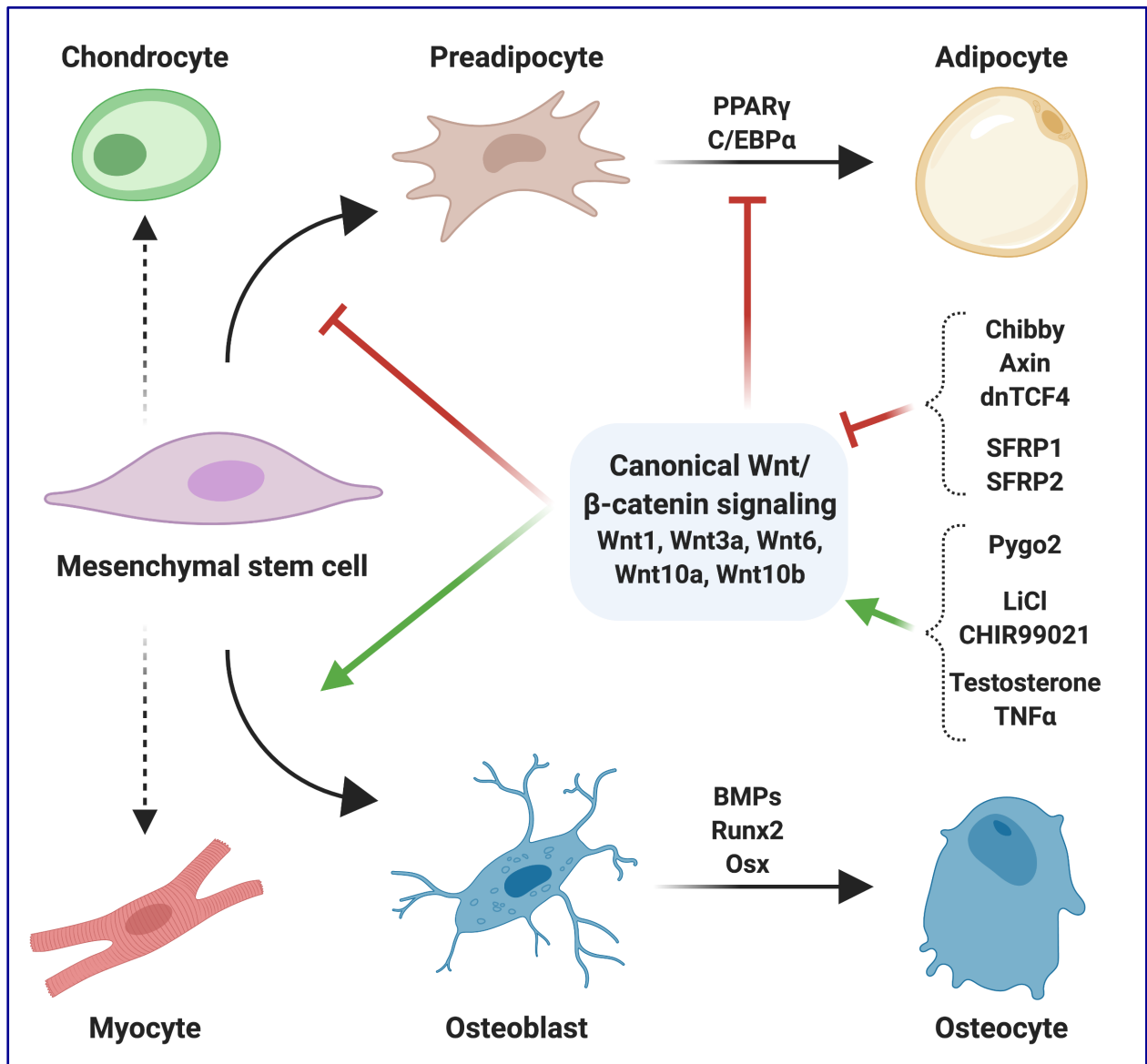


Figure 1.7. The canonical Wnt signaling pathway is an important endogenous regulator of cell fate determination. Activation of canonical Wnt/ β -catenin signaling in mesenchymal stem cells suppresses adipogenesis and promotes osteoblastogenesis. Wnt signaling suppresses adipocyte differentiation by inhibiting expression of PPAR γ and C/EBP α , the central regulators of adipogenesis.

References

1. Kadereit B, Kumar P, Wang WJ, et al. Evolutionarily conserved gene family important for fat storage. *Proc Natl Acad Sci U S A*. 2008;105(1):94-99.
2. Martin S, Parton RG. Lipid droplets: a unified view of a dynamic organelle. *Nat Rev Mol Cell Biol*. 2006;7(5):373-378.
3. Gesta S, Tseng YH, Kahn CR. Developmental origin of fat: tracking obesity to its source. *Cell*. 2007;131(2):242-256.
4. Cinti S. The adipose organ at a glance. *Dis Model Mech*. 2012;5(5):588-594.
5. Rosen ED, Spiegelman BM. What we talk about when we talk about fat. *Cell*. 2014;156(1-2):20-44.
6. Ingalls AM, Dickie MM, Snell GD. Obese, a new mutation in the house mouse. *J Hered*. 1950;41(12):317-318.
7. Zhang Y, Proenca R, Maffei M, Barone M, Leopold L, Friedman JM. Positional cloning of the mouse obese gene and its human homologue. *Nature*. 1994;372(6505):425-432.
8. Halaas JL, Gajiwala KS, Maffei M, et al. Weight-reducing effects of the plasma protein encoded by the obese gene. *Science*. 1995;269(5223):543-546.
9. Montague CT, Farooqi IS, Whitehead JP, et al. Congenital leptin deficiency is associated with severe early-onset obesity in humans. *Nature*. 1997;387(6636):903-908.
10. Farooqi IS, Jebb SA, Langmack G, et al. Effects of recombinant leptin therapy in a child with congenital leptin deficiency. *N Engl J Med*. 1999;341(12):879-884.
11. Jaacks LM, Vandevijvere S, Pan A, et al. The obesity transition: stages of the global epidemic. *Lancet Diabetes Endocrinol*. 2019;7(3):231-240.
12. Chooi YC, Ding C, Magkos F. The epidemiology of obesity. *Metabolism*. 2019;92:6-10.
13. Bluher M. Obesity: global epidemiology and pathogenesis. *Nat Rev Endocrinol*. 2019;15(5):288-298.
14. Kim DD, Basu A. Estimating the Medical Care Costs of Obesity in the United States: Systematic Review, Meta-Analysis, and Empirical Analysis. *Value Health*. 2016;19(5):602-613.
15. Tremmel M, Gerdtham UG, Nilsson PM, Saha S. Economic Burden of Obesity: A Systematic Literature Review. *Int J Environ Res Public Health*. 2017;14(4).
16. Vazquez-Vela ME, Torres N, Tovar AR. White adipose tissue as endocrine organ and its role in obesity. *Arch Med Res*. 2008;39(8):715-728.
17. Unger RH, Clark GO, Scherer PE, Orci L. Lipid homeostasis, lipotoxicity and the metabolic syndrome. *Biochim Biophys Acta*. 2010;1801(3):209-214.
18. Despres JP, Lemieux I. Abdominal obesity and metabolic syndrome. *Nature*. 2006;444(7121):881-887.
19. Agarwal AK, Garg A. Genetic basis of lipodystrophies and management of metabolic complications. *Annu Rev Med*. 2006;57:297-311.
20. Hussain I, Garg A. Lipodystrophy Syndromes. *Endocrinol Metab Clin North Am*. 2016;45(4):783-797.
21. Cinti S. The adipose organ. *Prostaglandins Leukot Essent Fatty Acids*. 2005;73(1):9-15.

22. Bagchi DP, Forss I, Mandrup S, MacDougald OA. SnapShot: Niche Determines Adipocyte Character I. *Cell Metab.* 2018;27(1):264-264 e261.
23. Bagchi DP, Forss I, Mandrup S, MacDougald OA. SnapShot: Niche Determines Adipocyte Character II. *Cell Metab.* 2018;27(1):266-266 e261.
24. Bagchi DP, MacDougald OA. Identification and Dissection of Diverse Mouse Adipose Depots. *J Vis Exp.* 2019(149).
25. Tchkonja T, Thomou T, Zhu Y, et al. Mechanisms and metabolic implications of regional differences among fat depots. *Cell Metab.* 2013;17(5):644-656.
26. Lee MJ, Wu Y, Fried SK. Adipose tissue heterogeneity: implication of depot differences in adipose tissue for obesity complications. *Mol Aspects Med.* 2013;34(1):1-11.
27. Kahn CR, Wang G, Lee KY. Altered adipose tissue and adipocyte function in the pathogenesis of metabolic syndrome. *J Clin Invest.* 2019;129(10):3990-4000.
28. Kissebah AH, Krakower GR. Regional adiposity and morbidity. *Physiol Rev.* 1994;74(4):761-811.
29. Smith RE, Horwitz BA. Brown fat and thermogenesis. *Physiol Rev.* 1969;49(2):330-425.
30. Zhang F, Hao G, Shao M, et al. An Adipose Tissue Atlas: An Image-Guided Identification of Human-like BAT and Beige Depots in Rodents. *Cell Metab.* 2018;27(1):252-262 e253.
31. Sanchez-Gurmaches J, Guertin DA. Adipocyte lineages: tracing back the origins of fat. *Biochim Biophys Acta.* 2014;1842(3):340-351.
32. Sanchez-Gurmaches J, Guertin DA. Adipocytes arise from multiple lineages that are heterogeneously and dynamically distributed. *Nat Commun.* 2014;5:4099.
33. Kajimura S, Spiegelman BM, Seale P. Brown and Beige Fat: Physiological Roles beyond Heat Generation. *Cell Metab.* 2015;22(4):546-559.
34. Frontini A, Cinti S. Distribution and development of brown adipocytes in the murine and human adipose organ. *Cell Metab.* 2010;11(4):253-256.
35. Cannon B, Nedergaard J. Brown adipose tissue: function and physiological significance. *Physiol Rev.* 2004;84(1):277-359.
36. Ricquier D. Uncoupling protein 1 of brown adipocytes, the only uncoupler: a historical perspective. *Front Endocrinol (Lausanne).* 2011;2:85.
37. Kozak LP, Harper ME. Mitochondrial uncoupling proteins in energy expenditure. *Annu Rev Nutr.* 2000;20:339-363.
38. Petrovic N, Walden TB, Shabalina IG, Timmons JA, Cannon B, Nedergaard J. Chronic peroxisome proliferator-activated receptor gamma (PPARgamma) activation of epididymally derived white adipocyte cultures reveals a population of thermogenically competent, UCP1-containing adipocytes molecularly distinct from classic brown adipocytes. *J Biol Chem.* 2010;285(10):7153-7164.
39. Wu J, Bostrom P, Sparks LM, et al. Beige adipocytes are a distinct type of thermogenic fat cell in mouse and human. *Cell.* 2012;150(2):366-376.
40. Vitali A, Murano I, Zingaretti MC, Frontini A, Ricquier D, Cinti S. The adipose organ of obesity-prone C57BL/6J mice is composed of mixed white and brown adipocytes. *J Lipid Res.* 2012;53(4):619-629.
41. Harms M, Seale P. Brown and beige fat: development, function and therapeutic potential. *Nat Med.* 2013;19(10):1252-1263.

42. Wu J, Cohen P, Spiegelman BM. Adaptive thermogenesis in adipocytes: is beige the new brown? *Genes Dev.* 2013;27(3):234-250.
43. Seale P, Bjork B, Yang W, et al. PRDM16 controls a brown fat/skeletal muscle switch. *Nature.* 2008;454(7207):961-967.
44. Xue B, Rim JS, Hogan JC, Coulter AA, Koza RA, Kozak LP. Genetic variability affects the development of brown adipocytes in white fat but not in interscapular brown fat. *J Lipid Res.* 2007;48(1):41-51.
45. Cypess AM, Lehman S, Williams G, et al. Identification and importance of brown adipose tissue in adult humans. *N Engl J Med.* 2009;360(15):1509-1517.
46. Virtanen KA, Lidell ME, Orava J, et al. Functional brown adipose tissue in healthy adults. *N Engl J Med.* 2009;360(15):1518-1525.
47. Orava J, Nuutila P, Lidell ME, et al. Different metabolic responses of human brown adipose tissue to activation by cold and insulin. *Cell Metab.* 2011;14(2):272-279.
48. Nedergaard J, Bengtsson T, Cannon B. Unexpected evidence for active brown adipose tissue in adult humans. *Am J Physiol Endocrinol Metab.* 2007;293(2):E444-452.
49. Saito M, Okamatsu-Ogura Y, Matsushita M, et al. High incidence of metabolically active brown adipose tissue in healthy adult humans: effects of cold exposure and adiposity. *Diabetes.* 2009;58(7):1526-1531.
50. Trayhurn P, Arch JR. New Physiological Aspects of Brown Adipose Tissue. *Curr Obes Rep.* 2014;3(4):414-421.
51. Harper JA, Dickinson K, Brand MD. Mitochondrial uncoupling as a target for drug development for the treatment of obesity. *Obes Rev.* 2001;2(4):255-265.
52. Zwick RK, Guerrero-Juarez CF, Horsley V, Plikus MV. Anatomical, Physiological, and Functional Diversity of Adipose Tissue. *Cell Metab.* 2018;27(1):68-83.
53. Li Z, Hardij J, Bagchi DP, Scheller EL, MacDougald OA. Development, regulation, metabolism and function of bone marrow adipose tissues. *Bone.* 2018;110:134-140.
54. Scheller EL, Doucette CR, Learman BS, et al. Region-specific variation in the properties of skeletal adipocytes reveals regulated and constitutive marrow adipose tissues. *Nat Commun.* 2015;6:7808.
55. Scheller EL, Cawthorn WP, Burr AA, Horowitz MC, MacDougald OA. Marrow Adipose Tissue: Trimming the Fat. *Trends Endocrinol Metab.* 2016;27(6):392-403.
56. Alexander CM, Kasza I, Yen CL, et al. Dermal white adipose tissue: a new component of the thermogenic response. *J Lipid Res.* 2015;56(11):2061-2069.
57. Kruglikov IL, Scherer PE. Dermal Adipocytes: From Irrelevance to Metabolic Targets? *Trends Endocrinol Metab.* 2016;27(1):1-10.
58. Festa E, Fretz J, Berry R, et al. Adipocyte lineage cells contribute to the skin stem cell niche to drive hair cycling. *Cell.* 2011;146(5):761-771.
59. Schmidt BA, Horsley V. Intradermal adipocytes mediate fibroblast recruitment during skin wound healing. *Development.* 2013;140(7):1517-1527.
60. Iacobellis G. Local and systemic effects of the multifaceted epicardial adipose tissue depot. *Nat Rev Endocrinol.* 2015;11(6):363-371.

61. Cherian S, Lopaschuk GD, Carvalho E. Cellular cross-talk between epicardial adipose tissue and myocardium in relation to the pathogenesis of cardiovascular disease. *Am J Physiol Endocrinol Metab.* 2012;303(8):E937-949.
62. Addison O, Marcus RL, Lastayo PC, Ryan AS. Intermuscular fat: a review of the consequences and causes. *Int J Endocrinol.* 2014;2014:309570.
63. Pond CM, Mattacks CA. The activation of the adipose tissue associated with lymph nodes during the early stages of an immune response. *Cytokine.* 2002;17(3):131-139.
64. Pond CM. Adipose tissue and the immune system. *Prostaglandins Leukot Essent Fatty Acids.* 2005;73(1):17-30.
65. Kloppenburg Al-FM. An emerging player in knee osteoarthritis: the infrapatellar fat pad. *Arthritis Research & Therapy.* 2013;15(225):1-9.
66. Nusse R, Varmus HE. Many tumors induced by the mouse mammary tumor virus contain a provirus integrated in the same region of the host genome. *Cell.* 1982;31(1):99-109.
67. Nusslein-Volhard C, Wieschaus E. Mutations affecting segment number and polarity in *Drosophila*. *Nature.* 1980;287(5785):795-801.
68. Rijsewijk F, Schuermann M, Wagenaar E, Parren P, Weigel D, Nusse R. The *Drosophila* homolog of the mouse mammary oncogene int-1 is identical to the segment polarity gene wingless. *Cell.* 1987;50(4):649-657.
69. Loh KM, van Amerongen R, Nusse R. Generating Cellular Diversity and Spatial Form: Wnt Signaling and the Evolution of Multicellular Animals. *Dev Cell.* 2016;38(6):643-655.
70. Clevers H. Wnt/beta-catenin signaling in development and disease. *Cell.* 2006;127(3):469-480.
71. Miller JR. The Wnts. *Genome Biol.* 2002;3(1):REVIEWS3001.
72. Logan CY, Nusse R. The Wnt signaling pathway in development and disease. *Annu Rev Cell Dev Biol.* 2004;20:781-810.
73. Wiese KE, Nusse R, van Amerongen R. Wnt signalling: conquering complexity. *Development.* 2018;145(12).
74. Clevers H, Nusse R. Wnt/beta-catenin signaling and disease. *Cell.* 2012;149(6):1192-1205.
75. Moon RT, Bowerman B, Boutros M, Perrimon N. The promise and perils of Wnt signaling through beta-catenin. *Science.* 2002;296(5573):1644-1646.
76. Cadigan KM, Liu YI. Wnt signaling: complexity at the surface. *J Cell Sci.* 2006;119(Pt 3):395-402.
77. Niehrs C. The complex world of WNT receptor signalling. *Nat Rev Mol Cell Biol.* 2012;13(12):767-779.
78. Grigoryan T, Wend P, Klaus A, Birchmeier W. Deciphering the function of canonical Wnt signals in development and disease: conditional loss- and gain-of-function mutations of beta-catenin in mice. *Genes Dev.* 2008;22(17):2308-2341.
79. Nishisho I, Nakamura Y, Miyoshi Y, et al. Mutations of chromosome 5q21 genes in FAP and colorectal cancer patients. *Science.* 1991;253(5020):665-669.
80. Kinzler KW, Nilbert MC, Vogelstein B, et al. Identification of a gene located at chromosome 5q21 that is mutated in colorectal cancers. *Science.* 1991;251(4999):1366-1370.

81. Kinzler KW, Nilbert MC, Su LK, et al. Identification of FAP locus genes from chromosome 5q21. *Science*. 1991;253(5020):661-665.
82. Rubinfeld B, Souza B, Albert I, et al. Association of the APC gene product with beta-catenin. *Science*. 1993;262(5140):1731-1734.
83. Su LK, Vogelstein B, Kinzler KW. Association of the APC tumor suppressor protein with catenins. *Science*. 1993;262(5140):1734-1737.
84. Nusse R, Clevers H. Wnt/beta-Catenin Signaling, Disease, and Emerging Therapeutic Modalities. *Cell*. 2017;169(6):985-999.
85. Polakis P. The many ways of Wnt in cancer. *Curr Opin Genet Dev*. 2007;17(1):45-51.
86. Cadigan KM, Nusse R. Wnt signaling: a common theme in animal development. *Genes Dev*. 1997;11(24):3286-3305.
87. Dierick H, Bejsovec A. Cellular mechanisms of wingless/Wnt signal transduction. *Curr Top Dev Biol*. 1999;43:153-190.
88. Coudreuse D, Korswagen HC. The making of Wnt: new insights into Wnt maturation, sorting and secretion. *Development*. 2007;134(1):3-12.
89. Tanaka K, Kitagawa Y, Kadowaki T. Drosophila segment polarity gene product porcupine stimulates the posttranslational N-glycosylation of wingless in the endoplasmic reticulum. *J Biol Chem*. 2002;277(15):12816-12823.
90. Hofmann K. A superfamily of membrane-bound O-acyltransferases with implications for wnt signaling. *Trends Biochem Sci*. 2000;25(3):111-112.
91. Rios-Esteves J, Haugen B, Resh MD. Identification of key residues and regions important for porcupine-mediated Wnt acylation. *J Biol Chem*. 2014;289(24):17009-17019.
92. Kadowaki T, Wilder E, Klingensmith J, Zachary K, Perrimon N. The segment polarity gene porcupine encodes a putative multitransmembrane protein involved in Wingless processing. *Genes Dev*. 1996;10(24):3116-3128.
93. Rios-Esteves J, Resh MD. Stearoyl CoA desaturase is required to produce active, lipid-modified Wnt proteins. *Cell Rep*. 2013;4(6):1072-1081.
94. Willert K, Brown JD, Danenberg E, et al. Wnt proteins are lipid-modified and can act as stem cell growth factors. *Nature*. 2003;423(6938):448-452.
95. Takada R, Satomi Y, Kurata T, et al. Monounsaturated fatty acid modification of Wnt protein: its role in Wnt secretion. *Dev Cell*. 2006;11(6):791-801.
96. Galli LM, Barnes TL, Secrest SS, Kadowaki T, Burrus LW. Porcupine-mediated lipid-modification regulates the activity and distribution of Wnt proteins in the chick neural tube. *Development*. 2007;134(18):3339-3348.
97. van den Heuvel M, Harryman-Samos C, Klingensmith J, Perrimon N, Nusse R. Mutations in the segment polarity genes wingless and porcupine impair secretion of the wingless protein. *EMBO J*. 1993;12(13):5293-5302.
98. Proffitt KD, Virshup DM. Precise regulation of porcupine activity is required for physiological Wnt signaling. *J Biol Chem*. 2012;287(41):34167-34178.
99. Burrus LW, McMahon AP. Biochemical analysis of murine Wnt proteins reveals both shared and distinct properties. *Exp Cell Res*. 1995;220(2):363-373.
100. Tang X, Wu Y, Belenkaya TY, et al. Roles of N-glycosylation and lipidation in Wg secretion and signaling. *Dev Biol*. 2012;364(1):32-41.

101. Komekado H, Yamamoto H, Chiba T, Kikuchi A. Glycosylation and palmitoylation of Wnt-3a are coupled to produce an active form of Wnt-3a. *Genes Cells*. 2007;12(4):521-534.
102. Franch-Marro X, Wendler F, Griffith J, Maurice MM, Vincent JP. In vivo role of lipid adducts on Wingless. *J Cell Sci*. 2008;121(Pt 10):1587-1592.
103. Banziger C, Soldini D, Schutt C, Zipperlen P, Hausmann G, Basler K. Wntless, a conserved membrane protein dedicated to the secretion of Wnt proteins from signaling cells. *Cell*. 2006;125(3):509-522.
104. Bartscherer K, Pelte N, Ingelfinger D, Boutros M. Secretion of Wnt ligands requires Evi, a conserved transmembrane protein. *Cell*. 2006;125(3):523-533.
105. Goodman RM, Thombre S, Firtina Z, et al. Sprinter: a novel transmembrane protein required for Wg secretion and signaling. *Development*. 2006;133(24):4901-4911.
106. Jin J, Morse M, Frey C, Petko J, Levenson R. Expression of GPR177 (Wntless/Evi/Sprinter), a highly conserved Wnt-transport protein, in rat tissues, zebrafish embryos, and cultured human cells. *Dev Dyn*. 2010;239(9):2426-2434.
107. Yu HM, Jin Y, Fu J, Hsu W. Expression of Gpr177, a Wnt trafficking regulator, in mouse embryogenesis. *Dev Dyn*. 2010;239(7):2102-2109.
108. Fu J, Jiang M, Mirando AJ, Yu HM, Hsu W. Reciprocal regulation of Wnt and Gpr177/mouse Wntless is required for embryonic axis formation. *Proc Natl Acad Sci U S A*. 2009;106(44):18598-18603.
109. Gasnereau I, Herr P, Chia PZ, Basler K, Gleeson PA. Identification of an endocytosis motif in an intracellular loop of Wntless protein, essential for its recycling and the control of Wnt protein signaling. *J Biol Chem*. 2011;286(50):43324-43333.
110. Yang PT, Lorenowicz MJ, Silhankova M, Coudreuse DY, Betist MC, Korswagen HC. Wnt signaling requires retromer-dependent recycling of MIG-14/Wntless in Wnt-producing cells. *Dev Cell*. 2008;14(1):140-147.
111. Pan CL, Baum PD, Gu M, Jorgensen EM, Clark SG, Garriga G. C. elegans AP-2 and retromer control Wnt signaling by regulating mig-14/Wntless. *Dev Cell*. 2008;14(1):132-139.
112. Port F, Kuster M, Herr P, et al. Wingless secretion promotes and requires retromer-dependent cycling of Wntless. *Nat Cell Biol*. 2008;10(2):178-185.
113. Korkut C, Ataman B, Ramachandran P, et al. Trans-synaptic transmission of vesicular Wnt signals through Evi/Wntless. *Cell*. 2009;139(2):393-404.
114. Coombs GS, Yu J, Canning CA, et al. WLS-dependent secretion of WNT3A requires Ser209 acylation and vacuolar acidification. *J Cell Sci*. 2010;123(Pt 19):3357-3367.
115. Herr P, Basler K. Porcupine-mediated lipidation is required for Wnt recognition by Wls. *Dev Biol*. 2012;361(2):392-402.
116. Harterink M, Port F, Lorenowicz MJ, et al. A SNX3-dependent retromer pathway mediates retrograde transport of the Wnt sorting receptor Wntless and is required for Wnt secretion. *Nat Cell Biol*. 2011;13(8):914-923.
117. Yu J, Chia J, Canning CA, Jones CM, Bard FA, Virshup DM. WLS retrograde transport to the endoplasmic reticulum during Wnt secretion. *Dev Cell*. 2014;29(3):277-291.

118. Coudreuse DY, Roel G, Betist MC, Destree O, Korswagen HC. Wnt gradient formation requires retromer function in Wnt-producing cells. *Science*. 2006;312(5775):921-924.
119. Carpenter AC, Rao S, Wells JM, Campbell K, Lang RA. Generation of mice with a conditional null allele for Wntless. *Genesis*. 2010;48(9):554-558.
120. McMahon AP, Bradley A. The Wnt-1 (int-1) proto-oncogene is required for development of a large region of the mouse brain. *Cell*. 1990;62(6):1073-1085.
121. Thomas KR, Capecchi MR. Targeted disruption of the murine int-1 proto-oncogene resulting in severe abnormalities in midbrain and cerebellar development. *Nature*. 1990;346(6287):847-850.
122. Liu P, Wakamiya M, Shea MJ, Albrecht U, Behringer RR, Bradley A. Requirement for Wnt3 in vertebrate axis formation. *Nat Genet*. 1999;22(4):361-365.
123. Ikeya M, Lee SM, Johnson JE, McMahon AP, Takada S. Wnt signalling required for expansion of neural crest and CNS progenitors. *Nature*. 1997;389(6654):966-970.
124. Brault V, Moore R, Kutsch S, et al. Inactivation of the beta-catenin gene by Wnt1-Cre-mediated deletion results in dramatic brain malformation and failure of craniofacial development. *Development*. 2001;128(8):1253-1264.
125. Belenkaya TY, Wu Y, Tang X, et al. The retromer complex influences Wnt secretion by recycling wntless from endosomes to the trans-Golgi network. *Dev Cell*. 2008;14(1):120-131.
126. Fu J, Ivy Yu HM, Maruyama T, Mirando AJ, Hsu W. Gpr177/mouse Wntless is essential for Wnt-mediated craniofacial and brain development. *Dev Dyn*. 2011;240(2):365-371.
127. Zhu X, Zhu H, Zhang L, et al. Wls-mediated Wnts differentially regulate distal limb patterning and tissue morphogenesis. *Dev Biol*. 2012;365(2):328-338.
128. Zhong Z, Zylstra-Diegel CR, Schumacher CA, et al. Wntless functions in mature osteoblasts to regulate bone mass. *Proc Natl Acad Sci U S A*. 2012;109(33):E2197-2204.
129. Zhong ZA, Zahatnansky J, Snider J, Van Wieren E, Diegel CR, Williams BO. Wntless spatially regulates bone development through beta-catenin-dependent and independent mechanisms. *Dev Dyn*. 2015;244(10):1347-1355.
130. Jiang M, Ku WY, Fu J, Offermanns S, Hsu W, Que J. Gpr177 regulates pulmonary vasculature development. *Development*. 2013;140(17):3589-3594.
131. van Amerongen R. Alternative Wnt pathways and receptors. *Cold Spring Harb Perspect Biol*. 2012;4(10).
132. Semenov MV, Habas R, Macdonald BT, He X. SnapShot: Noncanonical Wnt Signaling Pathways. *Cell*. 2007;131(7):1378.
133. Macdonald BT, Semenov MV, He X. SnapShot: Wnt/beta-catenin signaling. *Cell*. 2007;131(6):1204.
134. Willert K, Jones KA. Wnt signaling: is the party in the nucleus? *Genes Dev*. 2006;20(11):1394-1404.
135. Ozawa M, Baribault H, Kemler R. The cytoplasmic domain of the cell adhesion molecule uvomorulin associates with three independent proteins structurally related in different species. *EMBO J*. 1989;8(6):1711-1717.

136. Wieschaus E, Riggleman R. Autonomous requirements for the segment polarity gene armadillo during Drosophila embryogenesis. *Cell*. 1987;49(2):177-184.
137. Peifer M, Wieschaus E. The segment polarity gene armadillo encodes a functionally modular protein that is the Drosophila homolog of human plakoglobin. *Cell*. 1990;63(6):1167-1176.
138. Orsulic S, Peifer M. An in vivo structure-function study of armadillo, the beta-catenin homologue, reveals both separate and overlapping regions of the protein required for cell adhesion and for wingless signaling. *J Cell Biol*. 1996;134(5):1283-1300.
139. Riggleman B, Schedl P, Wieschaus E. Spatial expression of the Drosophila segment polarity gene armadillo is posttranscriptionally regulated by wingless. *Cell*. 1990;63(3):549-560.
140. Graham TA, Weaver C, Mao F, Kimelman D, Xu W. Crystal structure of a beta-catenin/Tcf complex. *Cell*. 2000;103(6):885-896.
141. Huber AH, Weis WI. The structure of the beta-catenin/E-cadherin complex and the molecular basis of diverse ligand recognition by beta-catenin. *Cell*. 2001;105(3):391-402.
142. Eklof Spink K, Fridman SG, Weis WI. Molecular mechanisms of beta-catenin recognition by adenomatous polyposis coli revealed by the structure of an APC-beta-catenin complex. *EMBO J*. 2001;20(22):6203-6212.
143. Poy F, Lepourcelet M, Shivdasani RA, Eck MJ. Structure of a human Tcf4-beta-catenin complex. *Nat Struct Biol*. 2001;8(12):1053-1057.
144. Peifer M, McCrea PD, Green KJ, Wieschaus E, Gumbiner BM. The vertebrate adhesive junction proteins beta-catenin and plakoglobin and the Drosophila segment polarity gene armadillo form a multigene family with similar properties. *J Cell Biol*. 1992;118(3):681-691.
145. Stepniak E, Radice GL, Vasioukhin V. Adhesive and signaling functions of cadherins and catenins in vertebrate development. *Cold Spring Harb Perspect Biol*. 2009;1(5):a002949.
146. MacDonald BT, Tamai K, He X. Wnt/beta-catenin signaling: components, mechanisms, and diseases. *Dev Cell*. 2009;17(1):9-26.
147. Kimelman D, Xu W. beta-catenin destruction complex: insights and questions from a structural perspective. *Oncogene*. 2006;25(57):7482-7491.
148. Liu C, Li Y, Semenov M, et al. Control of beta-catenin phosphorylation/degradation by a dual-kinase mechanism. *Cell*. 2002;108(6):837-847.
149. Aberle H, Bauer A, Stappert J, Kispert A, Kemler R. beta-catenin is a target for the ubiquitin-proteasome pathway. *EMBO J*. 1997;16(13):3797-3804.
150. Hart M, Concordet JP, Lassot I, et al. The F-box protein beta-TrCP associates with phosphorylated beta-catenin and regulates its activity in the cell. *Curr Biol*. 1999;9(4):207-210.
151. Ross SE, Hemati N, Longo KA, et al. Inhibition of adipogenesis by Wnt signaling. *Science*. 2000;289(5481):950-953.
152. Bennett CN, Ross SE, Longo KA, et al. Regulation of Wnt signaling during adipogenesis. *J Biol Chem*. 2002;277(34):30998-31004.

153. Valenta T, Hausmann G, Basler K. The many faces and functions of beta-catenin. *EMBO J.* 2012;31(12):2714-2736.
154. Stamos JL, Chu ML, Enos MD, Shah N, Weis WI. Structural basis of GSK-3 inhibition by N-terminal phosphorylation and by the Wnt receptor LRP6. *Elife.* 2014;3:e01998.
155. Behrens J, von Kries JP, Kuhl M, et al. Functional interaction of beta-catenin with the transcription factor LEF-1. *Nature.* 1996;382(6592):638-642.
156. Li VS, Ng SS, Boersema PJ, et al. Wnt signaling through inhibition of beta-catenin degradation in an intact Axin1 complex. *Cell.* 2012;149(6):1245-1256.
157. Hoppler S, Kavanagh CL. Wnt signalling: variety at the core. *J Cell Sci.* 2007;120(Pt 3):385-393.
158. Mosimann C, Hausmann G, Basler K. Beta-catenin hits chromatin: regulation of Wnt target gene activation. *Nat Rev Mol Cell Biol.* 2009;10(4):276-286.
159. Archbold HC, Yang YX, Chen L, Cadigan KM. How do they do Wnt they do?: regulation of transcription by the Wnt/beta-catenin pathway. *Acta Physiol (Oxf).* 2012;204(1):74-109.
160. Andrzejewska A, Lukomska B, Janowski M. Concise Review: Mesenchymal Stem Cells: From Roots to Boost. *Stem Cells.* 2019;37(7):855-864.
161. Farmer SR. Transcriptional control of adipocyte formation. *Cell Metab.* 2006;4(4):263-273.
162. Rosen ED, MacDougald OA. Adipocyte differentiation from the inside out. *Nat Rev Mol Cell Biol.* 2006;7(12):885-896.
163. Rosen ED, Walkey CJ, Puigserver P, Spiegelman BM. Transcriptional regulation of adipogenesis. *Genes Dev.* 2000;14(11):1293-1307.
164. Rangwala SM, Lazar MA. Transcriptional control of adipogenesis. *Annu Rev Nutr.* 2000;20:535-559.
165. Siersbaek R, Nielsen R, John S, et al. Extensive chromatin remodelling and establishment of transcription factor 'hotspots' during early adipogenesis. *EMBO J.* 2011;30(8):1459-1472.
166. Steger DJ, Grant GR, Schupp M, et al. Propagation of adipogenic signals through an epigenomic transition state. *Genes Dev.* 2010;24(10):1035-1044.
167. Lefterova MI, Haakonsson AK, Lazar MA, Mandrup S. PPARgamma and the global map of adipogenesis and beyond. *Trends Endocrinol Metab.* 2014;25(6):293-302.
168. Lefterova MI, Zhang Y, Steger DJ, et al. PPARgamma and C/EBP factors orchestrate adipocyte biology via adjacent binding on a genome-wide scale. *Genes Dev.* 2008;22(21):2941-2952.
169. Darlington GJ, Ross SE, MacDougald OA. The role of C/EBP genes in adipocyte differentiation. *J Biol Chem.* 1998;273(46):30057-30060.
170. Fischer L, Boland G, Tuan RS. Wnt-3A enhances bone morphogenetic protein-2-mediated chondrogenesis of murine C3H10T1/2 mesenchymal cells. *J Biol Chem.* 2002;277(34):30870-30878.
171. Hoppler S, Brown JD, Moon RT. Expression of a dominant-negative Wnt blocks induction of MyoD in *Xenopus* embryos. *Genes Dev.* 1996;10(21):2805-2817.
172. Cossu G, Borello U. Wnt signaling and the activation of myogenesis in mammals. *EMBO J.* 1999;18(24):6867-6872.

173. Prestwich TC, Macdougald OA. Wnt/beta-catenin signaling in adipogenesis and metabolism. *Curr Opin Cell Biol.* 2007;19(6):612-617.
174. Christodoulides C, Lagathu C, Sethi JK, Vidal-Puig A. Adipogenesis and WNT signalling. *Trends Endocrinol Metab.* 2009;20(1):16-24.
175. Sethi JK, Vidal-Puig A. Wnt signalling and the control of cellular metabolism. *Biochem J.* 2010;427(1):1-17.
176. Krishnan V, Bryant HU, Macdougald OA. Regulation of bone mass by Wnt signaling. *J Clin Invest.* 2006;116(5):1202-1209.
177. Cawthorn WP, Bree AJ, Yao Y, et al. Wnt6, Wnt10a and Wnt10b inhibit adipogenesis and stimulate osteoblastogenesis through a beta-catenin-dependent mechanism. *Bone.* 2012;50(2):477-489.
178. Kang S, Bennett CN, Gerin I, Rapp LA, Hankenson KD, Macdougald OA. Wnt signaling stimulates osteoblastogenesis of mesenchymal precursors by suppressing CCAAT/enhancer-binding protein alpha and peroxisome proliferator-activated receptor gamma. *J Biol Chem.* 2007;282(19):14515-14524.
179. Rawadi G, Vayssiere B, Dunn F, Baron R, Roman-Roman S. BMP-2 controls alkaline phosphatase expression and osteoblast mineralization by a Wnt autocrine loop. *J Bone Miner Res.* 2003;18(10):1842-1853.
180. Kennell JA, O'Leary EE, Gummow BM, Hammer GD, MacDougald OA. T-cell factor 4N (TCF-4N), a novel isoform of mouse TCF-4, synergizes with beta-catenin to coactivate C/EBPalpha and steroidogenic factor 1 transcription factors. *Mol Cell Biol.* 2003;23(15):5366-5375.
181. Moldes M, Zuo Y, Morrison RF, et al. Peroxisome-proliferator-activated receptor gamma suppresses Wnt/beta-catenin signalling during adipogenesis. *Biochem J.* 2003;376(Pt 3):607-613.
182. Cristancho AG, Schupp M, Lefterova MI, et al. Repressor transcription factor 7-like 1 promotes adipogenic competency in precursor cells. *Proc Natl Acad Sci U S A.* 2011;108(39):16271-16276.
183. Xie YY, Mo CL, Cai YH, et al. Pygo2 Regulates Adiposity and Glucose Homeostasis via β -Catenin-Axin2-GSK3 β Signaling Pathway. *Diabetes.* 2018;67(12):2569-2584.
184. Singh R, Artaza JN, Taylor WE, et al. Testosterone inhibits adipogenic differentiation in 3T3-L1 cells: nuclear translocation of androgen receptor complex with beta-catenin and T-cell factor 4 may bypass canonical Wnt signaling to down-regulate adipogenic transcription factors. *Endocrinology.* 2006;147(1):141-154.
185. Cawthorn WP, Heyd F, Hegyi K, Sethi JK. Tumour necrosis factor-alpha inhibits adipogenesis via a beta-catenin/TCF4(TCF7L2)-dependent pathway. *Cell Death Differ.* 2007;14(7):1361-1373.
186. Li FQ, Singh AM, Mofunanya A, et al. Chibby promotes adipocyte differentiation through inhibition of beta-catenin signaling. *Mol Cell Biol.* 2007;27(12):4347-4354.
187. Takemaru K, Yamaguchi S, Lee YS, Zhang Y, Carthew RW, Moon RT. Chibby, a nuclear beta-catenin-associated antagonist of the Wnt/Wingless pathway. *Nature.* 2003;422(6934):905-909.

188. Arango NA, Szotek PP, Manganaro TF, Oliva E, Donahoe PK, Teixeira J. Conditional deletion of beta-catenin in the mesenchyme of the developing mouse uterus results in a switch to adipogenesis in the myometrium. *Dev Biol.* 2005;288(1):276-283.
189. Longo KA, Wright WS, Kang S, et al. Wnt10b inhibits development of white and brown adipose tissues. *J Biol Chem.* 2004;279(34):35503-35509.
190. Wright WS, Longo KA, Dolinsky VW, et al. Wnt10b inhibits obesity in ob/ob and agouti mice. *Diabetes.* 2007;56(2):295-303.
191. Bennett CN, Longo KA, Wright WS, et al. Regulation of osteoblastogenesis and bone mass by Wnt10b. *Proc Natl Acad Sci U S A.* 2005;102(9):3324-3329.
192. Gong Y, Slee RB, Fukai N, et al. LDL receptor-related protein 5 (LRP5) affects bone accrual and eye development. *Cell.* 2001;107(4):513-523.
193. Little RD, Carulli JP, Del Mastro RG, et al. A mutation in the LDL receptor-related protein 5 gene results in the autosomal dominant high-bone-mass trait. *Am J Hum Genet.* 2002;70(1):11-19.
194. Boyden LM, Mao J, Belsky J, et al. High bone density due to a mutation in LDL-receptor-related protein 5. *N Engl J Med.* 2002;346(20):1513-1521.
195. Van Wesenbeeck L, Cleiren E, Gram J, et al. Six novel missense mutations in the LDL receptor-related protein 5 (LRP5) gene in different conditions with an increased bone density. *Am J Hum Genet.* 2003;72(3):763-771.
196. Mani A, Radhakrishnan J, Wang H, et al. LRP6 mutation in a family with early coronary disease and metabolic risk factors. *Science.* 2007;315(5816):1278-1282.
197. Balemans W, Ebeling M, Patel N, et al. Increased bone density in sclerosteosis is due to the deficiency of a novel secreted protein (SOST). *Hum Mol Genet.* 2001;10(5):537-543.
198. Faqeih E, Shaheen R, Alkuraya FS. WNT1 mutation with recessive osteogenesis imperfecta and profound neurological phenotype. *J Med Genet.* 2013;50(7):491-492.
199. Zheng HF, Tobias JH, Duncan E, et al. WNT16 influences bone mineral density, cortical bone thickness, bone strength, and osteoporotic fracture risk. *PLoS Genet.* 2012;8(7):e1002745.
200. Maupin KA, Droscha CJ, Williams BO. A Comprehensive Overview of Skeletal Phenotypes Associated with Alterations in Wnt/beta-catenin Signaling in Humans and Mice. *Bone Res.* 2013;1(1):27-71.
201. Rivadeneira F, Styrkarsdottir U, Estrada K, et al. Twenty bone-mineral-density loci identified by large-scale meta-analysis of genome-wide association studies. *Nat Genet.* 2009;41(11):1199-1206.
202. Hsu YH, Zillikens MC, Wilson SG, et al. An integration of genome-wide association study and gene expression profiling to prioritize the discovery of novel susceptibility Loci for osteoporosis-related traits. *PLoS Genet.* 2010;6(6):e1000977.
203. Day TF, Guo X, Garrett-Beal L, Yang Y. Wnt/beta-catenin signaling in mesenchymal progenitors controls osteoblast and chondrocyte differentiation during vertebrate skeletogenesis. *Dev Cell.* 2005;8(5):739-750.

204. Chen J, Long F. β -catenin promotes bone formation and suppresses bone resorption in postnatal growing mice. *J Bone Miner Res.* 2013;28(5):1160-1169.
205. Rodda SJ, McMahon AP. Distinct roles for Hedgehog and canonical Wnt signaling in specification, differentiation and maintenance of osteoblast progenitors. *Development.* 2006;133(16):3231-3244.
206. Holmen SL, Zylstra CR, Mukherjee A, et al. Essential role of beta-catenin in postnatal bone acquisition. *J Biol Chem.* 2005;280(22):21162-21168.
207. Glass DA, 2nd, Bialek P, Ahn JD, et al. Canonical Wnt signaling in differentiated osteoblasts controls osteoclast differentiation. *Dev Cell.* 2005;8(5):751-764.
208. Bennett CN, Ouyang H, Ma YL, et al. Wnt10b increases postnatal bone formation by enhancing osteoblast differentiation. *J Bone Miner Res.* 2007;22(12):1924-1932.
209. Veverka V, Henry AJ, Slocombe PM, et al. Characterization of the structural features and interactions of sclerostin: molecular insight into a key regulator of Wnt-mediated bone formation. *J Biol Chem.* 2009;284(16):10890-10900.
210. Li X, Zhang Y, Kang H, et al. Sclerostin binds to LRP5/6 and antagonizes canonical Wnt signaling. *J Biol Chem.* 2005;280(20):19883-19887.
211. Semenov M, Tamai K, He X. SOST is a ligand for LRP5/LRP6 and a Wnt signaling inhibitor. *J Biol Chem.* 2005;280(29):26770-26775.
212. Amrein K, Amrein S, Drexler C, et al. Sclerostin and its association with physical activity, age, gender, body composition, and bone mineral content in healthy adults. *J Clin Endocrinol Metab.* 2012;97(1):148-154.
213. Daniele G, Winnier D, Mari A, et al. Sclerostin and Insulin Resistance in Prediabetes: Evidence of a Cross Talk Between Bone and Glucose Metabolism. *Diabetes Care.* 2015;38(8):1509-1517.
214. Kim SP, Frey JL, Li Z, et al. Sclerostin influences body composition by regulating catabolic and anabolic metabolism in adipocytes. *Proc Natl Acad Sci U S A.* 2017;114(52):E11238-E11247.
215. Christodoulides C, Scarda A, Granzotto M, et al. WNT10B mutations in human obesity. *Diabetologia.* 2006;49(4):678-684.
216. Kanazawa A, Tsukada S, Sekine A, et al. Association of the gene encoding wingless-type mammary tumor virus integration-site family member 5B (WNT5B) with type 2 diabetes. *Am J Hum Genet.* 2004;75(5):832-843.
217. Van Camp JK, Beckers S, Zegers D, Verrijken A, Van Gaal LF, Van Hul W. Common genetic variation in sFRP5 is associated with fat distribution in men. *Endocrine.* 2014;46(3):477-484.
218. Shungin D, Winkler TW, Croteau-Chonka DC, et al. New genetic loci link adipose and insulin biology to body fat distribution. *Nature.* 2015;518(7538):187-196.
219. Heid IM, Jackson AU, Randall JC, et al. Meta-analysis identifies 13 new loci associated with waist-hip ratio and reveals sexual dimorphism in the genetic basis of fat distribution. *Nat Genet.* 2010;42(11):949-960.
220. Hao HX, Xie Y, Zhang Y, et al. ZNRF3 promotes Wnt receptor turnover in an R-spondin-sensitive manner. *Nature.* 2012;485(7397):195-200.
221. Saarinen A, Saukkonen T, Kivela T, et al. Low density lipoprotein receptor-related protein 5 (LRP5) mutations and osteoporosis, impaired glucose

- metabolism and hypercholesterolaemia. *Clin Endocrinol (Oxf)*. 2010;72(4):481-488.
222. Singh R, Smith E, Fathzadeh M, et al. Rare nonconservative LRP6 mutations are associated with metabolic syndrome. *Hum Mutat*. 2013;34(9):1221-1225.
 223. Loh NY, Neville MJ, Marinou K, et al. LRP5 regulates human body fat distribution by modulating adipose progenitor biology in a dose- and depot-specific fashion. *Cell Metab*. 2015;21(2):262-273.
 224. Zou Y, Ning T, Shi J, et al. Association of a gain-of-function variant in LGR4 with central obesity. *Obesity (Silver Spring)*. 2017;25(1):252-260.
 225. Styrkarsdottir U, Thorleifsson G, Sulem P, et al. Nonsense mutation in the LGR4 gene is associated with several human diseases and other traits. *Nature*. 2013;497(7450):517-520.
 226. Grant SF, Thorleifsson G, Reynisdottir I, et al. Variant of transcription factor 7-like 2 (TCF7L2) gene confers risk of type 2 diabetes. *Nat Genet*. 2006;38(3):320-323.
 227. Lyssenko V, Lupi R, Marchetti P, et al. Mechanisms by which common variants in the TCF7L2 gene increase risk of type 2 diabetes. *J Clin Invest*. 2007;117(8):2155-2163.
 228. Jin T. Current Understanding on Role of the Wnt Signaling Pathway Effector TCF7L2 in Glucose Homeostasis. *Endocr Rev*. 2016;37(3):254-277.
 229. Chen M, Lu P, Ma Q, et al. CTNNB1/beta-catenin dysfunction contributes to adiposity by regulating the cross-talk of mature adipocytes and preadipocytes. *Sci Adv*. 2020;6(2):eaax9605.
 230. Mori H, Prestwich TC, Reid MA, et al. Secreted frizzled-related protein 5 suppresses adipocyte mitochondrial metabolism through WNT inhibition. *J Clin Invest*. 2012;122(7):2405-2416.
 231. Geoghegan G, Simcox J, Seldin MM, et al. Targeted deletion of Tcf7l2 in adipocytes promotes adipocyte hypertrophy and impaired glucose metabolism. *Mol Metab*. 2019;24:44-63.
 232. Savage DB. Mouse models of inherited lipodystrophy. *Dis Model Mech*. 2009;2(11-12):554-562.
 233. Rochford JJ. Mouse models of lipodystrophy and their significance in understanding fat regulation. *Curr Top Dev Biol*. 2014;109:53-96.
 234. Das S, Yu S, Sakamori R, Stypulkowski E, Gao N. Wntless in Wnt secretion: molecular, cellular and genetic aspects. *Front Biol (Beijing)*. 2012;7(6):587-593.
 235. Xu W, Kimelman D. Mechanistic insights from structural studies of beta-catenin and its binding partners. *J Cell Sci*. 2007;120(Pt 19):3337-3344.
 236. Palomer E, Buechler J, Salinas PC. Wnt Signaling Deregulation in the Aging and Alzheimer's Brain. *Front Cell Neurosci*. 2019;13:227.

CHAPTER II

Methodology for Dissection of Diverse Murine Adipose Depots

Adapted from:

Bagchi DP, MacDougald OA. Identification and Dissection of Diverse Mouse Adipose Depots. *J. Vis. Exp.* 2019 Jul 11; (149), e59499, doi:10.3791/59499. PMID: 31355801.

Bagchi DP, Forss I, Mandrup S, MacDougald OA. SnapShot: Niche Determines Adipocyte Character I. *Cell Metab.* 2018 Jan 9;27(1):264-264.e1. doi: 10.1016/j.cmet.2017.11.012. PMID: 29320707.

Bagchi DP, Forss I, Mandrup S, MacDougald OA. SnapShot: Niche Determines Adipocyte Character II. *Cell Metab.* 2018 Jan 9;27(1):266-266.e1. doi: 10.1016/j.cmet.2017.11.013. PMID: 29320708.

Abstract

Adipose tissues are complex organs with a wide array of functions, including storage and mobilization of energy in response to local and global needs, uncoupling of metabolism to generate heat, and secretion of adipokines to regulate whole-body homeostasis and immune responses. Emerging research is identifying important regional differences in the developmental, molecular, and functional profiles of adipocytes located in discrete depots throughout the body. Different properties of the depots are medically relevant since metabolic diseases often demonstrate depot-specific effects. This protocol will provide investigators with a detailed anatomic atlas and dissection guide for the reproducible and accurate identification and excision of diverse mouse adipose tissues. Standardized dissection of discrete adipose depots will allow detailed comparisons of their molecular and metabolic characteristics and contributions to local and systemic pathologic states under various nutritional and environmental conditions.

Introduction

Adipose tissues play critical roles in whole-body homeostasis, including storage and release of energy in response to local and global needs, thermoregulation, and secretion of adipokines to regulate energy balance, metabolism, and immune responses^{1,2}. Adipocytes are located throughout the body in discrete depots³⁻⁵, as well as singly and in small clusters associated with vascular and lymphatic structures, and in some cases serve specialized roles within their microenvironments^{6,7}. Although adipocytes throughout the body have overlapping molecular and metabolic characteristics, the degree to which these properties are realized may depend on the specific niches in which these cells reside.

Most adipocytes are distributed in subcutaneous and visceral white adipose tissues (WAT)^{8,9}. Subcutaneous adipocytes are contained within the anterior and posterior subcutaneous depots. The interscapular depot contains multilocular brown adipocytes, which are rich in mitochondria¹⁰. Brown and brown-like adipocytes express uncoupling protein 1 (UCP1), which when activated can uncouple mitochondrial respiration, leading to non-shivering thermogenesis¹¹. This increased mitochondrial respiration also promotes glucose and fatty acid uptake and oxidation in brown adipocytes^{12,13}. Some WAT depots are prone to browning; although the posterior subcutaneous depot appears to be continuous, centrally located inguinal adipocytes become brown-like more readily than those in adjacent depots. However, at very low environmental temperatures, even epididymal adipose tissue is recruited to form brown-like thermogenic adipocytes¹⁴.

The intra-abdominal depots, such as the mesenteric, perirenal, retroperitoneal, and gonadal fat pads, are contained within the peritoneal cavity. Relative to adipocytes in subcutaneous depots, intra-abdominal adipocytes are typically larger and secrete less leptin. In addition, expansion of the intra-abdominal depots is highly associated with development of systemic insulin resistance. With positive energy balance, subcutaneous adipose tissue expands by adipocyte hypertrophy and hyperplasia¹⁵. In contrast, intra-abdominal depots expand during obesity predominantly by adipocyte hypertrophy¹⁵, which is associated with metabolic dysfunction because larger adipocytes have increased lipolysis, attract inflammatory macrophages, and are insulin

resistant. Thus, the different characteristics of these depots are important for differential susceptibility to metabolic diseases^{2,7,9,16-18}.

Marrow adipose tissue accounts for ~10% of total fat mass in healthy humans, and in rodents can be classified as constitutive or regulated. Studies have demonstrated region-specific differences in marrow adipocyte properties, including development, regulation, gene expression, and lipid composition¹⁹. In addition to serving as a lipid reservoir, marrow adipose tissue is a disproportionate source of circulating adiponectin, and because of its enclosure within bone, is integral to our understanding of osteoblasts, osteoclasts, and hematopoietic cells^{20,21}.

In addition to the adipose depots discussed above, there are several other understudied depots that are likely to have important local roles yet to be discovered. These include intramuscular, periarticular, paracardial, epicardial, and retro-orbital adipocytes²²⁻²⁵. The popliteal depot provides lipids for expansion of lymphatic tissue following infection²⁶. The dermal depot has roles in thermal insulation, wound healing, and hair follicle growth, and serves as a barrier to infection²⁷⁻³⁰.

Although regional differences in adipocyte character and function are under intense study, the field is currently limited by the lack of a standardized protocol for the identification and dissection of diverse mouse depots. Previously published methods have typically described the isolation of one or two specific depots and lack the level of detail required for uniform excision^{31,32}. The protocol described herein provides a comprehensive guide for the specific anatomic locations and isolation steps of many different mouse adipose depots. Although WAT depots are the primary focus, the excision of interscapular BAT is also described in detail. Adipose tissues excised using this protocol can be used for a wide variety of experimental endpoints, including explant studies, histology, and gene expression analyses.

The goal of this protocol is to provide investigators with a detailed protocol to clearly and precisely identify and isolate both prominent and less-studied murine adipose depots (**Figure 2.1**). This resource will facilitate a more complete investigation of the developmental, molecular, and functional characteristics of adipocytes within diverse niches.

Protocol

All animal procedures are performed with the approval of the Institutional Animal Care and Use Committee (IACUC) of the University of Michigan.

Euthanization

1. Place the mouse in an isoflurane vaporizer chamber and adjust the isoflurane flow rate to 5% or greater. Continue isoflurane exposure until one minute after breathing stops. Then remove the mouse from the vaporizer chamber and confirm euthanasia using an approved secondary measure.
2. Place the euthanized mouse on the dissection pan. Sterilize the dorsal and ventral external surfaces of the mouse using 70% ethanol. Ensure that the external surface of the mouse is sufficiently wet to minimize contamination from fur during dissection.

Identification and isolation of major subcutaneous WAT depots (anterior subcutaneous, dorsolumbar, inguinal, gluteal) and interscapular BAT

Anterior subcutaneous WAT

This method isolates both anterior subcutaneous WAT and interscapular BAT. Anterior subcutaneous WAT is located between the scapulae, descending from the nape of the neck to the axillae of the mouse¹¹. This depot has alternatively been described as suprascapular¹⁰ or interscapular³³ WAT and lies directly on top of the interscapular BAT depot.

1. To isolate the anterior subcutaneous depot, lay the mouse on its stomach in a prone position. Secure the upper and lower limbs to the dissection pan with dissection pins.
2. Use forceps to lift the dorsal skin at the nape of the neck. Use iris scissors to make a small (1 mm) cut in the skin.
3. Insert one blade of the iris scissors into the initial cut and make a midline vertical incision (2–3 cm) through the skin, beginning at the nape of the neck and descending along the spine to mid-back.

4. Make two horizontal incisions (1 cm each) using the iris scissors, extending laterally from midline, at the top and bottom of the initial vertical incision.
5. Use forceps to carefully peel back the skin and expose the anterior subcutaneous depot.
6. Use iris scissors to remove the depot following the natural borders of the tissue.
7. Place the dissected depot on the dissection pan and carefully remove the contaminating BAT using iris scissors.

Classical BAT

Classical BAT is located beneath the anterior subcutaneous WAT depot.

1. To isolate BAT, use iris scissors to cut horizontally along the bottom edge of the anterior subcutaneous tissue, following the natural border of the depot.
2. Then, use iris scissors to make two vertical incisions along the lateral edges of the depot, following the natural borders of the tissue.
3. Use forceps to carefully flip the depot up and reveal the butterfly-shaped interscapular BAT embedded within the WAT. Carefully dissect the BAT out from the surrounding WAT.

Posterior subcutaneous WAT

1. Lay the mouse on its back in a supine position.
2. After securing the upper and lower limbs with dissection pins, use forceps to lift up the skin at the base of the sternum and make a small (1 mm) cut in the skin.
3. Insert one blade of the iris scissors into the initial cut and make a midline incision (4–5 cm) through the skin, beginning at the base of the sternum and descending to the base of the tail. Exercise caution when making this incision because the ventral skin is very thin and is closely associated with the underlying peritoneal cavity wall.
4. Make two horizontal incisions (1 cm each) using iris scissors, extending laterally from midline, at the top of the initial vertical incision.
5. Use forceps to carefully peel back the skin from the peritoneal cavity and the leg to find posterior subcutaneous WAT, which should remain associated with the skin.

Secure the outstretched skin with dissection pins to ease complete excision of the WAT.

Although posterior subcutaneous WAT appears to be continuous, it is actually comprised of three discrete depots: dorsolumbar, inguinal, and gluteal¹. The dorsolumbar depot extends from the lumbar spine to the base of the hindlimb. The triangular inguinal depot extends from the base of the hindlimb ventrally across the groin and contains a prominent lymph node. The gluteal depot extends inferiorly from the base of the groin and wraps around the leg to the base of the tail.

Identification and isolation of visceral WAT depots (gonadal, perirenal, retroperitoneal, omental, pericardial)

WAT depots, which are largely contained within the thoracic and peritoneal cavities, keep the mouse in a supine position. Secure the upper and lower limbs to the dissection pan with dissection pins.

1. Use forceps to lift up the thin peritoneal cavity wall at the base of the sternum and make a small cut (1 mm) using iris scissors.
2. Insert one blade of the iris scissors into the cut and make a descending vertical incision (4–5 cm) from the top of the peritoneal cavity (base of the sternum) to the rectum.
3. Make two horizontal incisions (1 cm each) with iris scissors, extending laterally from midline, at the top and bottom of the vertical incision.
4. Use forceps to peel back the peritoneum and expose the abdominal cavity contents. Pin the outstretched peritoneum to the dissection pan.

Gonadal WAT

Gonadal WAT surrounds the uterus and ovaries in females (ovarian or parametrial) and the epididymis and testes in males (epididymal). Ovarian WAT surrounds the ovaries, uterus, and bladder. In obese animals, gonadal and perirenal WAT can appear to be continuous – in this case, separate the depots at the uterine horn and ovaries.

Epididymal WAT is found bound to the epididymis, testes, and the prominent epididymal blood vessel.

1. Locate the gonads (testes or ovaries) and use forceps to lift up the associated gonadal WAT.
2. Use iris scissors to carefully excise the WAT from the gonads.

Perirenal WAT

Perirenal WAT surrounds the kidneys bilaterally. In obese animals, this depot can appear to extend inferiorly to the top of the uterine horn and ovaries. Although the perirenal WAT has traditionally been classified as a visceral depot³, several groups have identified it as a brown depot based on lineage tracing and radiolabeled glucose uptake studies^{10,33,34}. Histologically it is comprised of a mixture of white and brown adipocytes.

1. To excise the perirenal depot, locate the kidney and use forceps to lift it up and pull it midline to see a clear division between the perirenal and retroperitoneal depots.
2. Excise the WAT directly associated with the kidneys. Ensure that the adrenal glands, located above the kidneys, are removed from the WAT.

Retroperitoneal WAT

Retroperitoneal WAT is located in a paravertebral position, along the border between the posterior abdominal wall and the spinal cord.

1. To excise this depot, use forceps to lift the kidney up and towards midline to clearly see the border between the perirenal and retroperitoneal depots.
Note: In obese animals, identifying this border can be challenging.
2. Then, use iris scissors to carefully dissect the retroperitoneal WAT from the posterior peritoneal wall.

Omental WAT

Omental WAT is located along the greater curvature of the stomach. Although omental adipose is an important depot in humans, it is generally only readily visible in morbidly obese mice.

1. To identify visceral omental WAT, use forceps to lift the stomach up. Use iris scissors to remove the associated adipose tissue along the inferior border of the stomach. Do not confuse omental WAT with the pancreas.

Mesenteric WAT

Mesenteric WAT is a web-like structure surrounding and associated with the small and large intestines.

1. To excise this depot, remove the intestines from the rest of the digestive tract by cutting at the base of the stomach and the rectum. Use forceps to lift the intestines out of the visceral cavity and unravel them.
2. Use iris scissors to carefully dissect the mesenteric WAT away from the intestines, beginning at the duodenum and continuing to the end of the colon. Carefully remove lymph nodes that are closely associated with the mesenteric depot.

Pericardial WAT

Pericardial WAT is located outside the visceral pericardium and on the external surface of the parietal pericardium, often along the inferior aspect of the heart²⁴.

1. To gain access to the thoracic cavity, keep the mouse in a supine position. Secure the upper and lower limbs to the dissection pan with dissection pins.
2. Use forceps to lift the xyphoid process (cartilage at the base of the sternum) and make a small (1 mm) cut in the thoracic cavity wall.
3. Insert one blade of the iris scissors into the cut and make two horizontal incisions (1 cm each) extending laterally from the base of the sternum. This will expose the diaphragm and inferior border of the thoracic cavity.

4. Use dissecting scissors to make two ascending vertical incisions (3–4 cm) through the ribcage, extending superiorly from the lateral borders of the thoracic cavity to the clavicle.
5. Use forceps to lift up the ventral half of the ribcage. Use dissecting scissors to make a final cut (2 cm) along the inferior length of the clavicle to remove the ribcage and expose the thoracic cavity contents.
6. If present, carefully dissect the pericardial adipose from the outer surface of the pericardium.

Identification and isolation of other adipose depots

Epicardial WAT

Epicardial WAT is contained within the visceral pericardium and is directly associated with the surface of the myocardium.

1. If present, epicardial adipocytes can be observed histologically after isolation and fixation of the perfused heart in 10% neutral buffered formalin for 24 h.

Popliteal WAT

Popliteal WAT is located in the popliteal fossa in the posterior knee and contains a large lymph node. This depot is not typically visible in young animals.

1. To isolate popliteal WAT, use iris scissors to carefully remove the skin from the base of the hind limb to the foot.
2. Place the patella against the dissection pan and secure the outstretched leg with a pin in the foot. Ensure that the popliteal fossa at the back of the knee is facing upward.
3. Use iris scissors to make a cut at the inferior border of the medial and lateral heads of the gastrocnemius muscle. Use forceps to lift up the muscle and reveal the triangular popliteal depot.
4. Use iris scissors to excise the depot along the natural tissue borders.

Dermal WAT

Dermal WAT is a thin layer of adipocytes located between the reticular dermis and the panniculus carnosus muscle layer.

1. To identify dermal adipocytes by histological methods, place the mouse on its stomach in a prone position. After securing the upper and lower limbs with dissection pins, spray the external surface of the mouse with 70% ethanol to wet the skin.
2. Use a scalpel to remove the wetted fur from a square portion of skin on the back of the mouse.
3. Use iris scissors to carefully excise the shaved portion of skin, which will include the reticular dermis, dermal WAT, panniculus carnosus, and some subcutaneous WAT.
4. Use a scalpel to cut the excised skin into thin vertical strips.
5. Position the thin vertical strips with the sticky subcutaneous WAT layer facing down.
6. Starting at one end, roll the strip onto itself to form a spiral. The sticky subcutaneous WAT layer on the outside of the spiral will allow the roll to maintain its shape during fixation.
7. Place the spiral in a well of a 24-well plate containing 10% neutral buffered formalin for 24 h prior to histological processing³⁵.

Intermuscular WAT

Intermuscular WAT is broadly defined as adipocytes located beneath the deep fascia of muscles. This term includes adipocytes interspersed between muscle fibers of skeletal muscle, also known as intramuscular WAT, and adipocytes located within muscle bundles themselves. Wildtype mice generally do not have large numbers of intermuscular adipocytes. However, it is possible under certain conditions to identify intermuscular WAT by histological methods. Under some conditions, intermuscular adipocytes can also be found in smooth muscles, such as the diaphragm.

1. To isolate the tibialis anterior (TA) muscle, for example, place the mouse on its back in a supine position and secure the lower limbs to the dissection pan using dissection pins. Wet the skin with 70% ethanol to minimize contamination with fur.

2. Use iris scissors to carefully remove the skin from the leg and expose the quadriceps muscle group, located above the knee on the femur shaft, and the TA located below the knee on the ventral surface of the tibia.

Note: The TA is thick near the proximal end of the tibia and more tendinous near the distal end.

3. Use iris scissors to excise a piece of the muscle and fix in 10% neutral buffered formalin for 24 h prior to histological processing³⁵.

Intra-articular WAT depots

Intra-articular WAT depots are located within synovial joints.

1. To identify infrapatellar WAT, for example, by histological methods, harvest leg bones as detailed in the BMAT section.
2. After the removing the femur-tibial complex, use iris scissors and gauze pads to remove as much muscle and connective tissue as possible. Do not break the tibiofemoral joint.
3. Fix the femur-tibial complex in 10% neutral buffered formalin for 24 h prior to decalcification and histological processing (described below).

Bone marrow adipose tissues

Bone marrow adipose tissue (BMAT) is contained within bones, interspersed with hematopoietic cells. Anatomically, BMAT can be classified as constitutive (distal tibia and caudal vertebrae) or regulated (mid-to-proximal tibia, femur, and lumbar vertebrae)^{21,36}. Clean isolation of bone marrow adipocytes for RNA and protein analyses is challenging in mice. However, mouse bones can readily be harvested, fixed, decalcified and paraffin-embedded for histological analyses.

1. To harvest leg bones, for example, first remove the legs from the mouse. Use dissection scissors to cut the acetabulofemoral joint, keeping the femoral head intact.
2. Use iris scissors to carefully remove the skin from the leg, revealing the leg muscles.

3. Carefully dissect away the main muscles from the femur and tibia using iris scissors and gauze pads.
4. When the femur is exposed, follow the edge of the bone to the articulation of the pelvis and femur and carefully release the femoral head from the acetabulofemoral joint. Use gauze to clean any remaining tissue from the femur.
5. Follow the border of the tibia to the ankle joint. Carefully release the medial malleolus, located at the tip of the tibia, from the ankle joint.
6. Once the femur-tibial complex has been isolated, remove as much muscle and connective tissue as possible using iris scissors and/or gauze.
7. Separate the tibia from the femur by inserting one blade of the iris scissors into the tibiofemoral joint and gently cut through the medial and lateral collateral ligaments and the anterior and posterior cruciate ligaments. Do not remove the capsule of the knee joint to ensure that the tibia remains intact. Use gauze to clean any remaining tissue from the tibia.
8. Fix bones in 10% neutral buffered formalin for 24 h at room temperature and then wash and store according to future needs.
 1. To analyze bone parameters using microcomputed tomography (μ CT), store bones in Sorensen's phosphate buffer, pH 7.4¹⁹.
 2. For BMAT quantification and histological analyses, decalcify bones in 14% EDTA, pH 7.4, for 10-14 days.
 3. Following decalcification, use osmium tetroxide staining and μ CT analysis to quantify BMAT³⁷. Otherwise, process and paraffin-embed bones for histology¹⁹.

Discussion

As the importance of the diverse molecular and functional characteristics of discrete adipocyte clusters is increasingly recognized, it is crucial that investigators within the field uniformly identify and excise adipose depots for further analyses. To date, few protocols exist for standardized localization and isolation of the wide range of mouse adipose depots. Previously published methods are focused primarily on one or two depots and lack the details necessary for uniform identification and excision by different investigators^{31,32}. This protocol is a novel and important contribution to the field of adipose biology since it provides an in-depth guide to the anatomic location and precise dissection of commonly studied and lesser-known depots throughout the mouse. Gross anatomical location (**Figure 2.2**) and histological analyses (**Figure 2.3**) are provided to demonstrate the diversity of adipocyte niches.

Successful isolation of discrete adipose depots using this protocol is dependent on several critical steps. Maintenance of a clean dissection environment is crucial; 70% ethanol can be used as necessary to remove contaminating hairs or blood from the dissection tray and tools. When isolating posterior subcutaneous WAT, it is imperative that the initial incision in the skin does not penetrate the closely associated peritoneal cavity so that the two layers can be efficiently separated to expose the WAT. Similarly, when cutting through the peritoneal wall to expose the abdominal cavity contents, incisions must not perforate the underlying intestines to prevent contamination with digestive elements. Interscapular BAT must be carefully excised from the surrounding tissue to prevent WAT contamination, which will skew future analyses. Consistent identification of the posterior subcutaneous dorsolumbar, inguinal, and gluteal depots depends on the utilization of precise anatomic landmarks described in the protocol. The distinction between these depots is particularly important; although the depots can appear to be continuous, centrally located inguinal adipocytes acquire brown-like characteristics more readily than their surrounding counterparts.

The adipose tissues isolated using this protocol can be analyzed using a variety of techniques. In addition to histological evaluation (i.e. immunohistochemistry, H&E staining), adipose tissues can be used for a wide array of molecular analyses, from regulation of transcription through to posttranslational protein modifications. Adipocytes

and stromal vascular cells within individual depots can be isolated by collagenase digestion and differential centrifugation. These fractions can then be used for molecular, metabolic, and cell culture studies. Depot explants can also be used for *ex vivo* metabolic and enzymatic assays.

Several challenges and limitations arise during the isolation and excision of mouse adipose tissues. First, some depots that are physiologically important in humans are not commonly present in lean, adult mice. For example, omental WAT, which is the major visceral depot in humans, can only be seen in genetically- or diet-induced obese mice. The expansion of some depots can, however, be induced by nutritional challenges or drug treatments. For example, high fat diet (HFD) feeding can cause the expansion of omental and pericardial WAT. Intermuscular WAT can be induced by skeletal muscle injury^{38,39} or HFD⁴⁰. Regulated BMAT also expands in response to various challenges, including HFD, calorie restriction and thiazolidinedione treatment^{36,41}.

Second, due to the small size of mice, obtaining enough sample for molecular or metabolic analyses can be difficult. For example, isolation of enough pure bone marrow adipocytes for subsequent analyses is challenging, even after pooling bones from multiple mice. Third, accurately defining borders of certain depots can be difficult. For example, posterior subcutaneous WAT appears to be one continuous depot but is actually comprised of discrete dorsolumbar, inguinal, and gluteal depots. Additionally, the perirenal can appear to be fused to both the gonadal and retroperitoneal depots in very obese animals. The lack of distinct borders between adjacent depots can make clean isolation of these tissues challenging. However, this dissection protocol provides investigators with a detailed atlas and step-by-step guidance for accurate and reproducible dissection of a wide range of mouse adipose depots.

Field-wide standardization of the identification and isolation of discrete mouse adipose depots described above will undoubtedly help further elucidate differences in the development, gene expression, and local and systemic functions of previously under-studied adipocyte niches.

Figure 2.1

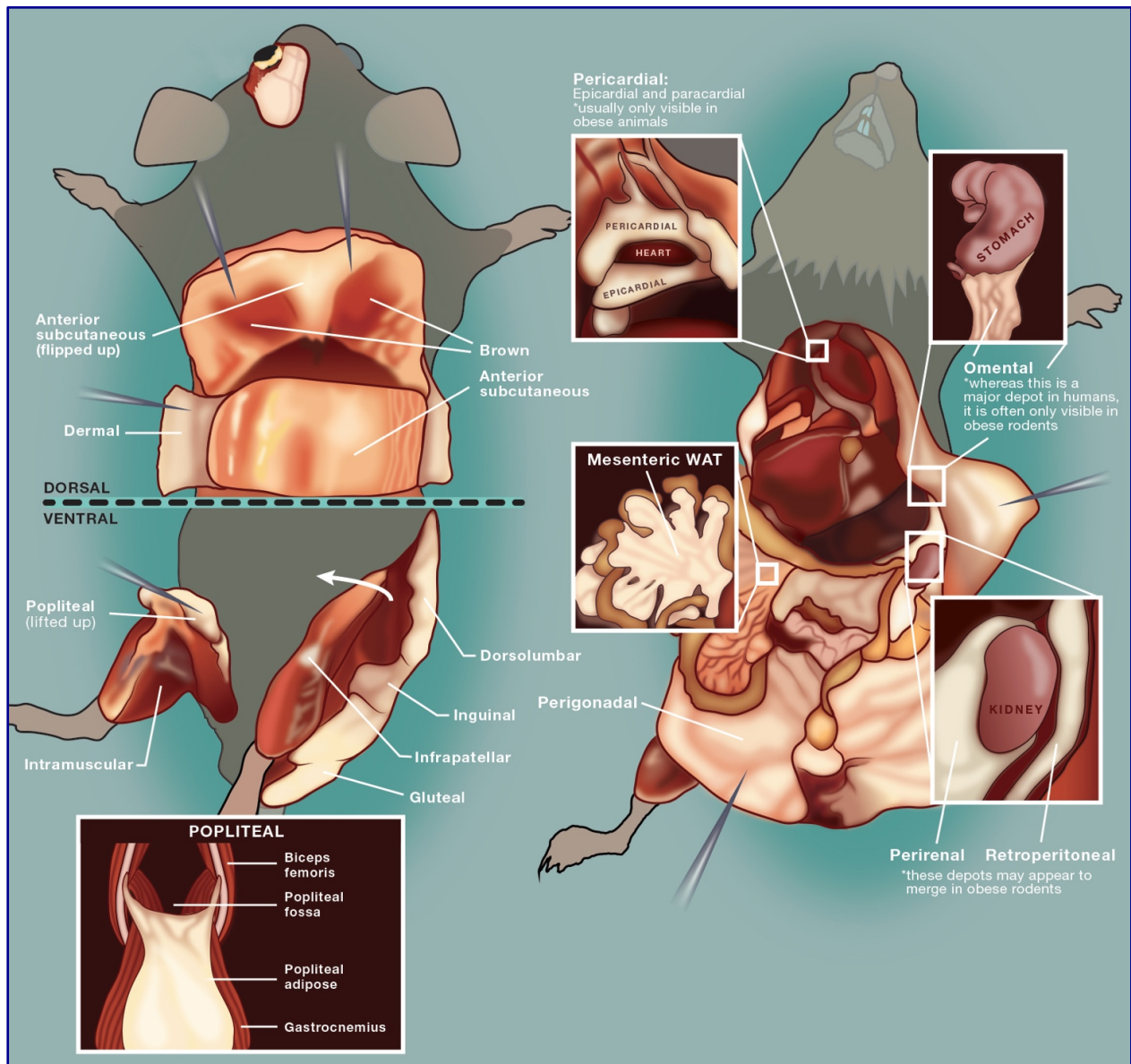


Figure 2.1. Schematic depiction of dissected mouse adipose depots. Adipocytes are located throughout the body in discrete depots, as well as singly and in small clusters associated with vascular and lymphatic structures. Although adipocytes throughout the body have overlapping molecular and metabolic characteristics, the degree to which these properties are realized will undoubtedly depend on the specific niches in which these cells reside.

Figure 2.2

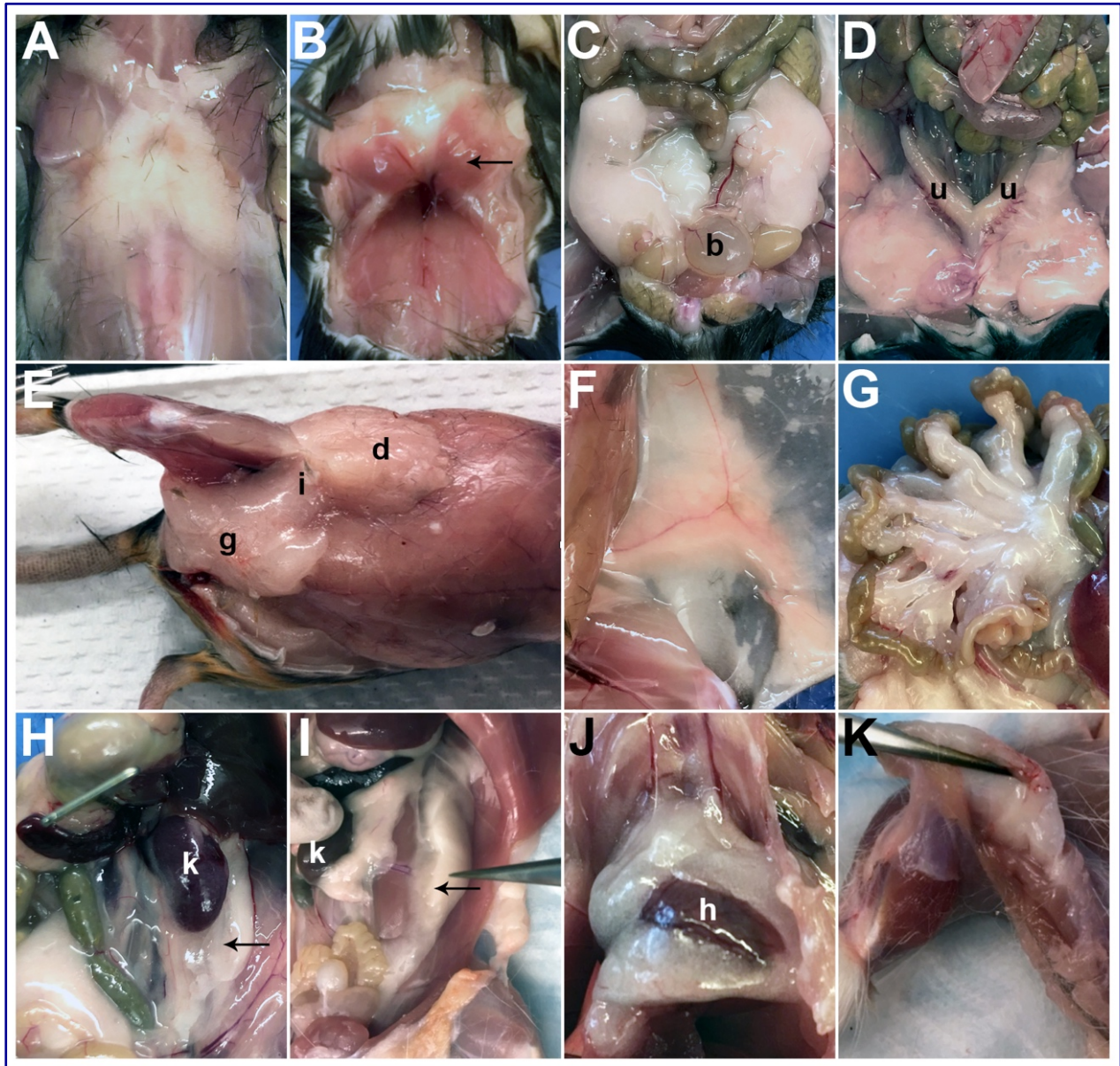


Figure 2.2. Gross anatomical locations of mouse adipose depots. Gross anatomy of (A) anterior subcutaneous; (B) brown; (C) epididymal (b, bladder); (D) ovarian (u, uterine horns); (E) posterior subcutaneous (dorsolumbar (d), inguinal (i), gluteal (g)); (F) inguinal; (G) mesenteric; (H) perirenal (k, kidney); (I) retroperitoneal (k, kidney); (J) pericardial (h, heart); and (K) popliteal adipose depots in C57BL/6J adult mice. Arrows point to specific depots if multiple depots are depicted. Relevant organs are designated by appropriate letters.

Figure 2.3

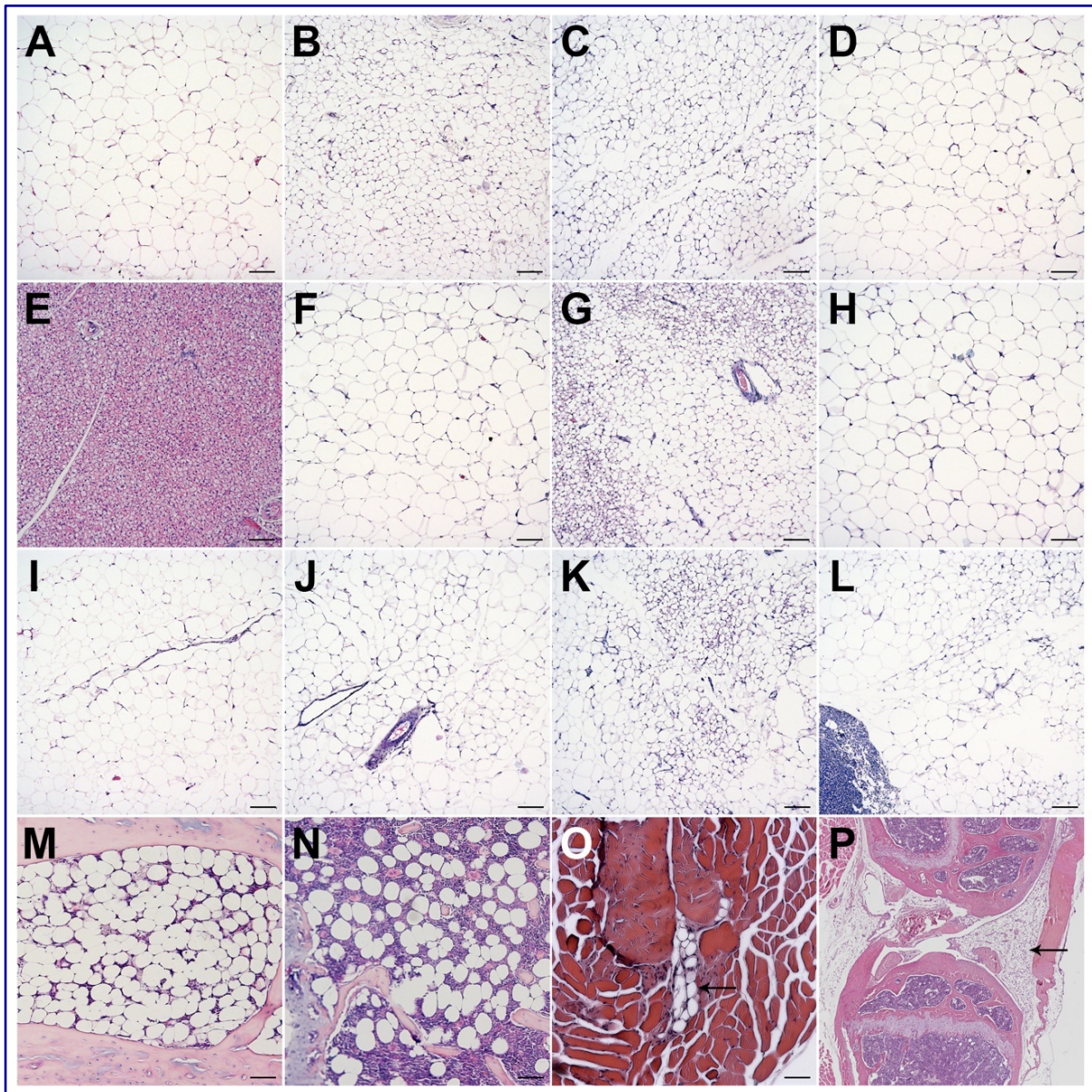


Figure 2.3. Histological evaluation of discrete mouse adipose depots. Histology of (A) anterior subcutaneous; (B) dorsolumbar; (C) inguinal; (D) gluteal; (E) brown; (F) gonadal; (G) perirenal; (H) retroperitoneal; (I) omental; (J) mesenteric; (K) pericardial; (L) popliteal; (M) constitutive and (N) regulated bone marrow adipose; (O) intermuscular; and (P) infrapatellar depots in C57BL/6J adult mice. Tissues were isolated according to the presented protocol, fixed overnight in 10% neutral buffered formalin, processed, and embedded in paraffin. 5 μ m sections were stained with H&E. Most images were taken at 100x magnification; scale bar = 100 μ m.

References

1. Cinti S. The adipose organ at a glance. *Dis Model Mech.* 2012;5(5):588-594.
2. Rosen ED, Spiegelman BM. What we talk about when we talk about fat. *Cell.* 2014;156(1-2):20-44.
3. Cinti S. The adipose organ. *Prostaglandins Leukot Essent Fatty Acids.* 2005;73(1):9-15.
4. Bagchi DP, Forss I, Mandrup S, MacDougald OA. SnapShot: Niche Determines Adipocyte Character I. *Cell Metab.* 2018;27(1):264-264 e261.
5. Bagchi DP, Forss I, Mandrup S, MacDougald OA. SnapShot: Niche Determines Adipocyte Character II. *Cell Metab.* 2018;27(1):266-266 e261.
6. Sanchez-Gurmaches J, Guertin DA. Adipocyte lineages: tracing back the origins of fat. *Biochim Biophys Acta.* 2014;1842(3):340-351.
7. Tchkonja T, Thomou T, Zhu Y, et al. Mechanisms and metabolic implications of regional differences among fat depots. *Cell Metab.* 2013;17(5):644-656.
8. Kahn CR, Wang G, Lee KY. Altered adipose tissue and adipocyte function in the pathogenesis of metabolic syndrome. *J Clin Invest.* 2019;129(10):3990-4000.
9. Lee MJ, Wu Y, Fried SK. Adipose tissue heterogeneity: implication of depot differences in adipose tissue for obesity complications. *Mol Aspects Med.* 2013;34(1):1-11.
10. Zhang F, Hao G, Shao M, et al. An Adipose Tissue Atlas: An Image-Guided Identification of Human-like BAT and Beige Depots in Rodents. *Cell Metab.* 2018;27(1):252-262 e253.
11. Frontini A, Cinti S. Distribution and development of brown adipocytes in the murine and human adipose organ. *Cell Metab.* 2010;11(4):253-256.
12. Kajimura S, Spiegelman BM, Seale P. Brown and Beige Fat: Physiological Roles beyond Heat Generation. *Cell Metab.* 2015;22(4):546-559.
13. Cannon B, Nedergaard J. Brown adipose tissue: function and physiological significance. *Physiol Rev.* 2004;84(1):277-359.
14. Yang X, Sui W, Zhang M, et al. Switching harmful visceral fat to beneficial energy combustion improves metabolic dysfunctions. *JCI Insight.* 2017;2(4):e89044.
15. Jeffery E, Wing A, Holtrup B, et al. The Adipose Tissue Microenvironment Regulates Depot-Specific Adipogenesis in Obesity. *Cell Metab.* 2016;24(1):142-150.
16. Gesta S, Tseng YH, Kahn CR. Developmental origin of fat: tracking obesity to its source. *Cell.* 2007;131(2):242-256.
17. Despres JP, Lemieux I. Abdominal obesity and metabolic syndrome. *Nature.* 2006;444(7121):881-887.
18. Kissebah AH, Krakower GR. Regional adiposity and morbidity. *Physiol Rev.* 1994;74(4):761-811.
19. Scheller EL, Doucette CR, Learman BS, et al. Region-specific variation in the properties of skeletal adipocytes reveals regulated and constitutive marrow adipose tissues. *Nat Commun.* 2015;6:7808.
20. Cawthorn WP, Scheller EL, Learman BS, et al. Bone marrow adipose tissue is an endocrine organ that contributes to increased circulating adiponectin during caloric restriction. *Cell Metab.* 2014;20(2):368-375.

21. Li Z, Hardij J, Bagchi DP, Scheller EL, MacDougald OA. Development, regulation, metabolism and function of bone marrow adipose tissues. *Bone*. 2018;110:134-140.
22. Addison O, Marcus RL, Lastayo PC, Ryan AS. Intermuscular fat: a review of the consequences and causes. *Int J Endocrinol*. 2014;2014:309570.
23. Cherian S, Lopaschuk GD, Carvalho E. Cellular cross-talk between epicardial adipose tissue and myocardium in relation to the pathogenesis of cardiovascular disease. *Am J Physiol Endocrinol Metab*. 2012;303(8):E937-949.
24. Iacobellis G. Local and systemic effects of the multifaceted epicardial adipose tissue depot. *Nat Rev Endocrinol*. 2015;11(6):363-371.
25. Kloppenburg Al-FM. An emerging player in knee osteoarthritis: the infrapatellar fat pad. *Arthritis Research & Therapy*. 2013;15(225):1-9.
26. Pond CM. Adipose tissue and the immune system. *Prostaglandins Leukot Essent Fatty Acids*. 2005;73(1):17-30.
27. Alexander CM, Kasza I, Yen CL, et al. Dermal white adipose tissue: a new component of the thermogenic response. *J Lipid Res*. 2015;56(11):2061-2069.
28. Kasza I, Suh Y, Wollny D, et al. Syndecan-1 is required to maintain intradermal fat and prevent cold stress. *PLoS Genet*. 2014;10(8):e1004514.
29. Kruglikov IL, Scherer PE. Dermal Adipocytes: From Irrelevance to Metabolic Targets? *Trends Endocrinol Metab*. 2016;27(1):1-10.
30. Festa E, Fretz J, Berry R, et al. Adipocyte lineage cells contribute to the skin stem cell niche to drive hair cycling. *Cell*. 2011;146(5):761-771.
31. Mann A, Thompson A, Robbins N, Blomkalns AL. Localization, Identification, and Excision of Murine Adipose Depots. *Journal of Visualized Experiments*. 2014(94).
32. Casteilla LP, L; Cousin, B; Calise, D. Choosing an adipose tissue depot for sampling: factors in selection and depot specificity. *Methods in Molecular Biology*.155:1-22.
33. de Jong JM, Larsson O, Cannon B, Nedergaard J. A stringent validation of mouse adipose tissue identity markers. *Am J Physiol Endocrinol Metab*. 2015;308(12):E1085-1105.
34. Sanchez-Gurmaches J, Guertin DA. Adipocytes arise from multiple lineages that are heterogeneously and dynamically distributed. *Nat Commun*. 2014;5:4099.
35. Parlee SD, Lentz SI, Mori H, MacDougald OA. Quantifying size and number of adipocytes in adipose tissue. *Methods Enzymol*. 2014;537:93-122.
36. Scheller EL, Cawthorn WP, Burr AA, Horowitz MC, MacDougald OA. Marrow Adipose Tissue: Trimming the Fat. *Trends Endocrinol Metab*. 2016;27(6):392-403.
37. Scheller EL, Troiano N, Vanhoutan JN, et al. Use of osmium tetroxide staining with microcomputerized tomography to visualize and quantify bone marrow adipose tissue in vivo. *Methods Enzymol*. 2014;537:123-139.
38. Lukjanenko L, Brachat S, Pierrel E, Lach-Trifilieff E, Feige JN. Genomic profiling reveals that transient adipogenic activation is a hallmark of mouse models of skeletal muscle regeneration. *PLoS One*. 2013;8(8):e71084.
39. Pagano AF, Demangel R, Briocche T, et al. Muscle Regeneration with Intermuscular Adipose Tissue (IMAT) Accumulation Is Modulated by Mechanical Constraints. *PLoS One*. 2015;10(12):e0144230.

40. Khan IM, Perrard XY, Brunner G, et al. Intermuscular and perimuscular fat expansion in obesity correlates with skeletal muscle T cell and macrophage infiltration and insulin resistance. *Int J Obes (Lond)*. 2015;39(11):1607-1618.
41. Sulston RJ, Learman BS, Zhang B, et al. Increased Circulating Adiponectin in Response to Thiazolidinediones: Investigating the Role of Bone Marrow Adipose Tissue. *Front Endocrinol (Lausanne)*. 2016;7:128.

CHAPTER III

Wntless Regulates Lipogenic Gene Expression in Adipocytes and Protects Against Diet-Induced Metabolic Dysfunction

Adapted from:

Bagchi DP, Li Z, Corsa CA, Hardij J, Mori H, Learman BS, Lewis KT, Schill RL, Romanelli SM, MacDougald OA. Wntless regulates lipogenic gene expression in adipocytes and protects against diet-induced metabolic dysfunction. *Mol Metab.* 2020 Apr 20; doi: 10.1016/j.molmet.2020.100992. PMID: 32325263.

Abstract

Objective: Obesity is a key risk factor for many secondary chronic illnesses, including type 2 diabetes and cardiovascular disease. Canonical Wnt/ β -catenin signaling is well-established as an important endogenous inhibitor of adipogenesis. This pathway is operative in mature adipocytes; however, its roles in this context remain unclear due to complexities of Wnt signaling and differences in experimental models. Herein, we use novel cultured cell and mouse models to investigate functional roles of Wnts secreted from adipocytes. *Methods:* We generated adipocyte-specific Wntless (*Wls*) knockout mice and cultured cell models to investigate molecular and metabolic consequences of disrupting Wnt secretion from mature adipocytes. To characterize *Wls*-deficient cultured adipocytes, we evaluated expression of Wnt target and lipogenic genes, and downstream functional effects on carbohydrate and lipid metabolism. In addition, we investigated the impact of adipocyte-specific *Wls* deletion on adipose tissues and global glucose metabolism in mice fed normal chow or high fat diets. *Results:* We report that many aspects of the Wnt signaling apparatus are expressed and operative in mature adipocytes, including the Wnt chaperone Wntless. Deletion of Wntless in cultured adipocytes results in inhibition of *de novo* lipogenesis and lipid monounsaturations, likely through repression of *Srebf1* (SREBP1c) and *Mlxipl* (ChREBP), and impaired cleavage

of immature SREBP1c into its active form. Adipocyte-specific *Wls* knockout mice (*Wls*^{-/-}) have lipogenic gene expression in adipose tissues and isolated adipocytes similar to that of controls when fed a normal chow diet. However, closer investigation reveals that a subset of Wnts and downstream signaling targets are up-regulated within stromal-vascular cells of *Wls*^{-/-} mice, suggesting that adipose tissues defend loss of Wnt secretion from adipocytes. Interestingly, this compensation is lost with long-term high fat diet challenge. Thus, after six months of high fat diet, *Wls*^{-/-} mice are characterized by decreased adipocyte lipogenic gene expression, reduced visceral adiposity, and improved glucose homeostasis. *Conclusion:* Taken together, these studies demonstrate that adipocyte-derived Wnts regulate *de novo* lipogenesis and lipid desaturation, and coordinate expression of lipogenic genes in adipose tissues. In addition, we report that Wnt signaling within adipose tissues is defended, such that a loss of Wnt secretion from adipocytes is sensed and compensated for by neighboring stromal-vascular cells. With chronic overnutrition, this compensatory mechanism is lost, revealing that *Wls*^{-/-} mice are resistant to diet-induced obesity, adipocyte hypertrophy, and metabolic dysfunction.

Introduction

Wnts are members of an evolutionarily conserved family of secreted glycoproteins with well-established roles in cell proliferation and differentiation during tissue development^{1,2}. When canonical Wnts bind to their membrane-spanning frizzled (Fzd) receptors and low-density lipoprotein receptor-related protein (LRP) co-receptors, they trigger an intracellular signaling cascade that stabilizes free cytosolic β -catenin, which then translocates to the nucleus and coactivates DNA-binding T-cell factor/lymphoid enhancer-binding factor (TCF/LEF) proteins to mediate downstream gene transcription¹⁻³. The endogenous Wnt pathway is a critical regulator of mesenchymal cell fate where it inhibits adipogenesis and promotes osteogenesis⁴⁻¹⁸.

Genetic studies in humans have also identified associations between Wnt pathway members and body fat distribution, obesity and metabolic function. For example, genome-wide association studies across diverse human populations have found strong correlations between polymorphisms in the canonical Wnt transcriptional effector *TCF7L2* and susceptibility to type 2 diabetes¹⁹⁻²¹; indeed, *TCF7L2* is one of the strongest risk loci for development of type 2 diabetes. In addition, loss-of-function mutations in Wnt co-receptors *LRP5* and *LRP6* are associated with impaired glucose tolerance, osteoporosis, and cardiovascular disease^{22,23}, whereas gain-of-function *LRP5* mutations are associated with increased adiposity and altered fat distribution²⁴. Common variants in Wnt signaling inhibitor *ZNRF3* and Wnt signaling activator *RSPO3* are associated with increased waist-to-hip ratio²⁵⁻²⁷. Further, gain-of-function mutations in *LGR4*, a protein that stabilizes Wnt receptors, are correlated with increased visceral adiposity²⁸. Polymorphisms in the *SFRP5* locus have been associated with decreased adiposity in men²⁹, whereas missense variants in *WNT10B* and certain *WNT5B* single nucleotide polymorphisms are correlated with higher risk of obesity and type 2 diabetes, respectively^{30,31}. Finally, variants in *CTNNB1* (β -catenin) have been associated with increased body mass index and risk of obesity³². Taken together, these studies provide strong genetic evidence for the influence of Wnt/ β -catenin signaling on white adipose tissue (WAT) function, body composition, and metabolic health.

Although recent studies have demonstrated that Wnt signaling is active in mature adipocytes, its functional roles in this context remain unclear due to complexity of the

Wnt pathway, and differences in experimental models, approaches, and results^{13,14,32-34}. For example, stabilization of Wnt signaling through global deletion of secreted frizzled-related protein 5 (SFRP5) - an adipocyte protein highly induced by obesity that binds to and sequesters Wnts - causes resistance to diet-induced obesity in mice³³. Whereas total adipocyte numbers are unaffected, adipocytes in *Sfrp5* mutant mice have increased mitochondrial number and are smaller in size compared to control mice, resulting in reduced WAT and improved glucose tolerance. Adipocyte-specific deletion of β -catenin has also been reported to cause decreased subcutaneous WAT mass and improved glycemic control in diet-induced obese mice³². In contrast, adipocyte-specific deletion of the transcription factor *Tcf7l2* leads to adipocyte hypertrophy and impaired glucose homeostasis with diet-induced obesity³⁴. These reports provide the first evidence that canonical Wnt signaling regulates ability of existing adipocytes to accommodate excess energy. Additional studies targeting the Wnt pathway in adipocytes are required to further understand how various components of this pathway differentially contribute to adipocyte metabolism.

Although it is clear that Wnt signaling is important within adipose tissues, one significant gap in our knowledge is the cellular source of physiologically relevant Wnts. To address this shortfall, we have targeted Wntless (*Wls*), an evolutionarily conserved chaperone protein required for transport of Wnts from the endoplasmic reticulum (ER) and Golgi apparatus to the cell membrane for secretion^{35,36}. Wnt proteins are modified with palmitoleic acid (C16:1) at conserved serine residues, and the lipocalin-like structure of Wntless may facilitate binding to these hydrophobic modifications³⁷⁻⁴¹. In fact, palmitoleoylation at Ser209 of Wnt3a, which is required for Wnt activity, is required for its physical binding to Wntless and subsequent release from the ER^{37,42,43}. Deletion of Wntless in vertebrate and invertebrate animal models results in phenotypes consistent with loss of Wnt function, suggesting that Wntless regulates signaling at the level of Wnt transport and secretion in signal-producing cells^{36,44-50}.

Here, we report that Wntless is expressed in mature adipocytes and that adipocyte-specific *Wls* deletion (hereby designated as *Wls*^{-/-}) leads to reduced *de novo* lipogenesis (DNL) and lipid monounsaturations. Further, inhibition of a network of lipogenic genes is correlated with repression of *Srebf1* and *Mlxipl*, which encode

SREBP1c and ChREBP, known transcriptional regulators of this gene set⁵¹⁻⁵³. Of particular interest, in mice fed a normal chow diet (NCD), loss of adipocyte-specific Wnt secretion is defended by increased expression of Wnts in surrounding stromal-vascular cells (SVC); however, this compensation is lost in mice fed a high fat diet (HFD). Thus, *Wnt1*^{-/-} mice challenged with long-term HFD demonstrate decreased adipocyte lipogenic gene expression, reduced size of epididymal adipocytes and WAT, and resistance to HFD-induced metabolic dysfunction. Studies from the cancer field have firmly established that inhibition of stearoyl CoA desaturase 1 (SCD1), which catalyzes the synthesis of palmitoleic acid, results in suppression of Wnt/ β -catenin signaling^{41,54-61}. Our studies reveal a reciprocal relationship in which Wnts are required for expression of lipogenic genes and DNL, including expression of SCD1 and formation of palmitoleic acid. Thus, these results highlight the novel and important roles of adipocyte-derived Wnts in critical mature adipocyte functions, including accumulation of lipid in WAT with HFD.

Results

Wntless is expressed in mature adipocytes and is up-regulated by diet-induced obesity.

Canonical Wnt signaling has previously been well-established as a significant endogenous regulator of adipogenesis⁴. Although recent studies have provided compelling evidence that this pathway also plays a role in the metabolism of adipocytes³²⁻³⁴, particularly under obesogenic conditions, the contribution of adipocyte-derived Wnt proteins has not been directly studied in this context. To this end, we first evaluated whether Wntless, the chaperone protein required for secretion of Wnts, is expressed and regulated in cultured adipocytes and WAT. In cultured MSCs derived from wildtype C57BL/6J mice, expression of *Wls* mRNA and protein was high in precursors, transiently repressed during differentiation, and elevated again in mature adipocytes (**Figure 3.1 A-B**). As expected, mRNA and protein expression of the adipocyte marker *Adipoq* (Adiponectin) increased during adipogenesis, whereas expression of the preadipocyte marker *Dlk1* (Pref1) decreased (**Figure 3.1 A-B**).

In addition to adipocytes, WAT contain myriad cell types, including preadipocytes, stromal cells, endothelial cells, and immune cells. These cells comprise the SVF of WAT and many have been shown to have active Wnt signaling in other contexts^{5,6,62-64}. We measured *Wls* mRNA in fractionated eWAT and iWAT of C57BL/6J mice and found that it is expressed at higher levels in isolated adipocytes than in the SVF (**Figure 3.1 C**). We then performed immunoblot analyses on various mouse tissues and observed that Wntless is highly expressed in diverse adipose depots (**Figure 3.1 D**), with relatively low abundance in lung and pancreas. Once we established that *Wls* is expressed in mouse adipose tissues, we explored whether its expression in WAT is regulated by nutritional or environmental challenges. We found that *Wls* gene expression in eWAT and iWAT is up-regulated by diet-induced obesity (**Figure 3.1 E**); notably, this increase in *Wls* expression occurs specifically in the adipocyte fraction and not in the SVF of eWAT and iWAT (**Supplemental Figure 3.1 A**). Further, *Wls* is specifically regulated by HFD feeding as its expression is not altered by acute fasting, fasting/refeeding, calorie restriction or acute cold exposure (**Supplemental Figure 3.1**

B). Wntless protein expression is also up-regulated by diet-induced obesity in eWAT and iWAT (**Figure 3.1 F**). We also queried the publicly available GTEx dataset to determine the distribution of *Wls* gene expression across male and female human tissues and found that *Wls* is expressed at higher levels in WAT depots when compared to liver or skeletal muscle (**Supplemental Figure 3.1 C**). These data suggest that Wntless, which is expressed in adipocytes and induced by obesity, likely plays a metabolic role in these cells, particularly under obesogenic conditions.

Wnt/ β -catenin signaling is operative in cultured adipocytes.

Although previous studies have characterized in detail the mechanisms by which Wnt signaling represses adipogenesis of mesenchymal precursors and promotes alternative cell fates^{4,5,15,17,18}, the expression pattern and roles of Wnt-related proteins in mature adipocytes is less clear. RNA-seq analyses of cultured MSCs and differentiated adipocytes reveals that many Wnts are induced during adipogenesis, including *Wnt2b*, *Wnt4*, *Wnt5b*, *Wnt8b*, *Wnt9a*, and *Wnt9b* (**Figure 3.1 G**). We also observed induction of *Fzd4* and *Fzd9* receptors and constitutive expression of other pathway members, such as *Ctnnb1* (β -catenin), *Lrp5*, *Lrp6*, *Sfrp1*, *Dvl1*, *Dvl2*, *Dvl3*, *Wnt16*, *Wnt2*, and *Wnt7b* (**Supplemental Figure 3.1 D**). Consistent with all major components of the signaling pathway being either induced or expressed constitutively, a number of downstream Wnt targets were elevated in mature adipocytes, including *Wisp1*, *Wisp2*, *Axin2*, *Tcf7l2* and *Tcf7l1*, amongst others. Further, treatment of mature adipocytes with recombinant Wnt3a regulates many Wnt pathway genes involved in negative feedback, as well as many adipocyte genes (**Figure 3.1 H**; data not shown). Taken together, these data indicate that the canonical Wnt signaling apparatus is operative in mature adipocytes.

Wntless deletion in cultured adipocytes inhibits DNL and lipid monounsaturations.

To study the molecular functions of Wntless in adipocytes, we isolated and cultured MSCs from *Wls*^{fl/fl} mice. This model allowed us to perform metabolic and mechanistic studies in cells derived directly from our mouse model. *Wls*^{fl/fl} MSCs were differentiated into adipocytes using a standard adipogenic cocktail. At day four of differentiation, adipocytes were infected in serum-free medium with adenoviral GFP as a control or

adenoviral Cre recombinase to induce *Wls* gene deletion. Adipocytes were allowed to recover following infection and were analyzed at day 12 to 14 of differentiation (**Figure 3.2 A**). Recombination of the floxed allele was confirmed by a 3-primer PCR system (**Figure 3.2 B**). Both qPCR and immunoblot analyses of Cre-infected adipocytes showed efficient deletion of *Wls* at the mRNA (**Figure 3.2 C**) and protein (**Figure 3.2 D**) levels. Deletion of *Wntless* does not affect differentiation and lipid accumulation, as assessed by adiponectin protein expression (**Figure 3.2 D**), phase-contrast microscopy, Oil Red-O staining (**Figure 3.2 E**), and measurement of TAG (**Figure 3.2 F**). To investigate whether Wnt signaling is altered by *Wls* deletion, we measured expression of known targets and found that Wnt-induced genes, including *Axin2*, *Tcf7l2*, *Cmyc*, and *Ppard* are down-regulated, whereas Wnt-suppressed gene *Id2* is up-regulated in *Wls*^{-/-} adipocytes (**Figure 3.2 G**). The downregulation of Wnt target genes in *Wls*^{-/-} adipocytes is relatively mild, suggesting that other pathways contribute to basal expression of these genes.

Of note, *Ctnnb1* mRNA is not altered, which is consistent with its primary regulation through protein turnover^{6,65}. Free cytosolic β -catenin, which is not bound to E-cadherins and comprises a very small and highly regulated proportion of total cellular β -catenin in preadipocytes, is the pool that mediates Wnt signaling^{5,6,66,67}. Thus, we measured free cytosolic β -catenin as a surrogate for Wnt signaling downstream of adipocyte-derived Wnts. Compared to *Wls*^{fl/fl} cells, we found that free cytosolic β -catenin is significantly lower (~33%) in *Wls*^{-/-} MSCs at baseline (**Figure 3.2 H**; quantified in **Supplemental Figure 3.2 A**). Interestingly, free cytosolic β -catenin also appears to be lower in *Wls*^{-/-} MSCs upon stimulation with Wnt3a, which may be secondary to desensitization of the Wnt signaling pathway in the absence of *Wntless* and secreted Wnts. In contrast, similar levels of membrane β -catenin are observed in control and *Wls*^{-/-} MSCs (**Figure 3.2 H**; quantified in **Supplemental Figure 3.2 A**). These data suggest that Wnt signaling is active in mature adipocytes and impaired secretion of adipocyte-derived Wnts influences downstream signaling in an autocrine/paracrine manner.

Since *Wntless* functions to chaperone Wnt proteins from the ER and Golgi apparatus to the plasma membrane for secretion, we hypothesized that its deletion might influence the adipocyte proteome. We therefore performed untargeted proteomic

analyses of *Wls^{fl/fl}* and *Wls^{-/-}* cultured adipocytes and observed substantial up- and down-regulation of adipocyte proteins (**Supplemental Figure 3.2 B**). Of these potential Wnt targets, we focused our investigations on the down-regulation of SCD1, an important adipocyte enzyme in the ER that catalyzes the desaturation of palmitic (C16:0) and stearic (C18:0) acids into palmitoleic (C16:1, n-7) and oleic (C18:1, n-9) acids, respectively^{68,69}. In addition to its role as the rate-limiting enzyme in fatty acid desaturation, SCD1 is also a key member of the DNL pathway (**Figure 3.3 A**), which converts excess dietary carbohydrates and amino acids into fatty acids. A subset of these fatty acids are esterified to form TAG, which can later be hydrolyzed and fatty acids either secreted or metabolized by β -oxidation to provide energy for the adipocyte^{70,71}. Consistent with proteomic data (**Supplemental Figure 3.2 B**), we found that Wntless deficiency in adipocytes down-regulates expression of *Scd1* mRNA (**Figure 3.3 A**) and protein (**Figure 3.3 B**). In addition, we also observed coordinate regulation of several enzymes involved in DNL and lipid metabolism (**Figure 3.3 A-B**; quantified in **Supplemental Figure 3.3 A**). Given the ~75% inhibition of SCD1 following *Wls* deletion, we hypothesized that *Wls^{-/-}* adipocytes would have impaired fatty acid monounsaturations and therefore a larger proportion of saturated fatty acids. Thus, we next used GC to analyze the composition of esterified fatty acids in total lipids extracted from *Wls^{fl/fl}* and *Wls^{-/-}* adipocytes. Consistent with our hypothesis, we found that *Wls^{-/-}* adipocytes contain a smaller proportion of monounsaturated fatty acids compared to *Wls^{fl/fl}* adipocytes (**Figure 3.3 C**). More specifically, when compared to control adipocytes, differentiated *Wls^{-/-}* cells contain higher levels of palmitic (C16:0) and stearic (C18:0) acids and lower amounts of myristoleic (C14:1, n-5), palmitoleic (C16:1, n-7) and vaccenic acids (C18:1, n-7) (**Figure 3.3 D-F**). Of note, *Wls^{-/-}* adipocytes contain mildly elevated levels of oleic acid (C18:1, n-9), consistent with previous reports of SCD1 inhibition in 3T3-L1 adipocytes⁷².

In addition to SCD1, *Wls* deletion also regulates expression of genes involved in lipid metabolism, including repression of ATP citrate lyase (ACLY), acetyl-CoA carboxylase (*Acaca*/ACC1) and fatty acid synthase (*Fasn*/FASN) (**Figure 3.3 A-B**). We therefore performed DNL assays using [¹⁴C]-acetate to determine whether this pathway is less active in *Wls^{-/-}* adipocytes. Cultured adipocytes were incubated in medium

containing [^{14}C]-acetate for 1, 2, 4 or 8 hours. Cells were then collected, and lipids were extracted to measure radiolabel incorporation into TAG, diacylglycerol (DAG), and phospholipid (PL) fractions. Analyses of conditioned media (**Figure 3.3 G**) and whole cell lysates (**Figure 3.3 H**) demonstrated that *Wls*^{-/-} adipocytes take up less labeled acetate over time. Importantly, *Wls*^{-/-} adipocytes incorporate significantly less radiolabel over time into the TAG fraction of cellular lipid (**Figure 3.3 I-J**) but not the PL or DAG fractions (**Figure 3.3 I**; quantified in **Supplementary Figure 3.3 B**). Thus, down-regulation of the DNL pathway secondary to Wntless deficiency is rate-limiting in adipocytes. Taken together, these data demonstrate that deletion of Wntless coordinately represses the network of lipogenic genes, thus altering the rate of lipogenesis and steady-state lipid composition in cultured adipocytes.

Wntless regulation of lipogenic genes is likely mediated by SREBP1c and ChREBP, and is independent of insulin responsiveness.

We next sought to understand the mechanism by which Wntless regulates the expression of *Scd1* and other lipogenic genes. Sterol regulatory element-binding protein 1c (SREBP1c) and carbohydrate-responsive element-binding protein (ChREBP) are known key upstream transcriptional regulators in WAT and liver of many genes involved in DNL, including *Acaca*, *Fasn*, and *Scd1*⁵¹⁻⁵³. Thus, we were interested in exploring whether these proteins are regulated in *Wls*^{-/-} adipocytes. We found that expression of *Srebf1* and *Mlxipl*, which encode SREBP1c and ChREBP respectively, are both down-regulated following loss of Wntless, whereas other transcription factors involved in adipogenesis and adipocyte metabolism, including *Pparg*, *Lxra*, and *Lxrb*, are not influenced (**Figure 3.4 A**). Although PPAR γ protein was unchanged, *Cebpa* mRNA and protein were both slightly repressed in *Wls*^{-/-} adipocytes, suggesting that this adipogenic transcription factor may also regulate lipogenic genes in mature adipocytes (**Figure 3.4 A-B**). Importantly, immunoblot analyses revealed that SREBP1c and ChREBP proteins were both repressed in *Wls*^{-/-} adipocytes (**Figure 3.4 B**), which is of interest since the literature to date has not reported regulation by Wnt signaling of *Srebf1* or *Mlxipl* in mature adipocytes. In addition, SREBP1c is post-translationally cleaved at the ER and only mature, soluble SREBP1c translocates to the nucleus to mediate gene

transcription. Of note, we observed that whereas the mature form of SREBP1c (~50 kDa relative mobility) is significantly decreased in *Wls*^{-/-} adipocytes, the larger immature form (~100 kDa) is reciprocally increased (**Figure 3.4 B-C**). Taken together, these data suggest that Wntless regulates lipogenic gene expression through expression of ChREBP, C/EBP α , and SREBP1c mRNA and proteins, with SREBP1c also potentially regulated at the post-translational level.

Previous studies have established insulin as an important regulator of *Srebf1* gene expression in the liver⁷³⁻⁷⁶. We therefore next investigated whether decreased responsiveness to insulin mediates the effects of *Wls* deletion on SREBP1c and ChREBP in adipocytes. We first measured basal and insulin-stimulated glucose uptake and did not observe differences between *Wls*^{fl/fl} and *Wls*^{-/-} adipocytes (**Figure 3.4 D**). We next assessed signaling downstream of insulin by immunoblot analyses, and found that phosphorylation on specific serine or threonine amino acids in AKT was not impaired in *Wls*^{-/-} adipocytes (**Figure 3.4 E**). Although insulin has been shown to promote *Srebf1* mRNA expression in the liver, insulin treatment did not induce *Srebf1* or *Mlxipl* gene expression in either *Wls*^{fl/fl} or *Wls*^{-/-} adipocytes (**Figure 3.4 F**). After translation, SREBP1 is anchored to the ER by a protein complex that includes SREBP cleavage-activating protein (SCAP) and insulin-induced gene 1 or 2 (Insig1 or Insig2)^{51,73,77-79}. The Insigs function to prevent the maturation of SREBP1. In response to stimuli, including insulin, Insig activity is decreased and SCAP escorts SREBP1 from the ER to the Golgi apparatus, where it is cleaved into a soluble and transcriptionally active form^{79,80}. We therefore explored whether SCAP mRNA or protein expression is altered by *Wls* deletion but found both to be unchanged in *Wls*^{-/-} adipocytes (**Figure 3.4 G-H**). Taken together, these data support the conclusion that in adipocytes, Wntless regulates SREBP1c and ChREBP through mechanisms independent of insulin responsiveness.

Adipose-specific Wntless deletion does not influence body composition or whole-body metabolism in mice on NCD.

Our studies thus far demonstrate that Wntless expression is promoted by diet-induced obesity, and Wntless deficiency suppresses a network of lipogenic genes and DNL, and reduces fatty acid monounsaturations of adipocyte lipids. Thus, we hypothesized that

Wntless plays an important role *in vivo* in the appropriate storage of circulating nutrients, particularly under obesogenic conditions. To test this hypothesis, we generated adipose-specific *Wls* knockout mice by crossing *Wls^{fl/fl}* mice with adiponectin-Cre mice. Adiponectin-Cre has been well-established as a model to delete floxed genes specifically and efficiently in adipocytes⁸¹. In our model, genetic recombination of *Wls* is only observed in adipose depots, and not in other tissues, such as liver, pancreas, and muscle (**Figure 3.5 A**). As expected, we found that Wntless mRNA (**Figure 3.5 B**) and protein (**Figure 3.5 C**) were decreased in iWAT and eWAT of *Wls^{-/-}* mice on NCD, when compared to *Wls^{fl/fl}* counterparts. Analyses of mRNA from fractionated WAT demonstrated that *Wls* deletion occurs specifically in the adipocyte fraction and not in the SVF of iWAT and eWAT depots (**Figure 3.5 D**). We then explored possible metabolic phenotypes in the *Wls^{-/-}* mice and did not detect differences in body composition (**Figure 3.5 E**), growth over time (**Figure 3.5 F**), glucose tolerance (**Figure 3.5 G**), or insulin sensitivity (**Figure 3.5 H**). Consistent with these data, *Wls^{-/-}* mice did not exhibit altered fed or fasted concentrations of blood glucose (**Figure 3.5 I**), or serum insulin (**Figure 3.5 J**), adiponectin (**Figure 3.5 K**), or TAG (**Figure 3.5 L**). Finally, tissue weights such as iWAT, eWAT, brown adipose tissue (BAT) or liver were not different between *Wls^{fl/fl}* and *Wls^{-/-}* mice (**Figure 3.5 M**). Similar results were observed in female mice fed NCD (**Supplemental Figure 3.4**). Histological analyses of tissues did not yield substantial differences in adipocyte size or number within iWAT, eWAT, perirenal WAT, or BAT (**Figure 3.6 A**; data not shown). In addition, liver morphology was unchanged (**Figure 3.6 A**).

Wnt signaling plays an important role in bone, where it increases bone mass and impairs marrow adiposity. For example, FABP4- or OCN-Wnt10b mice have extensive trabeculation throughout the entire endocortical compartment^{15,16}. We therefore evaluated whether marrow cells traced by adiponectin-Cre are a critical source of Wnts in the bone marrow niche^{82,83}. Histological analyses of tibia from both male and female cohorts suggest that Wntless deficiency does not influence size or number of marrow adipocytes (**Supplemental Figure 3.5 A**). In addition, micro-computed tomography (μ CT) analyses indicate that cortical and trabecular bone mass variables were not influenced by *Wls* deletion (**Supplemental Figure 3.5 B-I**).

Since Wntless was found to regulate lipogenic gene expression *in vitro*, we next measured expression of a subset of key DNL genes in eWAT and iWAT of *Wls^{fl/fl}* and *Wls^{-/-}* mice. As expected, *Wls* gene expression was significantly decreased in both eWAT and iWAT of *Wls^{-/-}* mice (**Figure 3.6 B**). Surprisingly, expression of most DNL pathway genes was not changed, with the exception of *Mlxipl* (**Figure 3.6 B**). We also did not observe changes in DNL gene expression within livers of *Wls^{-/-}* mice (**Supplemental Figure 3.6 A**). Analyses of isolated adipocytes from *Wls^{-/-}* mice showed that, despite efficient knockout of *Wls*, expression of lipogenic genes was not altered (**Figure 3.6 C**). This result was puzzling, so we next evaluated whether Wnt signaling is active within adipose tissues *in vivo*. To this end, we measured expression of downstream Wnt target genes in isolated adipocytes and SVF of *Wls^{-/-}* mice and their *Wls^{fl/fl}* counterparts, and found that expression of *Axin2* and *Id2* were dysregulated as expected in adipocytes with Wntless deficiency. Interestingly, for those adipocyte genes that were not suppressed as expected (i.e. *Cmyc*, *Tcf7l2*, and *Ppard*), compensatory up-regulation was observed in the SVF (**Figure 3.6 D**). Flow cytometric analyses of SVF isolated from *Wls^{fl/fl}* and *Wls^{-/-}* mice did not reveal differences in subpopulation proportions (**Supplemental Figure 3.6 B-C**); thus, we considered the possibility that SVCs of *Wls^{-/-}* mice sense the adipocyte-specific loss of Wnt secretion and respond by increasing their own production of Wnts to compensate for the deficiency. To this end, we measured the mRNA expression of many Wnts in SVF isolated from *Wls^{fl/fl}* or *Wls^{-/-}* mice fed NCD and found significantly increased expression of several Wnts, including *Wnt6*, *Wnt9b*, *Wnt10a*, *Wnt10b*, and *Wnt16* (**Figure 3.6 E**). We also observed decreased expression of *Wnt1*, *Wnt4*, and *Wnt8b*, whereas expression of *Wnt2a*, *Wnt2b*, *Wnt3*, *Wnt5a*, *Wnt5b*, and *Wnt11* was unchanged. These data provide strong evidence for altered Wnt production by neighboring SVCs in response to impaired secretion from adipocytes. Dramatic induction of *Wnt6*, *Wnt9b*, *Wnt10a*, *Wnt10b*, and *Wnt16*, along with induction of Wnt target genes, suggests that WATs rigorously defend adipocyte-specific loss of Wnts by increased signaling within SVCs.

***Wls*^{-/-} mice on HFD have decreased adipocyte DNL gene expression, reduced size of epididymal adipocytes and WAT, and are protected from metabolic dysfunction.**

Previous studies have suggested that Wnt signaling plays an important role in the metabolism of adipocytes under conditions of nutrient excess³²⁻³⁴. We have also found that *Wls* expression is up-regulated within both subcutaneous and visceral WAT with diet-induced obesity (**Figure 3.1 E-F; Supplemental Figure 3.1 A**). We therefore challenged *Wls*^{fl/fl} and *Wls*^{-/-} mice with 60% HFD for a minimum of 20 weeks and a striking metabolic phenotype emerged. Although HFD feeding did not cause a difference in body weight gain (**Figure 3.7 A**), *Wls*^{-/-} mice had decreased fat mass and increased lean mass (**Figure 3.7 B**), which was not due to altered daily food intake (**Supplemental Figure 3.7 A**). *Wls*^{-/-} mice had significantly improved glucose tolerance (**Figure 3.7 C**) and consistent with this, demonstrated higher random-fed (**Figure 3.7 D**) and glucose-induced circulating insulin concentrations (**Figure 3.7 E**) when compared to controls. Insulin sensitivity was not different (**Figure 3.7 F**), nor were random-fed or fasting blood glucose concentrations (**Figure 3.7 G**) or serum leptin (**Figure 3.7 H**), adiponectin (**Figure 3.7 I**), TAG (**Figure 3.7 J**), or free or total cholesterol (**Figure 3.7 K**). Consistent with leaner body composition, eWAT weights of *Wls*^{-/-} mice were decreased, whereas liver weights were increased (**Figure 3.7 L**).

Histological analyses of *Wls*^{-/-} tissues demonstrated significantly decreased eWAT adipocyte hypertrophy (**Figure 3.8 A-B**) with a trend toward smaller cells observed in iWAT (**Supplemental Figure 3.7 B**). Livers of *Wls*^{-/-} mice showed improved hepatosteatosis (**Figure 3.8 A**), likely contributing to the observed protection from glucose intolerance. Of note, we did not observe differences in histology of BAT or expression of UCP1 protein in *Wls*^{-/-} mice (**Supplemental Figure 3.7 C**), suggesting that metabolic effects of Wntless deletion are not secondary to altered BAT thermogenesis. We next isolated SVF and adipocytes from *Wls*^{-/-} mice fed HFD and measured Wnt target gene expression. We were intrigued to find that with HFD, SVF of *Wls*^{-/-} mice no longer had elevated Wnt expression or downstream signaling (**Figure 3.8 C; Supplemental Figure 3.7 D**). Analyses of the adipocyte fraction showed that Wnt target gene expression was significantly decreased (**Figure 3.8 C**), suggesting that HFD

challenge diminishes the ability of WAT to maintain Wnt signaling homeostasis. Consistent with this result, expression of several lipogenic genes, including *Mlxipl*, *Acaca*, *Fasn*, *Scd1* and *Elovl7*, was coordinately regulated in isolated epididymal adipocytes (**Figure 3.8 D-E**) and whole eWAT of *Wls^{-/-}* mice (**Figure 3.8 F**), remarkably consistent with our studies in cultured adipocytes (**Figures 3.3, 3.4**). A subset of these genes was also repressed in iWAT of *Wls^{-/-}* mice (**Figure 3.8 F**). Finally, to determine whether reduced WAT DNL was compensated for elsewhere, we isolated livers from *Wls^{-/-}* mice and found that they did not have altered DNL gene expression (**Supplemental Figure 3.7 E**). In summary, our studies support the conclusion that with chronic overnutrition, adipose tissues of *Wls^{-/-}* mice no longer defend Wnt signaling homeostasis, which leads to down-regulation of DNL enzyme expression, reduced adipocyte hypertrophy and adiposity, and overall improved metabolic health.

Discussion

An extensive literature has characterized mechanisms by which Wnt signaling in MSCs represses adipogenesis and promotes alternative cell fates, such as osteoblastogenesis^{5,12,17,18,84}. The Wnts expressed in MSCs that function cell-autonomously include Wnt10b, Wnt10a, and Wnt6, and other family members may conceivably participate as paracrine regulators^{5,6,12}. The preponderance of evidence indicates that canonical Wnt/ β -catenin signaling dominates control of MSC fate, with lesser contributions from the non-canonical pathway^{5,84}. In this regard, the expression of β -catenin is suppressed during adipogenesis in both mouse and human models, and its activity is further inhibited by induced expression of Wnt antagonist Chibby⁸⁵. Much of the early data within this field focused on the inhibition of adipogenesis by Wnt signaling, and coordinate suppression of many genes involved in Wnt/ β -catenin signaling during the early stages of differentiation. However, our work herein and other recently published reports demonstrate that repression of the canonical Wnt pathway during differentiation is transient, and that proteins including β -catenin, Wntless and Tcf7l2, play important functional roles in mature adipocytes^{32,34}.

Here, we report that essentially all aspects of the canonical Wnt signaling apparatus are expressed in mature adipocytes, including Wntless, Wnts, Fzd receptors, LRP co-receptors, Dishevelleds, β -catenin, TCF/LEFs, and modulatory proteins like Axin2, SFRP4 and SFRP5. Indeed, Wnt signaling in cultured adipocytes is likely to have contributions from many Wnt proteins, including Wnt16, Wnt2, and Wnt7b, which are expressed at similar levels in MSCs and adipocytes, and Wnt2b, Wnt4, Wnt5b, Wnt8b, Wnt9a, and Wnt9b, which are induced during adipogenesis. These Wnts are proposed to act through LRP5 and LRP6^{9,10}, in conjunction with Fzd4 and Fzd9, which are also increased during differentiation. We also observed induction of previously reported downstream Wnt targets WISP1 and WISP2, secreted adipokines that are increased with obesity and proposed to regulate whole-body insulin sensitivity^{86,87}. In some cases, there may also be interspecies differences that will be important for our long-term understanding of these complex processes⁸⁸. We have shown that the core Wnt/ β -catenin signaling molecules are expressed and operative within mature adipocytes, and expect that the unique combination of Wnts, receptors, and transcription factors

provides distinct functional specificity; however, the cellular processes in adipocytes controlled by this pathway were previously poorly understood.

To evaluate the cell-autonomous functions of Wnt signaling in adipocytes, we chose to block secretion of adipocyte-derived Wnts through deletion of the Wnt chaperone protein, Wntless. As expected, Wntless deletion and presumed impairment of Wnt secretion from cultured adipocytes suppressed accumulation of free cytosolic β -catenin and subsequent expression of several classic Wnt target genes such as *Axin2*, *Tcf7l2*, and *Cmyc*, responses that have been observed in many other cell types. In the context of adipocytes, we observed that Wnt secretion is also required for coordinate expression of lipogenic genes, including *Acly*, *Acaca*, *Fasn* and *Scd1*. Consistent with repression of these genes, *Wis^{-/-}* adipocytes exhibit functional impairments in DNL and lipid monounsaturations. These effects on adipocyte metabolism are highly specific: Wntless deletion does not influence insulin-stimulated glucose uptake, adrenergic stimulation of lipolysis, or β -oxidation (**Supplemental Figure 3.3 C-E**). These data are supported by that of Geoghegan *et al.*, who reported that *Tcf7l2* deletion in mesenchymal progenitors promotes adipogenesis and elevated expression of gene clusters involved in fatty acid and TAG metabolism³⁴, consistent with the repressive role of β -catenin and TCF/LEF signaling in this context⁵. *Tcf7l2* binding sites were reported within 1 kb of the transcriptional start site of most lipogenic genes, including *Acly*, *Fasn*, and *Scd1*, consistent with Wnt/ β -catenin signaling directly coordinating adipocyte lipid metabolism³⁴.

A common feature of Wnt signaling in a wide range of cell types and animal models is inhibitory feedback, which provides an intricate restraint on Wnt-dependent gene activation^{89,90}. Our lab previously observed Wnt1-induced feedback on members of the Wnt pathway in preadipocytes⁹¹; here, we uncovered a similar response to recombinant Wnt3a treatment of fully differentiated adipocytes. Thus, exogenous Wnt3a stimulates many of the classic inhibitory responses to limit the effects of Wnt signaling. These include induction of known feedback genes like *Nkd1*, *Nkd2*, *Axin2*, *Notum*, *Lgr5*, and *Tcf7*, coincident with repression of *Tcf7l2*, *Fzd8*, and *Lrp5*. Because Wnt secretion and functionality is largely dependent upon lipid modification by SCD1-derived palmitoleic acid⁴¹, inhibition of SCD1 results in reduced Wnt/ β -catenin signaling, an

observation extensively investigated within the cancer field⁵⁴⁻⁶¹. Herein, we have determined that the reciprocal relationship also holds true: endogenous Wnt signaling in adipocytes is required for lipogenesis and monounsaturating of lipids, including the formation of palmitoleic acid. Although signaling downstream of adipocyte Wnts is necessary for maintenance of lipogenic genes and production of palmitoleic acid, stimulation of adipocytes with exogenous Wnt3a does not further promote expression of these genes. These results may indicate that endogenous Wnt signaling plays a permissive role in expression of lipogenic genes, or perhaps that stimulation with a Wnt ligand other than Wnt3a may be necessary to observe dynamic regulation of this gene network.

In mice maintained on NCD, adipocyte-specific *Wls* deletion does not overtly influence body composition or whole-body metabolism. Consistent with our results, recent investigations into the role of Wnt signaling in mature adipocytes, including global deletion of *Sfrp5* or adipocyte-specific deletion of *Ctnnb1* or *Tcf7l2*, also did not yield metabolic phenotypes on a chow diet³²⁻³⁴. Although these previous studies did not probe further into a lack of detectable phenotype, our experiments uncovered a novel compensatory mechanism by which adipose tissues defend the loss of adipocyte-derived Wnt signaling in mice fed NCD. We found that despite efficient Wntless ablation at the DNA, RNA and protein levels, adipocytes isolated from *Wls*^{-/-} mice do not have altered Wnt target or DNL gene expression. However, upon further investigation, we observed that SVF cells isolated from *Wls*^{-/-} mice up-regulate Wnt mRNAs, including *Wnt6*, *Wnt9b*, *Wnt10a*, *Wnt10b*, and *Wnt16*. Consistent with these data, we also found elevated Wnt target gene expression in *Wls*^{-/-} SVCs, as evidenced by increased expression of *Cmyc*, *Tcf7l2*, and *Ppard*. These data suggest the intriguing possibility that under standard nutritional conditions, SVF cell populations sense the loss of adipocyte-derived Wnts and respond by up-regulating their own Wnt production and signaling to maintain downstream target gene expression within adipocytes.

Although mechanisms by which SVCs compensate for loss of adipocyte Wnts is not yet clear, a number of possibilities exist. Wntless deficiency may alter the SVF cellular composition, enriching for subpopulations that have highly active Wnt signaling. However, flow cytometry analysis of immune, endothelial, and stromal cell proportions

within the SVF did not yield observable differences between *Wls^{fl/fl}* and *Wls^{-/-}* mice, making this possibility less likely. Alternatively, a particular cell type within the SVF may detect loss of Wnt signaling from adipocytes and compensate by increasing its own Wnt production and secretion. It is also possible that the intricate intracellular feedback mechanisms described above may involve other families of secreted signaling molecules, including BMPs and FGFs, both of which are regulated in adipocytes by Wnt3a, and which have been shown in other contexts to interact with Wnt/ β -catenin signaling⁹²⁻⁹⁵. Wnts are low-abundance, lipid-modified proteins that act locally in an autocrine/paracrine manner; these characteristics create major technical challenges for isolating and quantifying Wnts from tissue or serum of *Wls^{fl/fl}* and *Wls^{-/-}* mice. Nevertheless, further studies will be necessary to fully elucidate the compensatory mechanisms by which specific SVF cells sense and respond to the loss of adipocyte-derived Wnt secretion.

Adipose tissues are critical for maintenance of insulin sensitivity and glucose homeostasis through storage of excess energy and secretion of adipokines⁹⁶⁻¹⁰⁰. To date, inhibition of adipose-specific Wnt signaling has been shown to influence whole-body glucose homeostasis under obesogenic conditions; however, discordant results have been reported between animal models that should, ostensibly, all be loss-of-function for Wnt signaling. For example, our work in *Wls^{-/-}* mice found that more than 20 weeks of HFD overrides the compensatory Wnt signaling in adipose SVCs, revealing a striking phenotype. *Wls^{-/-}* mice fed HFD are characterized by decreased fat and increased lean mass, improved glucose homeostasis, increased circulating insulin, and decreased lipogenic gene expression within WAT depots. Interestingly, these mice exhibit increased liver weight but improved hepatosteatosis by histological analysis. Although highly speculative, one possible explanation underlying this finding might be the existence of a Wnt-regulated adipocyte factor that signals to the pancreas to suppress insulin secretion. When this signal is removed by impaired Wnt secretion from adipose tissue, elevated circulating insulin may act upon the liver to suppress gluconeogenesis, stimulate glycogen storage and increase liver weight. Future quantitative measurements of regulated insulin secretion, glucose homeostasis, glycogen and TAG in whole livers, as well as examination of hepatic cell size and

number, may uncover mechanisms by which Wntless deficiency improves glucose tolerance in obese mice.

Consistent with our studies, adipocyte-specific β -catenin-deficient mice also exhibit decreased fat mass and improved glucose tolerance when fed HFD long-term³². In contrast, diet-induced obese *Tcf7l2*^{-/-} mice demonstrate increased adipose tissue mass, impaired glucose tolerance and greater insulin resistance³⁴. Expression of a subset of lipogenic genes, including *Acly* and *Scd1*, was elevated in WAT of these mice, in line with observed adipocyte hypertrophy, but counter to our results in cultured adipocytes and WAT from *Wls*^{-/-} mice. The bases for these apparently conflicting results may include reported discrepancies between their RNAseq and qPCR results, generation of alternative splice variants with differential cis-element binding or transcriptional activity, or compensatory binding of other TCF/LEF transcription factors to cis-elements¹⁰¹⁻¹⁰⁴. Alternatively, it is conceivable that there are distinctions between knockout of Wnt secretion and deletion of a downstream transcriptional effector of β -catenin; to this end, *Tcf7l2* has also been shown to have transcriptional activity independent of β -catenin in certain contexts¹⁰⁵ and its deletion may therefore impact distinct pathways. Indeed, Geogheghan *et al.* report that *Tcf7l2* deletion repressed expression of lipolytic genes, possibly contributing to adipocyte hypertrophy and subsequent metabolic dysfunction on HFD. In any case, results from both groups point to regulation of lipid metabolism by Wnt signaling in adipocytes.

In a gain-of-function Wnt signaling model, global *Sfrp5*^{Q27Stop} mice fed HFD were characterized by decreased adipocyte size and WAT mass, elevated mitochondrial variables including oxygen consumption, and a mild improvement in glucose homeostasis³³. These effects of SFRP5 on glucose homeostasis are largely supported by injection of SFRP5 neutralizing antibody¹⁰⁶. Consistent with these data, transgenic mice with enforced expression of Wnt10b from the FABP4 promoter have less WAT when maintained on NCD, are resistant to HFD-induced or genetic obesity, and are more glucose tolerant and insulin sensitive than controls^{13,14}. Taken together, these gain-of-function models support the notion that increased adipose Wnt signaling influences whole-body glucose homeostasis; however, further research is required to establish mechanisms and to resolve differences in experimental outcomes.

In summary, we have demonstrated that Wnt/ β -catenin signaling is active in adipocytes and adipocyte-derived Wnts are required for expression of a network of lipogenic genes. Further, adipocytes compensate for Wnt deficiency through cell-autonomous mechanisms, and WAT defends loss of adipocyte-derived Wnts by up-regulating Wnt signaling in SVCs (**Figure 3.9**). Finally, this compensatory mechanism for maintaining homeostasis is overridden by long-term HFD, revealing that *Wnt1*^{-/-} mice are resistant to diet-induced obesity, adipocyte hypertrophy, and metabolic dysfunction.

Materials and methods

Animals

Wls^{fl/fl} mice (#012888, Jackson Lab, Ellsworth, ME), which harbor loxP sites flanking exon 1, were crossed with Adiponectin (Adipoq)-Cre mice (#028020, Jackson Lab, Ellsworth, ME) to generate *Wls^{fl/fl}* or *Wls^{-/-}* mice. Animals were housed in a 12 h light/12 h dark cycle with free access to water and food. For HFD studies, mice were fed rodent diet with 60 kcal% from fat (#12492, Research Diets, New Brunswick, NJ). All animal studies were approved by and performed in compliance with policies of the University of Michigan Institutional Animal Care and Use Committee. Daily care of mice was overseen by the Unit for Laboratory Animal Medicine at the University of Michigan.

Body composition

Fat, lean, and free fluid masses were estimated with a Bruker Minispec LF90II NMR (Bruker, Billerica, MA) within the University of Michigan Mouse Metabolic Phenotyping Center.

Glucose and insulin tolerance tests

For glucose tolerance tests, mice were fasted for 16 h and then administered an intraperitoneal injection of glucose (1 mg/kg body weight). For insulin tolerance tests, mice were fasted for 6 h and then given an intraperitoneal injection of insulin (Eli Lilly, Indianapolis, IN). Mice on NCD received 0.5 U insulin/kg body weight whereas mice on HFD were administered 1.0 U insulin/kg body weight. Blood was collected from the tail vein, and glucose concentrations were monitored at 0, 15, 30, 60, and 120 minutes after intraperitoneal injection using a glucometer and Contour Next blood glucose strips (Bayer AG, Leverkusen, Germany).

Serum measurements

Blood was collected from the tail vein, or by cardiac puncture at time of harvest, and allowed to coagulate on ice for 2 h. After centrifugation at 2,000 x g for 20 min at 4°C, serum was transferred to a new tube and stored at -80°C. ELISA was used to estimate

concentrations of serum insulin (Crystal Chem USA, Elk Grove, IL), adiponectin (R&D Systems Inc., Minneapolis, MN), and leptin (PeproTech Inc., Rocky Hill, NJ). Triacylglycerols (TAG), and total and free cholesterol were measured by colorimetric assays (Cayman Chemical, Ann Arbor, MI; Abcam, Cambridge, UK, respectively).

Adipocyte and stromal-vascular cell fractionation

Inguinal WAT (iWAT) and epididymal WAT (eWAT) were excised from mice^{99,107}, minced with scissors and digested for 1 h at 37°C with shaking (600 rpm) in 2 mg/ml collagenase type I (Worthington Biochemical, Lakewood, NJ) in Krebs-Ringer-HEPES (KRH; pH 7.4) buffer containing 3% fatty acid-free bovine serum albumin (BSA; Gold Biotechnology, St. Louis, NJ), 1 g/L glucose, and 500 nM adenosine. The resulting cell suspensions were filtered through 100 µm cell strainers and centrifuged at 100 x g for 8 min to separate the stromal-vascular fraction (SVF) and the buoyant adipocytes. Fractions were washed 2x with KRH buffer containing 3% fatty acid-free BSA, 1 g/L glucose, and 500 nM adenosine. For immunoblot analyses, the fractions were subsequently washed 1x with KRH buffer containing 0.5% fatty acid-free BSA, 1 g/L glucose, and 500 nM adenosine.

Histology

Soft tissues were harvested and fixed in 10% neutral buffered formalin overnight at 4°C. Bones were fixed in 10% neutral buffered formalin for 24 h, rinsed with water and decalcified in 14% EDTA, pH 7.4 for 14 days. Paraffin-embedded tissues were sectioned at 5 µm thickness and stained with hematoxylin and eosin (H&E) as previously described¹⁰⁸. Stained sections were imaged using a Zeiss inverted microscope at 100x or 200x magnification.

Adipocyte histomorphometry

Adipocyte size and number were quantified from WAT sections stained with hematoxylin and eosin. After digital processing, individual adipocyte cross-sectional areas were quantified using MetaMorph Microscopy Automation & Image Analysis Software 2.0 (Molecular Devices, Sunnyvale, CA) as previously described¹⁰⁸. To

compare adipocyte sizes between genotypes, frequency distribution curves were generated with bin values as follows: bin range: 0 to 18,000 μm^2 ; bin width: 500 μm^2 . Nonlinear curves were fit to the data to visualize frequency distribution patterns.

Micro-computed tomography (μCT) analysis of bone

Harvested tibiae were fixed in 10% neutral buffered formalin for 24 h, washed with water, placed in Sorensen's phosphate buffer, pH 7.4, and stored at 4°C prior to μCT analysis. After placement in a 19-mm diameter tube, the length of each bone was scanned using a μCT system ($\mu\text{CT}100$ Scanco Medical, Bassersdorf, Switzerland). Scan settings were as follows: voxel size 12 μm , 70 kVp, 114 μA , 0.5 mm AL filter, integration time 500 ms. Density measurements were calibrated to the manufacturer's hydroxyapatite phantom. Analysis was performed with the manufacturer's evaluation software, using a threshold of 180 for trabecular bone and 280 for cortical bone.

Cell culture

Primary mesenchymal stem cells (MSC) were isolated from the ears of wildtype C57BL/6J (Jackson Labs, Bar Harbor, Maine) or *Wls^{fl/fl}* mice as previously described^{33,109,110} and cultured at 5% CO_2 . Subconfluent MSCs were maintained in DMEM:F12 medium (Thermo Fisher Scientific, Waltham, MA) containing 10% fetal bovine serum (FBS; Sigma-Aldrich, St. Louis, MO) and supplemented with 10 ng/ml recombinant basic fibroblast growth factor (PeproTech Inc., Rocky Hill, NJ). At two days post-confluence, adipogenesis was induced with 0.5 mM methylisobutylxanthine, 1 μM dexamethasone, 5 $\mu\text{g/ml}$ insulin and 5 μM rosiglitazone in DMEM:F12 containing 10% FBS. From day 2 to 4 of differentiation, cells were fed with fresh DMEM:F12 medium containing 10% FBS, 5 $\mu\text{g/ml}$ insulin and 5 μM rosiglitazone. Thereafter, cells were maintained in DMEM:F12 containing 10% FBS. Accumulation of neutral lipids in adipocytes was visualized with Oil Red-O staining¹¹¹. Briefly, cells were washed with phosphate-buffered saline (PBS), fixed in 0.5% glutaraldehyde in PBS for 5 min, incubated in Oil Red-O working solution for 10 min at room temperature with gentle agitation, and then washed 2x with PBS. Total TAG accumulation was quantified by colorimetric assay (Cayman Chemical, Ann Arbor, MI). Cells cultured for analyses of

lipid composition were differentiated from day 6 to 12 in DMEM:F12 containing 10% charcoal-stripped FBS (Sigma-Aldrich, St. Louis, MO). Where indicated, confluent MSCs or day 12 adipocytes were treated with 20 ng/ml recombinant Wnt3a (R&D Systems Inc., Minneapolis, MN) for 4 h prior to collection.

Genetic recombination in cultured cells

To induce gene deletion, *Wls^{fl/fl}* adipocytes were treated with adenoviral GFP or adenoviral Cre recombinase (1×10^{10} viral particles/ml) in serum-free maintenance medium from day 4 to 6 of differentiation. Adenoviruses were obtained from the University of Michigan Vector Core. Genetic recombination was confirmed by PCR with a three-primer system. Primer sequences as follows: P1, CTTCCCTGCTTCTTTAAGCGTC; P2, AGGCTTCGAACGTAAGTACC; P3, CTCAGAACTCCCTTCTTGAAGC; floxed band: 556 bp; recombined band: 410 bp.

Cellular fraction for isolation of free cytosolic and membrane β -catenin

To evaluate levels of free cytosolic β -catenin, confluent MSCs were treated for 4 h with 20 ng/ml recombinant Wnt3a (R&D Systems Inc., Minneapolis, MN) and cellular fractionation was performed as previously described. Briefly, cells were washed twice with cold PBS and homogenized using a BioVortexer mixer (Chemglass, Vineland, NJ) in ice-cold buffer containing 10 mM Tris pH 7.4, 140 mM NaCl, 5 mM EDTA, 2mM DTT, 1:100 protease inhibitor cocktail (Sigma-Aldrich, St. Louis, MO). Lysates were then centrifuged for 10 min at 500 x g at 4°C to remove cellular debris. Lysates were subsequently ultracentrifuged at 100,000 x g for 90 min at 4°C to obtain the cytosolic (supernatant) and membrane (pellet) fractions. Protein concentrations of cell fractions were measured by BCA protein assay (Thermo Scientific, Waltham, MA) and β -catenin expression was measured by immunoblotting^{6,66}.

De novo lipogenesis (DNL) assay

Cultured adipocytes were incubated overnight in fresh serum-free DMEM:F12 medium prior to evaluation of DNL. Cells were then incubated in fresh DMEM:F12 medium (containing 0.5 mM sodium pyruvate, 0.5 mM L-glutamine, 2.5 mM glucose)

supplemented with 1% fatty acid-free BSA, and containing 0.5 μCi [^{14}C]-acetate (PerkinElmer, Waltham, MA) and 5 μM sodium acetate for 1, 2, 4, or 8 h at 37°C. At the end of the indicated incubation times, adipocytes were harvested, and lipids extracted for analyses by thin-layer chromatography and scintillation counting.

Insulin-stimulated glucose uptake

Cultured adipocytes were fasted for 6 h in Dulbecco's PBS (dPBS; without calcium, magnesium, phenol red; Thermo Fisher Scientific, Waltham, MA) with 0.7% fatty acid-free BSA at 37°C. Cells were washed 1x with dPBS. Adipocytes were then stimulated with 0, 2, 10, 20 or 100 nM insulin in dPBS containing 0.7% fatty acid-free BSA. After 30 min, 0.1 $\mu\text{Ci}/\text{ml}$ [^{14}C]-2-deoxy-glucose and 1 mM 2-deoxy-glucose was added per well and incubated for an additional 10 min. To measure background glucose uptake, 50 μM cytochalasin B (glucose transport inhibitor) was added to a subset of wells during the last 10 min of insulin stimulation. Glucose uptake was terminated with addition of 2-deoxy-glucose to a final concentration of 20 mM. Medium was aspirated and cells were washed 2x with ice-cold PBS. Adipocytes were lysed in 0.1% sodium dodecyl sulfate, lysates centrifuged for 10 min at 13,600 x g, and supernatants transferred to a new tube. Radioactivity in the supernatant was measured using a scintillation counter, background glucose uptake subtracted, and labeled glucose uptake normalized to protein concentration of lysed cells.

Lipolysis assay

Cultured adipocytes were washed 1x with PBS and then incubated in Hank's Balanced Salt Solution (HBSS; Thermo Fisher Scientific, Waltham, MA) containing 2% BSA for 1 h at 37°C. Cells were then stimulated with 1 μM isoproterenol, 5 μM forskolin, or 1 μM CL-316,243 in fresh HBSS containing 2% BSA for 3 h at 37°C; untreated cells were used to assess basal lipolysis. Conditioned medium was collected at the end of the incubation, released glycerol measured by colorimetric assay (Sigma-Aldrich, St. Louis, MO), and normalized to protein concentration of lysed cells.

β-oxidation assay

Cultured adipocytes were washed 1x with PBS and then incubated with 5 mCi/ml [³H]-palmitic acid and 22 μM palmitic acid in β-oxidation buffer (following manufacturer's guidelines; catalog #D5030; Sigma-Aldrich, St. Louis, MO) containing 10 mg/ml BSA and 200 μM L-carnitine for 3 h at 37°C. A subset of wells was pre-treated with 100 μM etomoxir (CPT1 inhibitor; Cayman Chemical, Ann Arbor, MI; Abcam, Cambridge, UK) to block mitochondrial β-oxidation. Fresh etomoxir was added to these wells for the duration of the assay. After 3 h, conditioned media from cells was passed through columns containing anion exchange resin and collected in scintillation vials. Columns were subsequently washed 2x with deionized water. Radioactivity in the supernatant was measured using a scintillation counter and normalized to protein concentration of lysed cells.

Lipid extraction for analyses by gas chromatography

Cultured adipocytes were washed 2x with PBS and then suspended in 500 μl of a 1:2.5 methanol/water mixture. The cell suspension was transferred to a borosilicate glass tube. Wells were rinsed with 500 μl of the 1:2.5 methanol/water mixture and the volume was transferred to the glass tube. Then 375 μl chloroform and 375 μl 0.9% NaCl were added to each tube, which were then vortexed vigorously and centrifuged at 2500 rpm for 20 min at 4°C. The lower organic chloroform layer containing total lipids was transferred to a new tube and stored at -20°C until analyzed.

Fatty acid composition by gas chromatography

Fatty acids within extracted lipids were derivatized into their methyl esters by transesterification with boron trifluoride-methanol as previously described¹¹². Derivatized methyl esters were re-dissolved in a small volume of hexane and purified by thin-layer chromatography using n-hexane-diethyl ether-acetic acid (50:50:2, v/v/v) as the developing solvents. After development, plates were dried and sprayed with Premulin. The products were identified under ultraviolet light by comparison to the retention flow of the methyl heptadecanoate (C17:0) standard (retention flow, 0.67) applied side-by-side on the same plate. Methyl esters were extracted from the thin-layer chromatography

powder with diethyl ether, concentrated under nitrogen, and re-dissolved in 100 μ l hexane. Fatty acid compositions of the lipids were analyzed by gas chromatography (GC) as follows. Analysis of FAMES was performed with 1 μ l sample injection on an Agilent GC machine, model 6890N equipped with flame ionization detector, an auto sampler and a Chemstation software for data analysis. An Agilent HP 88, 30 m GC column with a 0.25 mm inner diameter and 0.20 mm film thickness was used. Hydrogen was used as a carrier gas and nitrogen was used as a makeup gas. Analyses were carried out with a temperature programming of 125-220°C. Fatty acid components within unknown samples were identified with respect to the retention times of authentic standard methyl ester mixtures run side-by-side. Fatty acid components were quantified with respect to the known amount of internal standard added and the calibration ratio derived from each fatty acid of a standard methyl esters mixture and the methyl heptadecanoate internal standard. The coefficient of variation for GC analyses was found to be within 2.3-3.7%.

Quantitative RT-PCR

Total RNA was purified from frozen tissue or cultured cells using RNA STAT-60 (Tel Test, Alvin, TX) according to the manufacturer's instructions. One μ g of total RNA was reverse-transcribed to cDNA using M-MLV Reverse Transcriptase (Invitrogen, Carlsbad, CA). qRT-PCR was performed on the StepOnePlus System (Applied Biosystems, Foster City, CA) with qPCRBIO Sygreen Mix (Innovative Solutions, Beverly Hill, MI). Prior to use, all primers were validated with a cDNA titration curve and product specificity was confirmed by melting curve analyses and gel electrophoresis of qPCR products. Expression of each gene was calculated using a cDNA titration curve within each plate and was then normalized to the expression of peptidylprolyl isomerase A (PPIA) mRNA.

RNA sequencing (RNA-seq) analyses

Confluent MSCs or day 12 adipocytes were treated with 20 ng/ml recombinant Wnt3a (R&D Systems Inc., Minneapolis, MN) or vehicle for 4 h prior to lysis and RNA isolation.

After DNase treatment, purified RNA samples (n = 4 per condition) were submitted to the University of Michigan Advanced Genomics Core for quality control, library preparation, and sequencing on an Illumina Hi-Seq platform. Read files were downloaded and collated into a single .fastq file for each sample. Quality of raw read data was checked using FastQC (version v0.11.30) to identify features of the data that may indicate quality problems (i.e. low-quality scores, over-represented sequences, inappropriate GC content). The Tuxedo Suite software package was used for alignment, differential expression analysis, and post-analysis diagnostics. Briefly, reads were aligned to the UCSC reference genome using TopHat (version 2.0.13) and Bowtie2 (version 2.2.1). FastQC was used for a second round of quality control post-alignment to ensure that only high-quality data was input to expression quantitation and differential expression analyses. Differential expression analysis was done using two distinct methods: Cufflinks/CuffDiff and HTSeq/DESeq2, using UCSC build mm10 as the reference genome sequence. To generate lists of Wnt-related genes significantly regulated by adipogenesis or recombinant Wnt3a treatment, data were analyzed using GOrilla (Gene Ontology Enrichment Analysis and Visualization Tool) and the PANTHER Classification System. The Wnt Homepage (<http://web.stanford.edu/group/nusselab/cgi-bin/wnt/>) was also used to generate a list of established Wnt pathway genes. The complete RNAseq dataset was then mined to identify Wnt-related genes that are up- or down-regulated during adipogenesis, or in response to Wnt3a.

Untargeted proteomics analysis

Cultured day 12 *Wls^{fl/fl}* and *Wls^{-/-}* adipocytes were washed three times with PBS to remove serum. Cells were homogenized using a BioVortexer mixer (Chemglass, Vineland, NJ) in ice-cold lysis buffer (1% SDS, 12.7 mM EDTA, 60 mM Tris-HCl; pH 6.8) containing 1:100 protease inhibitor cocktail (Sigma-Aldrich, St. Louis, MO). Lysates were then centrifuged at 13,600 x g for 10 min at 4°C and the supernatant was submitted to the University of Michigan Proteomics and Peptide Synthesis Core for untargeted proteomics analysis. In short, 12 µl of each sample was processed by SDS-PAGE using a 10% Bis-Tris NuPAGE mini-gel (Invitrogen, Carlsbad, CA) with MES buffer. The gel was excised into 10 equally sized bands and processed by in-gel

digestion with trypsin using a Digilab ProGest robot (Accela, Prague, Czech Republic). Half of each digest was analyzed by nano LC-MS/MS with a Waters NanoAcquity HPLC system interfaced to a ThermoFisher Q Exactive. Peptides were loaded on a trapping column and eluted over a 75 μ m analytic column at 350 nL/min; both columns were packed with Luna C18 resin. The mass spectrometer was operated in data-dependent mode, with the Orbitrap operating at 70,000 FWHM and 17,500 FWHM for MS and MS/MS, respectively. The 15 most abundant ions were selected for MS/MS. Data was queried using Mascot with the following parameters: enzyme: Trypsin/P; database: SwissProt Mouse; fixed modification: carbamidomethyl (C); variable modifications: oxidation (M), acetyl (N-term), pyro-Glu (N-term Q); deamidation (N, Q); mass value: monoisotopic; peptide mass tolerance: 10 ppm; fragment mass tolerance: 0.02 Da; max missed cleavages: 2. Mascot DAT files were parsed into Scaffold (Proteome Software, Portland, OR) for validation, filtering and to create a non-redundant list per sample. Data were filtered using a 1% protein and peptide FDR and requiring at least 2 unique peptides per protein.

Immunoblot analyses

Tissues were collected from mice and homogenized using a BioVortexer mixer (Chemglass, Vineland, NJ) in ice-cold lysis buffer (1% SDS, 12.7 mM EDTA, 60 mM Tris-HCl; pH 6.8) containing 1:100 protease inhibitor cocktail (Sigma-Aldrich, St. Louis, MO). Lysates were then centrifuged at 13,600 x g for 10 min at 4°C. For WAT lysates, the top lipid layer was removed, and extracts were centrifuged again. Cultured cells were washed once with PBS and homogenized in lysis buffer containing 1:100 protease inhibitor cocktail. Lysates were then centrifuged at 13,600 x g for 10 min at 4°C. Protein concentrations of cell or tissue lysates were measured by BCA protein assay (Thermo Scientific, Waltham, MA). Lysates were diluted to equal protein concentrations in lysis buffer and Laemmli sample buffer, vortexed vigorously, and heated at 95°C for 5 min. Cell or tissue extracts (20 μ g) were separated by SDS-PAGE on 4-12% gradient polyacrylamide gels (Invitrogen, Carlsbad, CA) and transferred to Immobilon PVDF membranes (Millipore, Billerica, MA). Membranes were blocked in 5% non-fat dried milk in Tris-buffered saline, pH 7.4, containing 0.05% Tween-20 (TTBS) for 1 h at room

temperature and then immunoblotted with indicated primary antibodies (1:1000) in 5% BSA in TTBS overnight at 4°C. Blots were probed with horseradish peroxidase-conjugated secondary antibodies (1:5000) diluted in 5% non-fat dried milk in TTBS for 1.5 h at room temperature and visualized with Clarity Western ECL Substrate (Bio-Rad, Hercules, CA) or SuperSignal West Femto Maximum Sensitivity Substrate (Thermo Scientific, Waltham, MA).

Human gene expression data

Human *Wls* gene expression data were acquired from the publicly available Genotype-Tissue Expression (GTEx) database.

Statistics

All data are presented as mean \pm S.D. When comparing two groups, significance was determined using two-tailed Student's t-test. When comparing multiple experimental groups, an analysis of variance (ANOVA) was followed by post hoc analyses with Dunnett's or Sidak's test, as appropriate. Differences were considered significant at $p < 0.05$ and are indicated with asterisks.

Figure 3.1

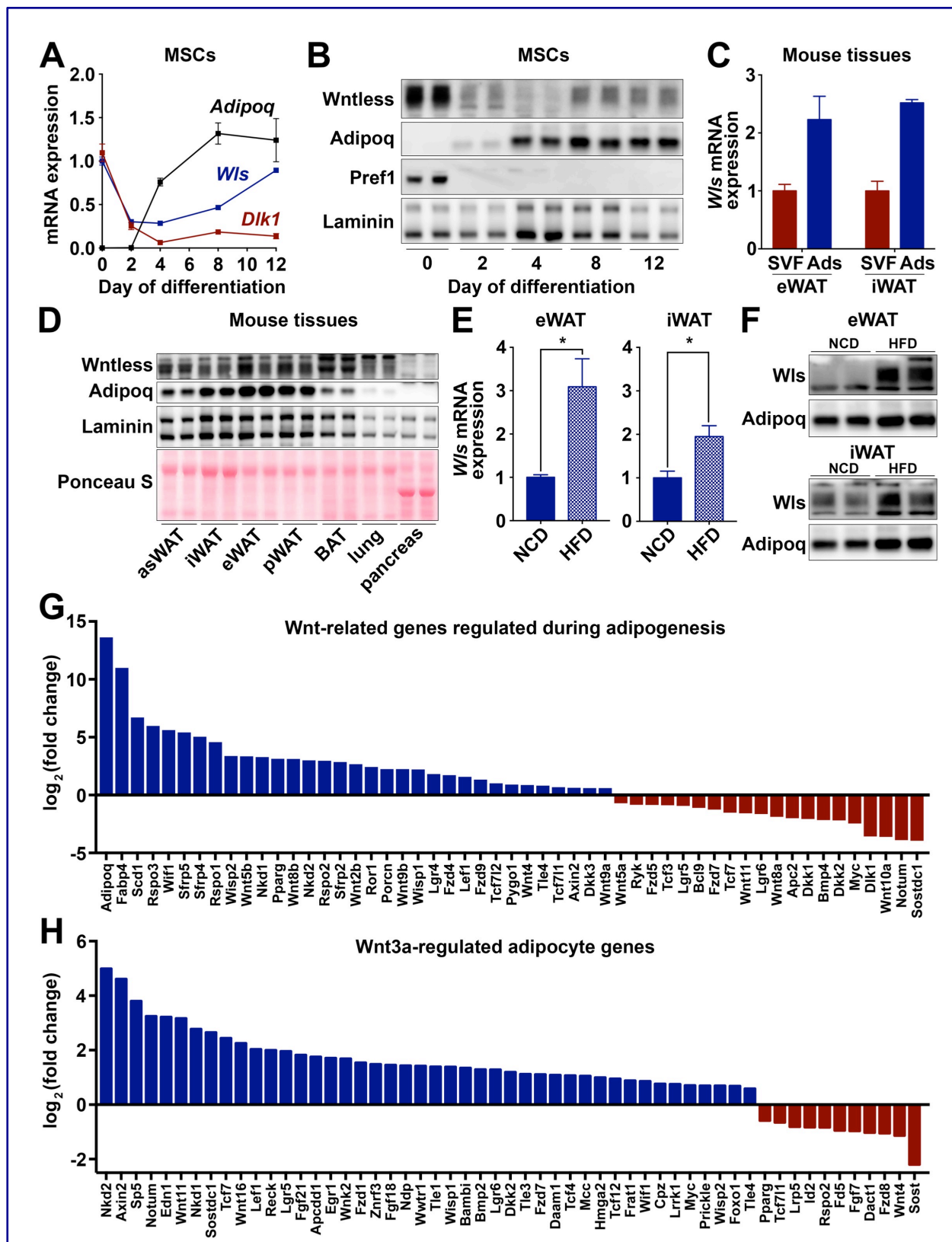
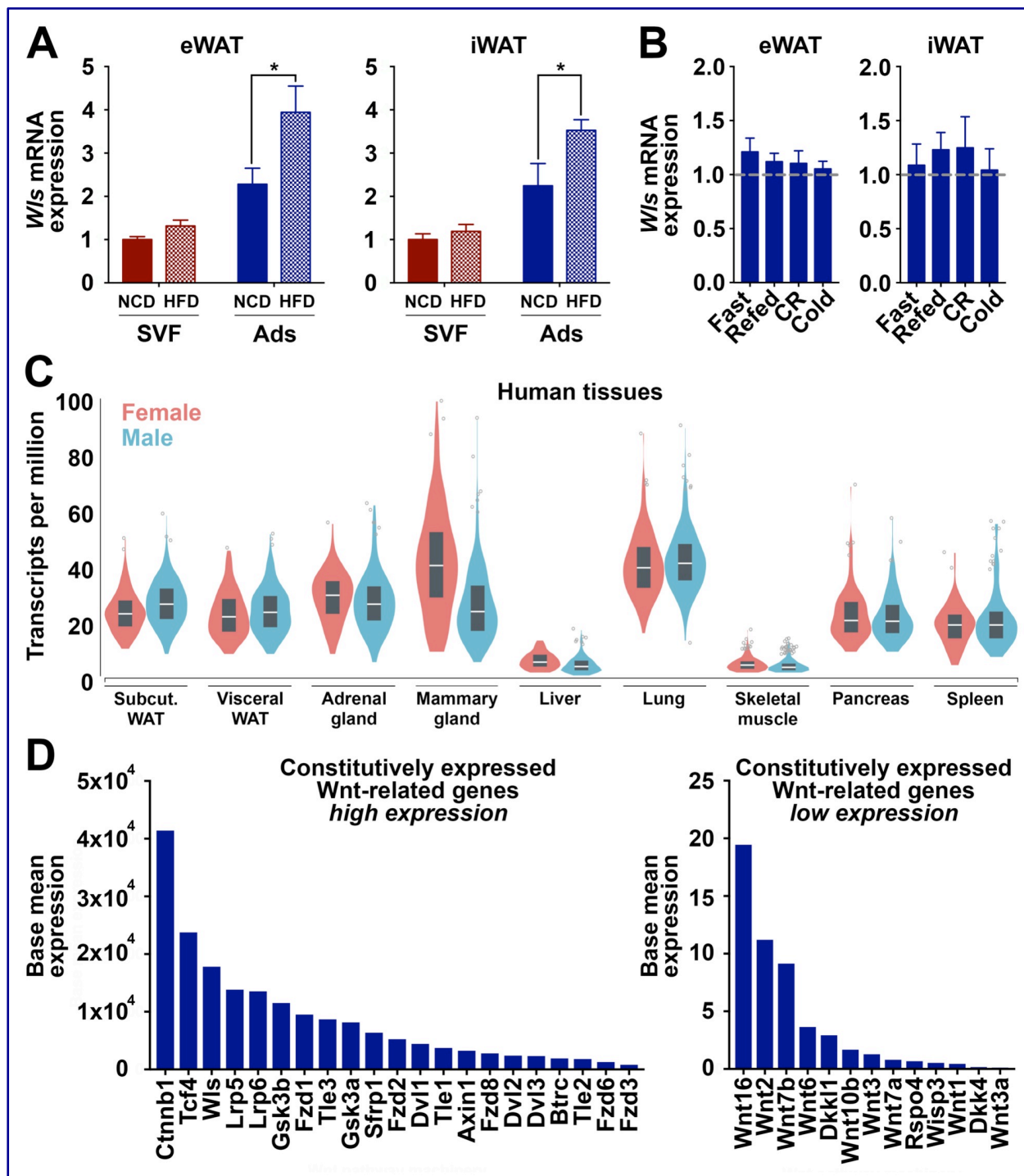


Figure 3.1. Canonical Wnt signaling is active in cultured adipocytes and Wntless is up-regulated by diet-induced obesity. (A-B) MSCs isolated from C57BL/6J mice were cultured under standard conditions and induced to differentiate. Wntless gene (n = 6) and protein expression at indicated days of differentiation. (C) Wntless gene expression in the stromal-vascular (SVF) and adipocyte (Ads) fractions isolated from epididymal (eWAT) and inguinal (iWAT) white adipose tissues of C57BL/6J mice (males; n = 6). (D) Representative immunoblot of Wntless protein expression across C57BL/6J mouse tissues (asWAT, anterior subcutaneous WAT; pWAT, perirenal WAT; BAT, brown adipose tissue); Adiponectin, Laminin, and Ponceau S included as controls. (E-F) Regulation of Wntless gene and protein expression in eWAT and iWAT of 16-week-old wildtype mice fed with normal chow diet (NCD) or 8 weeks of high fat diet (HFD) (males; n = 6). (G) Wnt-related genes found to be significantly up- or down-regulated by RNA-seq analyses of day 12 adipocytes vs. day 0 cultured MSCs (n = 4). (H) Select Wnt-related genes found to be significantly up- or down-regulated by RNA-seq analyses of day 12 cultured adipocytes treated with recombinant Wnt3a (20 ng/ml) for 4 h (n = 4). RNA expression normalized to PPIA. Data presented as mean \pm S.D. * indicates significance at $p < 0.05$.

Supplemental Figure 3.1



Supplemental Figure 3.1. (A) Wntless gene expression in the stromal-vascular (SVF) and adipocyte (Ads) fractions isolated from eWAT and inguinal iWAT of 16-week-old wildtype mice fed with NCD or 8 weeks of HFD (males; n = 6). (B) Regulation of Wntless gene expression in eWAT and iWAT by nutritional and environmental conditions: fast: 18 h; refed: 6 h after 18 h fast; 30% calorie restriction (CR): 6 wks; 4°C cold exposure: 6 hr. Each condition normalized to its individual experimental control set to 1 (indicated by grey dashed line). (C) Wntless gene expression in male and female human tissues; data obtained from the GTEx-RNA-Seq dataset. (D) Wnt-related genes found by RNA-seq analyses to be expressed at similar levels in both day 12 adipocytes and confluent day 0 cultured MSCs (n = 4). RNA expression normalized to PPIA. Data presented as mean \pm S.D. * indicates significance at $p < 0.05$.

Figure 3.2

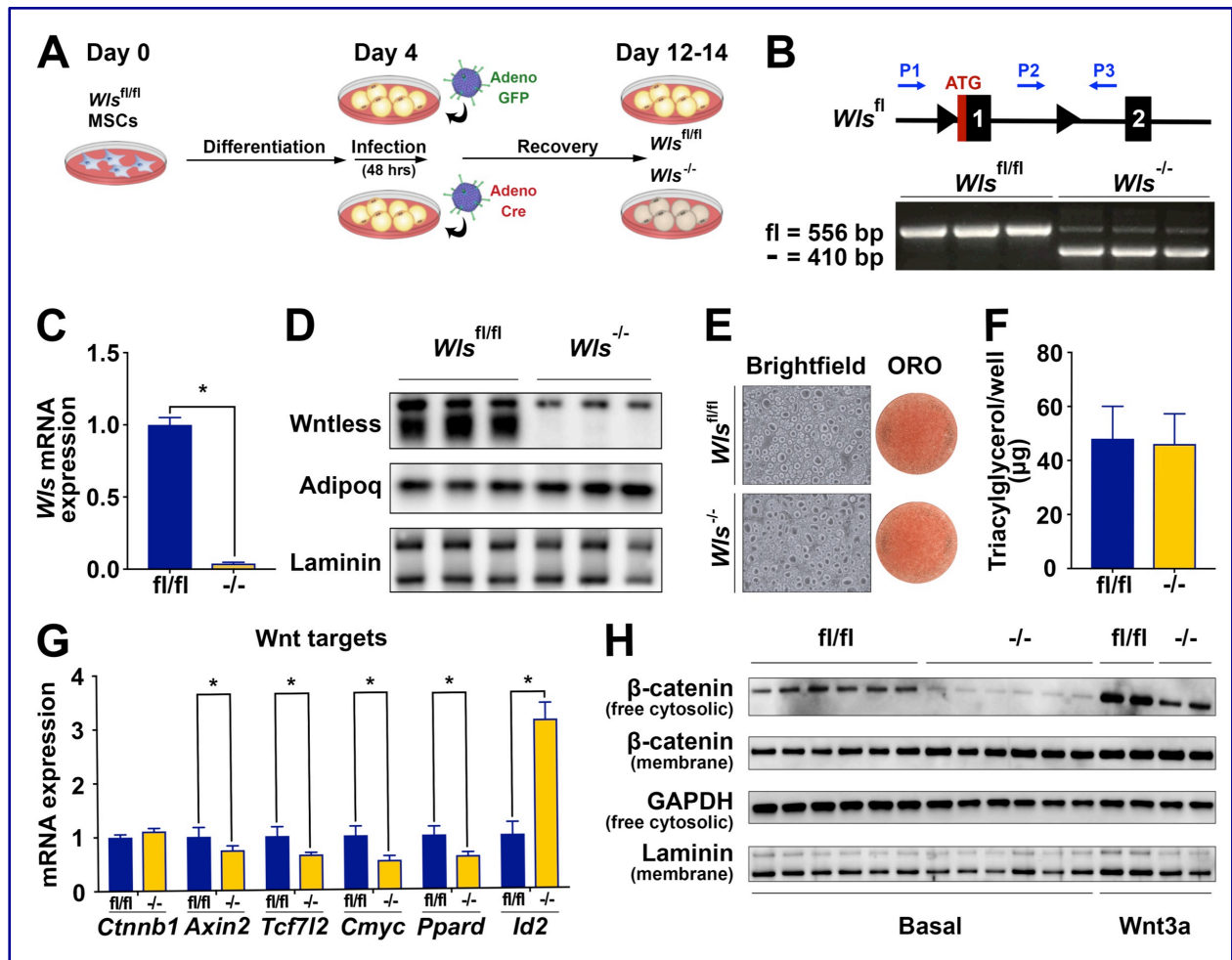
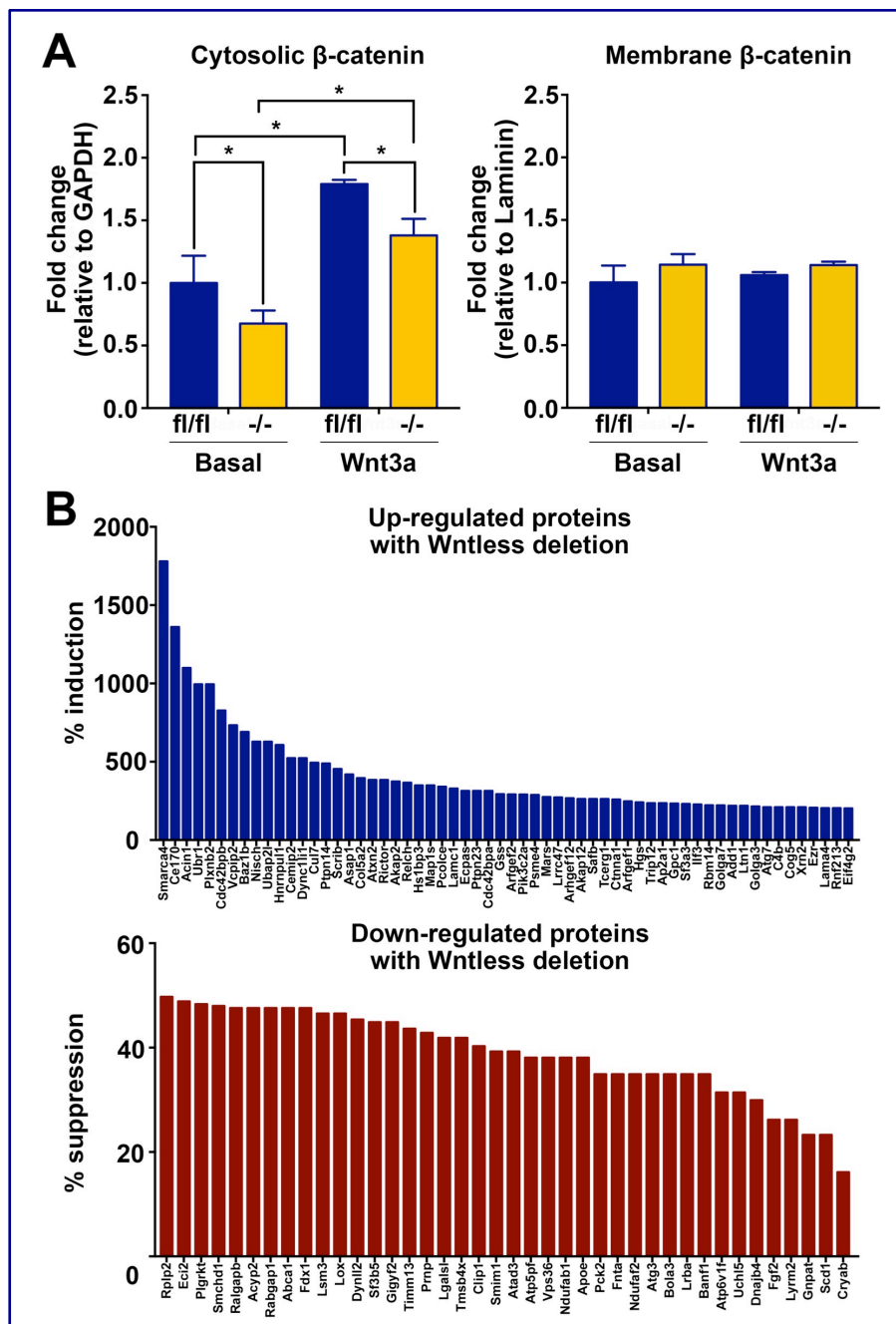


Figure 3.2. Wntless is required for canonical Wnt signaling in differentiated primary adipocytes. (A) Schematic model for deletion of Wntless in cultured adipocytes using adenoviral Cre recombinase. (B) Genetic recombination of Wntless in *Wls*^{fl/fl} and *Wls*^{-/-} adipocytes using a 3-primer PCR system (n = 3). (C-D) Wntless RNA and protein expression in adipocytes following adenoviral GFP or Cre infection (n = 3). (E) Representative brightfield and Oil Red-O images, and (F) triacylglycerol accumulation in *Wls*^{fl/fl} and *Wls*^{-/-} adipocytes (n = 4). (G) Expression of known Wnt target genes in *Wls*^{fl/fl} and *Wls*^{-/-} adipocytes (n = 3). (H) Free cytosolic and membrane β -catenin protein expression in *Wls*^{fl/fl} and *Wls*^{-/-} confluent MSCs under basal conditions (n = 6) and after 20 ng/ml Wnt3a treatment for 4 h (n = 2); GAPDH and laminin shown as cytosolic and membrane loading controls, respectively. RNA expression normalized to PPIA. Data presented as mean \pm S.D. * indicates significance at p < 0.05.

Supplemental Figure 3.2



Supplemental Figure 3.2. (A) Densitometry quantification of cytosolic and membranous β -catenin protein expression in $W/s^{fl/fl}$ and $W/s^{-/-}$ day 0 MSCs under basal conditions and after 20 ng/ml Wnt3a treatment for 4 h ($n = 6$). (B) Proteins found by untargeted proteomics analysis to be increased over 200% or decreased more than 50% in cultured day 12 $W/s^{-/-}$ adipocytes ($n = 1$). Data presented as mean \pm S.D. * indicates significance at $p < 0.05$.

Figure 3.3

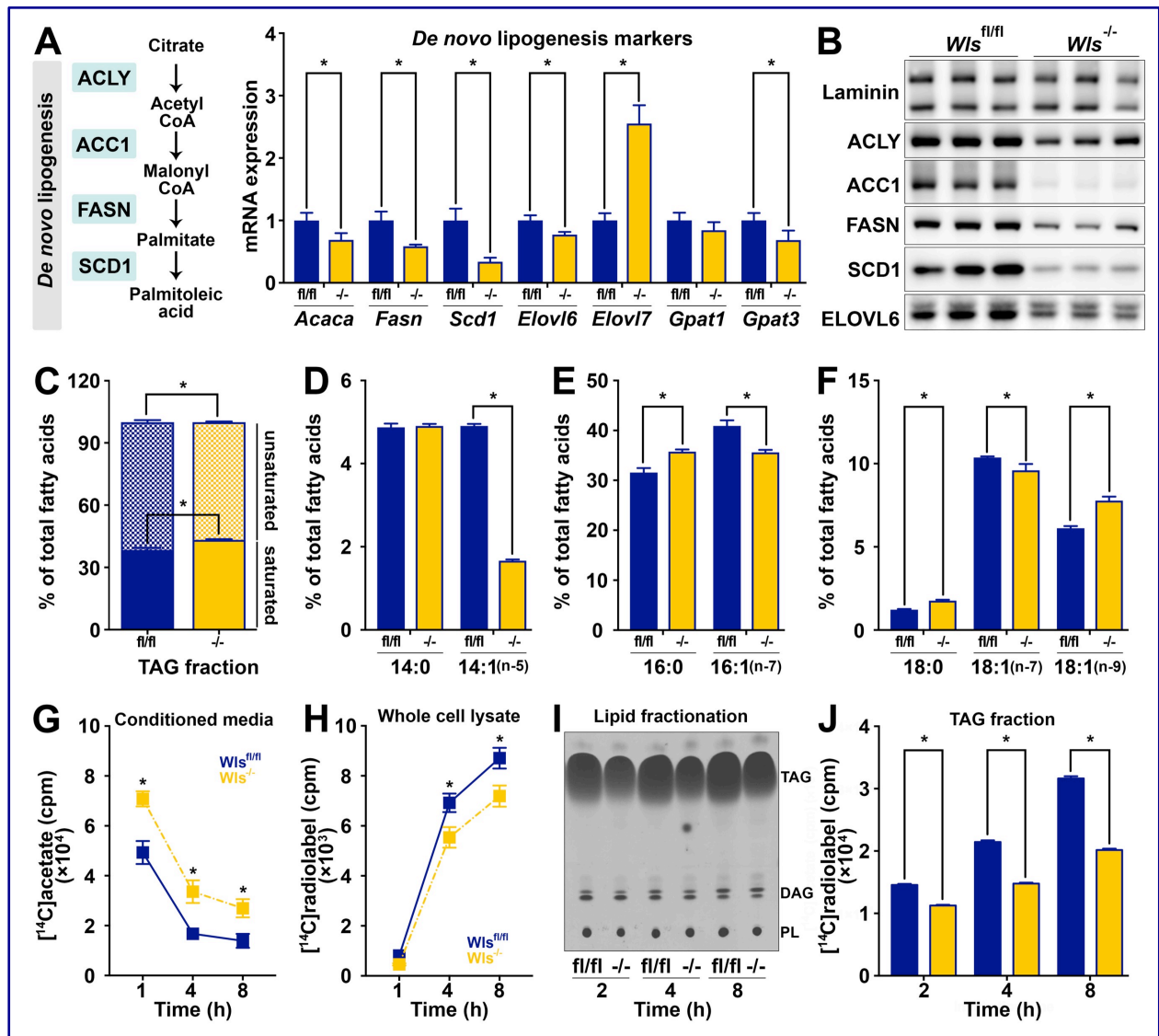
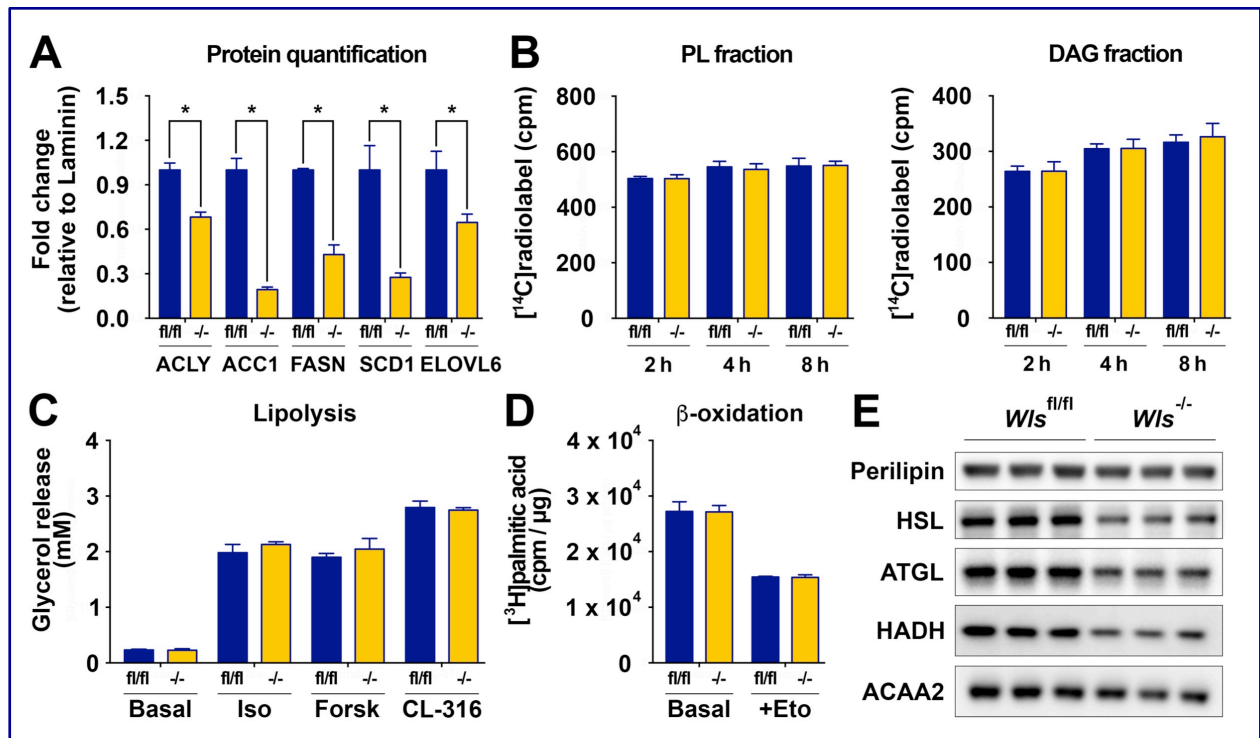


Figure 3.3. Adipocyte Wntless regulates expression of a network of lipogenic genes and influences triacylglycerol fatty acid composition and *de novo* lipogenesis. (A-B) Lipogenic gene and protein expression in *Wis*^{fl/fl} and *Wis*^{-/-} adipocytes (n = 3). RNA expression normalized to PPIA. (C) Proportion of total saturated (solid) versus unsaturated fatty acids (hatched) in lipids extracted from *Wis*^{fl/fl} and *Wis*^{-/-} adipocytes (n = 6). Relative proportions of (D) myristic (C14:0) versus myristoleic acid (C14:1), (E) palmitic (C16:0) versus palmitoleic acid (C16:1), and (F) stearic (C18:0) versus vaccenic (C18:1, n-7) or oleic acid (C18:1, n-9). *De novo* lipogenesis was evaluated in cultured *Wis*^{fl/fl} and *Wis*^{-/-} adipocytes using [¹⁴C]-acetate for 1, 2, 4 and 8 h. [¹⁴C]-radiolabel in (G) conditioned media versus (H) whole cell lysates after indicated incubation times was measured by scintillation counting (n = 3). (I) Representative thin-layer chromatography analysis of [¹⁴C]-acetate incorporation into lipid species over indicated incubation times; TAG, triacylglycerol; DAG, diacylglycerol;

PL, phospholipid. (J) Radiolabel incorporation into TAG fractions extracted from $Wts^{fl/fl}$ and $Wts^{-/-}$ adipocytes was quantified by scintillation counting (n = 3). Data presented as mean \pm S.D. * indicates significance at $p < 0.05$.

Supplemental Figure 3.3



Supplemental Figure 3.3. (A) Lipogenic proteins quantified by densitometry (n = 3). (B) *De novo* lipogenesis was evaluated in cultured *Wts^{fl/fl}* and *Wts^{-/-}* adipocytes using [¹⁴C]-acetate for 1, 2, 4 and 8 h. Radiolabel incorporation into PL and DAG fractions extracted from *Wts^{fl/fl}* and *Wts^{-/-}* adipocytes was quantified by scintillation counting (n = 3). (C) Basal and induced glycerol release from *Wts^{fl/fl}* and *Wts^{-/-}* adipocytes using 1 μM isoproterenol (Iso), 5 μM forskolin (Forsk), or 1 μM CL-316,243 (CL-316) for 3 h (n = 3). (D) β-oxidation of [³H]-palmitic acid; 100 μM etomoxir used as negative control (n = 3). (E) Expression of proteins related to lipolysis or β-oxidation (n = 3). Data presented as mean ± S.D. * indicates significance at p < 0.05.

Figure 3.4

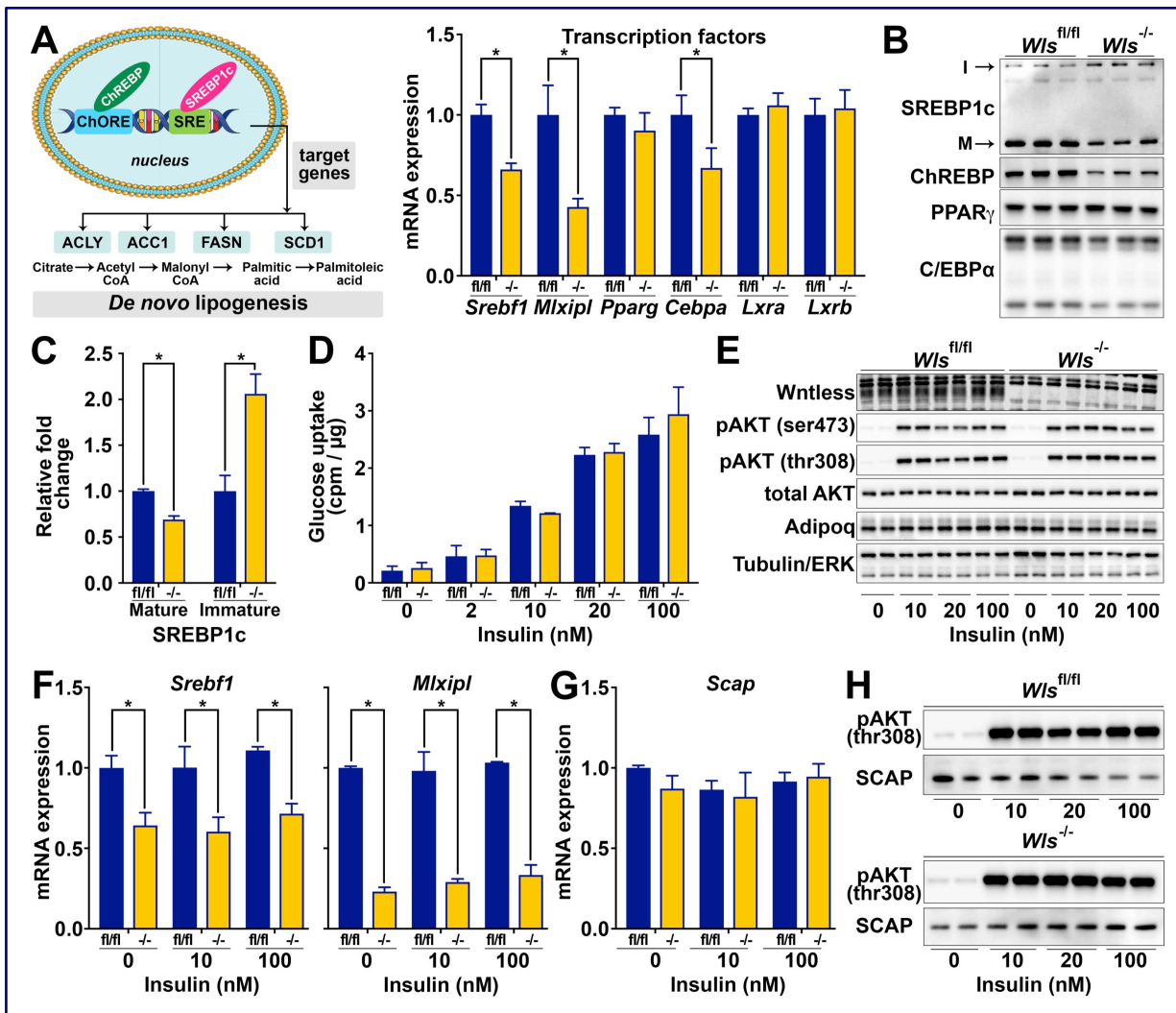
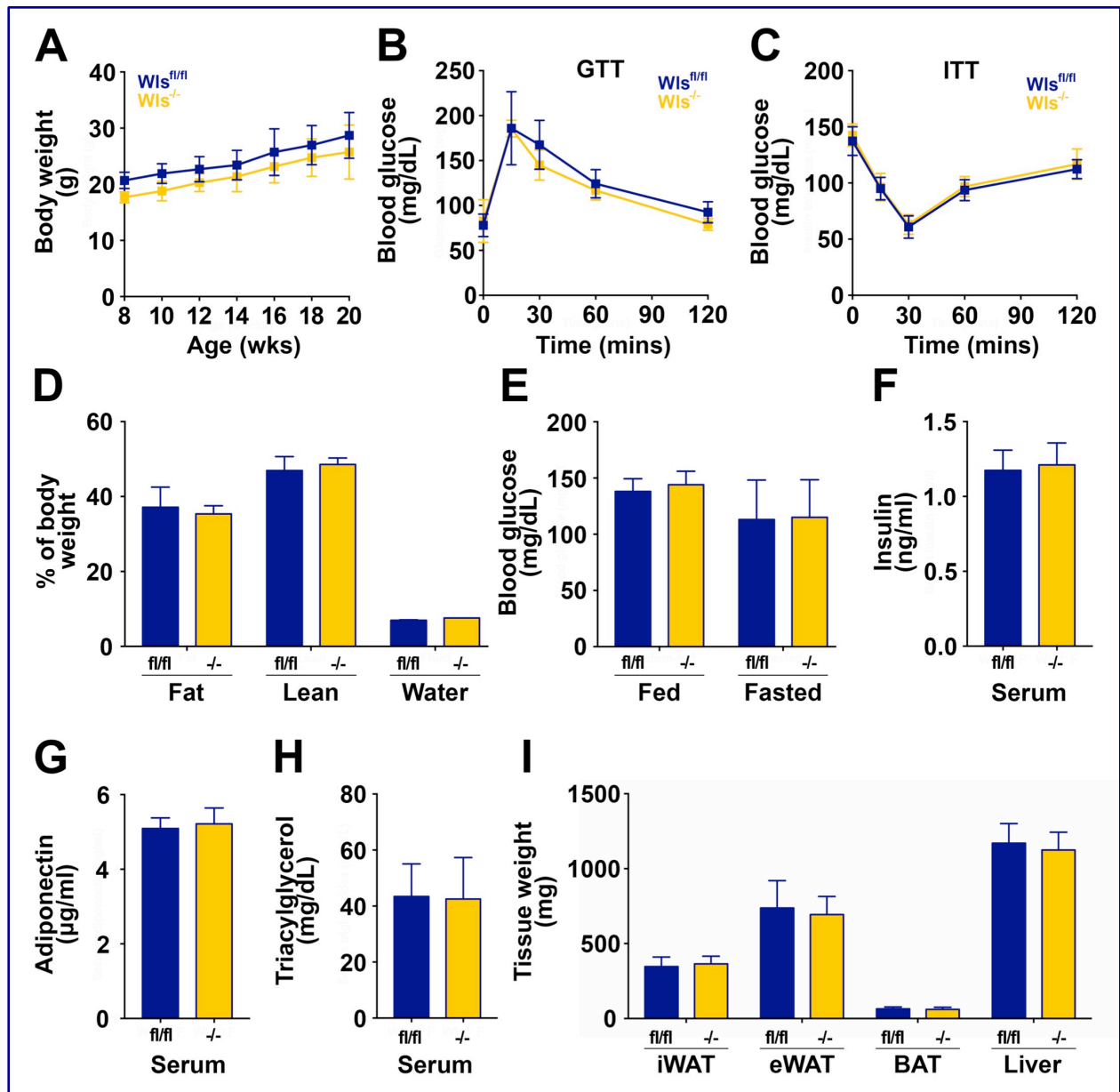


Figure 3.4. Wntless is required for expression of *Srebf1* and *Mlxipl*, transcriptional regulators of lipogenesis. (A-B) Gene and protein expression of indicated transcription factors (n = 3); I: immature, insoluble form of SREBP1c at relative mobility of 100 kDa; M: mature, soluble form of SREBP1c at 50 kDa. (C) Mature versus immature forms of SREBP1c quantified by densitometry. (D) Basal and insulin-stimulated glucose uptake into *Wts*^{fl/fl} and *Wts*^{-/-} adipocytes (n = 3). (E) Representative immunoblot of AKT phosphorylation in *Wts*^{fl/fl} and *Wts*^{-/-} adipocytes following treatment with indicated insulin concentrations for 10 min. (F) Expression of *Srebf1* or *Mlxipl* mRNAs in *Wts*^{fl/fl} and *Wts*^{-/-} adipocytes following treatment with indicated insulin concentrations for 24 h (n = 3). (G) Expression of *Scap* mRNA in *Wts*^{fl/fl} and *Wts*^{-/-} adipocytes following treatment with indicated insulin concentrations for 24 h (n = 3). (H) Representative immunoblot of SCAP protein expression in *Wts*^{fl/fl} and *Wts*^{-/-} adipocytes following treatment with indicated insulin concentrations for 10 min; pAKT(thr308) shown as a control for insulin response. RNA expression normalized to PPIA. Data presented as mean \pm S.D. * indicates significance at p < 0.05.

Supplemental Figure 3.4



Supplemental Figure 3.4. (A) Growth curve of 20-week-old female $Wis^{fl/fl}$ and $Wis^{-/-}$ mice on NCD. (B) Glucose tolerance test in 16-week-old $Wis^{fl/fl}$ and $Wis^{-/-}$ mice. (C) Insulin tolerance test in 18-week-old mice. (D) Body composition of 16-week-old $Wis^{fl/fl}$ and $Wis^{-/-}$ mice. (E) Blood glucose concentrations in random-fed and 16 h fasted mice. Serum concentrations of (F) insulin, (G) adiponectin, and (H) triacylglycerols in 20-week-old mice. (I) Tissue weights at time of sacrifice. $Wis^{fl/fl}$: n = 7; $Wis^{-/-}$: n = 9. Data presented as mean \pm S.D. * indicates significance at p < 0.05.

Figure 3.5

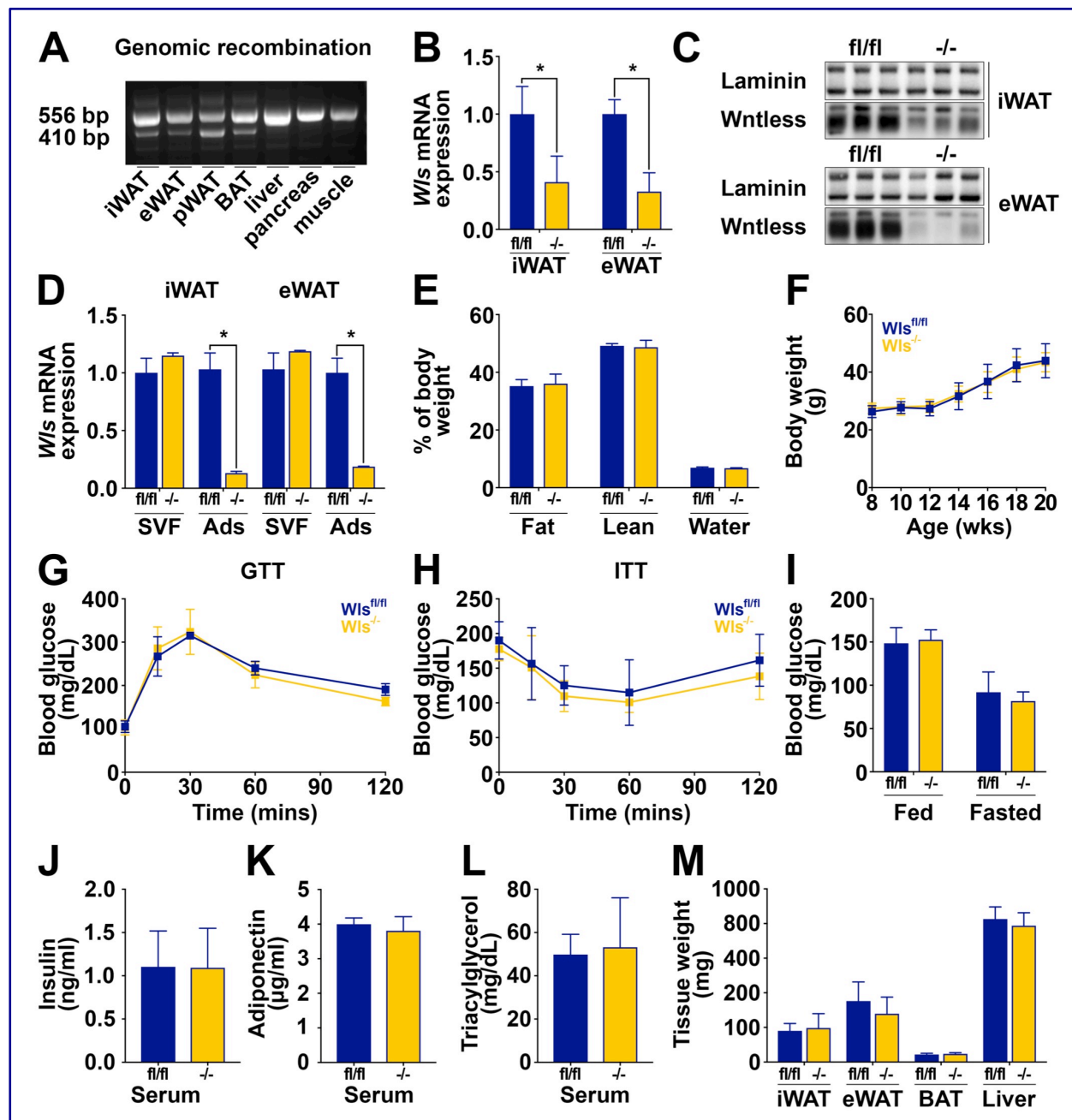
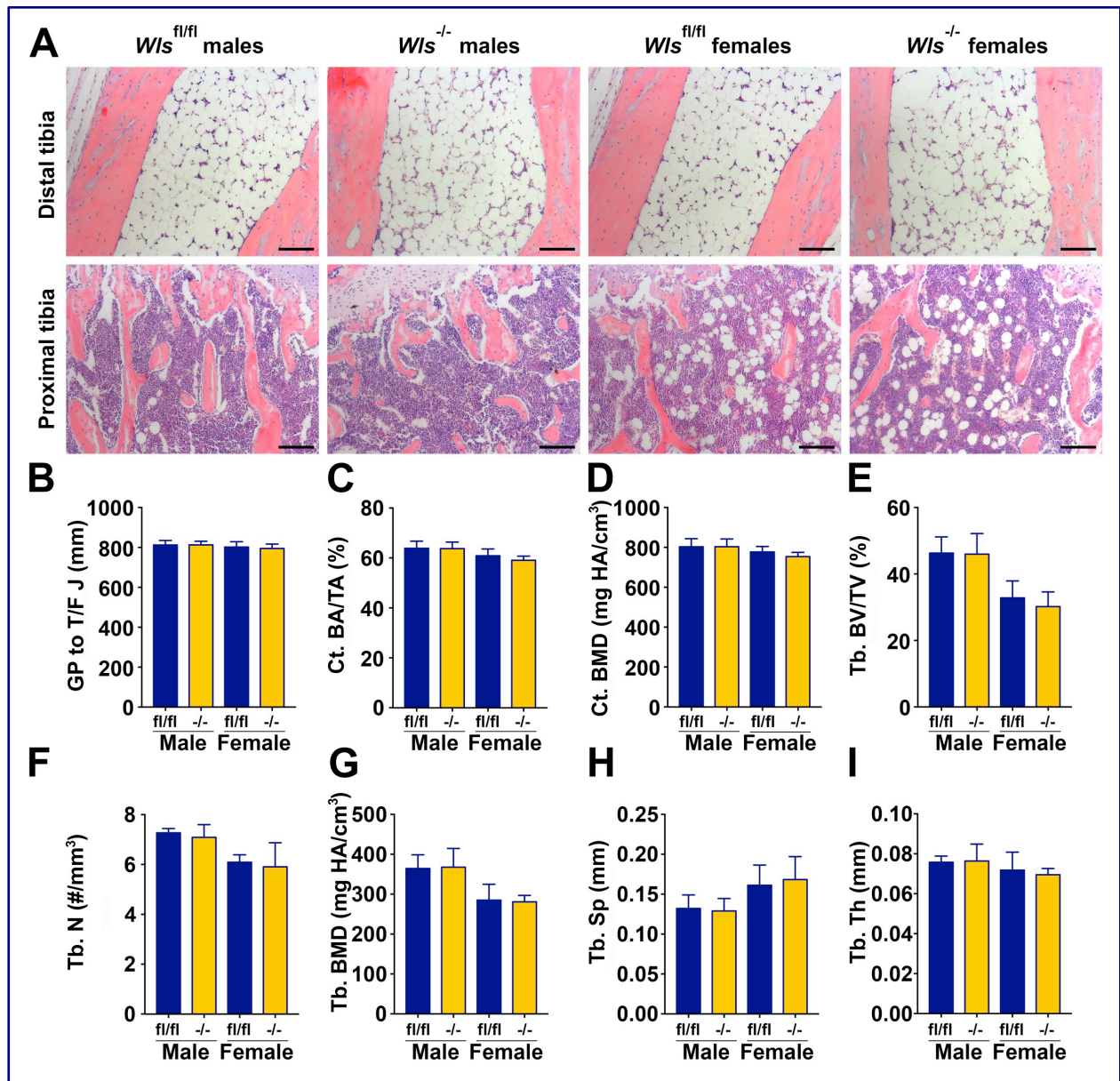


Figure 3.5. Adipose-specific Wntless deletion does not influence whole-body metabolism on a normal chow diet. (A) Genetic recombination of Wntless in tissues isolated from *Wts*^{-/-} mice. (B-C) Wntless mRNA and protein expression in iWAT and eWAT of *Wts*^{fl/fl} and *Wts*^{-/-} mice. (D) Wntless mRNA expression in SVF and adipocytes isolated from iWAT and eWAT of *Wts*^{fl/fl} and *Wts*^{-/-} mice (n = 3). (E) Body composition of 16-week-old *Wts*^{fl/fl} and *Wts*^{-/-} mice on NCD. (F) Growth curve of 20-week-old *Wts*^{fl/fl} and *Wts*^{-/-} mice on NCD. (G) Glucose tolerance test in 16-week-old *Wts*^{fl/fl} and *Wts*^{-/-} mice. (H) Insulin tolerance test in 18-week-old mice. (I) Blood glucose concentrations in random-fed and

16 h fasted mice. Serum concentrations of (**J**) insulin, (**K**) adiponectin, and (**L**) triacylglycerols in 20-week-old mice. (**M**) Tissue weights at time of sacrifice. RNA expression normalized to PPIA. Data shown in **E-M** from male mice, n = 5 per group. Data presented as mean \pm S.D. * indicates significance at $p < 0.05$.

Supplemental Figure 3.5



Supplemental Figure 3.5. (A) Representative histological images of H&E-stained distal and proximal tibia of male and female *Wls*^{fl/fl} and *Wls*^{-/-} mice fed NCD for 20 weeks; 100x magnification; scale bar, 50 μ m. μ CT analyses of (B) tibial length measured by distance from growth plate (GP) to tibia/fibula junction (T/F J), (C) mid-tibia cortical bone area (Ct. BA/TA), (D) bone mineral density (Ct. BMD), (E) tibial trabecular bone volume fraction (Tb. BV/TV), (F) trabecular number (Tb. N), (G) trabecular bone mineral density (Tb. BMD), (H) trabecular separation (Tb. Sp) and (I) trabecular thickness (Tb. Th). Data presented as mean \pm S.D. * indicates significance at $p < 0.05$.

Figure 3.6

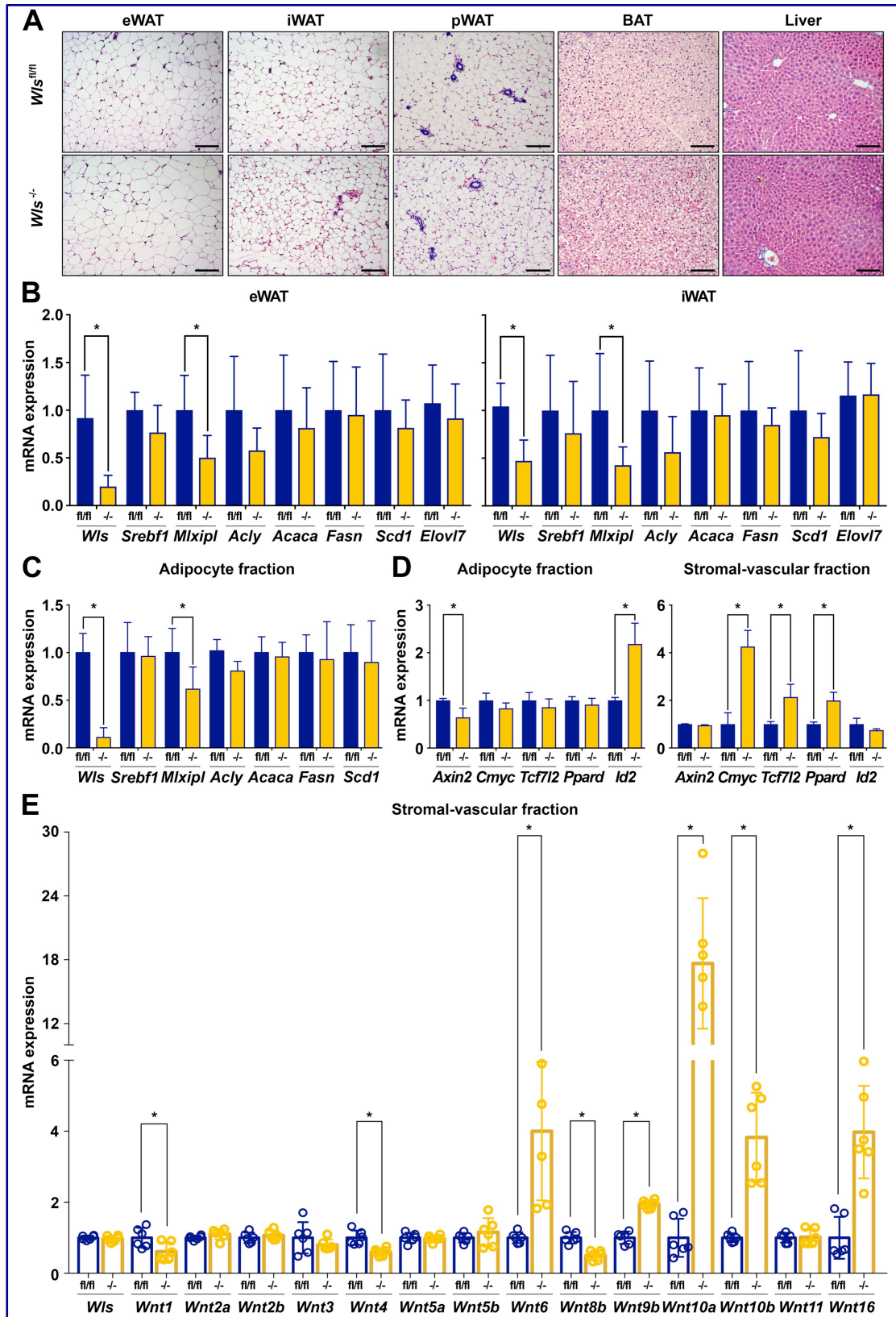
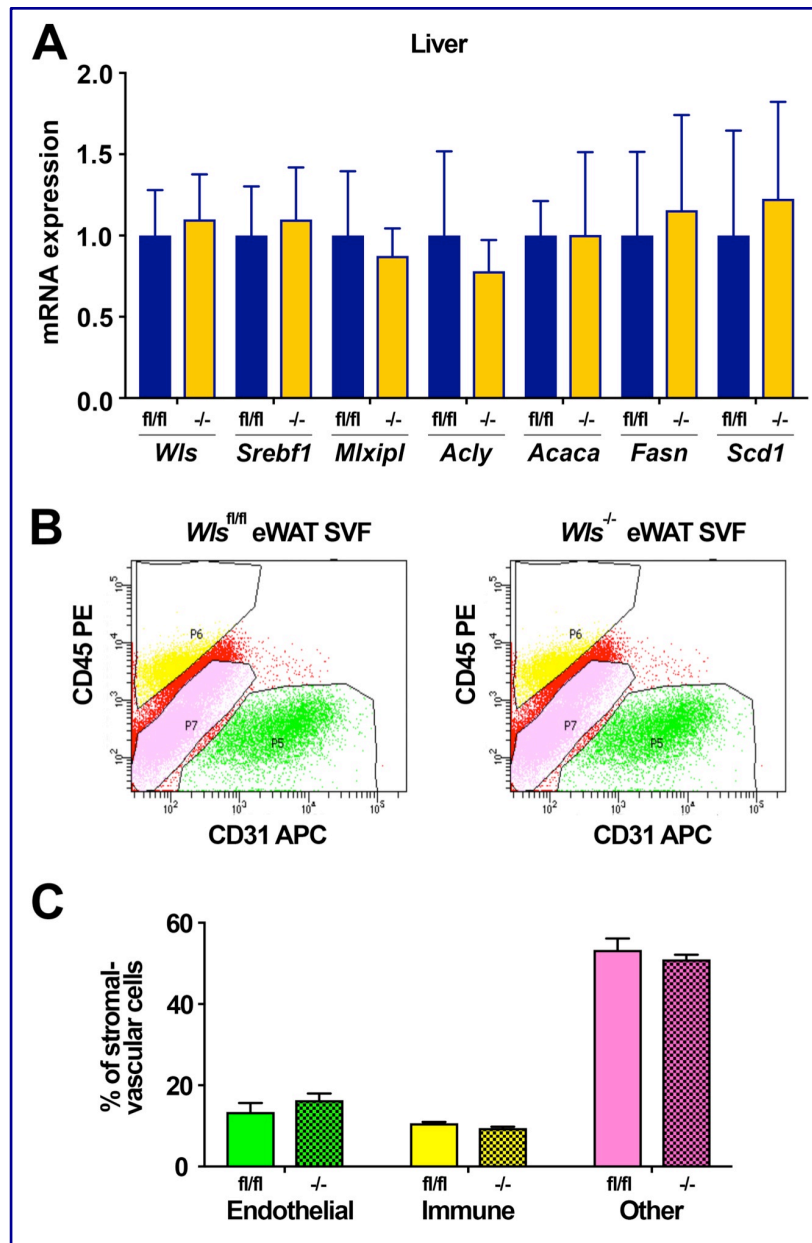


Figure 3.6. Adipose tissues compensate for adipocyte-specific Wntless deficiency by increasing Wnt signaling in stromal-vascular cells. (A) Representative histological images of H&E-stained tissues from *Wls^{fl/fl}* and *Wls^{-/-}* mice fed normal chow diet for 20 weeks; 200x magnification; scale bar, 100 μ m. (B) Lipogenic gene expression in eWAT and iWAT isolated from *Wls^{fl/fl}* and *Wls^{-/-}* mice. (C) Lipogenic gene expression in isolated eWAT adipocytes (n = 7). (D) Wnt target gene expression in isolated eWAT adipocytes and SVF of *Wls^{fl/fl}* and *Wls^{-/-}* mice (n = 5). (E) Expression of Wnt mRNAs in SVF isolated from eWAT of *Wls^{fl/fl}* and *Wls^{-/-}* mice (n = 6). Data shown from male mice. RNA expression normalized to PPIA. Data presented as mean \pm S.D. * indicates significance at $p < 0.05$.

Supplemental Figure 3.6



Supplemental Figure 3.6. (A) Lipogenic gene expression in livers isolated from male *Wts^{fl/fl}* and *Wts^{-/-}* mice on NCD. (B) Representative plots of flow cytometric analyses of eWAT SVF isolated from male *Wts^{fl/fl}* and *Wts^{-/-}* mice, stained with CD31-APC (endothelial cells) and CD45-PE (immune cells). (C) Quantification of SVF cell populations based on flow cytometric analyses (n = 6). RNA expression normalized to PPIA. Data presented as mean ± S.D. * indicates significance at p < 0.05.

Figure 3.7

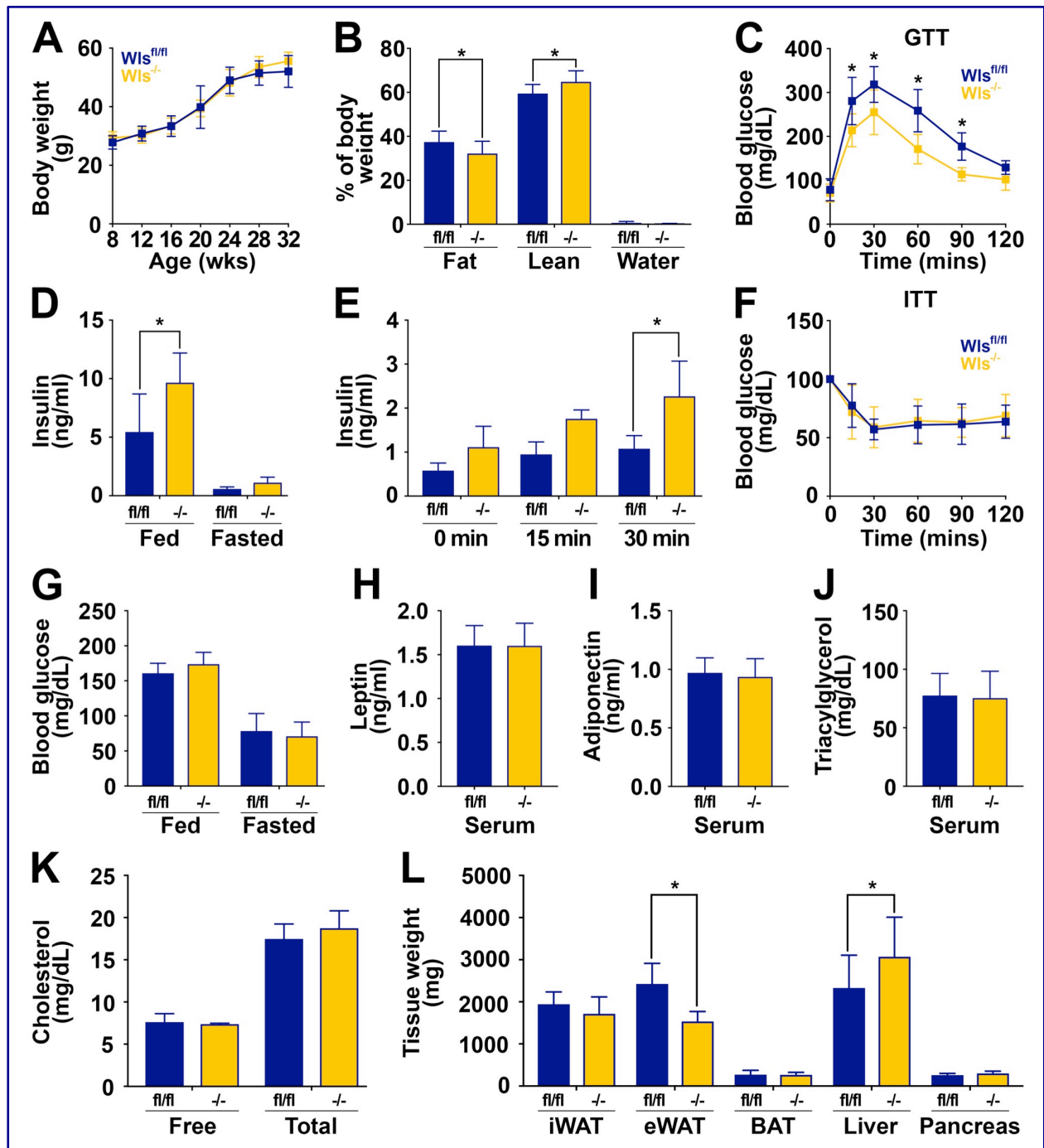
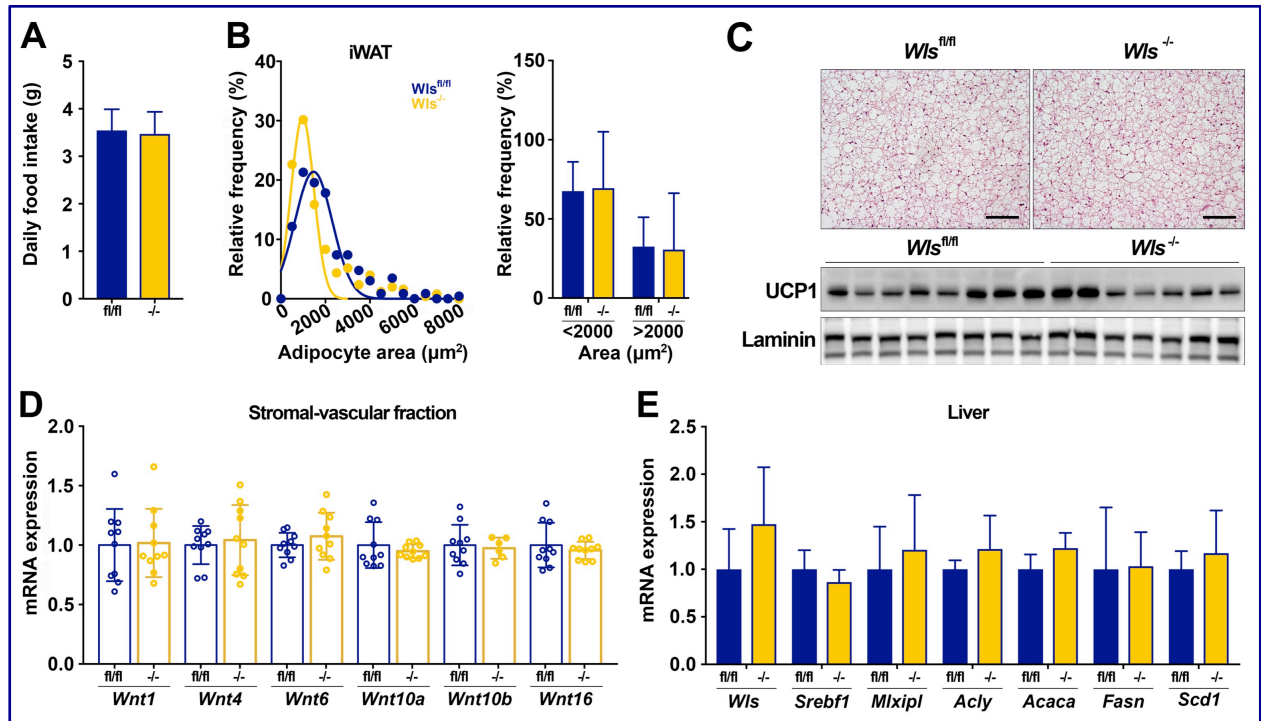


Figure 3.7. $Wts^{-/-}$ mice on HFD have decreased eWAT and improved glucose tolerance. (A) Growth curve over time of 32-week-old $Wts^{fl/fl}$ and $Wts^{-/-}$ mice fed 60% HFD for 24 weeks. (B) Body composition analysis of 28-week-old mice. (C) Glucose tolerance test in 28-week-old mice. (D) Serum insulin concentrations in fed and 16 h fasted mice. (E) Serum insulin concentrations in 16 h fasted mice at indicated times after intraperitoneal glucose injection (1 mg/kg body weight). (F) Insulin tolerance test in

30-week-old mice. **(G)** Blood glucose concentrations in random-fed and 16 h fasted mice. Circulating concentrations of **(H)** leptin, **(I)** adiponectin, **(J)** triacylglycerols, and **(K)** total and free cholesterol in 32-week-old mice. **(L)** Tissue weights of mice at time of sacrifice. Data shown from male mice; $W/s^{fl/fl}$: n = 8; $W/s^{-/-}$: n = 7. Data presented as mean \pm S.D. * indicates significance at $p < 0.05$.

Supplemental Figure 3.7



Supplemental Figure 3.7. (A) Daily food intake of male *Wls^{fl/fl}* and *Wls^{-/-}* mice fed HFD for 24 weeks. (B) Adipocyte size quantification of iWAT (400-500 adipocytes/mouse; n = 8, 7). (C) Representative H&E-stained images and UCP1 protein expression in BAT of male *Wls^{fl/fl}* and *Wls^{-/-}* mice fed HFD for 24 weeks; 200x magnification; scale bar, 100 μm . (D) Expression of Wnt mRNAs in SVF isolated from eWAT of HFD-fed male *Wls^{fl/fl}* and *Wls^{-/-}* mice (n = 10). (E) Lipogenic gene expression in livers isolated from male *Wls^{fl/fl}* and *Wls^{-/-}* mice on HFD. RNA expression normalized to PPIA. Data presented as mean \pm S.D. * indicates significance at p < 0.05.

Figure 3.8

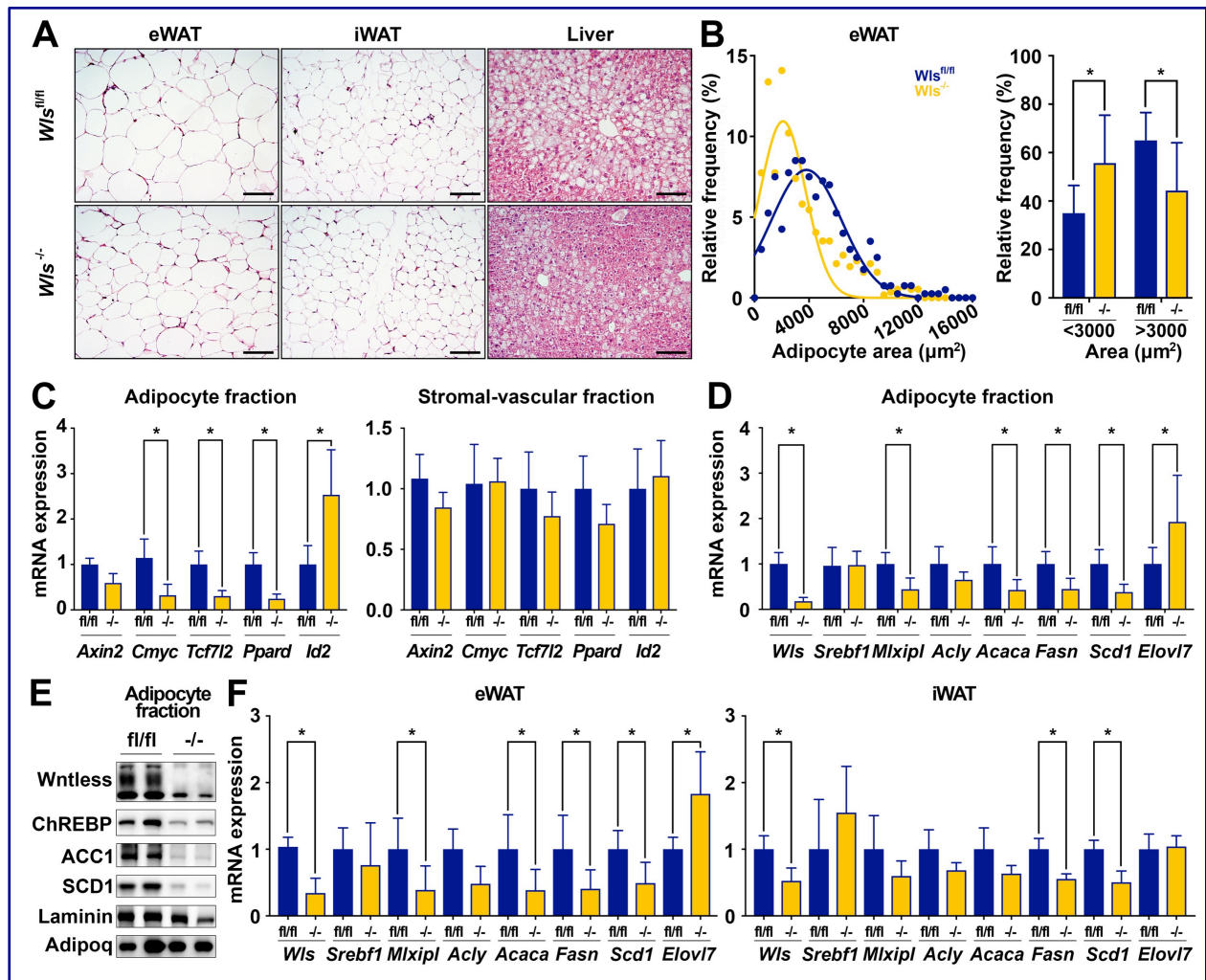


Figure 3.8. *Wts^{-/-}* mice on HFD have reduced epididymal adipocyte size and decreased DNL gene expression. (A) Representative histological images of H&E-stained tissues from *Wts^{fl/fl}* and *Wts^{-/-}* mice fed 60% HFD for 24 weeks; 200x magnification; scale bar, 100 μ m. (B) Adipocyte size quantification of eWAT (400-500 adipocytes/mouse, n = 8, 7). (C) Wnt target gene expression in adipocytes and SVF isolated from eWAT. (D-E) Lipogenic mRNA and protein expression in isolated eWAT adipocytes. (F) Lipogenic gene expression in eWAT and iWAT from *Wts^{fl/fl}* and *Wts^{-/-}* mice. Data shown from male mice. RNA expression normalized to PPIA. Data presented as mean \pm S.D. * indicates significance at p < 0.05.

Figure 3.9

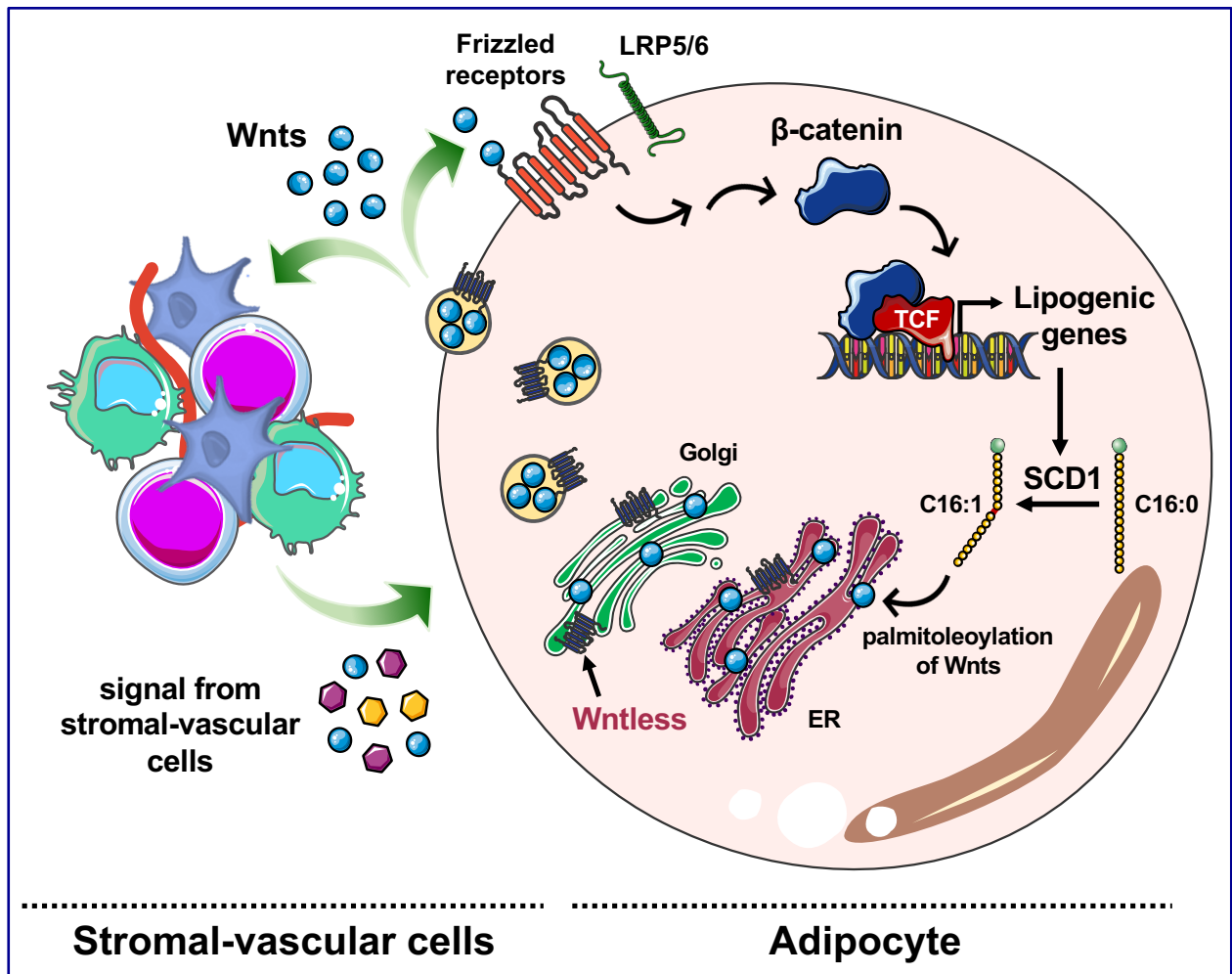


Figure 3.9. Schematic depicting the consequences of adipocyte-specific deletion of *Wntless*. Adipocyte-derived Wnts are required for expression of a network of lipogenic genes and loss of secreted Wnts in *Wls*^{-/-} adipocytes is sensed and compensated for by surrounding stromal-vascular cells to maintain tissue-wide Wnt signaling homeostasis.

References

1. Cadigan KM, Nusse R. Wnt signaling: a common theme in animal development. *Genes Dev.* 1997;11(24):3286-3305.
2. Clevers H. Wnt/beta-catenin signaling in development and disease. *Cell.* 2006;127(3):469-480.
3. Clevers H, Nusse R. Wnt/beta-catenin signaling and disease. *Cell.* 2012;149(6):1192-1205.
4. Prestwich TC, Macdougald OA. Wnt/beta-catenin signaling in adipogenesis and metabolism. *Curr Opin Cell Biol.* 2007;19(6):612-617.
5. Ross S. E. HN, Longo K. A., Bennett C. N., Lucas P. C., Erickson R. L., MacDougald O. A. Inhibition of adipogenesis by Wnt signaling. *Science.* 2000;289(5481):950-953.
6. Bennett CN, Ross SE, Longo KA, et al. Regulation of Wnt signaling during adipogenesis. *J Biol Chem.* 2002;277(34):30998-31004.
7. Moldes M, Zuo Y, Morrison RF, et al. Peroxisome-proliferator-activated receptor gamma suppresses Wnt/beta-catenin signalling during adipogenesis. *Biochem J.* 2003;376(Pt 3):607-613.
8. Villanueva CJ, Waki H, Godio C, et al. TLE3 is a dual-function transcriptional coregulator of adipogenesis. *Cell Metab.* 2011;13(4):413-427.
9. Christodoulides C, Lagathu C, Sethi JK, Vidal-Puig A. Adipogenesis and WNT signalling. *Trends Endocrinol Metab.* 2009;20(1):16-24.
10. Sethi JK, Vidal-Puig A. Wnt signalling and the control of cellular metabolism. *Biochem J.* 2010;427(1):1-17.
11. Lagathu C, Christodoulides C, Virtue S, et al. Dact1, a nutritionally regulated preadipocyte gene, controls adipogenesis by coordinating the Wnt/beta-catenin signaling network. *Diabetes.* 2009;58(3):609-619.
12. Cawthorn WP, Bree AJ, Yao Y, et al. Wnt6, Wnt10a and Wnt10b inhibit adipogenesis and stimulate osteoblastogenesis through a beta-catenin-dependent mechanism. *Bone.* 2012;50(2):477-489.
13. Longo KA, Wright WS, Kang S, et al. Wnt10b inhibits development of white and brown adipose tissues. *J Biol Chem.* 2004;279(34):35503-35509.
14. Wright WS, Longo KA, Dolinsky VW, et al. Wnt10b inhibits obesity in ob/ob and agouti mice. *Diabetes.* 2007;56(2):295-303.
15. Bennett CN, Longo KA, Wright WS, et al. Regulation of osteoblastogenesis and bone mass by Wnt10b. *Proc Natl Acad Sci U S A.* 2005;102(9):3324-3329.
16. Bennett CN, Ouyang H, Ma YL, et al. Wnt10b increases postnatal bone formation by enhancing osteoblast differentiation. *J Bone Miner Res.* 2007;22(12):1924-1932.
17. Kang S, Bennett CN, Gerin I, Rapp LA, Hankenson KD, Macdougald OA. Wnt signaling stimulates osteoblastogenesis of mesenchymal precursors by suppressing CCAAT/enhancer-binding protein alpha and peroxisome proliferator-activated receptor gamma. *J Biol Chem.* 2007;282(19):14515-14524.
18. Krishnan V, Bryant HU, Macdougald OA. Regulation of bone mass by Wnt signaling. *J Clin Invest.* 2006;116(5):1202-1209.

19. Grant SF, Thorleifsson G, Reynisdottir I, et al. Variant of transcription factor 7-like 2 (TCF7L2) gene confers risk of type 2 diabetes. *Nat Genet.* 2006;38(3):320-323.
20. Lyssenko V, Lupi R, Marchetti P, et al. Mechanisms by which common variants in the TCF7L2 gene increase risk of type 2 diabetes. *J Clin Invest.* 2007;117(8):2155-2163.
21. Jin T. Current Understanding on Role of the Wnt Signaling Pathway Effector TCF7L2 in Glucose Homeostasis. *Endocr Rev.* 2016;37(3):254-277.
22. Saarinen A, Saukkonen T, Kivela T, et al. Low density lipoprotein receptor-related protein 5 (LRP5) mutations and osteoporosis, impaired glucose metabolism and hypercholesterolaemia. *Clin Endocrinol (Oxf).* 2010;72(4):481-488.
23. Singh R, Smith E, Fathzadeh M, et al. Rare nonconservative LRP6 mutations are associated with metabolic syndrome. *Hum Mutat.* 2013;34(9):1221-1225.
24. Loh NY, Neville MJ, Marinou K, et al. LRP5 regulates human body fat distribution by modulating adipose progenitor biology in a dose- and depot-specific fashion. *Cell Metab.* 2015;21(2):262-273.
25. Shungin D, Winkler TW, Croteau-Chonka DC, et al. New genetic loci link adipose and insulin biology to body fat distribution. *Nature.* 2015;518(7538):187-196.
26. Heid IM, Jackson AU, Randall JC, et al. Meta-analysis identifies 13 new loci associated with waist-hip ratio and reveals sexual dimorphism in the genetic basis of fat distribution. *Nat Genet.* 2010;42(11):949-960.
27. Hao HX, Xie Y, Zhang Y, et al. ZNRF3 promotes Wnt receptor turnover in an R-spondin-sensitive manner. *Nature.* 2012;485(7397):195-200.
28. Zou Y, Ning T, Shi J, et al. Association of a gain-of-function variant in LGR4 with central obesity. *Obesity (Silver Spring).* 2017;25(1):252-260.
29. Van Camp JK, Beckers S, Zegers D, Verrijken A, Van Gaal LF, Van Hul W. Common genetic variation in sFRP5 is associated with fat distribution in men. *Endocrine.* 2014;46(3):477-484.
30. Christodoulides C, Scarda A, Granzotto M, et al. WNT10B mutations in human obesity. *Diabetologia.* 2006;49(4):678-684.
31. Kanazawa A, Tsukada S, Sekine A, et al. Association of the gene encoding wingless-type mammary tumor virus integration-site family member 5B (WNT5B) with type 2 diabetes. *Am J Hum Genet.* 2004;75(5):832-843.
32. Chen M, Lu P, Ma Q, et al. CTNNB1/beta-catenin dysfunction contributes to adiposity by regulating the cross-talk of mature adipocytes and preadipocytes. *Sci Adv.* 2020;6(2):eaax9605.
33. Mori H, Prestwich TC, Reid MA, et al. Secreted frizzled-related protein 5 suppresses adipocyte mitochondrial metabolism through WNT inhibition. *J Clin Invest.* 2012;122(7):2405-2416.
34. Geoghegan G, Simcox J, Seldin MM, et al. Targeted deletion of Tcf7l2 in adipocytes promotes adipocyte hypertrophy and impaired glucose metabolism. *Mol Metab.* 2019;24:44-63.
35. Das S, Yu S, Sakamori R, Stypulkowski E, Gao N. Wntless in Wnt secretion: molecular, cellular and genetic aspects. *Front Biol (Beijing).* 2012;7(6):587-593.

36. Banziger C, Soldini D, Schutt C, Zipperlen P, Hausmann G, Basler K. Wntless, a conserved membrane protein dedicated to the secretion of Wnt proteins from signaling cells. *Cell*. 2006;125(3):509-522.
37. Coombs GS, Yu J, Canning CA, et al. WLS-dependent secretion of WNT3A requires Ser209 acylation and vacuolar acidification. *J Cell Sci*. 2010;123(Pt 19):3357-3367.
38. Najdi R, Proffitt K, Sprowl S, et al. A uniform human Wnt expression library reveals a shared secretory pathway and unique signaling activities. *Differentiation*. 2012;84(2):203-213.
39. Herr P, Basler K. Porcupine-mediated lipidation is required for Wnt recognition by Wls. *Dev Biol*. 2012;361(2):392-402.
40. Rios-Esteves J, Haugen B, Resh MD. Identification of key residues and regions important for porcupine-mediated Wnt acylation. *J Biol Chem*. 2014;289(24):17009-17019.
41. Rios-Esteves J, Resh MD. Stearoyl CoA desaturase is required to produce active, lipid-modified Wnt proteins. *Cell Rep*. 2013;4(6):1072-1081.
42. Takada R, Satomi Y, Kurata T, et al. Monounsaturated fatty acid modification of Wnt protein: its role in Wnt secretion. *Dev Cell*. 2006;11(6):791-801.
43. Sun J, Yu S, Zhang X, et al. A Wntless-SEC12 complex on the ER membrane regulates early Wnt secretory vesicle assembly and mature ligand export. *J Cell Sci*. 2017;130(13):2159-2171.
44. Carpenter AC, Rao S, Wells JM, Campbell K, Lang RA. Generation of mice with a conditional null allele for Wntless. *Genesis*. 2010;48(9):554-558.
45. Fu J, Jiang M, Mirando AJ, Yu HM, Hsu W. Reciprocal regulation of Wnt and Gpr177/mouse Wntless is required for embryonic axis formation. *Proc Natl Acad Sci U S A*. 2009;106(44):18598-18603.
46. Preziosi M, Okabe H, Poddar M, Singh S, Monga SP. Endothelial Wnts regulate beta-catenin signaling in murine liver zonation and regeneration: A sequel to the Wnt-Wnt situation. *Hepatol Commun*. 2018;2(7):845-860.
47. Zhong Z, Zylstra-Diegel CR, Schumacher CA, et al. Wntless functions in mature osteoblasts to regulate bone mass. *Proc Natl Acad Sci U S A*. 2012;109(33):E2197-2204.
48. Jiang M, Ku WY, Fu J, Offermanns S, Hsu W, Que J. Gpr177 regulates pulmonary vasculature development. *Development*. 2013;140(17):3589-3594.
49. Cornett B, Snowball J, Varisco BM, Lang R, Whitsett J, Sinner D. Wntless is required for peripheral lung differentiation and pulmonary vascular development. *Dev Biol*. 2013;379(1):38-52.
50. Zhu X, Zhu H, Zhang L, et al. Wls-mediated Wnts differentially regulate distal limb patterning and tissue morphogenesis. *Dev Biol*. 2012;365(2):328-338.
51. Shao W, Espenshade PJ. Expanding roles for SREBP in metabolism. *Cell Metab*. 2012;16(4):414-419.
52. Horton JD, Goldstein JL, Brown MS. SREBPs: activators of the complete program of cholesterol and fatty acid synthesis in the liver. *J Clin Invest*. 2002;109(9):1125-1131.

53. Iizuka K, Bruick RK, Liang G, Horton JD, Uyeda K. Deficiency of carbohydrate response element-binding protein (ChREBP) reduces lipogenesis as well as glycolysis. *Proc Natl Acad Sci U S A*. 2004;101(19):7281-7286.
54. Mancini R, Noto A, Pisanu ME, De Vitis C, Maugeri-Sacca M, Ciliberto G. Metabolic features of cancer stem cells: the emerging role of lipid metabolism. *Oncogene*. 2018;37(18):2367-2378.
55. Mauvoisin D, Charfi C, Lounis AM, Rassart E, Mounier C. Decreasing stearoyl-CoA desaturase-1 expression inhibits beta-catenin signaling in breast cancer cells. *Cancer Sci*. 2013;104(1):36-42.
56. Fritz V, Benfodda Z, Rodier G, et al. Abrogation of de novo lipogenesis by stearoyl-CoA desaturase 1 inhibition interferes with oncogenic signaling and blocks prostate cancer progression in mice. *Mol Cancer Ther*. 2010;9(6):1740-1754.
57. Pisanu ME, Noto A, De Vitis C, et al. Blockade of Stearoyl-CoA-desaturase 1 activity reverts resistance to cisplatin in lung cancer stem cells. *Cancer Lett*. 2017;406:93-104.
58. Dai S, Yan Y, Xu Z, et al. SCD1 Confers Temozolomide Resistance to Human Glioma Cells via the Akt/GSK3beta/beta-Catenin Signaling Axis. *Front Pharmacol*. 2017;8:960.
59. Zhou Z, Lu Y, Wang Y, Du L, Zhang Y, Tao J. Let-7c regulates proliferation and osteodifferentiation of human adipose-derived mesenchymal stem cells under oxidative stress by targeting SCD-1. *Am J Physiol Cell Physiol*. 2019;316(1):C57-C69.
60. Jazurek-Ciesiolka M, Janikiewicz J, Dobrzyn P, Dziewulska A, Kozinski K, Dobrzyn A. Oleic acid increases the transcriptional activity of FoxO1 by promoting its nuclear translocation and beta-catenin binding in pancreatic beta-cells. *Biochim Biophys Acta Mol Basis Dis*. 2019;1865(10):2753-2764.
61. Ma XL, Sun YF, Wang BL, et al. Sphere-forming culture enriches liver cancer stem cells and reveals Stearoyl-CoA desaturase 1 as a potential therapeutic target. *BMC Cancer*. 2019;19(1):760.
62. Lengfeld JE, Lutz SE, Smith JR, et al. Endothelial Wnt/beta-catenin signaling reduces immune cell infiltration in multiple sclerosis. *Proc Natl Acad Sci U S A*. 2017;114(7):E1168-E1177.
63. Boulter L, Govaere O, Bird TG, et al. Macrophage-derived Wnt opposes Notch signaling to specify hepatic progenitor cell fate in chronic liver disease. *Nat Med*. 2012;18(4):572-579.
64. Chakrabarti R, Celia-Terrassa T, Kumar S, et al. Notch ligand Dll1 mediates cross-talk between mammary stem cells and the macrophageal niche. *Science*. 2018;360(6396).
65. Nusse R, Clevers H. Wnt/beta-Catenin Signaling, Disease, and Emerging Therapeutic Modalities. *Cell*. 2017;169(6):985-999.
66. Young CS, Kitamura M, Hardy S, Kitajewski J. Wnt-1 induces growth, cytosolic beta-catenin, and Tcf/Lef transcriptional activation in Rat-1 fibroblasts. *Mol Cell Biol*. 1998;18(5):2474-2485.

67. Miller JR, Moon RT. Analysis of the signaling activities of localization mutants of beta-catenin during axis specification in *Xenopus*. *J Cell Biol.* 1997;139(1):229-243.
68. Sampath H, Ntambi JM. The role of stearoyl-CoA desaturase in obesity, insulin resistance, and inflammation. *Ann N Y Acad Sci.* 2011;1243:47-53.
69. Paton CM, Ntambi JM. Biochemical and physiological function of stearoyl-CoA desaturase. *Am J Physiol Endocrinol Metab.* 2009;297(1):E28-37.
70. Ameer F, Scanduzzi L, Hasnain S, Kalbacher H, Zaidi N. De novo lipogenesis in health and disease. *Metabolism.* 2014;63(7):895-902.
71. Sanders FW, Griffin JL. De novo lipogenesis in the liver in health and disease: more than just a shunting yard for glucose. *Biol Rev Camb Philos Soc.* 2016;91(2):452-468.
72. Ralston JC, Badoud F, Cattrysse B, McNicholas PD, Mutch DM. Inhibition of stearoyl-CoA desaturase-1 in differentiating 3T3-L1 preadipocytes upregulates elongase 6 and downregulates genes affecting triacylglycerol synthesis. *Int J Obes (Lond).* 2014;38(11):1449-1456.
73. Wang Y, Viscarra J, Kim SJ, Sul HS. Transcriptional regulation of hepatic lipogenesis. *Nat Rev Mol Cell Biol.* 2015;16(11):678-689.
74. Tian J, Goldstein JL, Brown MS. Insulin induction of SREBP-1c in rodent liver requires LXRalpha-C/EBPbeta complex. *Proc Natl Acad Sci U S A.* 2016;113(29):8182-8187.
75. Linden AG, Li S, Choi HY, et al. Interplay between ChREBP and SREBP-1c coordinates postprandial glycolysis and lipogenesis in livers of mice. *J Lipid Res.* 2018;59(3):475-487.
76. Yabe D, Komuro R, Liang G, Goldstein JL, Brown MS. Liver-specific mRNA for Insig-2 down-regulated by insulin: implications for fatty acid synthesis. *Proc Natl Acad Sci U S A.* 2003;100(6):3155-3160.
77. Carobbio S, Hagen RM, Lelliott CJ, et al. Adaptive changes of the Insig1/SREBP1/SCD1 set point help adipose tissue to cope with increased storage demands of obesity. *Diabetes.* 2013;62(11):3697-3708.
78. Crewe C, Zhu Y, Paschoal VA, et al. SREBP-regulated adipocyte lipogenesis is dependent on substrate availability and redox modulation of mTORC1. *JCI Insight.* 2019;5.
79. Matsuda M, Korn BS, Hammer RE, et al. SREBP cleavage-activating protein (SCAP) is required for increased lipid synthesis in liver induced by cholesterol deprivation and insulin elevation. *Genes Dev.* 2001;15(10):1206-1216.
80. Yabe D, Brown MS, Goldstein JL. Insig-2, a second endoplasmic reticulum protein that binds SCAP and blocks export of sterol regulatory element-binding proteins. *Proc Natl Acad Sci U S A.* 2002;99(20):12753-12758.
81. Jeffery E, Berry R, Church CD, et al. Characterization of Cre recombinase models for the study of adipose tissue. *Adipocyte.* 2014;3(3):206-211.
82. Mukohira H, Hara T, Abe S, et al. Mesenchymal stromal cells in bone marrow express adiponectin and are efficiently targeted by an adiponectin promoter-driven Cre transgene. *Int Immunol.* 2019;31(11):729-742.

83. Li Z, Hardij J, Bagchi DP, Scheller EL, MacDougald OA. Development, regulation, metabolism and function of bone marrow adipose tissues. *Bone*. 2018;110:134-140.
84. Kennell JA, MacDougald OA. Wnt signaling inhibits adipogenesis through beta-catenin-dependent and -independent mechanisms. *J Biol Chem*. 2005;280(25):24004-24010.
85. Li FQ, Singh AM, Mofunanya A, et al. Chibby promotes adipocyte differentiation through inhibition of beta-catenin signaling. *Mol Cell Biol*. 2007;27(12):4347-4354.
86. Grunberg JR, Hoffmann JM, Hedjazifar S, et al. Overexpressing the novel autocrine/endocrine adipokine WISP2 induces hyperplasia of the heart, white and brown adipose tissues and prevents insulin resistance. *Sci Rep*. 2017;7:43515.
87. Murahovschi V, Pivovarova O, Ilkavets I, et al. WISP1 is a novel adipokine linked to inflammation in obesity. *Diabetes*. 2015;64(3):856-866.
88. Christodoulides C, Laudes M, Cawthorn WP, et al. The Wnt antagonist Dickkopf-1 and its receptors are coordinately regulated during early human adipogenesis. *J Cell Sci*. 2006;119(Pt 12):2613-2620.
89. Wiese KE, Nusse R, van Amerongen R. Wnt signalling: conquering complexity. *Development*. 2018;145(12).
90. Jho EH, Zhang T, Domon C, Joo CK, Freund JN, Costantini F. Wnt/beta-catenin/Tcf signaling induces the transcription of Axin2, a negative regulator of the signaling pathway. *Mol Cell Biol*. 2002;22(4):1172-1183.
91. Ross SE, Erickson RL, Gerin I, et al. Microarray analyses during adipogenesis: understanding the effects of Wnt signaling on adipogenesis and the roles of liver X receptor alpha in adipocyte metabolism. *Mol Cell Biol*. 2002;22(16):5989-5999.
92. ten Berge D, Brugmann SA, Helms JA, Nusse R. Wnt and FGF signals interact to coordinate growth with cell fate specification during limb development. *Development*. 2008;135(19):3247-3257.
93. Nakashima A, Katagiri T, Tamura M. Cross-talk between Wnt and bone morphogenetic protein 2 (BMP-2) signaling in differentiation pathway of C2C12 myoblasts. *J Biol Chem*. 2005;280(45):37660-37668.
94. Bertrand FE, Angus CW, Partis WJ, Sigounas G. Developmental pathways in colon cancer: crosstalk between WNT, BMP, Hedgehog and Notch. *Cell Cycle*. 2012;11(23):4344-4351.
95. Soshnikova N, Zechner D, Huelsken J, et al. Genetic interaction between Wnt/beta-catenin and BMP receptor signaling during formation of the AER and the dorsal-ventral axis in the limb. *Genes Dev*. 2003;17(16):1963-1968.
96. Carobbio S, Pellegrinelli V, Vidal-Puig A. Adipose Tissue Function and Expandability as Determinants of Lipotoxicity and the Metabolic Syndrome. *Adv Exp Med Biol*. 2017;960:161-196.
97. Qatanani M, Lazar MA. Mechanisms of obesity-associated insulin resistance: many choices on the menu. *Genes Dev*. 2007;21(12):1443-1455.
98. Kusminski CM, Bickel PE, Scherer PE. Targeting adipose tissue in the treatment of obesity-associated diabetes. *Nat Rev Drug Discov*. 2016;15(9):639-660.

99. Bagchi DP, Forss I, Mandrup S, MacDougald OA. SnapShot: Niche Determines Adipocyte Character I. *Cell Metab.* 2018;27(1):264-264 e261.
100. Bagchi DP, Forss I, Mandrup S, MacDougald OA. SnapShot: Niche Determines Adipocyte Character II. *Cell Metab.* 2018;27(1):266-266 e261.
101. Weise A, Bruser K, Elfert S, et al. Alternative splicing of Tcf7l2 transcripts generates protein variants with differential promoter-binding and transcriptional activation properties at Wnt/beta-catenin targets. *Nucleic Acids Res.* 2010;38(6):1964-1981.
102. Chen X, Ayala I, Shannon C, et al. The Diabetes Gene and Wnt Pathway Effector TCF7L2 Regulates Adipocyte Development and Function. *Diabetes.* 2018;67(4):554-568.
103. Kennell JA, O'Leary EE, Gummow BM, Hammer GD, MacDougald OA. T-cell factor 4N (TCF-4N), a novel isoform of mouse TCF-4, synergizes with beta-catenin to coactivate C/EBPalpha and steroidogenic factor 1 transcription factors. *Mol Cell Biol.* 2003;23(15):5366-5375.
104. Cristancho AG, Schupp M, Lefterova MI, et al. Repressor transcription factor 7-like 1 promotes adipogenic competency in precursor cells. *Proc Natl Acad Sci U S A.* 2011;108(39):16271-16276.
105. Hammond E, Lang J, Maeda Y, et al. The Wnt effector transcription factor 7-like 2 positively regulates oligodendrocyte differentiation in a manner independent of Wnt/beta-catenin signaling. *J Neurosci.* 2015;35(12):5007-5022.
106. Rulifson IC, Majeti JZ, Xiong Y, et al. Inhibition of secreted frizzled-related protein 5 improves glucose metabolism. *Am J Physiol Endocrinol Metab.* 2014;307(12):E1144-1152.
107. Bagchi DP, MacDougald OA. Identification and Dissection of Diverse Mouse Adipose Depots. *J Vis Exp.* 2019(149).
108. Parlee SD, Lentz SI, Mori H, MacDougald OA. Quantifying size and number of adipocytes in adipose tissue. *Methods Enzymol.* 2014;537:93-122.
109. Rim JS, Mynatt RL, Gawronska-Kozak B. Mesenchymal stem cells from the outer ear: a novel adult stem cell model system for the study of adipogenesis. *FASEB J.* 2005;19(9):1205-1207.
110. Gawronska-Kozak B. Preparation and differentiation of mesenchymal stem cells from ears of adult mice. *Methods Enzymol.* 2014;538:1-13.
111. Erickson RL, Hemati N, Ross SE, MacDougald OA. p300 coactivates the adipogenic transcription factor CCAAT/enhancer-binding protein alpha. *J Biol Chem.* 2001;276(19):16348-16355.
112. Scheller EL, Doucette CR, Learman BS, et al. Region-specific variation in the properties of skeletal adipocytes reveals regulated and constitutive marrow adipose tissues. *Nat Commun.* 2015;6:7808.

CHAPTER IV

Wnt/ β -catenin Signaling Regulates Adipose Tissue Lipogenesis and Adipocyte-Specific Loss is Rigorously Defended by Surrounding Stromal-Vascular Cells

Adapted from:

Bagchi DP, Li Z, Nishii A, DelProposto JB, Corsa CA, Hardij J, Mori H, Learman BS, Lumeng CN, MacDougald OA. Wnt/ β -catenin signaling regulates adipose tissue lipogenesis and adipocyte-specific loss is rigorously defended by neighboring stromal-vascular cells. *Mol Metab.* (accepted with minor revisions)

Abstract

Objective: Canonical Wnt/ β -catenin signaling is a well-studied endogenous regulator of mesenchymal cell fate determination, promoting osteoblastogenesis and inhibiting adipogenesis. However, emerging genetic evidence in humans links a number of Wnt pathway members to body fat distribution, obesity, and metabolic dysfunction, suggesting that this pathway also functions in adipocytes. Recent studies in mice have uncovered compelling evidence that the Wnt signaling pathway plays important roles in adipocyte metabolism, particularly under obesogenic conditions. However, complexities in Wnt signaling and differences in experimental models and approaches have thus far limited our understanding of its specific roles in this context. *Methods:* To investigate the roles of the canonical Wnt pathway in regulation of adipocyte metabolism, we generated adipocyte-specific β -catenin (*β -cat*) knockout mouse and culture cell models. We used RNA sequencing, ChIP sequencing, and molecular approaches to assess expression of Wnt targets and lipogenic genes. We then used functional assays to evaluate effects of β -catenin deficiency on adipocyte metabolism, including lipid and carbohydrate handling. In mice maintained on normal chow and high fat diets, we interrogated the cellular and functional consequences of adipocyte-specific β -catenin deletion on adipose tissues and systemic metabolism. *Results:* We report that in adipocytes, canonical Wnt/ β -catenin signaling regulates *de novo* lipogenesis (DNL) and fatty acid

monounsaturations. Further, β -catenin mediates effects of Wnt signaling on lipid metabolism in part by transcriptional regulation of *Mlxip1* and *Srebf1*. Intriguingly, adipocyte-specific loss of β -catenin is sensed and defended by CD45⁻/CD31⁻ stromal cells to maintain tissue-wide Wnt signaling homeostasis in chow-fed mice. With long-term high fat diet, this compensatory mechanism is overridden, revealing that β -catenin deletion promotes resistance to diet-induced obesity and adipocyte hypertrophy and subsequent protection from metabolic dysfunction. *Conclusions:* Taken together, these studies demonstrate that Wnt signaling in adipocytes is required for lipogenic gene expression, *de novo* lipogenesis, and lipid desaturation. In addition, adipose tissues rigorously defend Wnt signaling homeostasis under standard nutritional conditions, such that stromal-vascular cells sense and compensate for the adipocyte-specific loss. These findings underscore the critical importance of this pathway in adipocyte lipid metabolism and adipose tissue function.

Introduction

Canonical Wnt/ β -catenin signaling is an evolutionarily conserved pathway with well-established and diverse roles in cell proliferation and differentiation^{1,2}. Binding of canonical Wnts to their membrane-spanning frizzled receptors and low-density lipoprotein receptor-related protein (LRP) co-receptors activates a complex intracellular signaling cascade that results in the stabilization and accumulation of free cytosolic β -catenin^{3,4}. β -catenin can then translocate to the nucleus to bind to and coactivate DNA-binding T-cell factor/lymphoid enhancer-binding factor (TCF/LEF) proteins, thereby regulating Wnt target gene transcription^{2,5,6}.

Wnt signaling through the β -catenin-dependent pathway has been shown to have profound effects on mesenchymal cell fate determination and differentiation. Although this pathway is also involved in myogenesis and chondrogenesis⁷⁻⁹, its differential regulatory roles in adipogenesis and osteogenesis have been particularly well-studied. Indeed, stabilization of canonical signaling by enforced expression of Wnt3a, Wnt6, Wnt10a or Wnt10b, or a β -catenin stable mutant, in multipotent progenitor cells inhibits adipogenesis and promotes osteoblastogenesis¹⁰⁻¹⁴. Further, activation of canonical Wnt signaling in preadipocytes by enforced expression of Wnt1, Wnt10b, or a dominant-stable form of β -catenin, or pharmacological inhibition of glycogen synthase kinase 3, blocks adipogenesis by suppressing induction of the master adipogenic transcription factors PPAR γ and C/EBP α ¹⁵⁻¹⁷. In contrast, knockdown experiments in preadipocytes demonstrate that of the 19 Wnts, endogenous expression of Wnt6, Wnt10a, and Wnt10b contributes significantly to inhibition of adipogenesis¹⁰. Further, treatment of preadipocytes with soluble Wnt inhibitors sFRP1 or sFRP2, or overexpression of negative regulators of the canonical pathway, such as Axin or dominant-negative TCF4, results in spontaneous adipogenic differentiation^{18,19}. Enforced expression of β -catenin antagonist Chibby induces adipogenesis, whereas loss of Chibby up-regulates β -catenin transcriptional activity and inhibits adipogenic differentiation^{20,21}. Taken together, this significant body of work demonstrates that endogenous Wnt/ β -catenin signaling is a critical repressor of adipocyte differentiation.

Although Wnt signaling is an important regulator of adipose tissue development^{22,23}, increasing genetic evidence also links this pathway to adiposity, body fat distribution, and metabolic dysfunction in humans. For example, missense variations in canonical *WNT10B* are correlated with increased risk of type 2 diabetes²⁴, whereas polymorphisms in the Wnt inhibitor *SFRP5* locus are associated with decreased adiposity in men²⁵. In addition, common variants in *RSPO3* and *ZNRF3* have been implicated in increased waist-to-hip ratio²⁶⁻²⁸. Patients harboring loss-of-function mutations in Wnt co-receptors *LRP5* and *LRP6* are more likely to suffer from impaired glucose homeostasis, coronary disease, and osteoporosis^{29,30}; in contrast, gain-of-function mutations in *LRP5* are associated with increased adiposity and osteosclerosis³¹. Nonsense mutations in *LGR4*, a protein involved in stability of the Wnt co-receptor complex, are correlated with reduced adiposity and impaired bone formation and remodeling³², whereas patients with gain-of-function *LGR4* mutations are predisposed to increased visceral adiposity³³. Perhaps most striking, genome-wide association studies across a broad range of ethnic populations have strongly linked polymorphisms in the canonical Wnt transcriptional activator *TCF7L2* to increased susceptibility to type 2 diabetes³⁴⁻³⁶. Finally, during the course of our work, Chen *et al.* reported novel gain-of-function mutations in *CTNNB1* (β -catenin) that are associated with altered body fat distribution and predisposition to obesity³⁷. These studies provide compelling genetic evidence for distinct roles of canonical Wnt/ β -catenin signaling in body fat distribution and systemic metabolism.

A flurry of recent studies in mice have begun to investigate Wnt signaling in mature adipocytes, but its functional roles in this context remain unclear. For example, enforced expression of Wnt10b from the FABP4 promoter or stabilization of Wnt signaling through global deletion of the Wnt inhibitor secreted frizzled-related protein 5 (*SFRP5*) provides protection from diet-induced obesity^{22,23,38}. In contrast, adipocyte-specific *Tcf7l2* deletion in obese mice results in increased adipocyte hypertrophy and impaired glucose homeostasis³⁹. Work from our lab has demonstrated that loss of *Wntless*, and thus signaling by adipocyte-derived Wnts, protects mice from diet-induced obesity and metabolic dysfunction⁴⁰. Consistent with these findings, Chen *et al.* recently reported that β -catenin knockout mice are resistant to diet-induced obesity and exhibit

improved glucose homeostasis and insulin sensitivity compared to control counterparts³⁷. Taken together, these reports demonstrate that Wnt signaling plays an important role in mature adipocytes, particularly under obesogenic conditions. However, additional studies are required to unravel the detailed mechanisms by which different Wnt pathway members contribute to metabolic function of terminally-differentiated cells. To this end, we have chosen to investigate roles of β -catenin, the central protein in the canonical Wnt pathway, specifically in adipocytes.

Herein, we report for the first time that β -catenin is a key regulator of adipocyte *de novo* lipogenesis (DNL) and fatty acid desaturation. Although chow-fed adipocyte-specific β -catenin knockout mice do not exhibit an overt phenotype, deeper investigation reveals a striking phenomenon in which surrounding stromal-vascular cells (SVC) dramatically up-regulate β -catenin production and return mRNA and/or protein back to deficient adipocytes, such that knockout cells have sustained expression of β -catenin despite complete genomic deletion. Thus, Wnt signaling within and between cell types is monitored in white adipose tissue (WAT), and loss of β -catenin signaling in adipocytes is compensated for by CD45⁻/CD31⁻ stromal cells to maintain whole-tissue Wnt signaling homeostasis under standard nutritional conditions. This compensatory mechanism is overridden by diet-induced obesity such that high fat diet (HFD)-fed adipocyte-specific β -catenin knockout mice exhibit decreased adiposity and improved glucose homeostasis and hepatosteatosis. These findings underscore the critical importance of the canonical Wnt/ β -catenin pathway in adipocyte lipid metabolism and adipose tissue function.

Results

β -catenin is highly expressed in terminally differentiated adipocytes and up-regulated by obesity.

The canonical Wnt/ β -catenin pathway is a critical regulator of mesenchymal cell fate determination and an endogenous inhibitor of adipogenesis^{15,16}. Although Wnt signaling is commonly believed to be most important in precursors, recent studies have begun to shed light on important contributions of this pathway to functions within terminally-differentiated adipocytes³⁷⁻⁴⁰; however, specific roles of β -catenin in this context require further investigation. We thus first confirmed that β -catenin is expressed in mature adipocytes. *Ctnnb1* (β -catenin) mRNA and protein expression is high in cultured mesenchymal stem cells (MSC) derived from wildtype C57BL/6J mice, transiently suppressed during differentiation, and subsequently increased in terminally-differentiated adipocytes (**Figure 4.1 A-B**). Expression of the adipocyte marker *Adipoq* (adiponectin) increases during adipogenesis, whereas expression of the preadipocyte marker *Dlk1* (Pref1) decreases as expected (**Figure 4.1 A-B**).

To determine β -catenin levels in adipose tissues *in vivo*, we performed immunoblot analyses in various tissues isolated from wildtype mice and found that β -catenin is widely expressed, including in diverse adipose depots, pancreas and lung (**Supplemental Figure 4.1 A**). In addition to adipocytes, WAT is comprised of many other cell types, including endothelial, immune, and stromal cells and preadipocytes. These non-adipocyte cells are known as the stromal-vascular fraction (SVF) of WAT, and previous studies have demonstrated that β -catenin is widely expressed in many of these populations^{15,16,41-44}. To assess whether adipocyte-specific expression contributes significantly to β -catenin levels within whole adipose tissues, we measured *Ctnnb1* mRNA expression in fractionated epididymal (eWAT) and inguinal (iWAT) WAT of wildtype mice. We found that *Ctnnb1* is expressed highly in isolated adipocytes compared to the SVF (**Figure 4.1 C**), consistent with recently reported data³⁷. As expected, *Adipoq* expression is found exclusively in the adipocyte fractions, whereas *Dlk1* expression is limited to the SVF (**Supplemental Figure 4.1 B**), providing evidence of clean separation.

Recent studies have demonstrated that Wnt signaling plays a role in adipocyte metabolism under obesogenic conditions³⁷⁻⁴⁰. Thus, we examined the regulation of β -catenin in WAT after a number of nutritional and environmental treatments and found that its expression is up-regulated in both eWAT and iWAT with diet-induced obesity (**Figure 1D**), parallel with induction of *Lep* (leptin) (**Supplemental Figure 4.1 C**). Consistent with *Ctnnb1* expression patterns, downstream Wnt target *Nkd1* is increased in eWAT with HFD treatment; effects in iWAT are not statistically different (**Supplemental Figure 4.1 D**). Further, analyses of fractionated WAT demonstrate that up-regulation of *Ctnnb1* largely occurs in adipocytes, rather than in the SVF (**Figure 4.1 E**). This regulation is specific; *Ctnnb1* expression is not altered by other conditions, including acute fasting, fasting/refeeding, calorie restriction, or acute cold exposure (**Supplemental Figure 4.1 E**). Finally, we interrogated the GTEx database to determine distribution of *Ctnnb1* gene expression across male and female human tissues and found that β -catenin is highly expressed in subcutaneous and visceral WAT depots, with relatively low expression in liver, skeletal muscle, and pancreas (**Supplemental Figure 4.1 F**). Together, these data demonstrate that β -catenin is expressed in mature adipocytes and up-regulated by diet-induced obesity, and thus conceivably plays an important metabolic role in these cells.

Canonical Wnt signaling is operative in cultured adipocytes.

To interrogate the molecular functions of β -catenin in adipocytes, we utilized a cultured cell model using MSCs isolated directly from β -cat^{fl/fl} mice. To efficiently ablate β -catenin in either preadipocytes or adipocytes, we established a protocol for gene deletion using adenoviral Cre recombinase (**Supplemental Figure 4.1 G**). To induce gene deletion in preadipocytes, β -cat^{fl/fl} MSCs at 30-40% confluence were infected in serum-free medium with adenoviral GFP as a control, or adenoviral Cre to stimulate recombination. Preadipocytes were allowed to recover following infection and were analyzed at confluence. To induce gene deletion in adipocytes, β -cat^{fl/fl} MSCs were differentiated using a standard adipogenic cocktail and at day four of differentiation, adipocytes were infected with adenoviral GFP or Cre in serum-free medium. Cells were then allowed to recover and were subsequently analyzed at day 12 of differentiation. A 3-primer PCR

system was used to confirm recombination of the floxed allele (**Figure 4.1 F**, preadipocytes shown in **Supplemental Figure 4.1 H**). Efficient deletion of *Ctnnb1* mRNA (**Figure 4.1 G**) and protein (**Figure 4.1 H**, preadipocytes shown in **Supplemental Figure 4.1 H**) was observed in Cre-infected adipocytes. Adipocyte-specific β -catenin deletion does not affect differentiation status or lipid accumulation, as evidenced by adiponectin and perilipin protein expression (**Figure 4.1 H**), phase-contrast microscopy and Oil Red-O staining (**Figure 4.1 I**), and quantification of triacylglycerol (TAG) content per well (**Figure 4.1 J**). Importantly, protein levels of AXIN2 and WISP2, two known Wnt targets, are decreased in β -cat^{-/-} adipocytes (**Figure 4.1 H**, preadipocytes shown in **Supplemental Figure 4.1 H**).

Thus, we next investigated in more detail whether Wnt target genes are altered in adipocytes lacking β -catenin. To this end, we measured expression of well-characterized downstream genes under basal conditions and after stimulation with the small molecule CHIR99021, which stabilizes β -catenin through inhibition of GSK3 activity¹⁵. We found that Wnt-induced genes, including *Axin2*, *Nkd1*, and *Tcf7l2*, are down-regulated in β -cat^{-/-} adipocytes, whereas Wnt-repressed genes *Id2* and *Wif1* are up-regulated (**Figure 4.1 K**, **Supplemental Figure 4.1 I**). Importantly, Wnt pathway stimulation with CHIR99021 induces expression of most target genes only in β -cat^{fl/fl} adipocytes and not in β -cat^{-/-} cells, suggesting that expression of these genes is β -catenin-dependent in terminally differentiated cells (**Figure 4.1 K**, **Supplemental Figure 4.1 I**). Of note, *Id2* expression is down-regulated in both control and knockout adipocytes with CHIR99021 treatment, albeit to different degrees, suggesting that it is also regulated by other cellular pathways affected by GSK3 inhibition (**Figure 4.1 K**). Taken together, these data indicate that the canonical Wnt signaling pathway is operative in mature adipocytes, and likely regulates functions that are specialized to these cells.

β -catenin regulates metabolic pathways in adipocytes and exclusively mediates effects of canonical Wnt3a signaling.

Although β -catenin-dependent canonical Wnt signaling is a critical regulator of mesenchymal cell fate, the role of this pathway in mature adipocytes is less clear. To

identify the transcriptional pathways directly regulated by β -catenin in terminally-differentiated cells, we performed RNA-sequencing (RNA-seq) analyses of β -cat^{fl/fl} and β -cat^{-/-} adipocytes at baseline and following 4-hour treatment with recombinant Wnt3a (**Figure 4.2 A, E**). Of the 18,931 identified genes, β -catenin deletion in adipocytes resulted in significant up-regulation of 1,582 genes and down-regulation of 484 genes. We then used Gene Set Enrichment Analyses (GSEA) to identify significantly up- and down-regulated pathways in knockout cells. Strikingly, the majority of up-regulated pathways are related to inflammatory response, including TNF α , IL6, interferon γ , and interferon α signaling; in contrast, loss of β -catenin leads to suppression of several metabolic pathways, including those involved in glycolysis, oxidative phosphorylation, and fatty acid, cholesterol, and bile acid metabolism (**Figure 4.2 B**). Of note, mTORC1 signaling is also significantly down-regulated in β -cat^{-/-} adipocytes, which is of interest since this pathway has been shown to regulate lipid metabolism in adipocytes⁴⁵⁻⁴⁸.

Wnt3a treatment of β -cat^{fl/fl} adipocytes resulted in significant up-regulation of 535 genes and down-regulation of 417 genes, including dramatic induction of known Wnt targets *Axin2*, *Nkd1*, *Nkd2*, and *Wnt11* (**Figure 4.2 A, C**). Consistent with canonical Wnt/ β -catenin signaling predominating in adipocytes, Wnt3a treatment of β -cat^{-/-} adipocytes only altered expression of one gene, *Gpr161*, which has no known function (**Figure 4.2 D**). As expected, treatment of control adipocytes with Wnt3a stimulates the expression of genes known to be related to Wnt/ β -catenin signaling (**Figure 4.2 B**). Hedgehog and TGF β signaling, which have broad effects on differentiation and mature cell functions, are also up-regulated (**Figure 4.2 B**); cross-talk between these pathways and Wnt signaling have been reported in other contexts^{49,50}. Differential regulation of a subset of Wnt target genes was confirmed by qPCR analyses of control and knockout adipocytes treated with Wnt3a for different lengths of time (**Figure 4.2 F**).

Consistent with an extensive literature describing the role of Wnt signaling in precursors, RNA-seq analyses of β -cat^{fl/fl} and β -cat^{-/-} preadipocytes identified 866 up-regulated genes and 936 down-regulated genes (**Supplemental Figure 4.2 A, E**). Deletion of β -catenin in precursors suppresses many pathways critical for cell function, including DNA repair, proliferation, stress response, and glycolysis (**Supplemental**

Figure 4.2 B), consistent with known roles of Wnt signaling in cell proliferation and cancer metabolism⁵¹. Similar to observations in control adipocytes, Wnt3a treatment of β -cat^{fl/fl} preadipocytes promoted expression of many genes related to TGF β , Hedgehog and Notch signaling (**Supplemental Figure 4.2 A-C**). Unlike in β -cat^{-/-} adipocytes, Wnt3a treatment of β -cat^{-/-} preadipocytes resulted in up-regulation of 146 genes and down-regulation of 171 genes, including induction of Wnt target genes like *Axin2* and *Nkd1* (**Supplemental Figure 4.2 D-F**). These data indicate that in preadipocytes, Wnt target genes are also regulated by non-canonical Wnt signaling pathways, whereas in adipocytes, Wnt3a acts exclusively through a β -catenin-dependent mechanism.

β -catenin-dependent signaling regulates lipogenesis and fatty acid desaturation in adipocytes.

Lipogenesis and lipid accumulation are two specialized functions of adipocytes. Thus, we were intrigued to find that the RNA-seq dataset identified many genes related to lipid metabolism, including *Srebf1* and *Scd1*, as significantly down-regulated in β -cat^{-/-} adipocytes (**Figure 4.3 A-B**). Consistent with the RNA-seq data, we found that β -catenin deficiency in adipocytes down-regulates mRNA (**Figure 4.3 C**) and protein (**Figure 4.3 D**, quantification in **Supplemental Figure 4.3 A**) expression of many genes in the *de novo* lipogenesis (DNL) pathway, including ATP citrate lyase (*Acly*, ACLY), acetyl-CoA carboxylase (*Acaca*, ACC1), fatty acid synthase (*Fasn*, FASN), and stearoyl CoA desaturase 1 (*Scd1*, SCD1). DNL converts excess dietary amino acids and carbohydrates into fatty acids, a subset of which can be esterified into TAG and later mobilized to provide energy to adipocytes and other cells throughout the body^{52,53}. SCD1, a member of the DNL pathway, is the rate-limiting adipocyte enzyme localized to the endoplasmic reticulum that catalyzes desaturation of palmitic (C16:0) and stearic (18:0) acids into palmitoleic (C16:1, n-7) and oleic (C18:1, n-9) acids, respectively^{54,55}. Since SCD1 protein expression is inhibited by ~55% in β -cat^{-/-} adipocytes (**Figure 4.3 D**, **Supplemental Figure 4.3 A**), we hypothesized that TAG isolated from these cells would have decreased unsaturated fatty acids and increased saturated fatty acids. Indeed, we found that β -cat^{-/-} adipocytes contain a smaller proportion of monounsaturated fatty acid species compared to control adipocytes (**Figure 4.3 E**).

Closer examination revealed that compared to β -cat^{fl/fl} adipocytes, lipids isolated from terminally-differentiated β -cat^{-/-} cells contain significantly higher proportions of palmitic (16:0) and stearic (18:0) acids and less myristoleic (14:1, n-5) and palmitoleic (16:1, n-7) acids (**Figure 4.3 F, Supplemental Figure 4.3 B**). In addition, β -cat^{-/-} adipocytes also contain slightly elevated proportions of oleic (C18:1, n-9), vaccenic (C18:1, n-7), and arachidonic (C20:4) acids (**Supplemental Figure 4.3 B**, data not shown), consistent with previously published studies of SCD1 inhibition in 3T3-L1 adipocytes⁵⁶. Although it is surprising that ELOVL6 did not follow expression of other ChREBP- and SREBP1-regulated lipogenic genes, up-regulation of ELOVL7 has been observed in a variety of contexts in which Wnt signaling is repressed^{40,57-59}. The functional significance of increased ELOVL7 in adipocytes remains unclear since the proportion of very long chain saturated fatty acids was not altered in β -cat^{-/-} adipocytes (data not shown).

Since β -catenin deletion down-regulates a network of key DNL pathway members (**Figure 4.3 A-D**), we performed DNL assays using [¹⁴C]-acetate to evaluate whether lipogenesis is functionally impaired in β -cat^{-/-} adipocytes. Differentiated adipocytes were incubated in medium containing [¹⁴C]-acetate for 2, 4 or 8 hours. Cells were then lysed, and lipids extracted to measure the incorporation of radiolabel into TAG, diacylglycerol (DAG), and phospholipid (PL) fractions. Conditioned media (**Supplemental Figure 4.3 C**) and whole cell lysate (**Supplemental Figure 4.3 D**) analyses indicated that β -cat^{-/-} adipocytes take up less labeled acetate over time. Consistent with this, *Slc16a1* (*Mct1*), an acetate transporter, and *Acss2*, the cytosolic enzyme that catalyzes activation of acetate for use in lipid synthesis, are suppressed in β -cat^{-/-} adipocytes (**Supplemental Figure 4.3 B, E**). β -cat^{-/-} adipocytes incorporate significantly less radiolabel over time into the TAG and DAG fractions of cellular lipid (**Figure 4.3 G, Supplemental Figure 4.3 F**), but not the PL fraction (**Supplemental Figure 4.3 G**). This is important, as it suggests that acetate uptake is not the rate-limiting factor for radiolabel incorporation into TAG; indeed, decreased acetate incorporation in lipid synthesis may actually feedback to suppress transporter expression. Further, linear regression analyses demonstrate that decreased incorporation into TAG is not proportional to decreased acetate uptake (**Supplemental Figure 4.3 H-I**), strongly suggesting that suppressed expression of DNL enzymes, not

genes related to acetate transport or activation, is rate-limiting for lipogenesis in β -cat^{-/-} adipocytes. Thus, impaired DNL is secondary to loss of β -catenin-dependent Wnt signaling. These data suggest that adipocyte β -catenin signaling is required for lipogenic gene expression, DNL and steady-state lipid composition.

β -catenin exerts effects on lipogenesis through transcriptional regulation of Srebf1 and Mlxipl.

Extensive studies in liver have identified SREBP1c and ChREBP as key upstream transcriptional regulators of many genes involved in DNL, including *Acaca*, *Fasn*, and *Scd1*^{60,61}. We recently demonstrated for the first time that Wnt signaling mediates adipocyte lipogenic gene expression through regulation of sterol regulatory element-binding protein 1c (SREBP1c) and carbohydrate-responsive element-binding protein (ChREBP)⁴⁰. Thus, we next investigated whether these genes are specifically regulated by β -catenin-dependent Wnt signaling. Indeed, we found that expression of *Srebf1* and *Mlxipl*, which encode SREBP1c and ChREBP respectively, are both repressed in β -cat^{-/-} adipocytes; other transcription factors involved in adipogenesis and mature adipocyte function, including *Pparg* and *Cebpa*, are not altered (**Figure 4.3 A-B, H**). Consistent with expression of their respective mRNAs, SREBP1c and ChREBP protein levels are also decreased, whereas PPAR γ and C/EBP α levels are unaffected (**Figure 4.3 I**).

To establish whether repression of *Mlxipl* or *Srebf1* directly mediates impaired lipogenesis and fatty acid monounsaturations following β -catenin deletion, we evaluated the effects of increasing ChREBP or SREBP1c expression in β -catenin knockout adipocytes slightly above that observed in control adipocytes. Thus, we treated β -cat^{fl/fl} and β -cat^{-/-} adipocytes with adenoviral GFP as a control or adenoviruses encoding ChREBP or SREBP1c. Ectopic expression of ChREBP or SREBP1c was sufficient to induce SCD1 expression in control adipocytes, and partially rescue SCD1 mRNA and protein levels in β -cat^{-/-} adipocytes (**Figure 4.3 J, Supplemental Figure 4.3 J**). Expression of *Fasn* was also partially rescued by overexpression of these transcription factors (**Supplemental Figure 4.3 J**).

Since β -catenin coactivates TCF/LEF proteins like Tcf712 (Tcf4) to mediate transcription of downstream targets, we analyzed the promoter regions of *Mlxipl*, *Srebf1*, *Acaca*, *Fasn*, and *Scd1* and found multiple predicted Tcf712 binding sites on each gene (data not shown). Thus, we interrogated a recently published chromatin immunoprecipitation sequencing (ChIP-seq) dataset of Tcf712 binding in cultured *Tcf712^{fl/fl}* and *Tcf712^{-/-}* adipocytes³⁹ and found enrichment of Tcf712 binding sites in the promoter, exon and/or first intronic regions of *Mlxipl*, *Srebf1*, *Fasn*, and *Scd1*; binding occupancy of Tcf712 was subsequently lost in *Tcf712^{-/-}* cells (**Figure 4.3 K**). Taken together, these results support a model in which repressive effects of β -catenin deletion on lipogenic gene expression are mediated, in part, through down-regulation of ChREBP and SREBP1c. However, identification of Tcf712 binding sites in transcriptional regulatory regions of several lipogenic genes, including *Acaca*, *Fasn*, and *Scd1*, suggests that β -catenin likely regulates expression of these genes through a combination of direct (TCF/LEF) and indirect (ChREBP and SREBP1c) mechanisms.

Loss of β -catenin signaling within adipocytes does not influence global metabolism in chow-fed mice.

Our studies in cultured adipocytes revealed that canonical Wnt signaling through β -catenin is an important regulator of adipocyte lipogenesis and lipid desaturation (**Figure 4.3, Supplemental Figure 4.3**). We next hypothesized that β -catenin has effects on these pathways *in vivo* and thus generated adipocyte-specific β -catenin knockout mice by crossing *β -cat^{fl/fl}* mice with adiponectin-Cre mice. Genetic recombination is specifically observed in various adipose depots, but not in other tissues, including liver, muscle, pancreas, lung or heart (**Figure 4.4 A**). We evaluated possible metabolic phenotypes in *β -cat^{-/-}* mice maintained on normal chow diet (NCD) but did not observe differences in growth over time (**Figure 4.4 B**), body composition (**Figure 4.4 C**), or glucose and insulin tolerances (**Figure 4.4 D-E**). *β -cat^{-/-}* mice do not exhibit altered fed or fasted blood glucose (**Figure 4.4 F**), serum insulin concentrations (**4.4 G**), or circulating adiponectin levels (**Figure 4.4 H**). We did not detect differences in voluntary exercise capacity (**Supplemental Figure 4.4 A**), basal or induced lipolysis (**Figure 4.4**

I), or serum TAG levels (**Figure 4.4 J**). Upon harvest, weights of iWAT, eWAT, brown adipose tissue (BAT), perirenal WAT (pWAT), and liver were not different between β -cat^{fl/fl} and β -cat^{-/-} mice (**Figure 4.4 K**). Finally, histological analyses of tissues did not yield substantial differences in adipocyte size or number within BAT, iWAT, eWAT, or pWAT (**Figure 4.4 L**, data not shown), and liver morphology was not influenced (**Figure 4.4 L**). Similar results were found in female mice (**Supplemental Figure 4.4 B-J**).

Wnt signaling through β -catenin has been shown to have profound effects on determination of MSC fate and differentiation into adipocytes, osteocytes, chondrocytes or myocytes. The role of this pathway in fate selection between adipogenesis and osteogenesis has been particularly well-studied. Indeed, studies have demonstrated that Wnt signaling increases bone mass and trabeculation, and impairs accumulation of bone marrow adipocytes^{62,63}. We therefore examined whether marrow adiposity and bone characteristics are influenced by adipocyte-specific β -catenin deficiency. Histological analyses of tibia from both male and female mice suggest that β -catenin deletion does not alter size or number of regulated or constitutive marrow adipocytes (**Supplemental Figure 4.5 A, C**). Further, micro-computed tomography (μ CT) analyses did not yield differences in either trabecular or cortical bone mass variables in β -cat^{-/-} mice (**Supplemental Figure 4.5 B, D**).

β -catenin is up-regulated in the stromal-vascular fraction of adipose tissues from knockout mice.

Although we did not observe an overt metabolic phenotype in β -cat^{-/-} mice maintained on chow diet, we expected to find decreased DNL gene expression in eWAT and iWAT isolated from knockout mice. However, lipogenic gene expression is not influenced in whole eWAT or iWAT of β -cat^{-/-} mice (**Supplemental Figure 4.6 A-B**). We also did not observe changes in DNL gene expression within livers of β -cat^{-/-} mice (**Supplemental Figure 4.6 C**). Perhaps most perplexing, analyses of isolated adipocytes from β -cat^{-/-} mice did not demonstrate altered DNL gene expression, except for mild suppression of *Scd1* (**Supplemental Figure 4.6 D**). These data were concerning and suggested that perhaps β -catenin is not efficiently deleted *in vivo*. Indeed, we were surprised to find

that although β -catenin appears to be recombined at the genomic level in whole WAT of β -cat^{-/-} mice (**Figure 4.5 A**), suppression of *Ctnnb1* mRNA is much less substantial than expected (**Figure 4.5 B**). Further, β -catenin protein levels are virtually unaltered in eWAT and iWAT of β -cat^{-/-} mice (**Figure 4.5 C**).

Since SVF cell populations are known to express β -catenin, we considered the possibility that adipocyte-specific loss was being masked by the relatively high expression of β -catenin in SVCs. Thus, we fractionated WAT to determine whether efficient deletion occurs within adipocytes. Indeed, we found that β -catenin gene recombination occurs specifically in adipocytes and not SVCs of β -cat^{-/-} mice (**Figure 4.5 D**). However, we were surprised to find that *Ctnnb1* mRNA is only reduced by ~50% in the adipocyte fraction of β -cat^{-/-} mice, and its expression is highly induced in the SVF of knockout mice (**Figure 4.5 E**). We also observed sustained levels of β -catenin protein in knockout adipocytes, and significant induction of β -catenin protein within the SVF of β -cat^{-/-} mice (**Figure 4.5 F**). We next measured Wnt target genes in isolated adipocytes and SVCs of β -cat^{fl/fl} and β -cat^{-/-} mice. Consistent with β -catenin expression patterns, we found that most Wnt targets are not altered in the adipocyte fraction of β -cat^{-/-} mice (**Figure 4.5 G**), whereas these genes are significantly up-regulated in the SVF with β -catenin deficiency (**Figure 4.5 H**).

These striking findings suggest that adipose tissues are able to sense depletion of β -catenin and subsequently maintain canonical Wnt signaling across the tissue by up-regulating the pathway in SVCs. Thus, we next evaluated whether a specific cellular sub-population is enriched within the SVF of β -cat^{-/-} mice and found that several macrophage markers, including *Adgre1* (*F4/80*), *Cd68*, and *Cd11c*, are elevated, whereas markers for endothelial and stromal cells are not changed (**Supplemental Figure 4.6 E**). These data may suggest that macrophage number is increased in the SVF of β -cat^{-/-} mice; these macrophages may in turn contribute *Ctnnb1* mRNA or β -catenin protein back to deficient adipocytes, either directly via small extracellular vesicles (sEVs) or indirectly by stimulating production in neighboring cells. Although macrophage markers are increased, expression of classical inflammatory markers are decreased or unchanged in whole WAT of β -cat^{-/-} mice (**Supplemental Figure 4.6 F**).

We next performed flow cytometry analysis of SVF isolated from chow-fed β -*cat*^{fl/fl} and β -*cat*^{-/-} mice. We used CD45 and CD31 as markers for immune and endothelial cells, respectively; CD45⁻/CD31⁻ cells were designated as the stromal cell population. Flow cytometry analysis did not yield differences in proportions of CD45⁺, CD31⁺, or CD45⁻/CD31⁻ populations (**Figure 4.5 I-J**). Since proportions of different SVF cell types were not influenced by adipocyte-specific β -catenin deletion, we next hypothesized that a specific cell type might be up-regulating its own β -catenin expression. Thus, we used fluorescence-activated cell sorting (FACS) to separate CD45⁺, CD31⁺, and CD45⁻/CD31⁻ cell fractions. Expression of *F4/80*, *Pecam1*, and *Pdgfra* were evaluated by qPCR to confirm that we had specifically separated immune, endothelial, and stromal cell populations (**Supplemental Figure 4.6 G**). We next measured *Ctnnb1* mRNA expression in the three cell fractions and were intrigued to find that *Ctnnb1* is up-regulated in the CD45⁻/CD31⁻ population of chow-fed β -*cat*^{-/-} mice (**Figure 4.5 K**). Consistent with *Ctnnb1* expression patterns, downstream Wnt targets *Axin2* and *Nkd1* are also increased in CD45⁻/CD31⁻ cells isolated from β -*cat*^{-/-} mice (**Supplemental Figure 4.6 H**). These data suggest that a sub-population of CD45⁻/CD31⁻ stromal cells is able to sense the loss of adipocyte β -catenin, either directly or indirectly, and subsequently up-regulate its own expression to maintain Wnt signaling homeostasis within WAT of chow-fed mice. Further studies will be required to identify the specific cells within this population that mediate the observed compensatory effects.

β -*cat*^{-/-} mice are protected from diet-induced obesity and metabolic dysfunction.

Previous investigations into the role of Wnt signaling in WAT have found that this pathway is important in adipocyte metabolism under obesogenic conditions³⁷⁻⁴⁰. Consistent with these studies, we report that *Ctnnb1* expression is up-regulated within both eWAT and iWAT with diet-induced obesity (**Figure 4.1 D-E**). We thus challenged β -*cat*^{fl/fl} and β -*cat*^{-/-} mice with HFD and found that beginning at 20 weeks of feeding, knockout mice demonstrate decreased weight gain (**Figure 4.6 A**) and fat mass (**Figure 4.6 B**) compared to control mice, whereas lean mass is not affected. Of note, β -*cat*^{-/-} mice do not have decreased food intake (**Supplemental Figure 4.7 A**). Consistent with

decreased adiposity, β -cat^{-/-} mice exhibit significantly improved glucose tolerance (**Figure 4.6 C-D**). Although fasting and random-fed blood glucose concentrations are not different (**Figure 4.6 E**) and insulin sensitivity only trends toward improvement in knockout mice (**Figure 4.6 F, Supplemental Figure 4.7 B**), glucose-induced circulating insulin concentrations are decreased in β -cat^{-/-} mice compared to controls (**Figure 4.6 G**). Circulating TAG levels are decreased in knockout mice (**Figure 4.6 H**), whereas serum cholesterol (**Figure 4.6 I**) and adiponectin (**Figure 4.6 J**) are not changed. Upon harvest, weights of iWAT, eWAT and pWAT were significantly decreased in knockout mice, consistent with leaner body composition, whereas BAT, liver, and pancreas weights were unchanged (**Figure 4.6 K, Supplemental Figure 4.7 C**). Histological analyses of β -cat^{-/-} tissues suggest that adipocyte sizes within iWAT and eWAT are mildly decreased (**Figure 4.6 L**). In addition, livers of knockout mice have less hepatosteatosis compared to control counterparts (**Figure 4.6 L**), in line with recently reported findings³⁷. Consistent with the observed protection from glucose intolerance and the histological findings, livers of β -cat^{-/-} mice have decreased TAG content (**Figure 4.6 M**). *Cdf* (adipsin) mRNA levels are increased in eWAT of β -cat^{-/-} mice, whereas *Lep* expression is decreased and *Adipoq* and *Retn* (resistin) remain unchanged; similar trends were observed in iWAT of knockout mice (**Supplemental Figure 4.7 D-E**). Finally, expression of UCP1 protein in BAT of β -cat^{-/-} mice was unchanged despite a ~50% decrease in *Ctnnb1* expression (**Supplemental Figure 4.7 F**); these data, along with comparable BAT morphology (**Figure 4.6 L**), suggest that altered BAT thermogenesis is likely not responsible for improved metabolic function observed in obese β -catenin knockout mice.

We next measured *Ctnnb1* expression in eWAT and iWAT of β -cat^{-/-} mice fed HFD and found much lower mRNA levels in tissues of knockout mice (**Figure 4.7 A**). Further investigation revealed that *Ctnnb1* mRNA expression in isolated adipocytes is largely ablated in knockout mice, whereas expression in SVF is comparable to those of control mice (**Figure 4.7 B**). Consistent with these data, β -catenin protein is effectively deleted in the adipocyte fraction isolated from β -cat^{-/-} mice, and protein levels are no longer elevated in the SVF of these animals (**Figure 4.7 C**). These data are compelling

and suggest that with HFD, the compensatory increase in canonical Wnt signaling within stromal cells of knockout mice is lost. Indeed, the SVF of β -cat^{-/-} mice no longer exhibit elevated Wnt target gene expression (**Figure 4.7 D**). Further, analyses of the adipocyte fraction demonstrated decreased expression of Wnt targets, including *Axin2*, *Nkd1*, *Wnt10b*, and *Wnt16* (**Figure 4.7 E**).

Consistent with our *in vitro* studies showing the effects of β -catenin deletion on DNL, adipocytes of HFD-fed knockout mice are also characterized by decreased expression of key lipogenic genes, including *Srebf1*, *Mlxipl*, *Acly*, *Acaca*, *Fasn*, and *Scd1* (**Figure 4.7 F**). We also found that macrophage markers are decreased in the SVF of HFD-fed knockout mice (**Figure 4.7 G**), corroborating results reported by Chen *et al.*³⁷ and suggesting that these cells mediate the compensatory mechanism observed in chow-fed mice. Consistent with decreased immune cell markers, whole WAT of β -cat^{-/-} mice have suppressed expression of some inflammatory markers, including *Tnfa* and *Inos2* (**Figure 4.7 H-I**). Expression of *Saa3*, which encodes a secreted protein that activates macrophages, is also decreased in WAT of HFD-fed knockout mice (**Figure 4.7 H-I**). Thus, taken together, our findings demonstrate that diet-induced obesity overrides stromal compensation for adipocyte-specific β -catenin deletion, leading to impaired lipogenic gene expression, decreased adipose accumulation and adipocyte hypertrophy, and protection from metabolic dysfunction.

Discussion

Canonical β -catenin-dependent Wnt signaling is well-established as a key player in MSC fate determination, acting as a potent endogenous repressor of adipogenesis and promoter of osteoblastogenesis^{10,12,13,15}. The preponderance of data within adipocyte biology to date has focused on the inhibition of adipogenesis by Wnt signaling, undoubtedly because many genes involved in this pathway are suppressed during the early stages of differentiation⁶⁴. However, our work herein and recently published studies from our laboratory and others have demonstrated that canonical Wnt pathway members are present and operative in terminally-differentiated adipocytes, and thus have distinct functional roles in this context³⁷⁻⁴⁰.

To evaluate specific roles of canonical Wnt signaling in adipocyte function, we chose to ablate β -catenin, the central protein in the pathway. We report here that β -catenin deletion in cultured adipocytes suppresses expression of known downstream target genes, including *Axin2*, *Nkd1*, and *Tcf7l2*. Further, stimulation of Wnt signaling using either a GSK3 inhibitor or recombinant Wnt3a is largely blocked in adipocytes lacking β -catenin, suggesting that effects of canonical Wnt signaling are mediated exclusively by β -catenin in terminally-differentiated cells. Global RNA-seq analyses of β -cat^{fl/fl} and β -cat^{-/-} adipocytes identified several metabolic pathways as down-regulated by inhibition of Wnt signaling, including oxidative phosphorylation, glycolysis, and fatty acid, cholesterol, and bile acid metabolism. Of particular interest to adipocyte biology, we found that signaling through β -catenin is required for coordinate expression of many lipogenic genes, including *Acly*, *Acaca*, *Fasn*, and *Scd1*. Of note, RNA-seq analyses of livers from β -cat^{-/-} mice have also demonstrated decreased expression of lipogenic genes, including *Acly* and *Scd1*⁶⁵.

Consistent with repressed expression of DNL enzymes, we report that β -cat^{-/-} adipocytes are characterized by impaired lipogenesis and fatty acid monounsaturations. Effects of β -catenin deletion on adipocyte metabolism are specific, as knockout adipocytes do not exhibit altered insulin-stimulated glucose uptake, adrenergic stimulation of lipolysis, or β -oxidation of fatty acids (data not shown). These data are strongly supported by recently published work from our group showing that blocking

secretion and downstream signaling of adipocyte-derived Wnts also inhibits DNL and lipid unsaturation⁴⁰. In addition, Geoghegan *et al.* recently reported that *Tcf7l2* deletion in precursor cells stimulates adipogenesis and increased expression of genes related to lipid metabolism, providing further support for the presumptive role of β -catenin-dependent signaling in regulation of this process in adipocytes³⁹.

Extensive studies in the liver have identified *Srebf1* and *Mlxipl*, encoding SREBP1c and ChREBP respectively, as key upstream transcriptional regulators of DNL enzymes⁵³. Here, we report that expression of *Srebf1* and *Mlxipl* is significantly decreased in β -cat^{-/-} adipocytes, and that ectopic expression of ChREBP or SREBP1c partially rescues expression of DNL genes in adipocytes lacking β -catenin. These data are consistent with genome-wide ChIP-seq analysis of ChREBP binding sites in WAT, which identified binding sites on many genes related to metabolism, including *Acaca*, *Fasn*, and *Scd1*⁶⁶. Thus, β -catenin mediates effects on DNL genes in part by regulating expression of key transcription factors *Srebf1* and *Mlxipl*. Indeed, ChIP-seq analyses of *Tcf7l2* binding sites in cultured adipocytes, used as a surrogate for β -catenin/TCF/LEF activity, identified specific *Tcf7l2* occupancies in the regions surrounding the transcriptional start sites of *Mlxipl* and *Srebf1*, but also downstream lipogenic genes such as *Fasn* and *Scd1*. Although these data suggest that β -catenin regulates transcription of lipogenic genes through a combination of indirect (via ChREBP and SREBP1c) and direct mechanisms, ChIP-seq analyses of β -catenin binding sites in adipocytes will be required to further interrogate the direct versus indirect effects of β -catenin on transcription of lipogenic genes.

Adipocyte-specific β -catenin deletion does not appear to influence global metabolism in chow-fed mice. Indeed, consistent with our studies, recent investigations into roles of Wnt signaling in mature adipocytes, including global *Sfrp5* deletion or adipocyte-specific deletion of *Tcf7l2*, *Wntless*, or *Ctnnb1*, also did not reveal an overt metabolic phenotype in chow-fed mice³⁷⁻⁴⁰. However, we recently published a study showing that surrounding SVCs compensate for loss of adipocyte-derived Wnts secondary to *Wntless* deletion⁴⁰. Thus, we probed further into the lack of a detectable phenotype in β -cat^{-/-} mice and were surprised to find that although β -catenin is efficiently

ablated at the genomic level in β -cat^{-/-} adipocytes, the mRNA and protein are still detectable at levels much higher than expected. These data are consistent with those recently published by Chen *et al.*, who reported a ~50% reduction in β -catenin mRNA expression in adipocytes isolated from iWAT or eWAT of knockout mice³⁷. Perhaps unsurprisingly, given the substantial β -catenin expression remaining, we found that Wnt targets and lipogenic genes are not altered in isolated knockout adipocytes. However, further investigation revealed that SVCs isolated from β -cat^{-/-} mice exhibit significantly up-regulated expression of *Ctnnb1* and downstream Wnt targets, including *Axin2*, *Nkd1*, *Tcf7l2*, *Wnt10b*, and *Wnt16*. Although Chen *et al.* did not report elevated *Ctnnb1* expression in SVF of knockout mice, their data does suggest a trend toward increased expression in SVF isolated from eWAT³⁷. These data support the compelling conclusion that Wnt signaling is critical for autocrine and paracrine communication within WAT, such that loss of Wnt/ β -catenin signaling in adipocytes is sensed and compensated for by SVCs to maintain whole-tissue Wnt signaling homeostasis.

An important question raised by our studies is the underlying mechanism by which β -catenin expression is up-regulated in the SVF of knockout animals. Gene expression analysis of CD45⁺, CD31⁺ and CD45⁻/CD31⁻ populations isolated by FACS demonstrated that *Ctnnb1* and downstream targets *Axin2* and *Nkd1* are significantly up-regulated in CD45⁻/CD31⁻ stromal cells of knockout mice. These data suggest that a sub-population of CD45⁻/CD31⁻ cells, which include adipose stem cells, committed preadipocytes, and pericytes⁶⁷, is able to directly or indirectly sense the loss of adipocyte β -catenin and subsequently up-regulates its own expression to maintain Wnt signaling homeostasis within WAT of chow-fed mice. This compensatory mechanism may be the result of a dynamic network of intercellular Wnt signals; alternatively, it may conceivably arise from complex interactions between canonical Wnt signaling and other pathways, including Hedgehog, BMP and FGF signaling^{49,68,69}.

Gene expression analysis of whole SVF indicated that several macrophage markers, including *F4/80*, *Cd68*, and *Cd11c*, were increased in chow-fed β -cat^{-/-} mice. It is important to note that various isoforms of CD45 are present on almost all differentiated hematopoietic cells, and although *Cd68* and *Cd11c* are commonly used as macrophage markers, they are also expressed by non-hematopoietic cell types,

including endothelial and stromal cells^{70,71}. Thus, it is possible that β -catenin indeed causes a mild increase in macrophage number, but that this difference is not observed when using a broad marker like CD45, which stains virtually all hematopoietic cells. Further studies using single-cell RNA sequencing analysis of SVF from β -cat^{fl/fl} and β -cat^{-/-} mice may help clarify specific sub-population changes following adipocyte-specific loss of β -catenin.

The relatively high levels of *Ctnnb1* mRNA and β -catenin protein in knockout adipocytes also suggests the intriguing possibility that β -catenin is being delivered back to deficient cells, perhaps via SVF-derived sEVs. Many different cell types are known to secrete sEVs containing proteins, lipids, and genetic material; these sEVs serve as a unique mechanism for intercellular communication and have varied and intricate effects on receiving cells^{72,73}. This is of interest in the context of adipose biology, as WAT-derived sEVs have widespread effects^{74,75}, from regulation of hepatic FGF21 expression and glucose handling by the liver⁷⁶ to promotion of fatty acid oxidation within melanoma cells, contributing to aggressive tumor cell migration and invasion⁷⁷. sEVs are also secreted from non-adipocyte cell types within WAT, including macrophages⁷⁸, endothelial cells⁷⁹, and stromal cells⁸⁰ and can have profound effects on glucose homeostasis, insulin sensitivity, and inflammation. Recently, Crewe *et al.* found that endothelial-derived sEVs mediate cross-talk between adipocyte and SVF cell populations⁷⁹. Indeed, they reported a phenomenon strikingly similar to the one we observe in chow-fed β -cat^{-/-} mice: despite efficient genetic ablation of *Cav1* (caveolin-1), cav1 protein is readily detectable in deficient adipocytes. Ultimately, this was found to be the result of sEV-mediated trafficking of cav1 protein from surrounding endothelial cells back to *Cav1*^{-/-} adipocytes. In addition to cav1, proteomic analysis of isolated endothelial sEVs identified members of the Wnt signaling pathway, including β -catenin⁷⁹. Thus, a similar mechanism may explain the sustained expression of β -catenin protein in knockout adipocytes. In addition to identification of the cell population contributing elevated β -catenin expression, further studies will be required to determine whether β -catenin protein is being trafficked back to deficient adipocytes.

To date, studies of Wnt signaling in mature adipocytes have consistently reported that metabolic phenotypes are revealed with long-term HFD. However, conflicting results have emerged: our work in β -cat^{-/-} mice fed HFD demonstrate decreased weight gain and fat mass, significantly improved glucose homeostasis, decreased circulating TAG and glucose-stimulated insulin release, and protection from hepatosteatosis. Of note, the metabolic effects observed in our mice are remarkably consistent with data recently reported by Chen *et al.*; in their study deleting β -catenin from adipocytes, obese β -cat^{-/-} mice also exhibited decreased body weight and adiposity, accompanied by improved glucose tolerance, insulin sensitivity, and hepatosteatosis³⁷. Additionally, adipocyte-specific *Wntless*^{-/-} mice fed HFD are also characterized by decreased fat mass and protection from glucose intolerance and hepatosteatosis⁴⁰. In contrast, HFD-fed *Tcf712*^{-/-} mice demonstrated increased WAT mass, impaired glucose tolerance, and insulin insensitivity³⁹. Further, WAT isolated from *Tcf712* knockout mice had elevated lipogenic gene expression, including *Scd1*. There are many potential reasons for these discordant results, including the generation of alternative *Tcf712* splice variants⁸¹, compensatory activity of other TCF/LEF transcription factors^{18,19}, or downstream effects on signaling pathways independent of β -catenin⁸². Nevertheless, it is clear from these studies that Wnt signaling within adipocytes, while complex, plays a critical role in regulation of lipid metabolism.

One final point of interest is the functional protection from diet-induced obesity and subsequent metabolic dysfunction that loss of adipocyte-specific β -catenin signaling appears to afford mice. Chen *et al.* found that WAT of HFD-fed β -cat^{-/-} mice contained fewer PDGFR α ⁺ preadipocytes, indicating that reduced fat mass is caused by decreased hyperplasia³⁷. Further, they observed decreased expression of *Saa3*, a secreted protein that is elevated with obesity and type 2 diabetes, and which functions to activate macrophages to promote local inflammatory responses⁸³⁻⁸⁵. Thus, Chen *et al.* put forth the hypothesis that reduced *Saa3* in HFD-fed β -cat^{-/-} mice leads to less macrophage recruitment and activation, and subsequently less PDGFR α ⁺ cell proliferation. Indeed, global *Saa3*-deficient mice are resistant to diet-induced obesity, adipose tissue inflammation and dyslipidemia⁸⁶. Our own studies demonstrate that consistent with macrophage marker expression patterns, *Saa3* is mildly higher in β -cat^{-/-}

mice maintained on chow diet and is subsequently suppressed in knockout mice with HFD feeding. Thus, it is possible that β -catenin mediates cross-talk between mature adipocytes and surrounding cells through Saa3, but future studies will be required to directly answer this question.

In summary, we report that β -catenin-dependent canonical Wnt signaling regulates various metabolic pathways in mature adipocytes, including lipid metabolism (**Figure 4.8**). Indeed, β -catenin is required for coordinate regulation of DNL and fatty acid desaturation, partly mediated through the key transcription factors *Srebf1* and *Mlxipl*. Perhaps most interestingly, in chow-fed mice, CD45⁻/CD31⁻ stromal cells respond to adipocyte-specific β -catenin depletion by up-regulating β -catenin and downstream target gene expression to defend canonical Wnt signaling homeostasis within WAT. We contend that this compensatory mechanism may explain the lack of observable phenotypes under standard nutritional conditions in virtually all mouse models that have been developed to interrogate the function of Wnt signaling in adipocytes. Finally, HFD feeding obesity overrides this compensatory mechanism, revealing that β -cat⁻ mice are protected from diet-induced obesity and metabolic dysfunction. Together, these novel findings underscore the critical importance of Wnt signaling in regulation of glucose and lipid metabolism in mature adipocytes.

Materials and methods

Animals

Ctnnb1^{fl/fl} mice (hereby referred to as β -cat^{fl/fl}) (#004152, Jackson Lab, Ellsworth, ME), which harbor loxP sites flanking exons 2 to 6, were crossed with Adiponectin (Adipoq)-Cre mice (#028020, Jackson Lab, Ellsworth, ME) to generate β -cat^{fl/fl} or β -cat^{-/-} mice. Animals were housed in a 12 h light/12 h dark cycle with free access to water and food. For high fat diet (HFD) studies, mice were fed rodent diet with 60 kcal% from fat (#12492, Research Diets, New Brunswick, NJ). All animal studies were approved by and performed in compliance with policies of the University of Michigan Institutional Animal Care and Use Committee. Daily care of mice was overseen by the Unit for Laboratory Animal Medicine at the University of Michigan.

Body composition

Lean, fat, and free fluid masses were measured by a Bruker Minispec LF90II NMR (Bruker, Billerica, MA) at the University of Michigan Mouse Metabolic Phenotyping Center.

Glucose and insulin tolerance tests

For glucose tolerance tests, mice were fasted for 16 h and then given glucose (1 mg/kg body weight) via intraperitoneal injection. For insulin tolerance tests, mice were fasted for 6 h and then administered insulin (Eli Lilly, Indianapolis, IN) via intraperitoneal injection. Chow-fed mice received 0.5 U insulin/kg body weight, whereas HFD-fed mice were given 1.0 U insulin/kg body weight. Glucose concentrations were monitored in blood collected from the tail vein at 0, 15, 30, 60, and 120 minutes after injection using a glucometer and Contour Next blood glucose strips (Bayer AG, Leverkusen, Germany).

In vivo lipolysis

Mice were administered an intraperitoneal injection of saline as control or isoproterenol (10 mg/kg body weight) to stimulate lipolysis. Blood was collected from the tail vein immediately prior to and 15, 30, 60, and 120 minutes after injection. Blood was allowed

to coagulate on ice for 2 h. After centrifugation at 2,000 x g for 20 min at 4°C, serum was transferred to a new tube. Serum glycerol concentrations were measured by colorimetric assay (Sigma-Aldrich, St. Louis, MO).

Voluntary running wheel exercise

Mice were single-housed for one week prior to beginning exercise studies. Mice were then given free access to running wheels (Columbus Instruments, Columbus, OH) for voluntary exercise. Daily running totals were calculated from wheel revolutions collected at 1 min intervals for a total of six weeks.

Serum measurements

Blood was collected from the tail vein or by cardiac puncture at time of sacrifice. After coagulation on ice for 2 h and centrifugation at 2,000 x g for 20 min at 4°C, separated serum was transferred to a new tube and stored at -80°C until use. Serum insulin and adiponectin concentrations were measured by ELISA (Crystal Chem USA, Elk Grove, IL; R&D Systems Inc., Minneapolis, MN. respectively). Colorimetric assays were used to estimate triacylglycerols (TAG) and total cholesterol levels (Cayman Chemical, Ann Arbor, MI; Abcam, Cambridge, UK, respectively).

Adipocyte and stromal-vascular cell fractionation

Epididymal WAT (eWAT) and inguinal WAT (iWAT) depots were excised from mice as previously described^{87,88}. WAT depots were minced with scissors and digested in 2 mg/ml collagenase type I (Worthington Biochemical, Lakewood, NJ) in Krebs-Ringer-HEPES (KRH; pH 7.4) buffer containing 3% fatty acid-free bovine serum albumin (BSA; Gold Biotechnology, St. Louis, NJ), 1 g/L glucose, and 500 nM adenosine for 1 h at 37°C with shaking (600 rpm). Buoyant adipocytes were separated from the stromal-vascular fraction (SVF) by filtering cell suspensions through 100 µm cell strainers and then centrifuging at 100 x g for 8 min. Fractions were washed 2x with KRH buffer containing 3% fatty acid-free BSA, 1 g/L glucose, and 500 nM adenosine. For immunoblot samples, fractions were then washed 1x with KRH buffer containing 0.5% fatty acid-free BSA, 1 g/L glucose, and 500 nM adenosine.

Fluorescence-activated cell sorting of stromal-vascular cell sub-populations

Excised eWAT was digested at 37°C in RPMI medium (Thermo Fisher Scientific, Waltham, MA) containing 0.5% BSA and 1 mg/ml type II collagenase for 30 mins with shaking. In order to ensure sufficient cell numbers, three mice were combined per sample and three samples were analyzed per genotype. SVF was separated from buoyant adipocytes by differential centrifugation following filtration through 100 µm cell strainers. Cells were stained with anti-CD45-PE (clone 30-F11; eBioscience, San Diego, CA) and anti-CD31-APC (clone 390; eBioscience, San Diego, CA) antibodies prior to flow cytometry analysis. Fluorescence-activated cell sorting was performed on a BD FACSAria III cell sorter (BD Biosciences, San Jose, CA) and data were processed and analyzed using FlowJo software (BD Biosciences, San Jose, CA). Sorted cells were pelleted by 500 x g for 5 mins, and RNA was subsequently isolated for evaluation of gene expression.

Histology

After harvest, soft tissues were fixed overnight in 10% neutral buffered formalin at 4°C. Bones were fixed for 24 h in 10% neutral buffered formalin, rinsed with water and then decalcified for 14 days in 14% EDTA, pH 7.4. Tissues were then processed, paraffin-embedded, and sectioned at 5 µm thickness. Sections were stained with hematoxylin and eosin as previously described⁸⁹ and subsequently imaged using a Zeiss inverted microscope at 100x or 200x magnification, as indicated.

Micro-computed tomography (µCT) analysis of bone

Tibia were harvested and fixed in 10% neutral buffered formalin for 24 h, rinsed with water, and stored at 4°C in Sorensen's phosphate buffer, pH 7.4, prior to µCT analysis. For analysis, each bone was placed in a 19-mm diameter tube and its length was scanned using a µCT system as previously described⁴⁰ (µCT100 Scanco Medical, Bassersdorf, Switzerland). Analyses of bone parameters were performed with the manufacturer's evaluation software, using a threshold of 280 for cortical bone and 180 for trabecular bone.

Cell culture

Primary mesenchymal stem cells (MSC) were isolated from outer ears of wildtype C57BL/6J (Jackson Labs, Bar Harbor, Maine) or β -cat^{fl/fl} mice as previously described^{38,90} and cultured at 37°C in 5% CO₂. Subconfluent MSCs were maintained in DMEM:F12 medium (Thermo Fisher Scientific, Waltham, MA) containing 10% fetal bovine serum (FBS; Sigma-Aldrich, St. Louis, MO) and supplemented with 10 ng/ml recombinant basic fibroblast growth factor (PeproTech Inc., Rocky Hill, NJ). Adipogenesis was induced at two days post-confluence with 5 µg/ml insulin, 5 µM rosiglitazone, 1 µM dexamethasone, and 0.5 mM methylisobutylxanthine in DMEM:F12 containing 10% FBS. Cells were fed with fresh DMEM:F12 medium containing 10% FBS, 5 µg/ml insulin and 5 µM rosiglitazone from days 2 to 4 of differentiation. For the remainder of differentiation, cells were maintained in DMEM:F12 containing 10% FBS. Oil Red-O staining was used to visualize accumulation of neutral lipids, as previously described⁹¹. Colorimetric assay (Cayman Chemical, Ann Arbor, MI) was used to quantify total TAG accumulation per well. For lipid composition analyses, cells were differentiated in DMEM:F12 containing 10% charcoal-stripped FBS (Sigma-Aldrich, St. Louis, MO) from days 6 to 12. As indicated, confluent MSCs or mature adipocytes were treated with 3 µM CHIR99021 (Cayman Chemical, Ann Arbor, MI) or 20 ng/ml recombinant Wnt3a (R&D Systems Inc., Minneapolis, MN) for 4 h prior to lysis and RNA isolation.

Genetic recombination in cultured cells

To induce gene deletion in preadipocytes, β -cat^{fl/fl} precursors were treated at ~30% confluence with adenoviral GFP or adenoviral Cre recombinase (3 x 10⁹ viral particles/ml) in serum-free DMEM:F12 supplemented with 10 ng/ml recombinant basic fibroblast growth factor for 24 h. Preadipocytes were analyzed once they reached confluence. To induce gene recombination in adipocytes, β -cat^{fl/fl} cells were treated with adenoviral GFP or adenoviral Cre recombinase (1 x 10¹⁰ viral particles/ml) in serum-free DMEM:F12 from days 4 to 6 of differentiation. Adipocytes were then analyzed at day 12 of differentiation. Adenoviruses were obtained from the University of Michigan Vector Core. PCR with a three-primer system was used to confirm genetic recombination.

Primer sequences are as follows: P1, AAGGTAGAGTGATGAAAGTTGTT; P2, CACCATGTCCTCTGTCTATTC; P3, TACACTATTGAATCACAGGGACTT; floxed band: 324 bp, recombined band: 500 bp.

ChREBP or SREBP1c overexpression in cultured cells

β -cat^{fl/fl} and β -cat^{-/-} adipocytes were treated with adenoviral GFP, adenovirus overexpressing ChREBP, or adenovirus overexpressing SREBP1c (1 x 10⁵ viral particles/ml) in DMEM:F12 containing 10% FBS from days 9 to 12 of differentiation. Adipocytes were then analyzed at day 12 for rescue of DNL enzyme expression. Adenoviruses were obtained from Vector Biolabs (Vector Biolabs, Malvern, PA).

De novo lipogenesis (DNL) assay

Prior to evaluation of DNL, cultured adipocytes were incubated in fresh serum-free DMEM:F12 medium overnight. To measure DNL, cells were then incubated in fresh DMEM:F12 medium (with 0.5 mM sodium pyruvate, 0.5 mM L-glutamine, 2.5 mM glucose, 1% fatty acid-free BSA) containing 5 μ M sodium acetate and 0.5 μ Ci [¹⁴C]-acetate (PerkinElmer, Waltham, MA) for 2, 4, or 8 h at 37°C. Following indicated incubation times, cells were harvested and lipids extracted for analyses by scintillation counting and thin-layer chromatography.

Lipid extraction for analyses by gas chromatography

Lipids were extracted from cultured adipocytes as previously described⁴⁰. Briefly, cells were washed 2x with PBS and then collected in 500 μ l of a 1:2.5 methanol/water mixture. Cell suspensions were transferred to clean borosilicate glass tubes. Wells were rinsed with 500 μ l of the 1:2.5 methanol/water mixture and volumes were transferred to the glass tubes. After addition of 750 μ l chloroform and 375 μ l 0.9% NaCl, tubes were vortexed vigorously and centrifuged at 2,500 rpm for 20 min at 4°C. Lower organic chloroform layers containing total lipids were transferred to clean glass tubes and stored at -20°C until use.

Fatty acid composition by gas chromatography

Fatty acids within extracted lipids were derivatized into their methyl esters by transesterification with boron trifluoride-methanol, as previously described⁹². Derivatized methyl esters were re-dissolved in a small volume of hexane and purified by thin-layer chromatography using n-hexane-diethyl ether-acetic acid (50:50:2, v/v/v) as the developing solvent. Plates were dried and sprayed with Premulin after development. Products were identified under ultraviolet light by comparison to retention flow of the methyl heptadecanoate (C17:0) standard (retention flow, 0.67) applied side-by-side on the same plate. Methyl esters were extracted from thin-layer chromatography powder with diethyl ether, concentrated under nitrogen, and re-dissolved in 100 μ l hexane. Fatty acid compositions of lipids were analyzed by gas chromatography (GC) as follows: FAMES analysis was performed with 1 μ l sample injection on an Agilent GC machine, model 6890N equipped with flame ionization detector, an auto sampler and a Chemstation software for data analysis. An Agilent HP 88, 30 m GC column with a 0.25 mm inner diameter and 0.20 mm film thickness was used, with hydrogen as a carrier gas and nitrogen as a makeup gas. Analyses were carried out with a temperature programming of 125-220°C. Fatty acid components within unknown samples were identified with respect to retention times of authentic standard methyl ester mixtures run side-by-side. Fatty acid components were quantified with respect to a known amount of internal standard added and the calibration ratio derived from each fatty acid of a standard methyl esters mixture and the methyl heptadecanoate internal standard. Coefficient of variation for GC analyses was found to be 2.3-3.7%.

Quantitative RT-PCR

Total RNA was isolated and purified from cultured cells or frozen tissue using RNA STAT-60 (Tel Test, Alvin, TX) according to the manufacturer's instructions. M-MLV Reverse Transcriptase (Invitrogen, Carlsbad, CA) was used to reverse-transcribe 1 μ g RNA to cDNA. qRT-PCR was performed using qPCRBIO Sygreen Mix (Innovative Solutions, Beverly Hill, MI) on a StepOnePlus System (Applied Biosystems, Foster City, CA). All primers were validated with cDNA titration curves prior to use; qPCR product specificities were confirmed by melting curve analyses and gel electrophoresis. Gene

expression was calculated using a cDNA titration curve within each plate and was subsequently normalized to peptidylprolyl isomerase A (PPIA) mRNA expression.

RNA sequencing (RNA-seq) analyses

Confluent β -cat^{fl/fl} and β -cat^{-/-} preadipocytes and terminally-differentiated adipocytes were treated with 20 ng/ml recombinant Wnt3a (R&D Systems Inc., Minneapolis, MN) or vehicle for 4 h prior to lysis and RNA isolation (n = 4 per group). After DNase treatment, samples were submitted to the University of Michigan Advanced Genomics Core for quality control, library preparation, and sequencing on an Illumina Hi-Seq platform. Read files for each sample were subsequently downloaded and collated into a single .fastq file. FastQC (version v0.11.30) was used to evaluate the quality of raw read data and to identify problematic features (inappropriate GC content, over-represented sequences, low-quality scores). Alignment, differential expression analyses, and post-analysis diagnostics were performed using the Tuxedo Suite software package. Briefly, TopHat (version 2.0.13) and Bowtie2 (version 2.2.1) were used to align reads to the UCSC reference genome. A second round of quality control was performed post-alignment using FastQC to ensure that only high-quality data was used for gene expression quantitation and differential expression analyses. Differential expression analyses were performed using two independent methods: Cufflinks/CuffDiff and HTSeq/DESeq2, using UCSC build mm10 as the reference genome sequence. Pathway analyses were conducted on ranked lists of log₂ fold change using Gene Set Enrichment Analysis (GSEA) software v4.0.3 and Molecular Signature Database (MSigDB) by the Broad Institute⁹³. Prior to running analyses, mouse gene symbols were remapped to human ortholog symbols using chip annotation files. Mouse genes that did not have equivalent human orthologs were excluded from analyses. Output from DESeq2 analyses were used to generate lists of genes ranked by the metric $-\log_{10}$ FDR*log₂ fold change. The resulting lists were run through pre-ranked GSEA using the Molecular Signatures Database v7.1 (H, hallmark gene sets). Enriched pathways were defined by an FDR < 0.05. Normalized enrichment score (NES) is the primary metric from GSEA for evaluating the magnitude of differentially expressed pathways. Pathway impact analyses were conducted on AdvaitaBio's iPathwayGuide⁹⁴ to identify enriched

KEGG pathways. The ggplot2 package in R was used for further visualization of enriched pathways.

Chromatin immunoprecipitation (ChIP-seq) analyses

ChIP-seq data of Tcf712 binding sites in *Tcf712^{fl/fl}* and *Tcf712^{-/-}* cultured adipocytes was previously generated³⁹ and is publicly available. Data was obtained from Gene Expression Omnibus (GEO accession: GSE129403). The Integrative Genomics Viewer (IGV) was used for visualization of Tcf712 peaks⁹⁵.

Human gene expression data

Human *Ctnnb1* gene expression data were obtained from the publicly available Genotype-Tissue Expression (GTEx) database.

Immunoblot analyses

Tissue samples were homogenized with a BioVortexer mixer (Chemglass, Vineland, NJ) in ice-cold lysis buffer (1% SDS, 12.7 mM EDTA, 60 mM Tris-HCl; pH 6.8) containing 1:100 protease inhibitor cocktail (Sigma-Aldrich, St. Louis, MO). Lysates were centrifuged at 13,600 x g for 10 min at 4°C, the top lipid layer removed, and extracts were centrifuged again. Cultured cells were washed 2x with PBS, lysed in ice-cold lysis buffer containing 1:100 protease inhibitor cocktail, and homogenized. Lysates were then centrifuged at 13,600 x g for 10 min at 4°C. Protein concentrations of tissue or cell lysates were measured by BCA protein assay (Thermo Scientific, Waltham, MA). Lysates were diluted to equal protein concentrations in Laemmli sample buffer and lysis buffer, vigorously vortexed, and denatured at 95°C for 5 min. Tissue or cell extracts (20 µg) were separated by SDS-PAGE on 4-12% gradient polyacrylamide gels (Invitrogen, Carlsbad, CA) and transferred to Immobilon PVDF membranes (Millipore, Billerica, MA). Prior to immunoblotting with primary antibodies, membranes were blocked in 5% non-fat dried milk in Tris-buffered saline, pH 7.4, containing 0.05% Tween-20 (TTBS) for 1 h at room temperature. All primary antibodies were used at a concentration of 1:1000 in TTBS containing 5% BSA overnight at 4°C. Membranes were probed with horseradish peroxidase-conjugated secondary antibodies (1:5000) diluted in 5% non-fat dried milk in

TTBS for 1.5 h at room temperature and subsequently visualized with Clarity Western ECL Substrate (Bio-Rad, Hercules, CA) or SuperSignal West Femto Maximum Sensitivity Substrate (Thermo Scientific, Waltham, MA).

Statistics

All data are presented as mean \pm S.D. Significance was determined using two-tailed Student's t-test when comparing two groups. An analysis of variance (ANOVA) was followed by post hoc analyses with Dunnett's or Sidak's test, as appropriate, when comparing multiple experimental groups. Observed differences were considered to be significant at $p < 0.05$ and are indicated with asterisks.

Figure 4.1

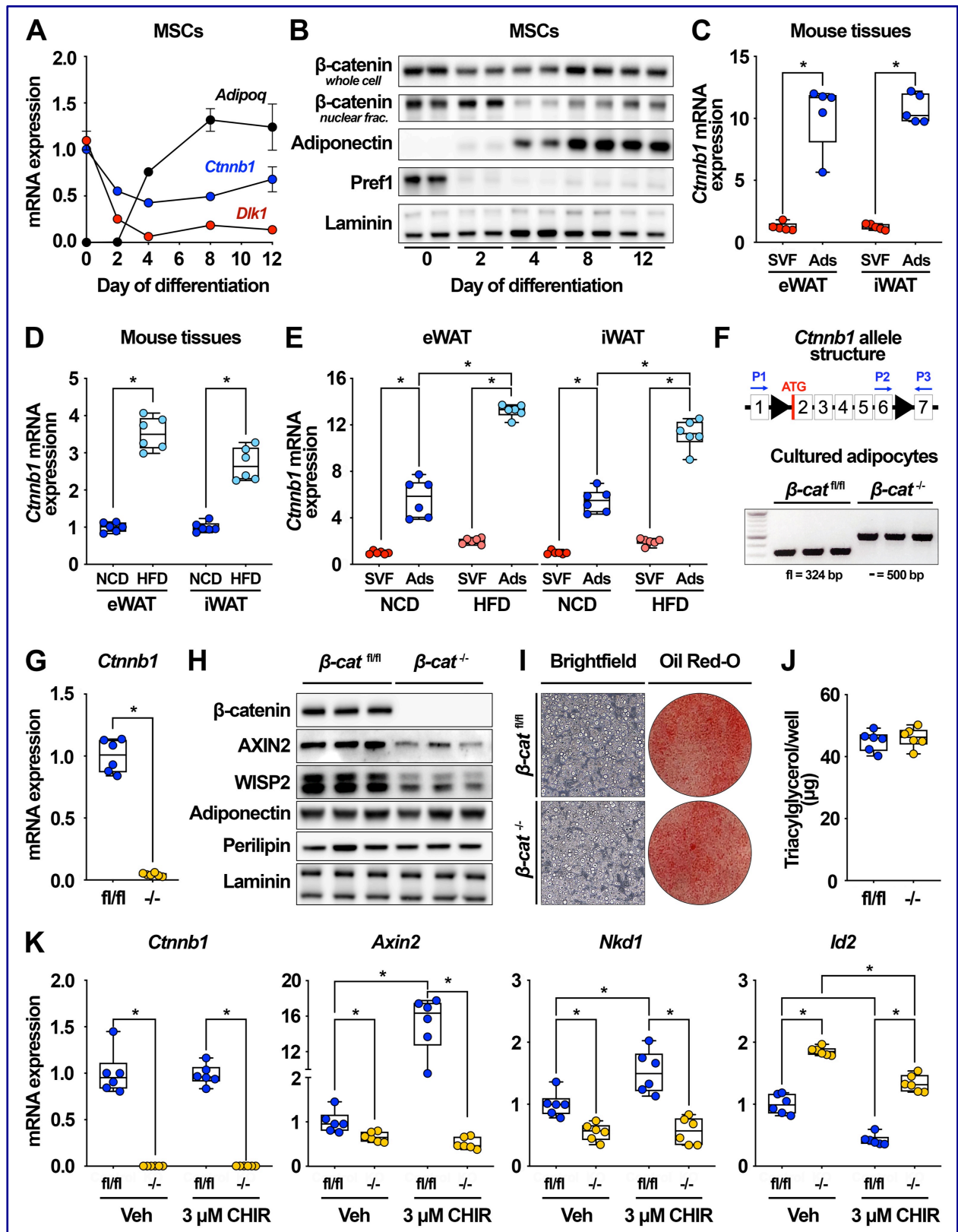
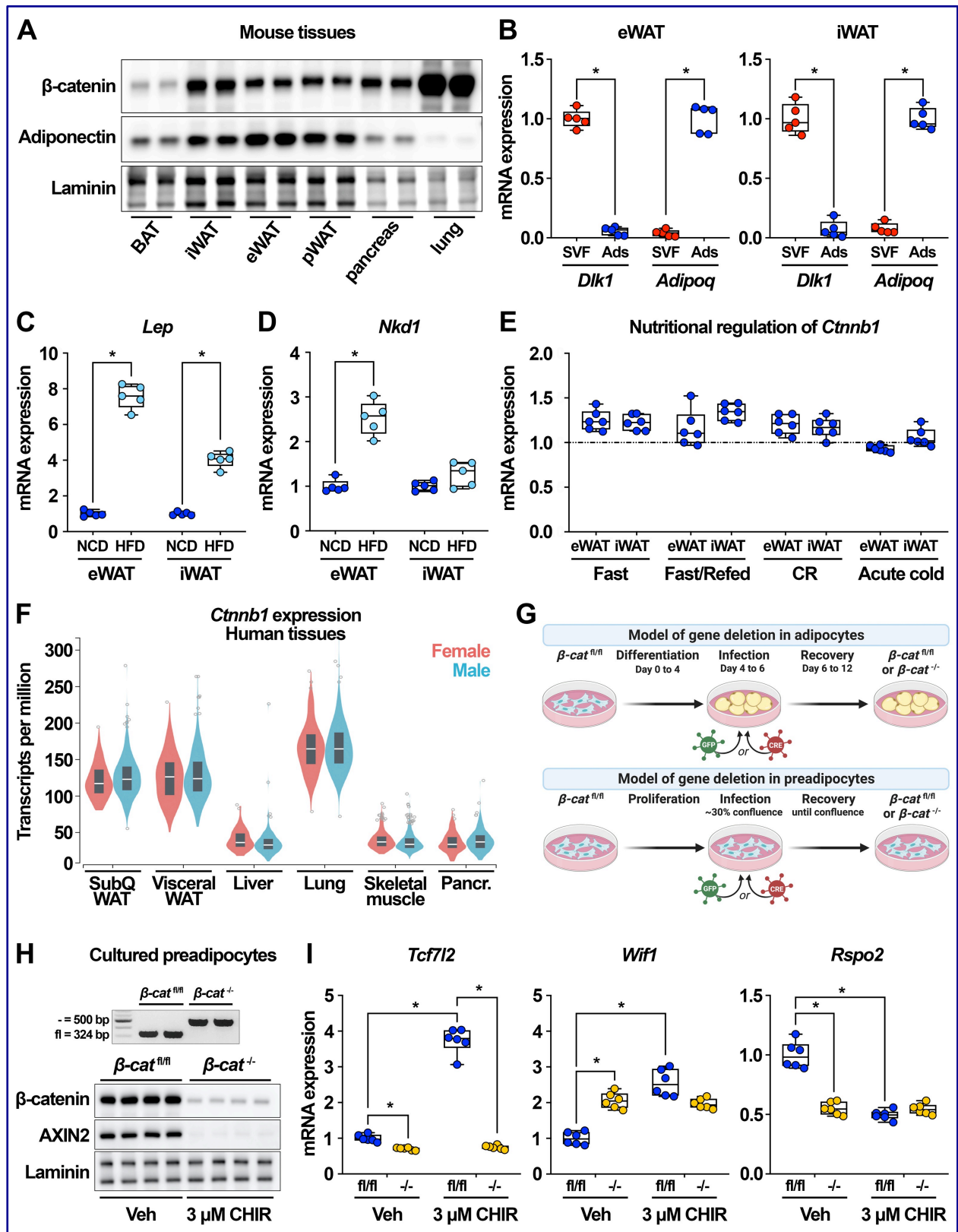


Figure 4.1. β -catenin is expressed in cultured and primary adipocytes and up-regulated by diet-induced obesity. (A-B) Mesenchymal stem cells (MSC) isolated from C57BL/6J mice were cultured under standard conditions and induced to differentiate. *Ctnnb1* gene (n = 6) and protein (n = 2) expression at indicated days of adipogenesis. (C) *Ctnnb1* gene expression in stromal-vascular (SVF) and adipocyte (Ads) fractions isolated from epididymal (eWAT) and inguinal (iWAT) white adipose tissues (WAT) of C57BL/6J mice (males; n = 5). (D) Expression of *Ctnnb1* in eWAT and iWAT of mice fed normal chow diet (NCD) or high fat diet (HFD) for 10 weeks. (E) *Ctnnb1* expression in SVF and Ads of eWAT and iWAT isolated from NCD- and HFD-fed mice (males; n = 5). (F) *Ctnnb1* allele structure and genetic recombination in β -cat^{fl/fl} and β -cat^{-/-} adipocytes using a 3-primer PCR system (n = 3). (G-H) *Ctnnb1* RNA (n = 6) and protein (n = 3) expression in adipocytes following adenoviral GFP or Cre infection. (I) Representative brightfield and Oil Red-O images, and (J) triacylglycerol (TAG) accumulation in β -cat^{fl/fl} and β -cat^{-/-} adipocytes (n = 6). (K) Expression of *Ctnnb1* and downstream Wnt target genes in β -cat^{fl/fl} and β -cat^{-/-} adipocytes treated with vehicle or 3 μ M CHIR99021 for 4 h (n = 6). RNA expression normalized to PPIA. Data presented as mean \pm S.D. * indicates significance at p < 0.05.

Supplemental Figure 4.1



Supplemental Figure 4.1. (A) Representative immunoblot of β -catenin protein expression across C57BL/6J mouse tissues (BAT, brown adipose tissue; pWAT, perirenal WAT); adiponectin and laminin included as controls. (B) *Dlk1* and *Adipoq* gene expression in SVF and adipocyte fractions isolated from eWAT and iWAT of C57BL/6J mice (males; n = 5). (C-D) *Lep* and *Nkd1* mRNA expression in SVF and adipocytes isolated from eWAT and iWAT of mice fed NCD or 10 weeks of HFD (males; n = 5). (E) Regulation of *Ctnnb1* gene expression in eWAT and iWAT by nutritional and environmental conditions: fast: 18 h; refed: 6 h after 18 h fast; 30% calorie restriction (CR): 6 weeks; 4°C cold exposure: 6 h. Each condition normalized to its individual experimental control set to 1 (indicated by dashed line; n = 6). (F) *Ctnnb1* gene expression in male and female human tissues; data obtained from the GTEx-RNA-Seq dataset. (G) Schematic model for deletion of β -catenin in cultured preadipocytes or adipocytes using adenoviral Cre recombinase. (H) *Ctnnb1* gene recombination (n = 2) and β -catenin protein expression (n = 4) in preadipocytes treated with adenoviral GFP or Cre. (I) Expression of downstream Wnt target genes in β -cat^{fl/fl} and β -cat^{-/-} adipocytes treated with vehicle or 3 μ M CHIR99021 for 4 h (n = 6). RNA expression normalized to PPIA. Data presented as mean \pm S.D. * indicates significance at p < 0.05.

Figure 4.2

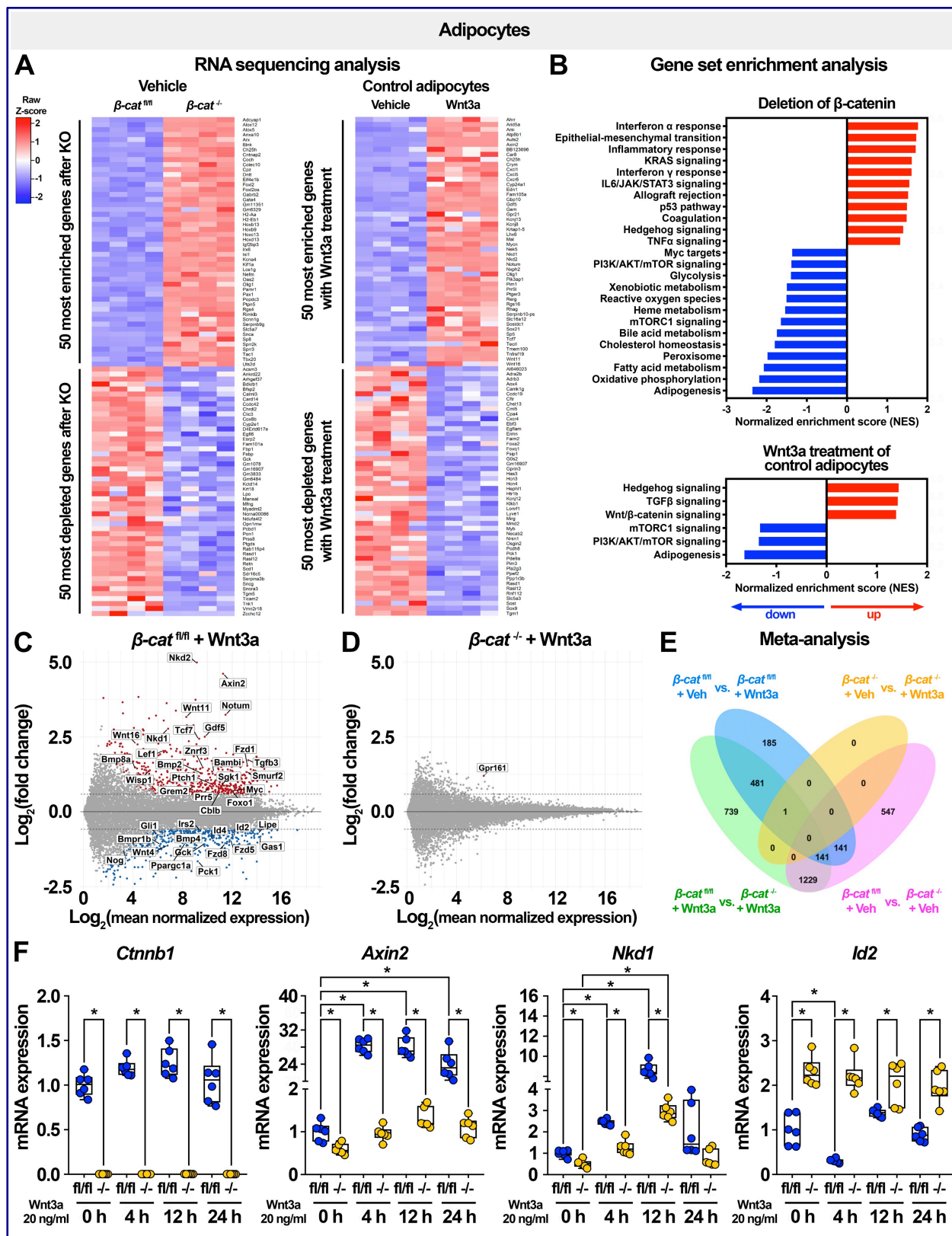
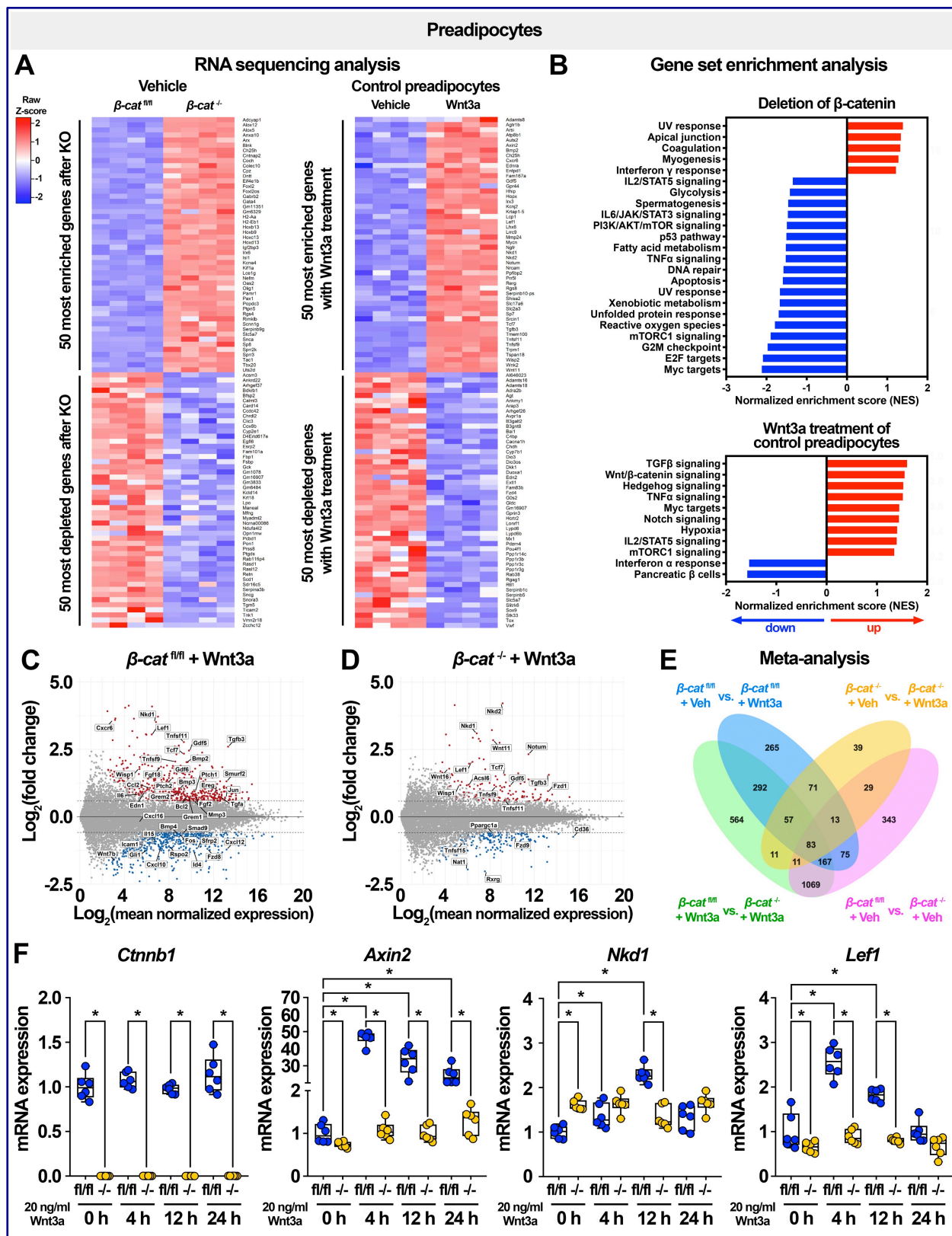


Figure 4.2. β -catenin regulates metabolic pathways in adipocytes and exclusively mediates effects of canonical Wnt3a signaling. RNA-seq analyses were performed on β -cat^{fl/fl} and β -cat^{-/-} adipocytes under basal conditions or after 4 h treatment with recombinant Wnt3a (20 ng/ml; n = 4 per group). **(A)** Heat maps of differential gene expression changes in β -cat^{fl/fl} and β -cat^{-/-} adipocytes under basal conditions (left panel) and β -cat^{fl/fl} cells treated with vehicle or Wnt3a (right panel). **(B)** Gene Set Enrichment Analyses (GSEA) of genes expressed in β -cat^{fl/fl} and β -cat^{-/-} adipocytes under basal conditions (top panel) and β -cat^{fl/fl} cells treated with vehicle or Wnt3a (bottom panel). **(C-D)** MA plots of gene expression changes following Wnt3a treatment of β -cat^{fl/fl} or β -cat^{-/-} adipocytes. **(E)** Venn diagram depicting meta-analysis of gene expression changes in β -cat^{fl/fl} or β -cat^{-/-} adipocytes treated with vehicle or Wnt3a for 4 h. **(F)** Expression of *Ctnnb1* and downstream Wnt target genes in β -cat^{fl/fl} and β -cat^{-/-} adipocytes treated with vehicle or 20 ng/ml recombinant Wnt3a for 4, 12 or 24 h (n = 6). RNA expression normalized to PPIA. Data presented as mean \pm S.D. * indicates significance at p < 0.05.

Supplemental Figure 4.2



Supplemental Figure 4.2. RNA-seq analyses were performed on β -cat^{fl/fl} and β -cat^{-/-} preadipocytes under basal conditions or after 4 h treatment with recombinant Wnt3a (20 ng/ml; n = 4 per group). **(A)** Heat maps of differential gene expression changes in β -cat^{fl/fl} and β -cat^{-/-} preadipocytes under basal conditions (left panel) and β -cat^{fl/fl} cells treated with vehicle or Wnt3a (right panel). **(B)** Gene Set Enrichment Analyses (GSEA) of genes in β -cat^{fl/fl} and β -cat^{-/-} preadipocytes under basal conditions (top panel) and β -cat^{fl/fl} cells treated with vehicle or Wnt3a (bottom panel). **(C-D)** MA plots of gene expression changes following Wnt3a treatment of β -cat^{fl/fl} or β -cat^{-/-} preadipocytes. **(E)** Venn diagram depicting meta-analysis of gene expression changes in β -cat^{fl/fl} or β -cat^{-/-} preadipocytes treated with vehicle or Wnt3a for 4 h. **(F)** Expression of *Ctnnb1* and downstream Wnt target genes in β -cat^{fl/fl} and β -cat^{-/-} preadipocytes treated with vehicle or 20 ng/ml recombinant Wnt3a for 4, 12 or 24 h (n = 6). RNA expression normalized to PPIA. Data presented as mean \pm S.D. * indicates significance at p < 0.05.

Figure 4.3

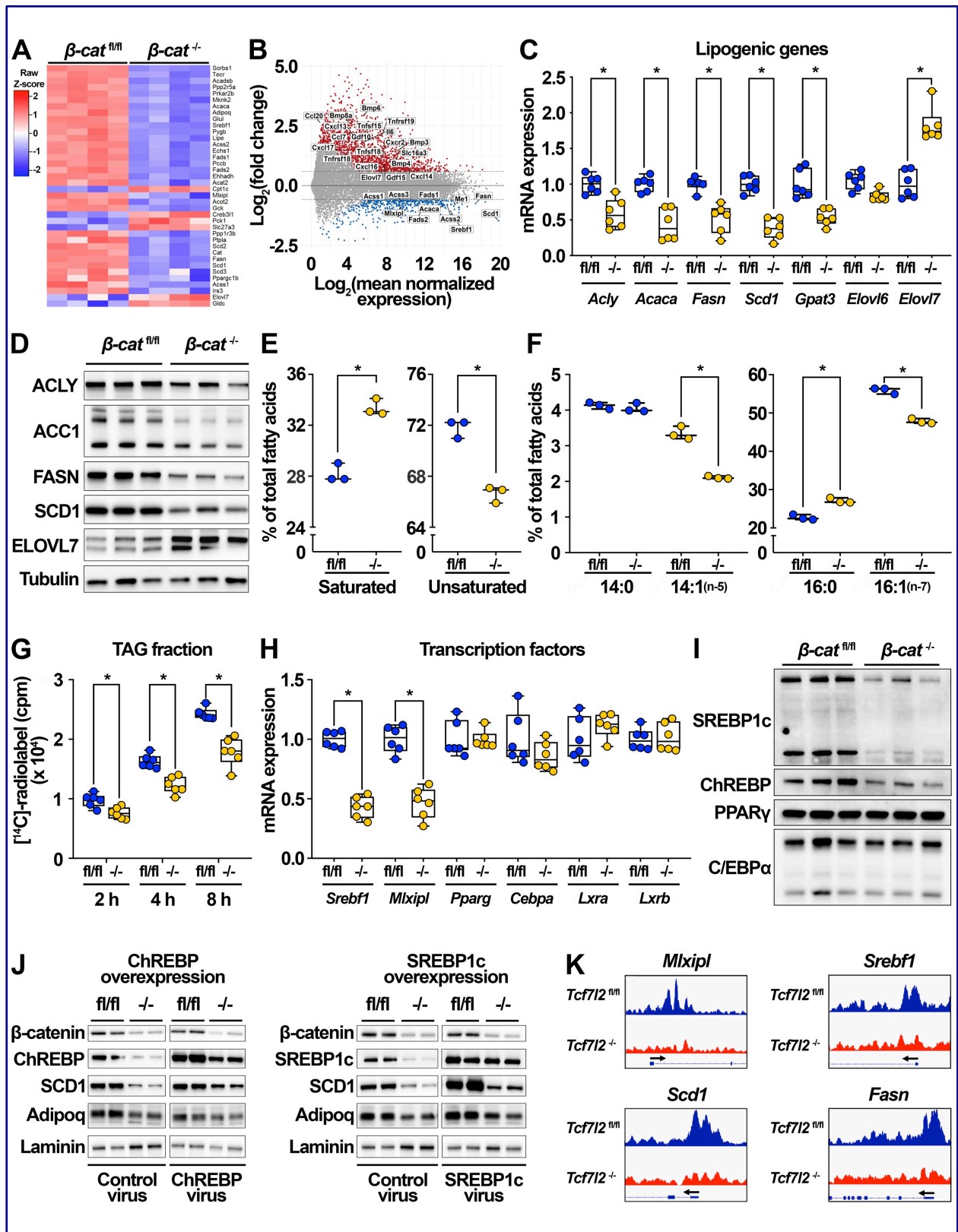
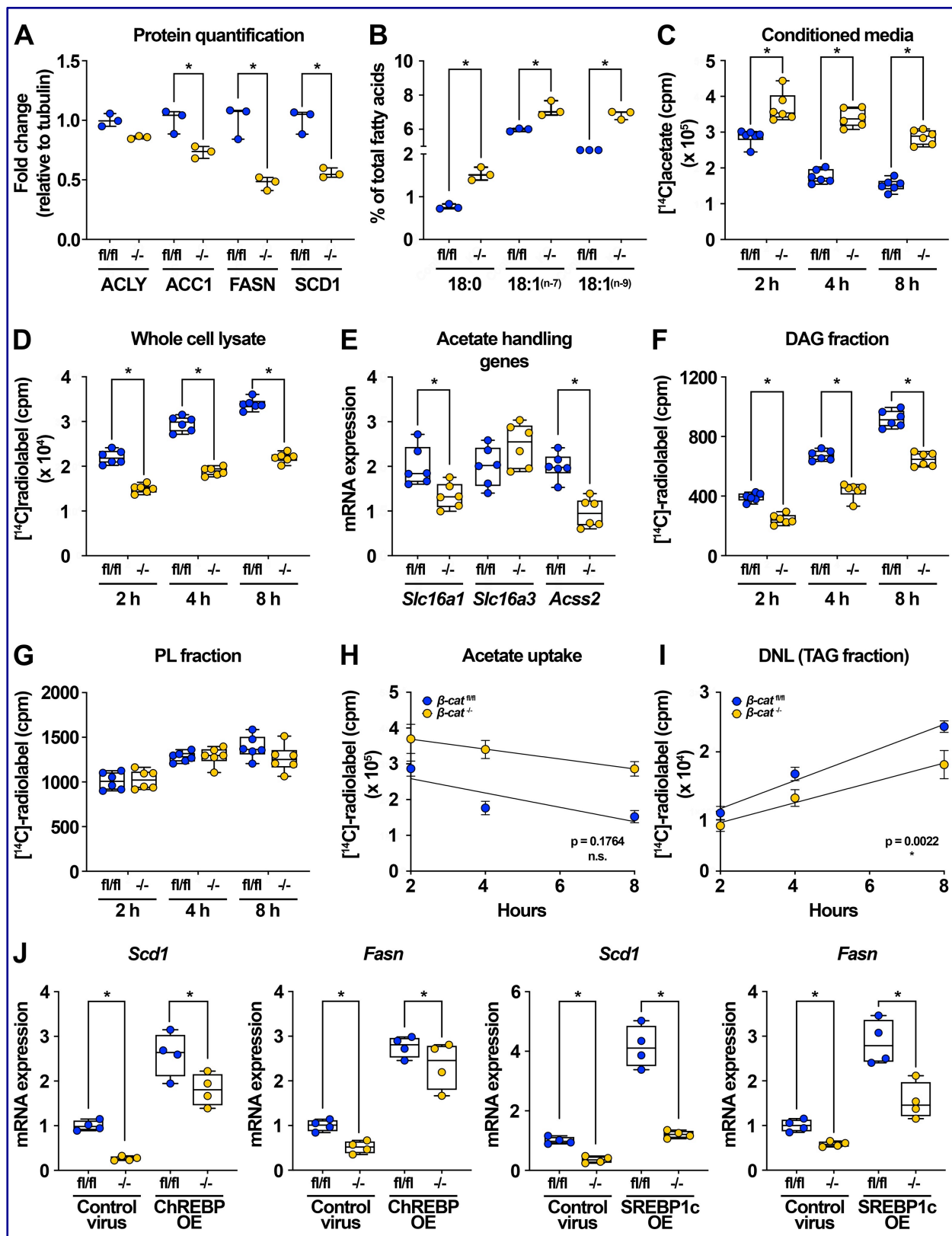


Figure 4.3. β -catenin-dependent Wnt signaling regulates lipogenesis and fatty acid desaturation in adipocytes. (A-B) Heat map and MA plot showing differentially expressed genes related to fatty acid, cholesterol, and bile acid metabolism in cultured β -cat^{fl/fl} and β -cat^{-/-} adipocytes (n = 4). (C-D) Lipogenic gene (n = 6) and protein (n = 3) expression in β -cat^{fl/fl} and β -cat^{-/-} adipocytes. (E) Proportion of total saturated versus unsaturated fatty acids in lipids extracted from β -cat^{fl/fl} and β -cat^{-/-} adipocytes (n = 3). (F) Relative proportions of myristic (C14:0) and palmitic (C16:0) versus myristoleic (C14:1, n-5) and palmitoleic (C16:1, n-7) acids (n = 3). (G) *De novo* lipogenesis (DNL) was evaluated in cultured β -cat^{fl/fl} and β -cat^{-/-} adipocytes using [¹⁴C]-acetate for 2, 4 and 8 h. Incorporation of [¹⁴C]-radiolabel into TAG fractions extracted from β -cat^{fl/fl} and β -cat^{-/-} adipocytes was quantified by scintillation counting (n = 6). (H-I) Gene (n = 6) and protein (n = 3) expression of indicated transcription factors in β -cat^{fl/fl} and β -cat^{-/-} adipocytes. (J) Protein expression in β -cat^{fl/fl} and β -cat^{-/-} adipocytes treated for 72 h with adenovirus expressing GFP, ChREBP, or SREBP1c (1 x 10⁵ viral particles/ml). (K) Integrative Genomics Viewer capture showing Tcf712 peaks (indicating binding occupancy) in the regions \pm 3 kb from transcription start sites (black arrows) of indicated genes in cultured Tcf712^{fl/fl} and Tcf712^{-/-} adipocytes. RNA expression normalized to PPIA. Data presented as mean \pm S.D. * indicates significance at p < 0.05.

Supplemental Figure 4.3



Supplemental Figure 4.3. (A) Lipogenic proteins quantified by densitometry (n = 3). (B) Relative proportions of stearic (C18:0) versus vaccenic (C18:1, n-7) and oleic (C18:1, n-9) acids in β -cat^{fl/fl} and β -cat^{-/-} adipocytes (n = 3). [¹⁴C]-radiolabel in (C) conditioned media versus (D) whole cell lysates after indicated incubation times measured by scintillation counting (n = 6). (E) Expression of genes related to acetate uptake and activation (n = 6). (F-G) Radiolabel incorporation into DAG and PL fractions extracted from β -cat^{fl/fl} and β -cat^{-/-} adipocytes quantified by scintillation counting (n = 6). (H) Linear regression analyses comparing slopes of acetate uptake over time from conditioned media into β -cat^{fl/fl} and β -cat^{-/-} adipocytes. (I) Linear regression analyses comparing slopes of radiolabel incorporation over time into TAG fractions of β -cat^{fl/fl} and β -cat^{-/-} adipocytes. (J) Gene expression in β -cat^{fl/fl} and β -cat^{-/-} adipocytes treated with adenovirus expressing GFP, ChREBP, or SREBP1c for 72 h (1 x 10⁵ viral particles/ml; n = 4). RNA expression normalized to PPIA. Data presented as mean ± S.D. * indicates significance at p < 0.05.

Figure 4.4

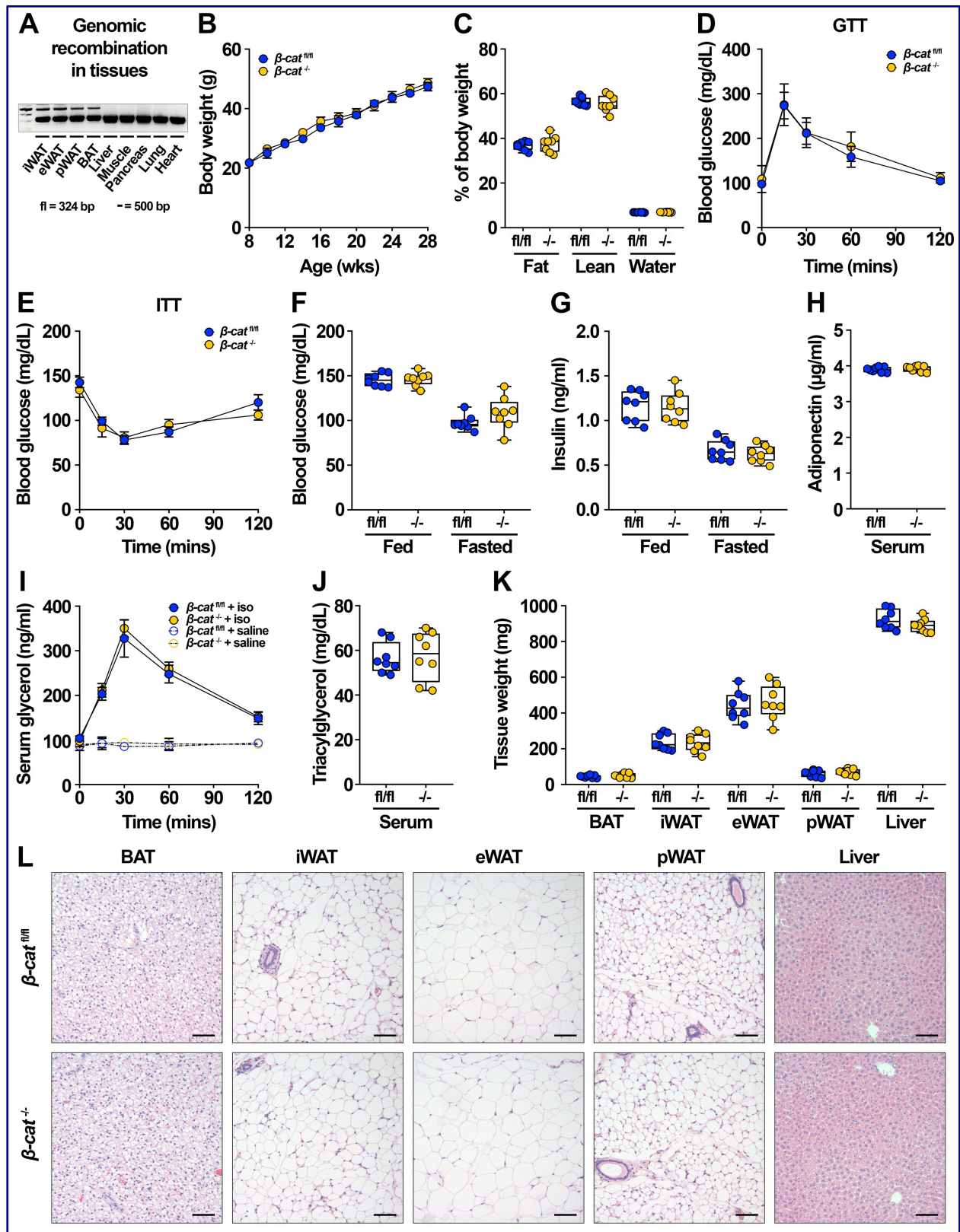
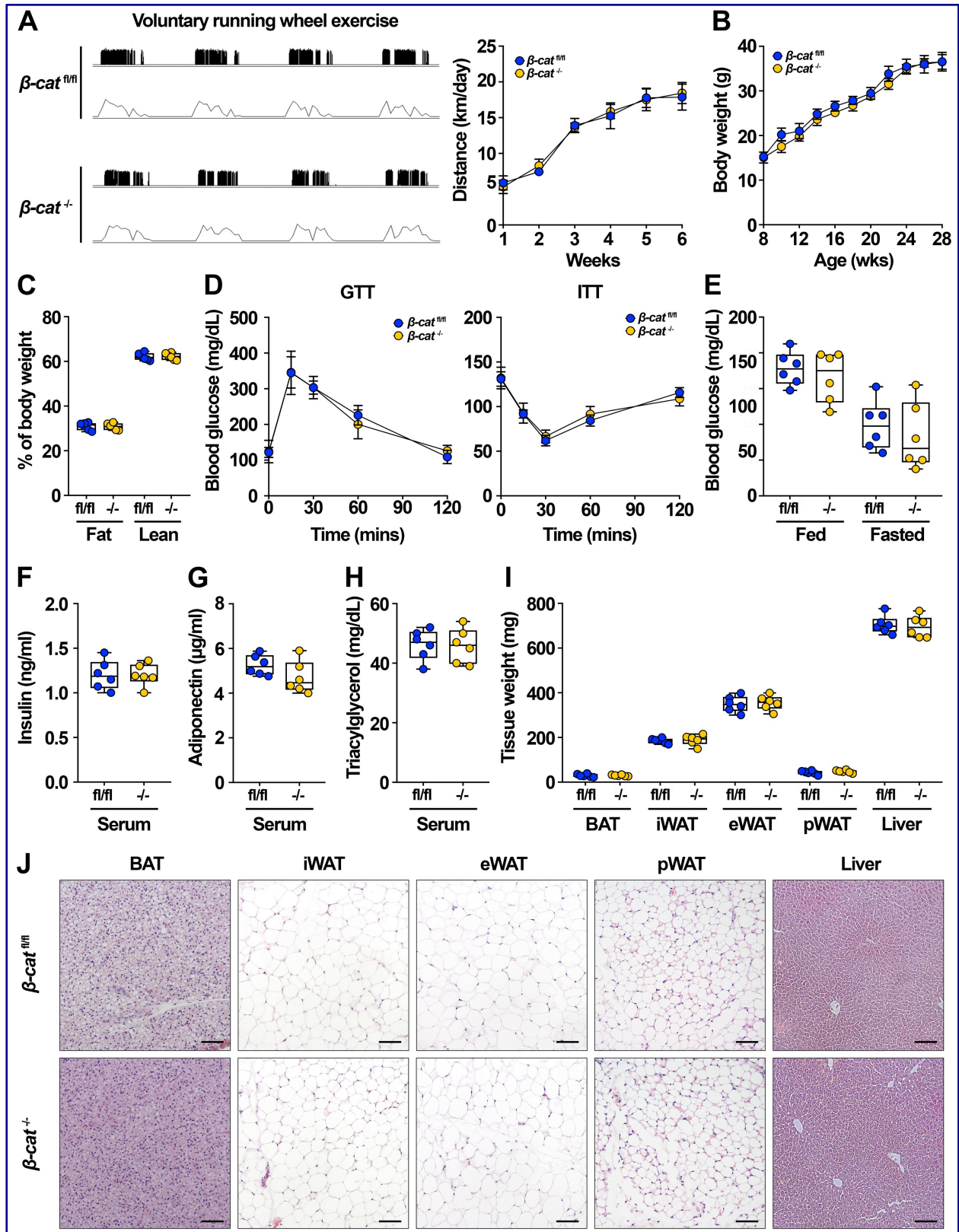


Figure 4.4. Adipocyte-specific β -catenin deletion does not influence global metabolism on a normal chow diet. (A) Genetic recombination in tissues isolated from β -cat^{-/-} mice. (B) Growth curve of 28-week-old β -cat^{fl/fl} and β -cat^{-/-} mice. (C) Body composition of 16-week-old β -cat^{fl/fl} and β -cat^{-/-} mice on NCD. (D) Glucose tolerance tests in 16-week-old β -cat^{fl/fl} and β -cat^{-/-} mice. (E) Insulin tolerance test in 19-week-old mice. (F) Blood glucose concentrations in random-fed and 16 h fasted mice. Serum concentrations of (G) random-fed and fasted insulin and (H) adiponectin levels in 28-week-old mice. (I) Basal and stimulated lipolysis in 22-week-old mice (iso, isoproterenol: 10 mg/kg body weight). (J) Serum TAG in 28-week-old mice. (K) Tissue weights at time of sacrifice. (L) Representative histological images of H&E-stained tissues from β -cat^{fl/fl} and β -cat^{-/-} mice fed NCD for 28 weeks; 200x magnification; scale bar, 100 μ m. Data in **B-L** from male mice, n = 8 per group. Data presented as mean \pm S.D. * indicates significance at p < 0.05.

Supplemental Figure 4.4



Supplemental Figure 4.4. (A) Representative traces and quantification of daily running distance in chow-fed male 23-week-old β -cat^{fl/fl} and β -cat^{-/-} mice given access to voluntary exercise wheels for six weeks. (B) Growth curve of 28-week-old female β -cat^{fl/fl} and β -cat^{-/-} mice. (C) Body composition of 16-week-old β -cat^{fl/fl} and β -cat^{-/-} mice on NCD. (D) Glucose and insulin tolerance tests in 16- and 19-week-old β -cat^{fl/fl} and β -cat^{-/-} mice, respectively. (E) Blood glucose concentrations in random-fed and 16 h fasted mice. Serum concentrations of (F) insulin, (G) adiponectin, and (H) TAG in 28-week-old mice. (I) Tissue weights at time of sacrifice. (J) Representative histological images of H&E-stained tissues from female β -cat^{fl/fl} and β -cat^{-/-} mice fed NCD for 28 weeks; 200x magnification; scale bar, 100 μ m. Data in **B-J** from female mice, n = 6 per group. Data presented as mean \pm S.D. * indicates significance at p < 0.05.

Figure 4.5

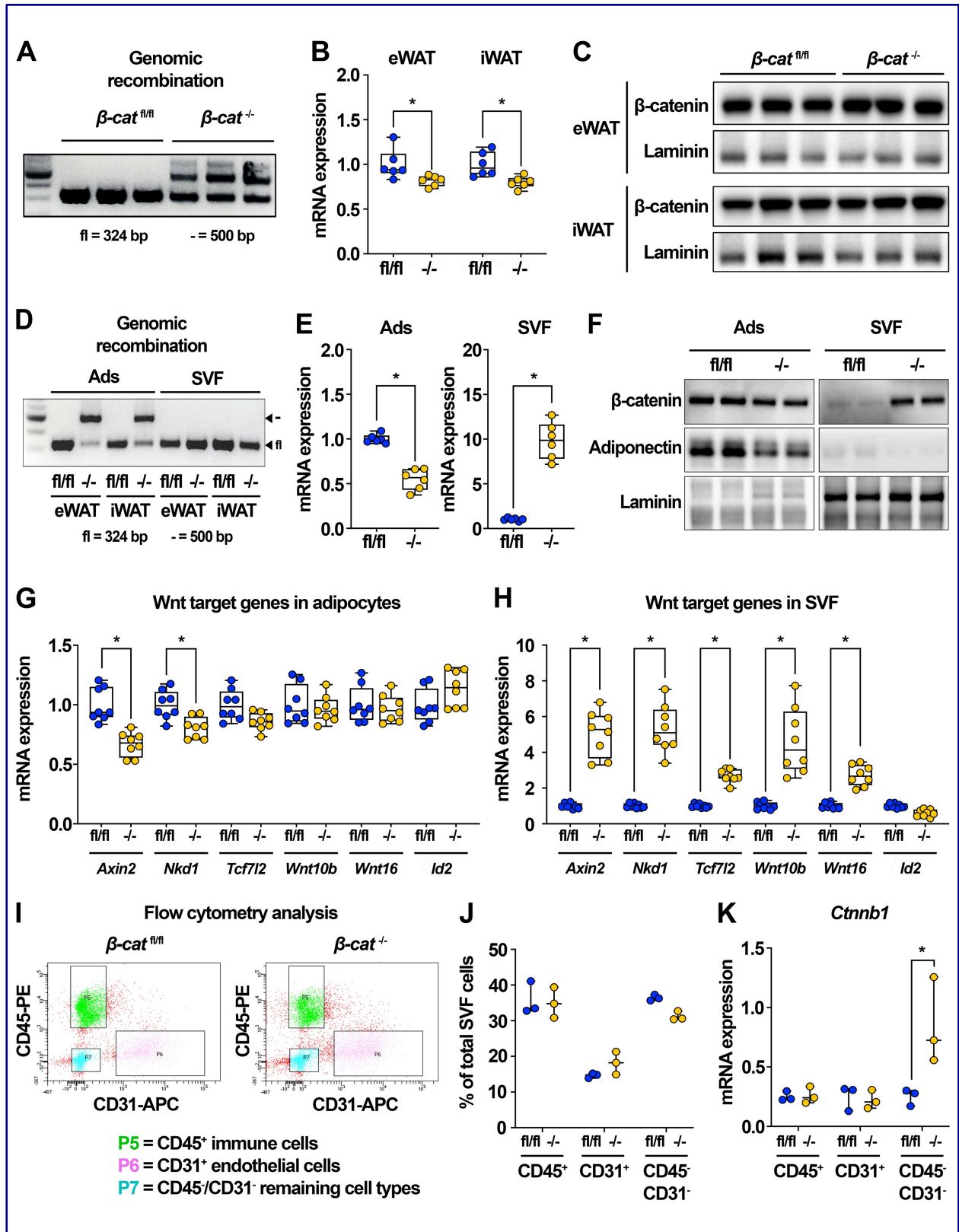
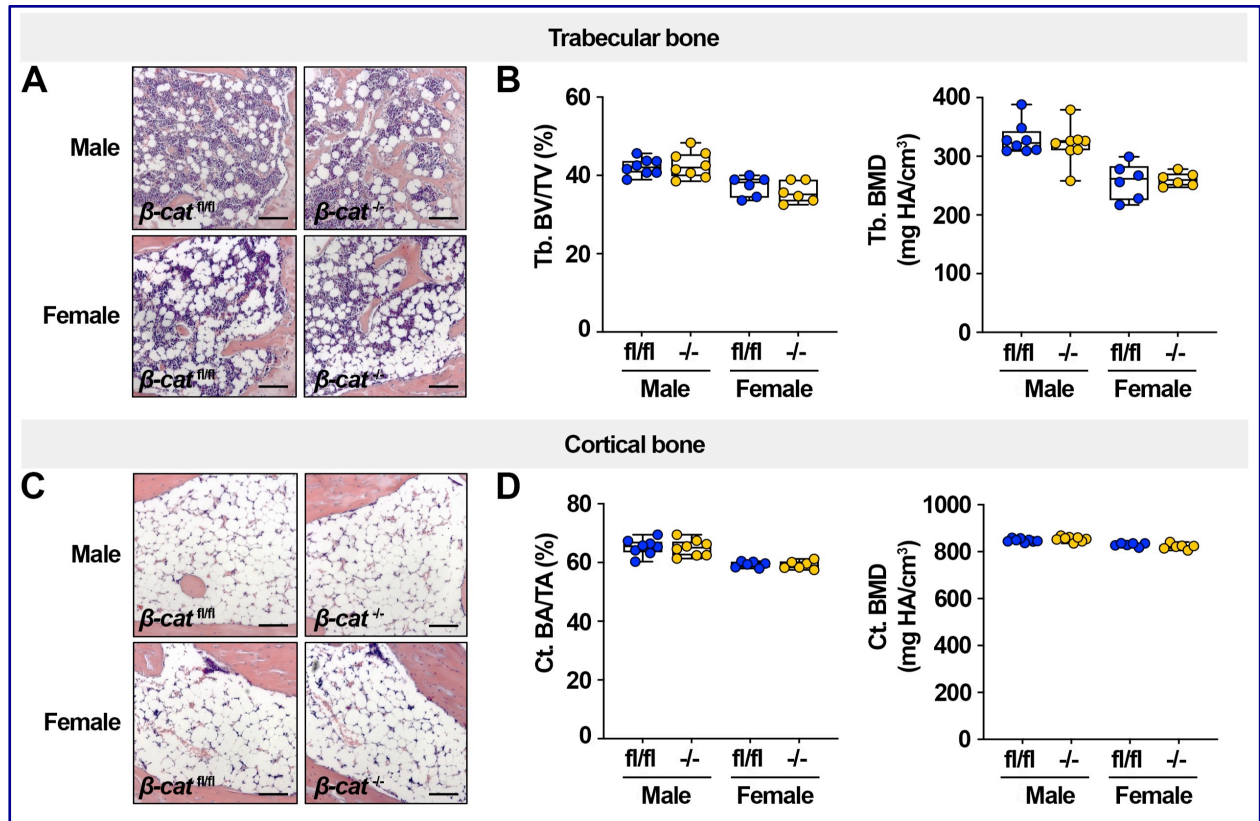


Figure 4.5. β -catenin is up-regulated in the stromal-vascular fraction of adipose tissues from knockout mice. (A) Genetic recombination in tissues isolated from β -cat^{fl/fl} and β -cat^{-/-} mice (n = 3). (B-C) *Ctnnb1* mRNA (n = 3) and protein (n = 6) expression in eWAT and iWAT of β -cat^{fl/fl} and β -cat^{-/-} mice. (D) Genomic recombination of β -catenin in adipocytes and SVF isolated from eWAT and iWAT of β -cat^{fl/fl} and β -cat^{-/-} mice. (E) *Ctnnb1* mRNA expression in isolated eWAT adipocytes and SVF of β -cat^{fl/fl} and β -cat^{-/-} mice (n = 6). (F) β -catenin protein expression in isolated eWAT adipocytes and SVF of β -cat^{fl/fl} and β -cat^{-/-} mice; adiponectin and laminin shown as protein loading controls. (G-H) Wnt target gene expression in adipocytes and SVF isolated from eWAT of β -cat^{fl/fl} and β -cat^{-/-} mice (n = 8). (I) Representative plots showing flow cytometry analysis of SVF isolated from β -cat^{fl/fl} and β -cat^{-/-} mice (3 mice per sample; n = 3 samples). (J) Quantification of SVF cell proportions evaluated by flow cytometry analysis (3 mice per sample; n = 3 samples). (K) *Ctnnb1* mRNA expression normalized to PPIA in cellular fractions isolated by FACS analysis (3 mice per sample; n = 3 samples). Data presented as mean \pm S.D. * indicates significance at p < 0.05.

Supplemental Figure 4.5



Supplemental Figure 4.5. (A) Representative histological images of H&E-stained proximal tibia (regulated bone marrow adipose tissue) of male and female $\beta\text{-cat}^{fl/fl}$ and $\beta\text{-cat}^{-/-}$ mice fed NCD for 28 weeks (male: n = 8; female: n = 6). (B) μ CT analyses of tibial trabecular bone volume fraction (Tb. BV/TV) and trabecular bone mineral density (Tb. BMD). (C) Representative histological images of H&E-stained distal tibia (constitutive bone marrow adipose tissue) of male and female $\beta\text{-cat}^{fl/fl}$ and $\beta\text{-cat}^{-/-}$ mice. (D) μ CT analyses of mid-tibial cortical bone area (Ct. BA/TA) and cortical bone mineral density (Ct. BMD). Histological images shown at 100x magnification; scale bar, 50 μ m. Data presented as mean \pm S.D. * indicates significance at p < 0.05.

Figure 4.6

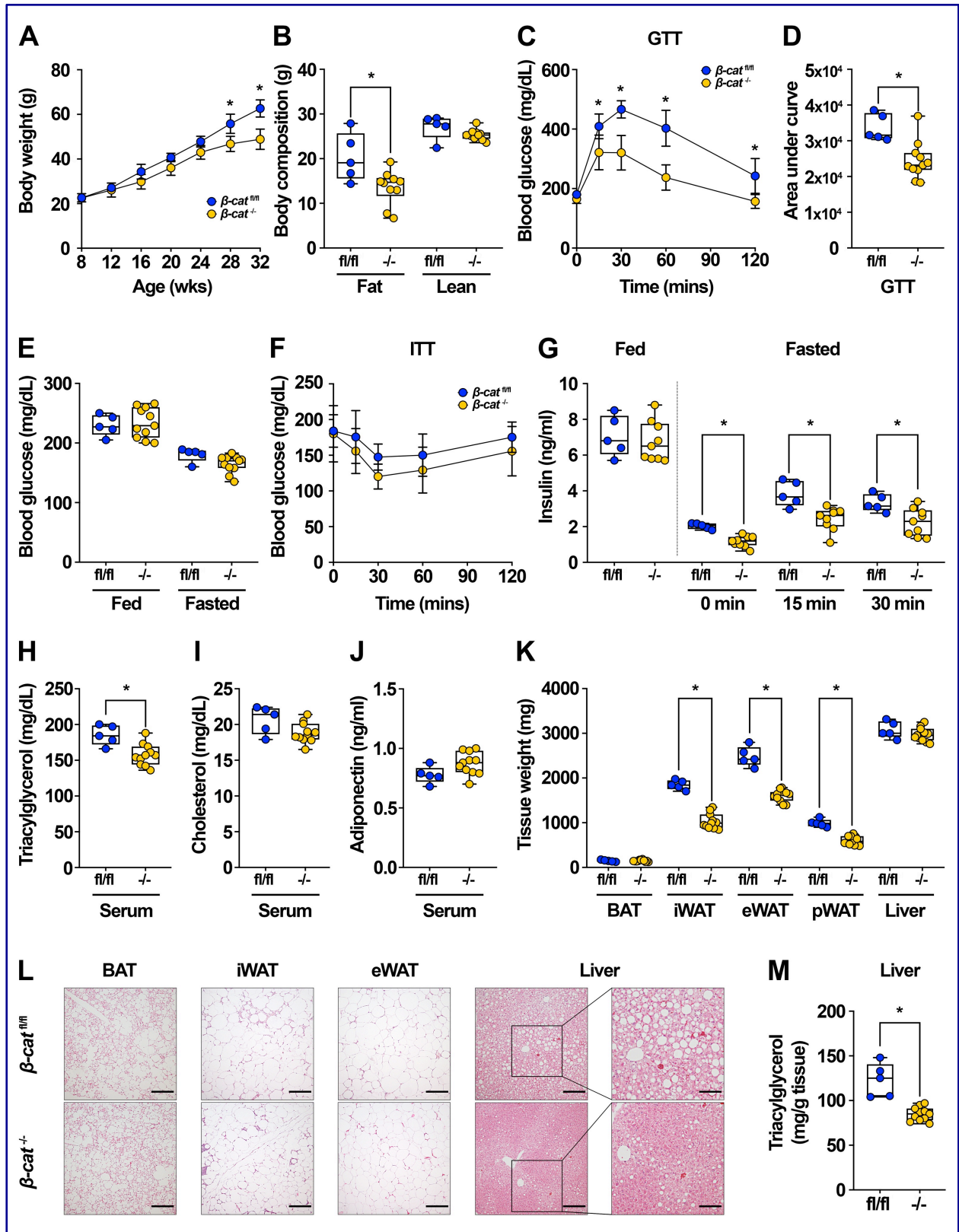
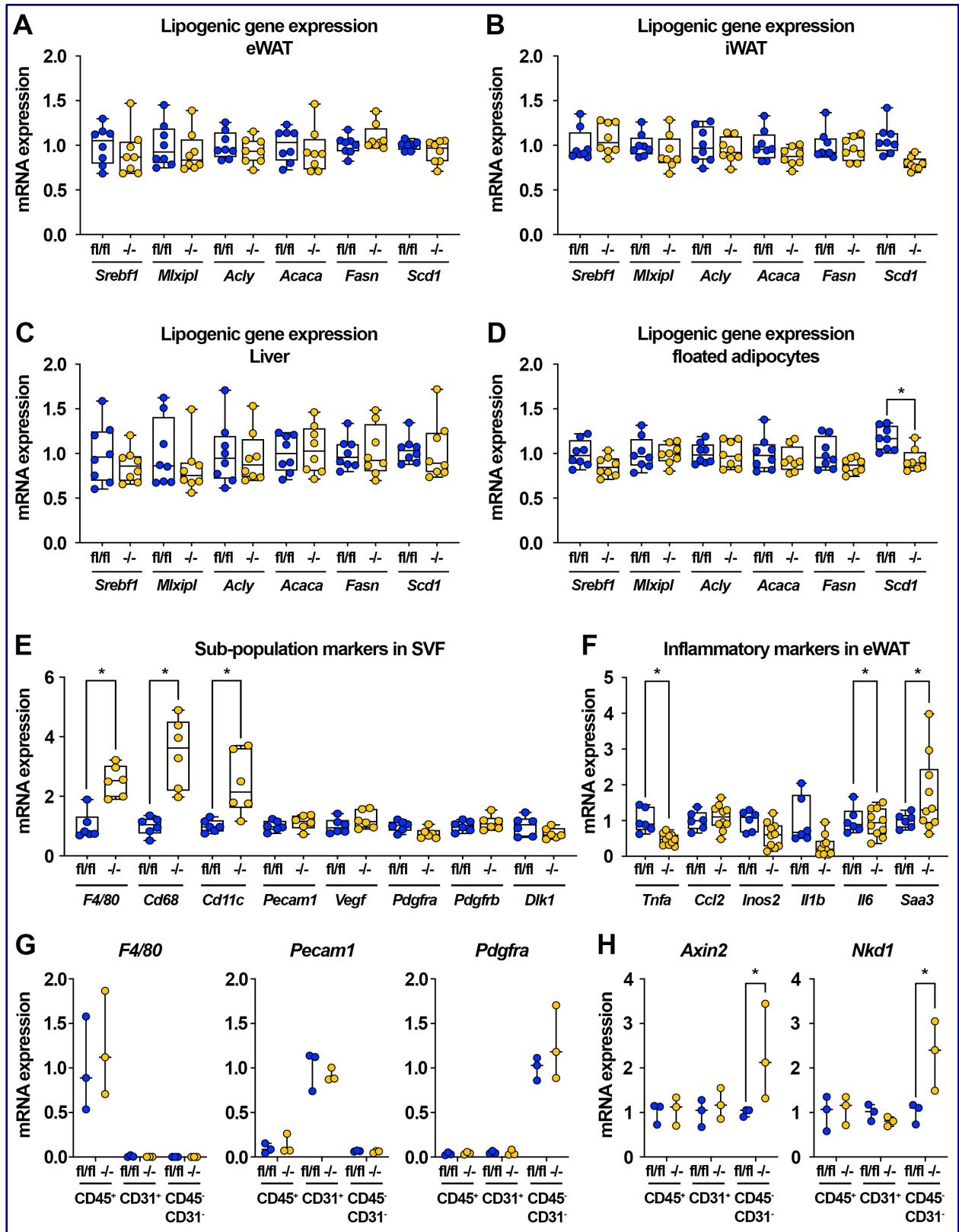


Figure 4.6. β -cat^{-/-} mice are protected from diet-induced obesity and metabolic dysfunction. (A) Growth curve over time of 32-week-old β -cat^{fl/fl} and β -cat^{-/-} mice fed 60% HFD for 24 weeks. (B) Body composition analysis of 28-week-old mice. (C-D) Glucose tolerance test and area under the curve analysis in 28-week-old mice. (E) Blood glucose concentrations in random-fed and 16 h fasted mice. (F) Insulin tolerance test in 30-week-old mice. (G) Serum insulin concentrations in random-fed mice or in 16 h fasted mice at indicated times after intraperitoneal glucose injection (1 mg/kg body weight). Serum (H) TAG, (I) total cholesterol, and (J) adiponectin in 32-week-old mice. (K) Tissue weights at time of sacrifice. (L) Representative histological images of H&E-stained tissues from β -cat^{fl/fl} and β -cat^{-/-} mice fed HFD for 24 weeks; 200x magnification; scale bar, 100 μ m. (M) Quantification of liver TAG in 32-week-old mice. Data shown from male mice; β -cat^{fl/fl}: n = 5, β -cat^{-/-}: n = 11. Data presented as mean \pm S.D. * indicates significance at p < 0.05.

Supplemental Figure 4.6



Supplemental Figure 4.6. (A-D) Lipogenic gene expression in whole eWAT, iWAT, liver, or isolated eWAT adipocytes of β -cat^{fl/fl} and β -cat^{-/-} mice (n = 8). (E) Expression of immune, endothelial, and stromal cell markers in SVF isolated from eWAT of β -cat^{fl/fl} and β -cat^{-/-} mice (n = 6). (F) Expression of inflammatory markers in whole eWAT of β -cat^{fl/fl} and β -cat^{-/-} mice (n = 6; n = 10). (G-H) Expression of cell markers and Wnt target genes in SVF sub-populations isolated by FACS analysis (3 mice per sample; n = 3 samples). RNA expression normalized to PPIA. Data presented as mean \pm S.D. * indicates significance at p < 0.05.

Figure 4.7

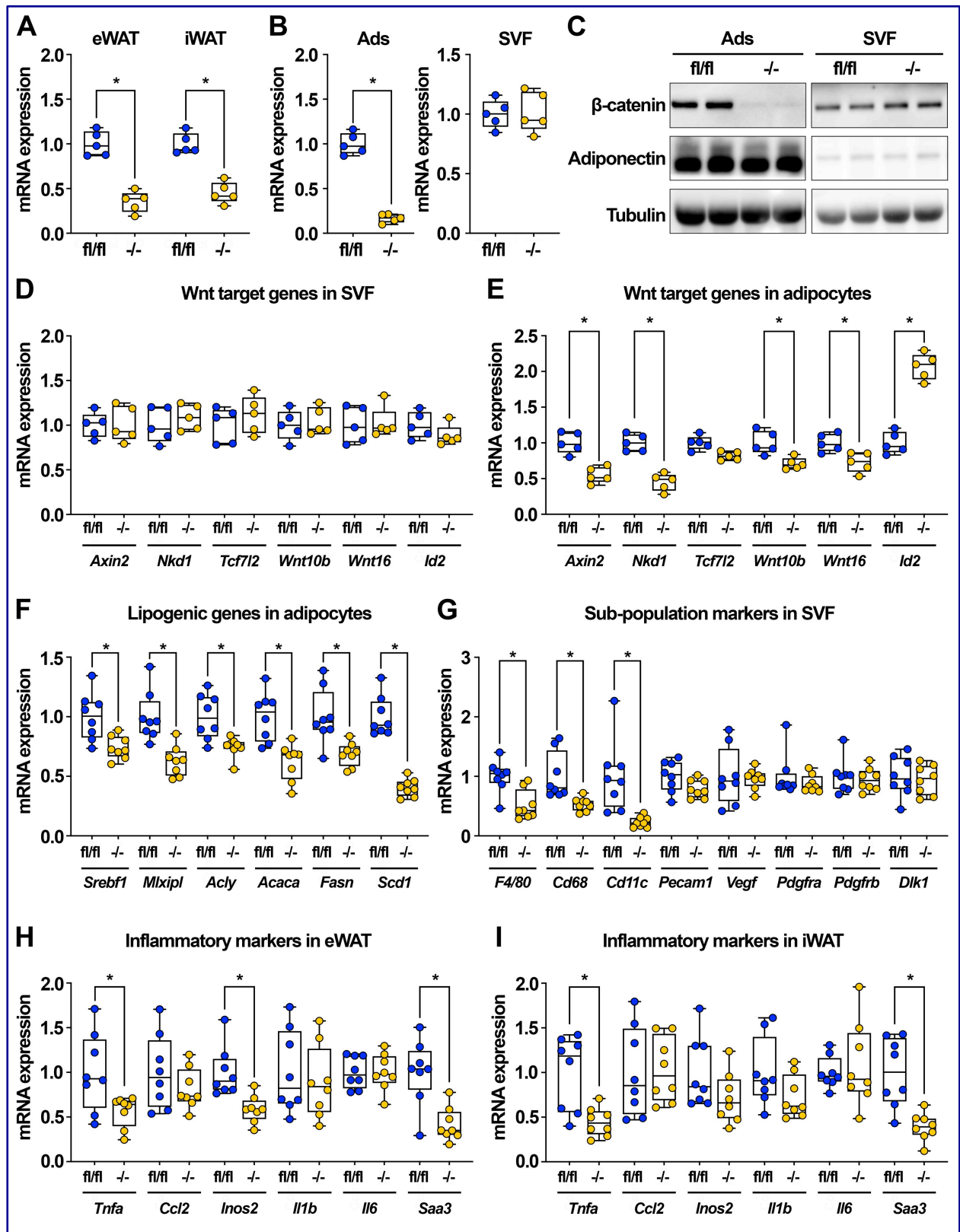
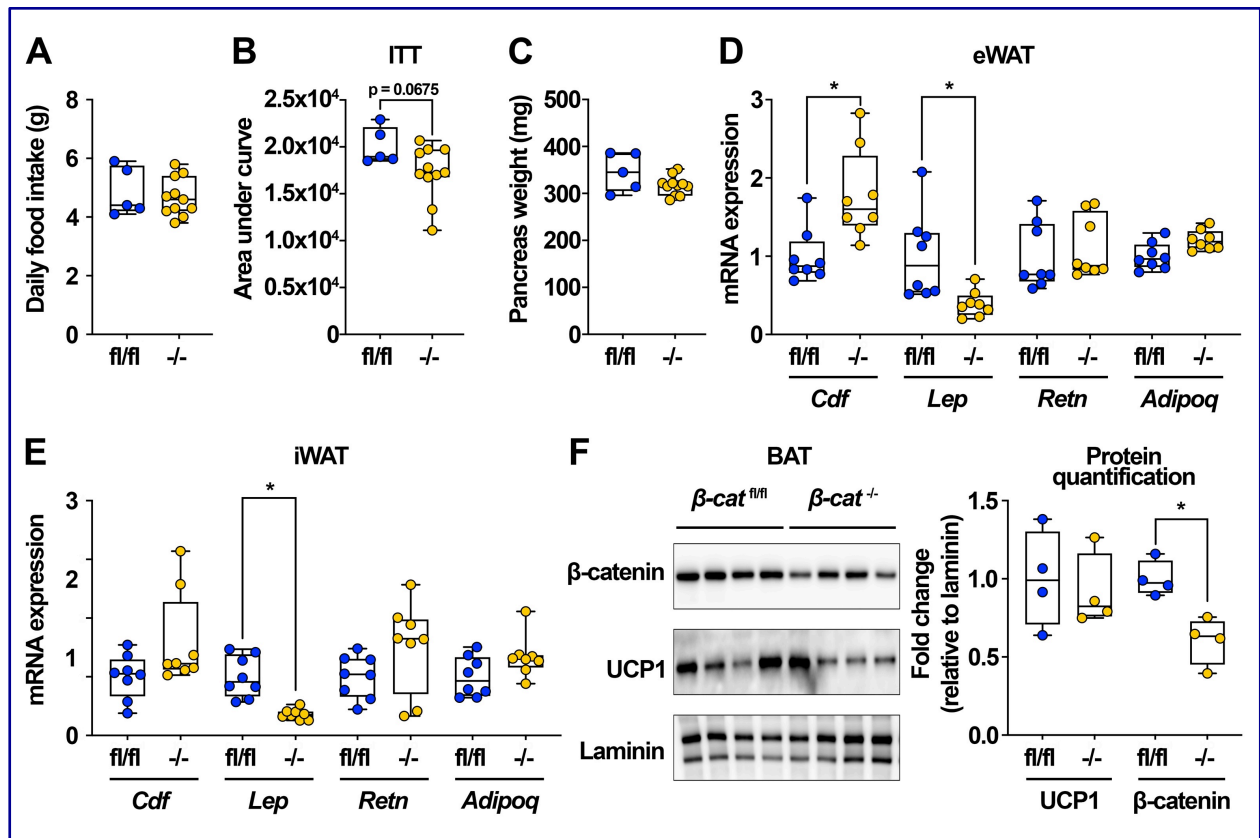


Figure 4.7. Diet-induced obesity overcomes compensatory up-regulation of Wnt/ β -catenin signaling in SVF of knockout mice. (A) *Ctnnb1* mRNA expression in eWAT and iWAT of β -cat^{fl/fl} and β -cat^{-/-} mice fed HFD for 28 weeks (n = 5). (B) *Ctnnb1* mRNA expression in isolated eWAT adipocytes and SVF of HFD-fed β -cat^{fl/fl} and β -cat^{-/-} mice (n = 5). (C) β -catenin protein expression in isolated eWAT adipocytes and SVF of β -cat^{fl/fl} and β -cat^{-/-} mice fed HFD; adiponectin and laminin shown as controls. (D-E) Wnt target gene expression in SVF and adipocytes isolated from eWAT of obese β -cat^{fl/fl} and β -cat^{-/-} mice (n = 5). (F) Lipogenic gene expression in eWAT adipocytes isolated from HFD-fed β -cat^{fl/fl} and β -cat^{-/-} mice (n = 8). (G) Expression of immune, endothelial, and stromal cell markers in SVF isolated from eWAT of obese β -cat^{fl/fl} and β -cat^{-/-} mice (n = 8). (H-I) Expression of inflammatory markers in whole eWAT and iWAT of β -cat^{fl/fl} and β -cat^{-/-} mice fed HFD (n = 8). RNA expression normalized to PPIA. Data presented as mean \pm S.D. * indicates significance at p < 0.05.

Supplemental Figure 4.7



Supplemental Figure 4.7. (A) Daily food intake of male $\beta\text{-cat}^{fl/fl}$ and $\beta\text{-cat}^{-/-}$ mice fed HFD for 24 weeks. (B) ITT area under the curve analysis of male $\beta\text{-cat}^{fl/fl}$ and $\beta\text{-cat}^{-/-}$ HFD-fed mice. (C) Pancreas weights at time of sacrifice of HFD-fed mice ($n = 5$, $n = 11$). (D-E) mRNA expression of adipokines in eWAT and iWAT of HFD-fed mice ($n = 8$). (F) Immunoblot and densitometry quantification of UCP1 and β -catenin protein expression in BAT isolated from HFD-fed $\beta\text{-cat}^{fl/fl}$ and $\beta\text{-cat}^{-/-}$ mice ($n = 4$). Data presented as mean \pm S.D. * indicates significance at $p < 0.05$.

Figure 4.8.

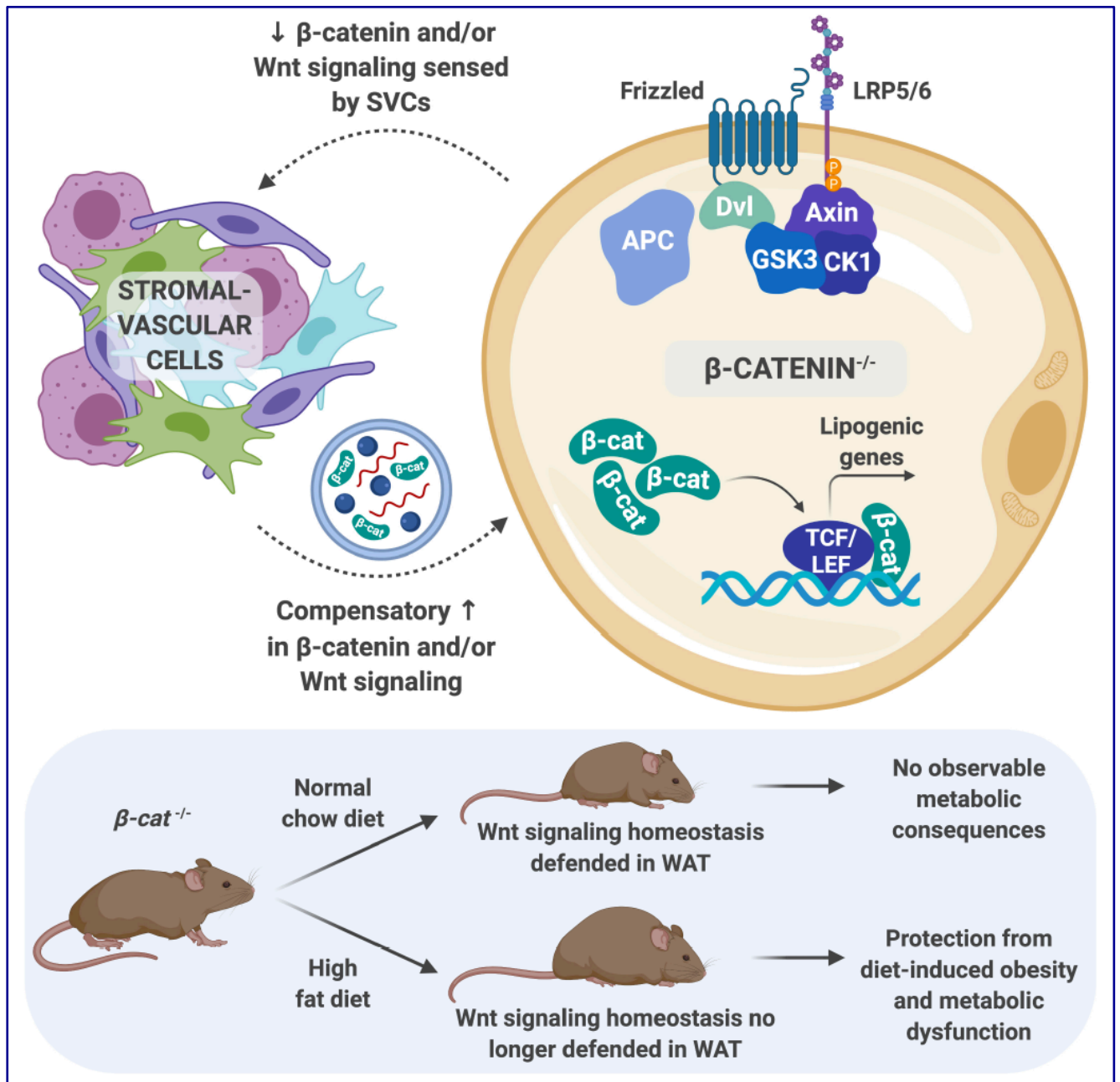


Figure 4.8. Schematic depicting the consequences of adipocyte-specific deletion of β -catenin. Canonical Wnt/ β -catenin signaling is required for coordinate regulation of adipocyte lipogenesis and fatty acid desaturation. In chow-fed mice, loss of adipocyte β -catenin is sensed and compensated for by neighboring stromal cells to defend tissue-wide canonical Wnt signaling homeostasis. Chronic overnutrition overrides this compensatory mechanism, revealing that adipocyte-specific β -catenin knockout mice are protected from diet-induced obesity and metabolic dysfunction.

References

- 1 Cadigan, K. M. & Nusse, R. Wnt signaling: a common theme in animal development. *Genes Dev* **11**, 3286-3305, doi:10.1101/gad.11.24.3286 (1997).
- 2 Clevers, H. Wnt/beta-catenin signaling in development and disease. *Cell* **127**, 469-480, doi:10.1016/j.cell.2006.10.018 (2006).
- 3 Logan, C. Y. & Nusse, R. The Wnt signaling pathway in development and disease. *Annu Rev Cell Dev Biol* **20**, 781-810, doi:10.1146/annurev.cellbio.20.010403.113126 (2004).
- 4 MacDonald, B. T., Tamai, K. & He, X. Wnt/beta-catenin signaling: components, mechanisms, and diseases. *Dev Cell* **17**, 9-26, doi:10.1016/j.devcel.2009.06.016 (2009).
- 5 Valenta, T., Hausmann, G. & Basler, K. The many faces and functions of beta-catenin. *EMBO J* **31**, 2714-2736, doi:10.1038/emboj.2012.150 (2012).
- 6 Willert, K. & Jones, K. A. Wnt signaling: is the party in the nucleus? *Genes Dev* **20**, 1394-1404, doi:10.1101/gad.1424006 (2006).
- 7 Fischer, L., Boland, G. & Tuan, R. S. Wnt-3A enhances bone morphogenetic protein-2-mediated chondrogenesis of murine C3H10T1/2 mesenchymal cells. *J Biol Chem* **277**, 30870-30878, doi:10.1074/jbc.M109330200 (2002).
- 8 Hoppler, S., Brown, J. D. & Moon, R. T. Expression of a dominant-negative Wnt blocks induction of MyoD in *Xenopus* embryos. *Genes Dev* **10**, 2805-2817, doi:10.1101/gad.10.21.2805 (1996).
- 9 Cossu, G. & Borello, U. Wnt signaling and the activation of myogenesis in mammals. *EMBO J* **18**, 6867-6872, doi:10.1093/emboj/18.24.6867 (1999).
- 10 Cawthorn, W. P. *et al.* Wnt6, Wnt10a and Wnt10b inhibit adipogenesis and stimulate osteoblastogenesis through a beta-catenin-dependent mechanism. *Bone* **50**, 477-489, doi:10.1016/j.bone.2011.08.010 (2012).
- 11 Christodoulides, C. *et al.* The Wnt antagonist Dickkopf-1 and its receptors are coordinately regulated during early human adipogenesis. *J Cell Sci* **119**, 2613-2620, doi:10.1242/jcs.02975 (2006).
- 12 Krishnan, V., Bryant, H. U. & Macdougald, O. A. Regulation of bone mass by Wnt signaling. *J Clin Invest* **116**, 1202-1209, doi:10.1172/JCI28551 (2006).
- 13 Kang, S. *et al.* Wnt signaling stimulates osteoblastogenesis of mesenchymal precursors by suppressing CCAAT/enhancer-binding protein alpha and peroxisome proliferator-activated receptor gamma. *J Biol Chem* **282**, 14515-14524, doi:10.1074/jbc.M700030200 (2007).
- 14 Rawadi, G., Vayssiere, B., Dunn, F., Baron, R. & Roman-Roman, S. BMP-2 controls alkaline phosphatase expression and osteoblast mineralization by a Wnt autocrine loop. *J Bone Miner Res* **18**, 1842-1853, doi:10.1359/jbmr.2003.18.10.1842 (2003).
- 15 Ross, S. E. *et al.* Inhibition of adipogenesis by Wnt signaling. *Science* **289**, 950-953, doi:10.1126/science.289.5481.950 (2000).
- 16 Bennett, C. N. *et al.* Regulation of Wnt signaling during adipogenesis. *J Biol Chem* **277**, 30998-31004, doi:10.1074/jbc.M204527200 (2002).

- 17 Moldes, M. *et al.* Peroxisome-proliferator-activated receptor gamma suppresses Wnt/beta-catenin signalling during adipogenesis. *Biochem J* **376**, 607-613, doi:10.1042/bj20030426 (2003).
- 18 Kennell, J. A., O'Leary, E. E., Gummow, B. M., Hammer, G. D. & MacDougald, O. A. T-cell factor 4N (TCF-4N), a novel isoform of mouse TCF-4, synergizes with beta-catenin to coactivate C/EBPalpha and steroidogenic factor 1 transcription factors. *Mol Cell Biol* **23**, 5366-5375, doi:10.1128/mcb.23.15.5366-5375.2003 (2003).
- 19 Cristancho, A. G. *et al.* Repressor transcription factor 7-like 1 promotes adipogenic competency in precursor cells. *Proc Natl Acad Sci U S A* **108**, 16271-16276, doi:10.1073/pnas.1109409108 (2011).
- 20 Li, F. Q. *et al.* Chibby promotes adipocyte differentiation through inhibition of beta-catenin signaling. *Mol Cell Biol* **27**, 4347-4354, doi:10.1128/MCB.01640-06 (2007).
- 21 Takemaru, K. *et al.* Chibby, a nuclear beta-catenin-associated antagonist of the Wnt/Wingless pathway. *Nature* **422**, 905-909, doi:10.1038/nature01570 (2003).
- 22 Longo, K. A. *et al.* Wnt10b inhibits development of white and brown adipose tissues. *J Biol Chem* **279**, 35503-35509, doi:10.1074/jbc.M402937200 (2004).
- 23 Wright, W. S. *et al.* Wnt10b inhibits obesity in ob/ob and agouti mice. *Diabetes* **56**, 295-303, doi:10.2337/db06-1339 (2007).
- 24 Christodoulides, C. *et al.* WNT10B mutations in human obesity. *Diabetologia* **49**, 678-684, doi:10.1007/s00125-006-0144-4 (2006).
- 25 Van Camp, J. K. *et al.* Common genetic variation in sFRP5 is associated with fat distribution in men. *Endocrine* **46**, 477-484, doi:10.1007/s12020-013-0088-7 (2014).
- 26 Heid, I. M. *et al.* Meta-analysis identifies 13 new loci associated with waist-hip ratio and reveals sexual dimorphism in the genetic basis of fat distribution. *Nat Genet* **42**, 949-960, doi:10.1038/ng.685 (2010).
- 27 Shungin, D. *et al.* New genetic loci link adipose and insulin biology to body fat distribution. *Nature* **518**, 187-196, doi:10.1038/nature14132 (2015).
- 28 Hao, H. X. *et al.* ZNRF3 promotes Wnt receptor turnover in an R-spondin-sensitive manner. *Nature* **485**, 195-200, doi:10.1038/nature11019 (2012).
- 29 Saarinen, A. *et al.* Low density lipoprotein receptor-related protein 5 (LRP5) mutations and osteoporosis, impaired glucose metabolism and hypercholesterolaemia. *Clin Endocrinol (Oxf)* **72**, 481-488, doi:10.1111/j.1365-2265.2009.03680.x (2010).
- 30 Singh, R. *et al.* Rare nonconservative LRP6 mutations are associated with metabolic syndrome. *Hum Mutat* **34**, 1221-1225, doi:10.1002/humu.22360 (2013).
- 31 Loh, N. Y. *et al.* LRP5 regulates human body fat distribution by modulating adipose progenitor biology in a dose- and depot-specific fashion. *Cell Metab* **21**, 262-273, doi:10.1016/j.cmet.2015.01.009 (2015).
- 32 Styrkarsdottir, U. *et al.* Nonsense mutation in the LGR4 gene is associated with several human diseases and other traits. *Nature* **497**, 517-520, doi:10.1038/nature12124 (2013).

- 33 Zou, Y. *et al.* Association of a gain-of-function variant in LGR4 with central obesity. *Obesity (Silver Spring)* **25**, 252-260, doi:10.1002/oby.21704 (2017).
- 34 Lyssenko, V. *et al.* Mechanisms by which common variants in the TCF7L2 gene increase risk of type 2 diabetes. *J Clin Invest* **117**, 2155-2163, doi:10.1172/JCI30706 (2007).
- 35 Grant, S. F. *et al.* Variant of transcription factor 7-like 2 (TCF7L2) gene confers risk of type 2 diabetes. *Nat Genet* **38**, 320-323, doi:10.1038/ng1732 (2006).
- 36 Jin, T. Current Understanding on Role of the Wnt Signaling Pathway Effector TCF7L2 in Glucose Homeostasis. *Endocr Rev* **37**, 254-277, doi:10.1210/er.2015-1146 (2016).
- 37 Chen, M. *et al.* CTNNB1/beta-catenin dysfunction contributes to adiposity by regulating the cross-talk of mature adipocytes and preadipocytes. *Sci Adv* **6**, eaax9605, doi:10.1126/sciadv.aax9605 (2020).
- 38 Mori, H. *et al.* Secreted frizzled-related protein 5 suppresses adipocyte mitochondrial metabolism through WNT inhibition. *J Clin Invest* **122**, 2405-2416, doi:10.1172/JCI63604 (2012).
- 39 Geoghegan, G. *et al.* Targeted deletion of Tcf7l2 in adipocytes promotes adipocyte hypertrophy and impaired glucose metabolism. *Mol Metab* **24**, 44-63, doi:10.1016/j.molmet.2019.03.003 (2019).
- 40 Bagchi, D. P. *et al.* Wntless regulates lipogenic gene expression in adipocytes and protects against diet-induced metabolic dysfunction. *Mol Metab*, 100992, doi:10.1016/j.molmet.2020.100992 (2020).
- 41 Lengfeld, J. E. *et al.* Endothelial Wnt/beta-catenin signaling reduces immune cell infiltration in multiple sclerosis. *Proc Natl Acad Sci U S A* **114**, E1168-E1177, doi:10.1073/pnas.1609905114 (2017).
- 42 Malsin, E. S., Kim, S., Lam, A. P. & Gottardi, C. J. Macrophages as a Source and Recipient of Wnt Signals. *Front Immunol* **10**, 1813, doi:10.3389/fimmu.2019.01813 (2019).
- 43 Boulter, L. *et al.* Macrophage-derived Wnt opposes Notch signaling to specify hepatic progenitor cell fate in chronic liver disease. *Nat Med* **18**, 572-579, doi:10.1038/nm.2667 (2012).
- 44 Tran, K. A. *et al.* Endothelial β -Catenin Signaling Is Required for Maintaining Adult Blood-Brain Barrier Integrity and Central Nervous System Homeostasis. *Circulation* **133**, 177-186, doi:10.1161/CIRCULATIONAHA.115.015982 (2016).
- 45 Crewe, C. *et al.* SREBP-regulated adipocyte lipogenesis is dependent on substrate availability and redox modulation of mTORC1. *JCI Insight* **5**, doi:10.1172/jci.insight.129397 (2019).
- 46 Peterson, T. R. *et al.* mTOR complex 1 regulates lipin 1 localization to control the SREBP pathway. *Cell* **146**, 408-420, doi:10.1016/j.cell.2011.06.034 (2011).
- 47 Porstmann, T. *et al.* SREBP activity is regulated by mTORC1 and contributes to Akt-dependent cell growth. *Cell Metab* **8**, 224-236, doi:10.1016/j.cmet.2008.07.007 (2008).
- 48 Soliman, G. A., Acosta-Jaquez, H. A. & Fingar, D. C. mTORC1 inhibition via rapamycin promotes triacylglycerol lipolysis and release of free fatty acids in 3T3-L1 adipocytes. *Lipids* **45**, 1089-1100, doi:10.1007/s11745-010-3488-y (2010).

- 49 Bertrand, F. E., Angus, C. W., Partis, W. J. & Sigounas, G. Developmental pathways in colon cancer: crosstalk between WNT, BMP, Hedgehog and Notch. *Cell Cycle* **11**, 4344-4351, doi:10.4161/cc.22134 (2012).
- 50 Dao, D. Y., Yang, X., Chen, D., Zuscik, M. & O'Keefe, R. J. Axin1 and Axin2 are regulated by TGF- and mediate cross-talk between TGF- and Wnt signaling pathways. *Ann N Y Acad Sci* **1116**, 82-99, doi:10.1196/annals.1402.082 (2007).
- 51 Nusse, R. & Clevers, H. Wnt/beta-Catenin Signaling, Disease, and Emerging Therapeutic Modalities. *Cell* **169**, 985-999, doi:10.1016/j.cell.2017.05.016 (2017).
- 52 Ameer, F., Scanduzzi, L., Hasnain, S., Kalbacher, H. & Zaidi, N. De novo lipogenesis in health and disease. *Metabolism* **63**, 895-902, doi:10.1016/j.metabol.2014.04.003 (2014).
- 53 Sanders, F. W. & Griffin, J. L. De novo lipogenesis in the liver in health and disease: more than just a shunting yard for glucose. *Biol Rev Camb Philos Soc* **91**, 452-468, doi:10.1111/brv.12178 (2016).
- 54 Sampath, H. & Ntambi, J. M. The role of stearoyl-CoA desaturase in obesity, insulin resistance, and inflammation. *Ann N Y Acad Sci* **1243**, 47-53, doi:10.1111/j.1749-6632.2011.06303.x (2011).
- 55 Paton, C. M. & Ntambi, J. M. Biochemical and physiological function of stearoyl-CoA desaturase. *Am J Physiol Endocrinol Metab* **297**, E28-37, doi:10.1152/ajpendo.90897.2008 (2009).
- 56 Ralston, J. C., Badoud, F., Cattrysse, B., McNicholas, P. D. & Mutch, D. M. Inhibition of stearoyl-CoA desaturase-1 in differentiating 3T3-L1 preadipocytes upregulates elongase 6 and downregulates genes affecting triacylglycerol synthesis. *Int J Obes (Lond)* **38**, 1449-1456, doi:10.1038/ijo.2014.35 (2014).
- 57 Charawi, S. *et al.* LKB1 signaling is activated in CTNNB1-mutated HCC and positively regulates β -catenin-dependent CTNNB1-mutated HCC. *J Pathol* **247**, 435-443, doi:10.1002/path.5202 (2019).
- 58 Palpant, N. J. *et al.* Inhibition of β -catenin signaling respecifies anterior-like endothelium into beating human cardiomyocytes. *Development* **142**, 3198-3209, doi:10.1242/dev.117010 (2015).
- 59 Sebastian, A. *High-throughput Analysis of WNT Signaling Pathway in Osteoblasts* Doctor of Philosophy thesis, University of California Merced (2016).
- 60 Wang, Y., Viscarra, J., Kim, S. J. & Sul, H. S. Transcriptional regulation of hepatic lipogenesis. *Nat Rev Mol Cell Biol* **16**, 678-689, doi:10.1038/nrm4074 (2015).
- 61 Linden, A. G. *et al.* Interplay between ChREBP and SREBP-1c coordinates postprandial glycolysis and lipogenesis in livers of mice. *J Lipid Res* **59**, 475-487, doi:10.1194/jlr.M081836 (2018).
- 62 Bennett, C. N. *et al.* Regulation of osteoblastogenesis and bone mass by Wnt10b. *Proc Natl Acad Sci U S A* **102**, 3324-3329, doi:10.1073/pnas.0408742102 (2005).
- 63 Bennett, C. N. *et al.* Wnt10b increases postnatal bone formation by enhancing osteoblast differentiation. *J Bone Miner Res* **22**, 1924-1932, doi:10.1359/jbmr.070810 (2007).
- 64 Rosen, E. D. & MacDougald, O. A. Adipocyte differentiation from the inside out. *Nat Rev Mol Cell Biol* **7**, 885-896, doi:10.1038/nrm2066 (2006).

- 65 Gougelet, A. *et al.* T-cell factor 4 and β -catenin chromatin occupancies pattern zonal liver metabolism in mice. *Hepatology* **59**, 2344-2357, doi:10.1002/hep.26924 (2014).
- 66 Pongvarin, N. *et al.* Genome-Wide Analysis of ChREBP Binding Sites on Male Mouse Liver and White Adipose Chromatin. *Endocrinology* **156**, 1982-1994, doi:10.1210/en.2014-1666 (2015).
- 67 Cawthorn, W. P., Scheller, E. L. & MacDougald, O. A. Adipose tissue stem cells meet preadipocyte commitment: going back to the future. *J Lipid Res* **53**, 227-246, doi:10.1194/jlr.R021089 (2012).
- 68 Soshnikova, N. *et al.* Genetic interaction between Wnt/beta-catenin and BMP receptor signaling during formation of the AER and the dorsal-ventral axis in the limb. *Genes Dev* **17**, 1963-1968, doi:10.1101/gad.263003 (2003).
- 69 ten Berge, D., Brugmann, S. A., Helms, J. A. & Nusse, R. Wnt and FGF signals interact to coordinate growth with cell fate specification during limb development. *Development* **135**, 3247-3257, doi:10.1242/dev.023176 (2008).
- 70 Russo, L. & Lumeng, C. N. Properties and functions of adipose tissue macrophages in obesity. *Immunology* **155**, 407-417, doi:10.1111/imm.13002 (2018).
- 71 Chistiakov, D. A., Killingsworth, M. C., Myasoedova, V. A., Orekhov, A. N. & Bobryshev, Y. V. CD68/macrosialin: not just a histochemical marker. *Lab Invest* **97**, 4-13, doi:10.1038/labinvest.2016.116 (2017).
- 72 van Niel, G., D'Angelo, G. & Raposo, G. Shedding light on the cell biology of extracellular vesicles. *Nat Rev Mol Cell Biol* **19**, 213-228, doi:10.1038/nrm.2017.125 (2018).
- 73 Raposo, G. & Stahl, P. D. Extracellular vesicles: a new communication paradigm? *Nat Rev Mol Cell Biol* **20**, 509-510, doi:10.1038/s41580-019-0158-7 (2019).
- 74 Chen, X. W., Li, S. & Lin, J. D. The Micro-Managing Fat: Exosomes as a New Messenger. *Trends Endocrinol Metab* **28**, 541-542, doi:10.1016/j.tem.2017.04.004 (2017).
- 75 Deng, Z. B. *et al.* Adipose tissue exosome-like vesicles mediate activation of macrophage-induced insulin resistance. *Diabetes* **58**, 2498-2505, doi:10.2337/db09-0216 (2009).
- 76 Thomou, T. *et al.* Adipose-derived circulating miRNAs regulate gene expression in other tissues. *Nature* **542**, 450-455, doi:10.1038/nature21365 (2017).
- 77 Lazar, I. *et al.* Adipocyte Exosomes Promote Melanoma Aggressiveness through Fatty Acid Oxidation: A Novel Mechanism Linking Obesity and Cancer. *Cancer Res* **76**, 4051-4057, doi:10.1158/0008-5472.CAN-16-0651 (2016).
- 78 Ying, W. *et al.* Adipose Tissue Macrophage-Derived Exosomal miRNAs Can Modulate In Vivo and In Vitro Insulin Sensitivity. *Cell* **171**, 372-384.e312, doi:10.1016/j.cell.2017.08.035 (2017).
- 79 Crewe, C. *et al.* An Endothelial-to-Adipocyte Extracellular Vesicle Axis Governed by Metabolic State. *Cell* **175**, 695-708.e613, doi:10.1016/j.cell.2018.09.005 (2018).

- 80 Zhao, H. *et al.* Exosomes From Adipose-Derived Stem Cells Attenuate Adipose Inflammation and Obesity Through Polarizing M2 Macrophages and Being in White Adipose Tissue. *Diabetes* **67**, 235-247, doi:10.2337/db17-0356 (2018).
- 81 Weise, A. *et al.* Alternative splicing of Tcf7l2 transcripts generates protein variants with differential promoter-binding and transcriptional activation properties at Wnt/beta-catenin targets. *Nucleic Acids Res* **38**, 1964-1981, doi:10.1093/nar/gkp1197 (2010).
- 82 Hammond, E. *et al.* The Wnt effector transcription factor 7-like 2 positively regulates oligodendrocyte differentiation in a manner independent of Wnt/beta-catenin signaling. *J Neurosci* **35**, 5007-5022, doi:10.1523/JNEUROSCI.4787-14.2015 (2015).
- 83 Sanada, Y. *et al.* Serum Amyloid A3 Gene Expression in Adipocytes is an Indicator of the Interaction with Macrophages. *Sci Rep* **6**, 38697, doi:10.1038/srep38697 (2016).
- 84 Fasshauer, M. *et al.* Serum amyloid A3 expression is stimulated by dexamethasone and interleukin-6 in 3T3-L1 adipocytes. *J Endocrinol* **183**, 561-567, doi:10.1677/joe.1.05699 (2004).
- 85 Han, C. Y. *et al.* Adipocyte-derived serum amyloid A3 and hyaluronan play a role in monocyte recruitment and adhesion. *Diabetes* **56**, 2260-2273, doi:10.2337/db07-0218 (2007).
- 86 den Hartigh, L. J. *et al.* Deletion of serum amyloid A3 improves high fat high sucrose diet-induced adipose tissue inflammation and hyperlipidemia in female mice. *PLoS One* **9**, e108564, doi:10.1371/journal.pone.0108564 (2014).
- 87 Bagchi, D. P., Forss, I., Mandrup, S. & MacDougald, O. A. SnapShot: Niche Determines Adipocyte Character I. *Cell Metab* **27**, 264-264 e261, doi:10.1016/j.cmet.2017.11.012 (2018).
- 88 Bagchi, D. P. & MacDougald, O. A. Identification and Dissection of Diverse Mouse Adipose Depots. *J Vis Exp*, doi:10.3791/59499 (2019).
- 89 Parlee, S. D., Lentz, S. I., Mori, H. & MacDougald, O. A. Quantifying size and number of adipocytes in adipose tissue. *Methods Enzymol* **537**, 93-122, doi:10.1016/B978-0-12-411619-1.00006-9 (2014).
- 90 Rim, J. S., Mynatt, R. L. & Gawronska-Kozak, B. Mesenchymal stem cells from the outer ear: a novel adult stem cell model system for the study of adipogenesis. *FASEB J* **19**, 1205-1207, doi:10.1096/fj.04-3204fje (2005).
- 91 Erickson, R. L., Hemati, N., Ross, S. E. & MacDougald, O. A. p300 coactivates the adipogenic transcription factor CCAAT/enhancer-binding protein alpha. *J Biol Chem* **276**, 16348-16355, doi:10.1074/jbc.m100128200 (2001).
- 92 Scheller, E. L. *et al.* Region-specific variation in the properties of skeletal adipocytes reveals regulated and constitutive marrow adipose tissues. *Nat Commun* **6**, 7808, doi:10.1038/ncomms8808 (2015).
- 93 Subramanian, A. *et al.* Gene set enrichment analysis: a knowledge-based approach for interpreting genome-wide expression profiles. *Proc Natl Acad Sci U S A* **102**, 15545-15550, doi:10.1073/pnas.0506580102 (2005).
- 94 Ahsan, S. & Drăghici, S. Identifying Significantly Impacted Pathways and Putative Mechanisms with iPathwayGuide. *Curr Protoc Bioinformatics* **57**, 7.15.11-17.15.30, doi:10.1002/cpbi.24 (2017).

- 95 Thorvaldsdóttir, H., Robinson, J. T. & Mesirov, J. P. Integrative Genomics Viewer (IGV): high-performance genomics data visualization and exploration. *Brief Bioinform* **14**, 178-192, doi:10.1093/bib/bbs017 (2013).

CHAPTER V

Discussion and Future Perspectives

The role of Wnt signaling in mesenchymal stem cell fate determination and differentiation is well-established¹⁻⁴. Indeed, the preponderance of data within the field of adipose biology to date has characterized Wnt inhibition of adipogenesis and promotion of other cell fates, including osteoblastogenesis, chondrogenesis, and myogenesis⁵⁻¹⁰. However, increasing genetic evidence in humans has linked various Wnt pathway members to body fat distribution, obesity, and metabolic dysfunction¹¹⁻²³. In recent years, a flurry of studies in mice has uncovered compelling evidence suggesting that Wnt signaling plays important roles in adipocyte metabolism, particularly under obesogenic conditions²⁴⁻²⁷. Perhaps unsurprisingly, given the breadth and complexity of this pathway and differences in experimental models, approaches and results, the exact functional roles of the Wnt pathway and its underlying molecular mechanisms in this context remain unclear.

Thus, against this backdrop, my doctoral work presented herein set out to unravel the unique contributions of Wnt pathway members to adipocyte metabolism. To this end, I generated novel cultured cell and mouse models to functionally characterize the differential roles of two key pathway members, Wntless (*Wls*) and β -catenin (*Ctnnb1*), in terminally-differentiated adipocytes. Deletion of Wntless, a dedicated intracellular chaperone for Wnts, allowed me to investigate the functional roles of both canonical and non-canonical Wnts secreted from adipocytes, whereas loss of β -catenin allowed me to specifically interrogate the contribution of canonical Wnt signaling to adipocyte function.

These studies revealed for the first time that loss of adipocyte-derived Wnts or canonical Wnt/ β -catenin signaling in adipocytes coordinately down-regulates lipogenic gene expression, resulting in impaired *de novo* lipogenesis (DNL) and fatty acid

monounsaturations. Further, effects on lipid metabolism are mediated by repression of *Srebf1* and *Mlxipl*, known transcriptional regulators of DNL enzymes. *In vivo*, Wntless and β -catenin do not appear to influence global metabolism in mice maintained on normal chow diet (NCD). However, deeper investigation reveals that adipose tissues are able to defend adipocyte-specific loss of Wntless or β -catenin by compensatory up-regulation of Wnt signaling in surrounding stromal-vascular cells (SVC). Finally, long-term overnutrition overrides this compensatory mechanism, such that both *Wls*^{-/-} and *β -cat*^{-/-} mice are resistant to diet-induced obesity and protected from metabolic dysfunction. These novel findings underscore the critical importance of Wnt signaling in adipocyte metabolism, and also raise some fascinating questions and lines of inquiry worthy of future investigation.

Does Wnt signaling directly regulate lipogenic gene transcription or are the effects mediated indirectly by *Srebf1* and *Mlxipl* activity?

Our studies reveal for the first time that both Wntless and β -catenin are required for coordinate expression of a network of lipogenic genes, including *Acly*, *Acaca*, *Fasn*, *Scd1*, *Elovl6*, and *Elovl7*. Extensive studies in the liver have identified SREBP1c and ChREBP as key upstream transcriptional regulators of many DNL enzymes²⁸⁻³⁰, and genome-wide ChIP-seq analysis in white adipose tissues (WAT) recently identified ChREBP binding sites on many genes related to metabolism, including *Acaca*, *Fasn*, and *Scd1*³¹. Thus, we hypothesized that effects of Wnt signaling on lipogenesis are also mediated by these transcription factors. We found that mRNA and protein levels of both *Srebf1* and *Mlxipl* are suppressed in *Wls*^{-/-} and *β -cat*^{-/-} adipocytes, whereas other transcription factors involved in adipogenesis and adipocyte metabolism, including *Pparg* and *Cebpa*, are unaffected. It is important to note that the consistent results observed in both Wntless and β -catenin knockout models suggest that adipocyte-derived Wnts largely signal through the canonical pathway to mediate effects on lipid metabolism. Further, overexpression of ChREBP or SREBP1c is sufficient to induce SCD1 in *β -cat*^{fl/fl} adipocytes, and to partially rescue SCD1 mRNA and protein levels in *β -cat*^{-/-} cells. Thus, loss of Wnt signaling results in impaired DNL at least in part due to suppression of *Mlxipl* and *Srebf1*.

A compelling question raised by these results is whether Wnt signaling directly regulates lipogenic gene transcription, or whether the effects are mediated indirectly by *Srebf1* and *Mlxipl* activity. Since β -catenin activates TCF/LEF proteins to mediate target gene transcription, a few possibilities exist. Perhaps β -catenin/TCF/LEF complexes bind directly to lipogenic genes to promote transcription; indeed, Geoghegan *et al.* reported Tcf7l2 binding sites within 1 kilobase of the transcriptional start site of many lipogenic genes, including *Acly*, *Fasn*, and *Scd1*²⁴. It is also possible that β -catenin/TCF/LEF complexes bind to and activate *Srebf1* and *Mlxipl*, which in turn regulate transcription of lipogenic genes. Analyses of the promoter regions of *Srebf1* and *Mlxipl*, as well as DNL enzymes like *Fasn* and *Scd1*, for potential TCF binding motifs may provide important clues regarding Wnt signaling regulation of these genes. ChIP-seq analyses of β -catenin binding sites in adipocytes will be required to identify the genes that are directly transcriptionally regulated by Wnt signaling. Decreased promoter occupancy of these genes in β -cat^{-/-} adipocytes and impaired expression of *Srebf1*, *Mlxipl*, or lipogenic genes following mutation of β -catenin binding sites will definitively prove the mechanisms underlying Wnt-mediated transcriptional regulation of lipid metabolism in adipocytes.

Pharmacological activation of Wnt signaling or enforced expression of β -catenin in *Srebf1*^{-/-} or *Mlxipl*^{-/-} adipocytes will also provide valuable insights into the requirement of these transcription factors for Wnt regulation of DNL enzymes. Experiments to determine whether there is increased expression of DNL enzymes above baseline with Wnt pathway activation in SREBP1c- or ChREBP-deficient cells would test if these transcription factors are required for basal or Wnt regulation of lipogenic genes in adipocytes. However, if Wnt activation does not up-regulate lipogenic gene expression in the absence of SREBP1c- or ChREBP, it is more likely that these transcription factors exclusively mediate the effects of Wnt signaling on DNL enzymes. These experiments and others will be necessary to more clearly define the mechanisms underlying Wnt regulation of lipogenesis in adipocytes.

Are other adipocyte functions regulated by Wnt signaling?

To obtain a global view of the transcriptional pathways regulated by canonical Wnt signaling in terminally differentiated cells, we performed RNA-seq analyses of β -cat^{fl/fl} and β -cat^{-/-} adipocytes. Gene set enrichment analyses (GSEA) of differentially expressed genes identified several metabolic pathways as being down-regulated with β -catenin deletion, including those involved in glycolysis, oxidative phosphorylation, and fatty acid, cholesterol, and bile acid metabolism. Pathways up-regulated by loss of β -catenin are largely related to inflammatory response, including TNF α , interferon- α , interferon- γ , and IL6/JAK/STAT3 signaling. Of note, Geogheghan *et al.* recently reported that Tcf7l2 also regulates many metabolic pathways in WAT, including cholesterol, fatty acyl-CoA and TAG biosynthesis and amino acid, carbohydrate, and peroxisomal lipid metabolism²⁴.

Since lipogenesis and lipid accumulation are two specialized functions of adipocytes, we focused our investigations on down-regulation of the DNL pathway in β -cat^{-/-} and *Wls*^{-/-} adipocytes. Although we did not observe effects on lipolysis, β -oxidation, or glucose uptake in β -cat^{-/-} or *Wls*^{-/-} cells, it is likely that Wnt signaling influences other metabolic pathways in adipocytes. Indeed, interactions between effects on distinct pathways may, in part, explain differences observed between reported phenotypes of impaired Wnt signaling in adipocytes²⁴⁻²⁷. Thorough characterization of the effects of impaired Wnt signaling on other cellular functions, including inflammation, glycolysis, mitochondrial activity, and cholesterol synthesis, may provide particularly important insights into the protective phenotypes observed in knockout mice with long-term high fat diet (HFD) feeding.

One pathway found to be down-regulated in both β -cat^{-/-} adipocytes and preadipocytes that may be of particular interest is mTORC1 signaling. mTORC1, which is a central integrator of several distinct signaling molecules and pathways, activates SREBP1c to promote lipogenesis in adipocytes^{32,33}. Thus, it is possible that Wnt signaling regulation of *Srebf1* and downstream lipogenic genes is mediated in part by mTORC1 activity. Evaluation of basal mTORC1 signaling in β -cat^{-/-} and *Wls*^{-/-} adipocytes compared to control cells will reveal whether this pathway is indeed

suppressed by impaired Wnt signaling. If enforced expression of mTORC1 signaling is sufficient to restore *Srebf1* levels to that of control cells, this pathway may be an important mediator of Wnt pathway effects on adipocyte lipid metabolism.

What is the compensatory mechanism by which stromal-vascular cells sense and respond to loss of adipocyte-specific Wnt signaling?

To date, virtually all models of impaired Wnt signaling in adipose tissues have reported a lack of phenotype in mice maintained on chow diet²⁴⁻²⁶. Consistent with these prior studies, adipocyte-specific Wntless or β -catenin deletion does not overtly influence body composition or whole-body metabolism. Surprisingly, given the effects of impaired Wnt signaling on lipogenesis in cultured adipocytes, DNL gene expression is not influenced in whole WAT or isolated adipocytes from β -cat^{-/-} and *Wls*^{-/-} mice.

Although previous studies did not probe further into a lack of detectable phenotype in chow-fed mice, our experiments have uncovered a striking compensatory mechanism by which adipose tissues defend adipocyte-specific loss of Wnt signaling. In *Wls*^{-/-} adipocytes, despite efficient ablation of Wntless at the DNA, RNA and protein levels, downstream Wnt signaling and lipogenic gene expression is maintained. Unexpectedly, surrounding SVF cells broadly up-regulate mRNAs of Wnts and their transcriptional targets, including *Cmyc*, *Tcf7l2*, and *Ppard*. Our observations in the β -catenin model are even more interesting: although β -catenin is completely recombined at the genomic level in β -cat^{-/-} adipocytes, *Ctnnb1* mRNA is only reduced by ~50% and over 80% of β -catenin protein remains. Paradoxically, we found dramatic induction of β -catenin mRNA and protein within the SVF of β -cat^{-/-} mice. Consistent with β -catenin expression patterns, many Wnt targets, including *Axin2*, *Nkd1*, *Tcf7l2*, *Wnt10b*, and *Wnt16*, were not altered in β -cat^{-/-} adipocytes; in contrast, these genes were significantly up-regulated in the SVF with β -catenin deficiency. Data from these two independent models support the compelling conclusion that impaired Wnt signaling in adipocytes is sensed by and compensated for by surrounding cells. Indeed, we contend that this compensatory mechanism may explain the lack of observable phenotypes under standard conditions in other mouse models that have been developed thus far to study Wnt signaling in adipocytes.

A fascinating unanswered question raised by our observations is undoubtedly the exact underlying mechanism by which Wnt signaling is sensed and up-regulated in the SVF of Wntless or β -catenin knockout animals. A number of possibilities emerge to explain this phenomenon. For example, impaired Wnt signaling may alter SVF cellular composition, enriching for subpopulations that have highly active Wnt signaling. Indeed, we observe elevated expression of macrophage markers, including *F4/80*, *Cd68*, and *Cd11c*, in SVF of β -cat^{-/-} mice, suggesting increased macrophage numbers. Flow cytometry analyses using CD45 and CD31 antibodies did not yield observable differences in proportions of immune or endothelial cells, respectively, between control and knockout SVF in either model; however, these cell surface markers may not be specific enough to highlight the regulated cell population. Thus, future experiments using more specific markers, including *F4/80* or *Cd11c*, will be required to more accurately quantify macrophage numbers in SVF of β -cat^{-/-} and *Wls*^{-/-} mice. Immunofluorescence staining using antibodies for F4/80 or CD68 to visualize macrophages may also provide suitable quantification of cell numbers in WAT tissue sections from control and knockout mice.

Alternatively, a particular cell type within the SVF may detect loss of Wnt signaling from adipocytes and respond by increasing its own Wnt or β -catenin production to maintain signaling homeostasis within the tissue. Evaluation of gene expression within CD45⁺, CD31⁺, and CD45⁻/CD31⁻ populations isolated by fluorescence-activated cell sorting reveals that CD45⁻/CD31⁻ stromal cells, which include adipose stem cells, committed preadipocytes and pericytes, are responsible at least in part for the observed compensation. Since β -catenin and Wnt proteins are broadly expressed, further studies using unbiased single-cell RNA-seq analysis of SVF sub-populations from control and knockout mice may prove to be more successful in specifically identify the cell populations that are up-regulating their Wnt signaling.

Of course, it is also possible and perhaps likely that the compensatory mechanism is more complex, involving cross-talk between multiple cell populations. For example, Chen *et al.* reported that in HFD-fed mice, β -catenin deletion suppresses WAT expression of *Saa3*, an adipokine known to activate macrophages²⁶. Further, they contend that down-regulation of *Saa3* results in impaired macrophage recruitment and

decreased preadipocyte proliferation²⁶. Although we found that macrophage markers and *Saa3* are down-regulated in WAT of HFD-fed β -cat^{-/-} mice, we observed only mild up-regulation in eWAT and no change in iWAT of chow-fed mice. Thus, *Saa3* probably does not mediate the compensatory effects observed in SVF of β -cat^{-/-} and *Wls*^{-/-} mice. However, unbiased transcriptome analyses of WAT and isolated SVF from chow-fed control and knockout animals may provide insights into secreted factors that are involved in cross-talk between adipocytes and surrounding cell populations. These experiments will shed much-needed light on the mechanism by which adipocyte-specific loss of Wnt signaling is sensed and defended.

Interestingly, we also found that diet-induced obesity overrides this compensatory mechanism in both models: SVF of HFD-fed *Wls*^{-/-} and β -cat^{-/-} mice no longer exhibit elevated Wnt signaling, and consequently, isolated adipocytes from these mice have decreased Wnt target and lipogenic gene expression. Additionally, β -catenin mRNA and protein expression is negligible in knockout adipocytes from HFD-fed mice. Long-term HFD feeding has well-established effects on adipose tissue inflammation, remodeling and SVF composition³⁴⁻³⁶. These changes likely contribute to the loss of compensation in HFD-fed knockout mice, but further experiments are required to fully understand why this occurs, revealing a phenotype in obese mice.

Is β -catenin delivered back to deficient adipocytes from stromal-vascular cells by extracellular vesicles?

Although secretion of Wnts is blocked in *Wls*^{-/-} adipocytes, the remaining signaling machinery, including β -catenin, is intact. Thus, a plausible mechanism for tissue-wide compensation in this model emerges readily. One might imagine that loss of adipocyte-derived Wnts is sensed by neighboring cells, which in turn respond by increasing their own Wnt production and secretion. Wnts from SVF cells are then able to act in a paracrine fashion to maintain downstream signaling in deficient adipocytes.

A model of compensation in β -catenin-deficient adipocytes is more complicated. The relatively high levels of β -catenin mRNA and protein observed in knockout adipocytes suggests the intriguing possibility that β -catenin is being delivered back to deficient cells, perhaps by SVF-derived small extracellular vesicles (sEV). Many

different cell types are known to secrete sEVs containing proteins, lipids, and genetic material; these sEVs mediate a unique mechanism for intercellular communication and have diverse and intricate effects on recipient cells^{37,38}. This is of particular interest in the context of adipose biology, since WAT-derived sEVs have widespread effects³⁹⁻⁴². sEVs are also secreted by various SVCs, including macrophages, endothelial cells, and stromal cells, and can have profound effects on metabolism⁴³⁻⁴⁵. Thus, sustained expression of β -catenin in knockout adipocytes may be the result of mRNA transfer and subsequent translation, or more direct trafficking of protein.

The possibility of direct β -catenin protein transfer is supported by recent findings by Crewe *et al.*, who reported that sEVs derived from endothelial cells mediate cross-talk between adipocytes and SVF cells populations⁴⁵. Indeed, they described a phenomenon strikingly similar to the one we observe in chow-fed β -cat^{-/-} mice. Despite efficient genetic ablation of *Cav1* (caveolin-1), cav1 protein is readily detectable in deficient adipocytes; this was found to be due to sEV-mediated trafficking of cav1 protein from surrounding endothelial cells back to *Cav1*^{-/-} adipocytes. In addition to cav1, proteomic analyses of isolated endothelial sEVs identified members of the Wnt signaling pathway, including β -catenin.

Thus, it is possible that a similar mechanism explains the sustained expression of β -catenin protein in knockout adipocytes. Evaluation of β -catenin expression in sEVs secreted from cultured SVF of control and knockout mice will provide insight into the potential trafficking of β -catenin mRNA or protein. If sEVs from SVF of β -cat^{-/-} mice contain higher amounts of β -catenin, this will provide compelling evidence for the delivery of β -catenin protein back to deficient adipocytes. Alternatively, SVF of knockout mice may secrete larger quantities of sEVs in order to maintain β -catenin expression in β -cat^{-/-} adipocytes.

Once a potential SVC subpopulation responsible for compensation is identified, studies ablating β -catenin from that particular cell type will be required to definitively establish a causal relationship. For example, if future studies provide compelling evidence for macrophages being the source of β -catenin up-regulation, experiments using different Cre drivers to simultaneously delete β -catenin from both adipocytes and

macrophages will be required; loss of compensation in these studies will conclusively define an adipocyte-SVF axis of Wnt regulation.

The animal models presented in this dissertation both used constitutively expressed adiponectin-Cre. We had originally bred $\beta\text{-cat}^{fl/fl}$ mice to a tamoxifen-inducible adiponectin-Cre^{ER} model, but sustained β -catenin expression in knockout mice led us to believe that a lack of phenotype in chow-fed mice was due to inefficient tamoxifen-induced gene recombination. Thus, all future studies were conducted using the constitutively active adiponectin-Cre. In hindsight, it is likely that we were observing the same compensatory mechanism later found with constitutive loss of β -catenin or Wntless.

Indeed, inducible deletion of adipocyte-specific Insig-1, a negative regulator of SREBP1c transcriptional activity, blocks DNL gene expression acutely⁴⁶. However, subsequent diminished efflux of citrate from mitochondria triggers production of reactive oxygen species, which activate mTORC1. Thus, an mTORC1-mediated compensatory mechanism rapidly restores SREBP1c and downstream lipogenic enzyme expression less than 72 hours after gene deletion. This study highlights the importance of maintaining lipogenic gene expression in adipocytes and may shed light on possible reasons that adipose tissues rigorously defend Wnt signaling. Thus, future studies using mice with inducible loss of Wntless or β -catenin may provide critical insights into the timing and mechanism of compensation.

How does adipocyte-specific loss of Wnt signaling provide functional protection from diet-induced obesity?

To date, studies of Wnt signaling in mature adipocytes have consistently revealed metabolic phenotypes with long-term HFD feeding²⁴⁻²⁶. Indeed, we found that both $Wls^{-/-}$ and $\beta\text{-cat}^{-/-}$ mice are resistant to diet-induced obesity and are protected from subsequent metabolic dysfunction. Specifically, HFD-fed Wntless knockout mice are characterized by decreased fat and increased lean mass, improved glucose homeostasis, and increased circulating insulin levels. $\beta\text{-cat}^{-/-}$ mice fed HFD demonstrate decreased weight gain and fat mass, significantly improved glucose homeostasis, and decreased circulating TAG and glucose-stimulated insulin release. Both knockout

models have decreased lipogenic gene expression within WAT depots and are protected from hepatosteatosis.

A point of interest is the mechanism underlying protection from diet-induced obesity and metabolic dysfunction that is afforded to mice lacking adipocyte-specific Wnt signaling. Although both *Wls*^{-/-} and *β-cat*^{-/-} mice exhibit decreased fat mass and liver TAG accumulation compared to their control counterparts, food intake is unaffected. If energy intake is the same but it is not being stored in WAT or liver, logic dictates that *Wls*^{-/-} and *β-cat*^{-/-} mice utilize more energy compared to controls. Thus, energy expenditure, oxygen consumption, and physical activity should be quantitatively measured in future cohorts of HFD-fed mice using the Comprehensive Lab Animal Monitoring System (CLAMS).

Another possible explanation for decreased energy storage in HFD-fed mice may be increased heat loss via the skin; global *Scd1*^{-/-} and keratinocyte-specific *Scd*^{-/-} mice are resistant to diet-induced obesity in part due to decreased insulation and thus increased heat loss through the skin⁴⁷⁻⁴⁹. Since obese *Wls*^{-/-} and *β-cat*^{-/-} mice exhibit decreased SCD1 expression in WAT and isolated adipocytes, it is possible that SCD1 expression is also suppressed in dermal WAT, leading to up-regulation of thermogenic pathways at the expense of nutrient utilization. Quantification of dermal adipocyte lipids and measurement of thermogenic genes will provide insights into the contribution of dermal WAT lipogenesis to the observed phenotype. Although unlikely since a difference in fat mass only emerges after at least 20 weeks of HFD, it is also possible that *Wls*^{-/-} and *β-cat*^{-/-} mice absorb less lipids from the intestine. The presence of a malabsorptive phenotype can be tested by measuring fecal lipids in knockout mice either under basal conditions or after intragastric fat challenge.

In addition to improved glucose tolerance, *β-cat*^{-/-} mice also demonstrate lower glucose-stimulated insulin concentrations and a trend toward improved systemic insulin sensitivity. Thus, protection from metabolic dysfunction in β-catenin knockout mice may be due to greater peripheral insulin sensitivity and glucose uptake. Measurement of phosphorylated AKT in WAT and muscle after insulin injection in HFD-mice may answer this question: increased pAKT levels in peripheral tissues of *β-cat*^{-/-} mice will suggest

improved peripheral insulin sensitivity. Hyperinsulinemic-euglycemic clamps can also be used to quantitatively assess insulin sensitivity in tissues of control and knockout mice.

In contrast to β -cat^{-/-} mice, Wntless knockout mice exhibit increased circulating random-fed and glucose-stimulated insulin concentrations; pancreas weights are not altered. Interestingly, *Wls*^{-/-} mice also demonstrate increased liver weight, despite less hepatosteatosis observed by histological analysis. One possible explanation for this constellation of findings is the existence of a Wnt-regulated adipokine that signals to the pancreas to suppress insulin secretion under normal conditions. When this signal is removed by loss of adipocyte-derived Wnt secretion, elevated circulating insulin may act upon the liver to suppress gluconeogenesis, stimulating glycogen synthesis and storage, and increase liver weight. Thus, quantitative measurements of pancreatic beta cell mass and number, liver TAG and glycogen levels, and hepatic cell size and number in future HFD cohorts may uncover mechanisms by which Wntless deficiency improves glucose homeostasis in obese mice.

Why does ablation of Wnt signaling confer resistance to diet-induced obesity and metabolic dysfunction?

Characterization of two independent animal models has revealed that Wnt signaling homeostasis is rigorously defended by adipose tissues under standard nutritional conditions. This finding suggests that Wnt signaling is critically important for the proper function of mature adipocytes. Indeed, RNA-seq and GSEA analyses revealed that loss of β -catenin up-regulates inflammatory pathways and down-regulates many metabolic pathways, including those related to mitochondrial function and lipid and cholesterol metabolism.

Our molecular studies in cultured adipocytes also revealed that Wnt signaling regulates lipogenesis and fatty acid desaturation, two essential adipocyte functions. Indeed, Wnt signaling is required for expression of a network of lipogenic enzymes, including FASN and SCD1. FASN mediates synthesis of palmitic acid (C16:0) and SCD1 catalyzes its desaturation to palmitoleic acid (C16:1). Adipocytes are largely responsible for *in vivo* production of palmitoleic acid (C16:1), a fatty acid with insulin-sensitizing and anti-inflammatory effects^{50,51}. In contrast, cytokine signaling and

inflammation, predicted to be increased with β -catenin deletion, are associated with adipose tissue dysfunction, dyslipidemia, and insulin resistance^{34-36,52}. Thus, one might reasonably expect that functional loss of Wnt signaling with HFD would have catastrophic effects on vital adipocyte functions, including lipid synthesis and storage, and promote WAT inflammation and whole-body metabolic dysfunction.

However, we and others have found that adipocyte-specific deletion of β -catenin or Wntless in mice provides protection from diet-induced obesity and subsequent metabolic dysfunction²⁶. Perhaps the most compelling question that has emerged from my doctoral work arises from these counter-intuitive findings and is partly philosophical in nature: why does adipocyte-specific loss of Wnt signaling confer resistance to diet-induced obesity and metabolic function?

Canonical Wnt signaling has been identified as a significant regulator of adipocyte lipogenesis and fatty acid desaturation. Thus, the answer to this question may lie in clearer understanding of the relative physiological importance of adipocyte DNL in global metabolism, particularly under obesogenic conditions. Unfortunately, genetic manipulation of DNL enzymes in adipocytes has thus far produced conflicting effects on systemic metabolism. Global *Scd1*^{-/-} mice fed HFD are characterized by reduced weight gain and fat accumulation and increased oxygen consumption and insulin sensitivity compared to controls; these effects persist despite significantly increased food intake by knockout mice⁴⁷. Surprisingly, adipocyte-specific SCD1 deletion does not confer resistance to diet-induced obesity or otherwise appear to influence systemic metabolism⁵³. Although mouse models of *Srebf1* deletion in adipose tissues have not been reported to date, adipocyte-specific loss of ChREBP results in altered WAT fatty acid composition, impaired glucose transport and profound insulin resistance⁵⁴. Inactivation of *Acaca* using the aP2-Cre causes reduced WAT accumulation in a fasting/refeeding paradigm⁵⁵; however, this Cre is known to leak outside of adipose tissues and consistent with this, *Acaca*^{-/-} mice also exhibit growth retardation, confounding these results.

Mice with adipocyte-specific deletion of FASN are characterized by increased energy expenditure, browning of WAT, and resistance to diet-induced obesity⁵⁶. Indeed, loss of FASN in WAT of HFD-fed mice using an inducible adiponectin-Cre promotes

browning and UCP1 expression in iWAT and is accompanied by improved glucose homeostasis. Effects on browning are mediated by increased sympathetic outflow, as evidenced by elevated tyrosine hydroxylase (TH) and neuropeptide Y (NPY) protein expression in iWAT. Interestingly, both *Th* (tyrosine hydroxylase) and *Npy* (neuropeptide Y) were identified by our RNA-seq dataset as up-regulated in β -*cat*^{-/-} adipocytes. Although we do not observe obvious signs of browning in histological sections of iWAT from HFD-fed β -*cat*^{-/-} mice, staining for UCP1, TH, and NPY and measurement of protein levels by immunoblotting will provide more quantitative assessments of browning in WAT of these mice.

The discordant results observed in these different mouse models of impaired adipose tissue DNL highlight the complexities of animal physiology. Nevertheless, detailed analyses of cytokines, circulating fatty acid species like palmitoleic acid, and measurement of oxygen consumption and energy expenditure in HFD-fed mice may yield clues as to the mechanisms by which loss of Wnt signaling confers protection from metabolic dysfunction. Further, an unbiased view of gene expression changes in control and knockout *Wls* and β -*cat* mice may shed light on novel metabolic pathways that are influenced *in vivo*.

Thus, although the roles of adipocyte Wnt signaling and lipogenesis in systemic metabolism remain unclear, the findings presented in this dissertation contribute novel knowledge to our burgeoning understanding of Wnt signaling in mature adipocyte function. Further, given the evolutionary conservation and ubiquitous nature of this pathway, it is highly likely that our findings will be widely applicable in the biology of diverse cell types.

References

1. Sethi JK, Vidal-Puig A. Wnt signalling and the control of cellular metabolism. *Biochem J*. 2010;427(1):1-17.
2. Christodoulides C, Lagathu C, Sethi JK, Vidal-Puig A. Adipogenesis and WNT signalling. *Trends Endocrinol Metab*. 2009;20(1):16-24.
3. Bennett CN, Ross SE, Longo KA, et al. Regulation of Wnt signaling during adipogenesis. *J Biol Chem*. 2002;277(34):30998-31004.
4. Ross SE, Hemati N, Longo KA, et al. Inhibition of adipogenesis by Wnt signaling. *Science*. 2000;289(5481):950-953.
5. Fischer L, Boland G, Tuan RS. Wnt-3A enhances bone morphogenetic protein-2-mediated chondrogenesis of murine C3H10T1/2 mesenchymal cells. *J Biol Chem*. 2002;277(34):30870-30878.
6. Hoppler S, Brown JD, Moon RT. Expression of a dominant-negative Wnt blocks induction of MyoD in *Xenopus* embryos. *Genes Dev*. 1996;10(21):2805-2817.
7. Cossu G, Borello U. Wnt signaling and the activation of myogenesis in mammals. *EMBO J*. 1999;18(24):6867-6872.
8. Krishnan V, Bryant HU, Macdougald OA. Regulation of bone mass by Wnt signaling. *J Clin Invest*. 2006;116(5):1202-1209.
9. Bennett CN, Longo KA, Wright WS, et al. Regulation of osteoblastogenesis and bone mass by Wnt10b. *Proc Natl Acad Sci U S A*. 2005;102(9):3324-3329.
10. Kang S, Bennett CN, Gerin I, Rapp LA, Hankenson KD, Macdougald OA. Wnt signaling stimulates osteoblastogenesis of mesenchymal precursors by suppressing CCAAT/enhancer-binding protein alpha and peroxisome proliferator-activated receptor gamma. *J Biol Chem*. 2007;282(19):14515-14524.
11. Grant SF, Thorleifsson G, Reynisdottir I, et al. Variant of transcription factor 7-like 2 (TCF7L2) gene confers risk of type 2 diabetes. *Nat Genet*. 2006;38(3):320-323.
12. Lyssenko V, Lupi R, Marchetti P, et al. Mechanisms by which common variants in the TCF7L2 gene increase risk of type 2 diabetes. *J Clin Invest*. 2007;117(8):2155-2163.
13. Saarinen A, Saukkonen T, Kivela T, et al. Low density lipoprotein receptor-related protein 5 (LRP5) mutations and osteoporosis, impaired glucose metabolism and hypercholesterolaemia. *Clin Endocrinol (Oxf)*. 2010;72(4):481-488.
14. Singh R, Smith E, Fathzadeh M, et al. Rare nonconservative LRP6 mutations are associated with metabolic syndrome. *Hum Mutat*. 2013;34(9):1221-1225.
15. Loh NY, Neville MJ, Marinou K, et al. LRP5 regulates human body fat distribution by modulating adipose progenitor biology in a dose- and depot-specific fashion. *Cell Metab*. 2015;21(2):262-273.
16. Shungin D, Winkler TW, Croteau-Chonka DC, et al. New genetic loci link adipose and insulin biology to body fat distribution. *Nature*. 2015;518(7538):187-196.
17. Heid IM, Jackson AU, Randall JC, et al. Meta-analysis identifies 13 new loci associated with waist-hip ratio and reveals sexual dimorphism in the genetic basis of fat distribution. *Nat Genet*. 2010;42(11):949-960.
18. Hao HX, Xie Y, Zhang Y, et al. ZNRF3 promotes Wnt receptor turnover in an R-spondin-sensitive manner. *Nature*. 2012;485(7397):195-200.

19. Zou Y, Ning T, Shi J, et al. Association of a gain-of-function variant in LGR4 with central obesity. *Obesity (Silver Spring)*. 2017;25(1):252-260.
20. Van Camp JK, Beckers S, Zegers D, Verrijken A, Van Gaal LF, Van Hul W. Common genetic variation in sFRP5 is associated with fat distribution in men. *Endocrine*. 2014;46(3):477-484.
21. Christodoulides C, Scarda A, Granzotto M, et al. WNT10B mutations in human obesity. *Diabetologia*. 2006;49(4):678-684.
22. Christodoulides C, Laudes M, Cawthorn WP, et al. The Wnt antagonist Dickkopf-1 and its receptors are coordinately regulated during early human adipogenesis. *J Cell Sci*. 2006;119(Pt 12):2613-2620.
23. Kanazawa A, Tsukada S, Sekine A, et al. Association of the gene encoding wingless-type mammary tumor virus integration-site family member 5B (WNT5B) with type 2 diabetes. *Am J Hum Genet*. 2004;75(5):832-843.
24. Geoghegan G, Simcox J, Seldin MM, et al. Targeted deletion of Tcf7l2 in adipocytes promotes adipocyte hypertrophy and impaired glucose metabolism. *Mol Metab*. 2019;24:44-63.
25. Mori H, Prestwich TC, Reid MA, et al. Secreted frizzled-related protein 5 suppresses adipocyte mitochondrial metabolism through WNT inhibition. *J Clin Invest*. 2012;122(7):2405-2416.
26. Chen M, Lu P, Ma Q, et al. CTNNB1/beta-catenin dysfunction contributes to adiposity by regulating the cross-talk of mature adipocytes and preadipocytes. *Sci Adv*. 2020;6(2):eaax9605.
27. Bagchi DP, Li Z, Corsa CA, et al. Wntless regulates lipogenic gene expression in adipocytes and protects against diet-induced metabolic dysfunction. *Mol Metab*. 2020:100992.
28. Shao W, Espenshade PJ. Expanding roles for SREBP in metabolism. *Cell Metab*. 2012;16(4):414-419.
29. Horton JD, Goldstein JL, Brown MS. SREBPs: activators of the complete program of cholesterol and fatty acid synthesis in the liver. *J Clin Invest*. 2002;109(9):1125-1131.
30. Iizuka K, Bruick RK, Liang G, Horton JD, Uyeda K. Deficiency of carbohydrate response element-binding protein (ChREBP) reduces lipogenesis as well as glycolysis. *Proc Natl Acad Sci U S A*. 2004;101(19):7281-7286.
31. Pongvarin N, Chang B, Imamura M, et al. Genome-Wide Analysis of ChREBP Binding Sites on Male Mouse Liver and White Adipose Chromatin. *Endocrinology*. 2015;156(6):1982-1994.
32. Danai LV, Guilherme A, Guntur KV, Straubhaar J, Nicoloso SM, Czech MP. Map4k4 suppresses Srebp-1 and adipocyte lipogenesis independent of JNK signaling. *J Lipid Res*. 2013;54(10):2697-2707.
33. Porstmann T, Santos CR, Griffiths B, et al. SREBP activity is regulated by mTORC1 and contributes to Akt-dependent cell growth. *Cell Metab*. 2008;8(3):224-236.
34. Duan Y, Zeng L, Zheng C, et al. Inflammatory Links Between High Fat Diets and Diseases. *Front Immunol*. 2018;9:2649.
35. Sun K, Kusminski CM, Scherer PE. Adipose tissue remodeling and obesity. *J Clin Invest*. 2011;121(6):2094-2101.

36. Choe SS, Huh JY, Hwang IJ, Kim JI, Kim JB. Adipose Tissue Remodeling: Its Role in Energy Metabolism and Metabolic Disorders. *Front Endocrinol (Lausanne)*. 2016;7:30.
37. van Niel G, D'Angelo G, Raposo G. Shedding light on the cell biology of extracellular vesicles. *Nat Rev Mol Cell Biol*. 2018;19(4):213-228.
38. Raposo G, Stahl PD. Extracellular vesicles: a new communication paradigm? *Nat Rev Mol Cell Biol*. 2019;20(9):509-510.
39. Chen XW, Li S, Lin JD. The Micro-Managing Fat: Exosomes as a New Messenger. *Trends Endocrinol Metab*. 2017;28(8):541-542.
40. Lazar I, Clement E, Dauvillier S, et al. Adipocyte Exosomes Promote Melanoma Aggressiveness through Fatty Acid Oxidation: A Novel Mechanism Linking Obesity and Cancer. *Cancer Res*. 2016;76(14):4051-4057.
41. Deng ZB, Poliakov A, Hardy RW, et al. Adipose tissue exosome-like vesicles mediate activation of macrophage-induced insulin resistance. *Diabetes*. 2009;58(11):2498-2505.
42. Thomou T, Mori MA, Dreyfuss JM, et al. Adipose-derived circulating miRNAs regulate gene expression in other tissues. *Nature*. 2017;542(7642):450-455.
43. Zhao H, Shang Q, Pan Z, et al. Exosomes From Adipose-Derived Stem Cells Attenuate Adipose Inflammation and Obesity Through Polarizing M2 Macrophages and Beiging in White Adipose Tissue. *Diabetes*. 2018;67(2):235-247.
44. Ying W, Riopel M, Bandyopadhyay G, et al. Adipose Tissue Macrophage-Derived Exosomal miRNAs Can Modulate In Vivo and In Vitro Insulin Sensitivity. *Cell*. 2017;171(2):372-384.e312.
45. Crewe C, Joffin N, Rutkowski JM, et al. An Endothelial-to-Adipocyte Extracellular Vesicle Axis Governed by Metabolic State. *Cell*. 2018;175(3):695-708.e613.
46. Crewe C, Zhu Y, Paschoal VA, et al. SREBP-regulated adipocyte lipogenesis is dependent on substrate availability and redox modulation of mTORC1. *JCI Insight*. 2019;5.
47. Ntambi JM, Miyazaki M, Stoehr JP, et al. Loss of stearoyl-CoA desaturase-1 function protects mice against adiposity. *Proc Natl Acad Sci U S A*. 2002;99(17):11482-11486.
48. Sampath H, Flowers MT, Liu X, et al. Skin-specific deletion of stearoyl-CoA desaturase-1 alters skin lipid composition and protects mice from high fat diet-induced obesity. *J Biol Chem*. 2009;284(30):19961-19973.
49. Sampath H, Ntambi JM. Role of stearoyl-CoA desaturase-1 in skin integrity and whole body energy balance. *J Biol Chem*. 2014;289(5):2482-2488.
50. Cao H, Gerhold K, Mayers JR, Wiest MM, Watkins SM, Hotamisligil GS. Identification of a lipokine, a lipid hormone linking adipose tissue to systemic metabolism. *Cell*. 2008;134(6):933-944.
51. Guo X, Li H, Xu H, et al. Palmitoleate induces hepatic steatosis but suppresses liver inflammatory response in mice. *PLoS One*. 2012;7(6):e39286.
52. Pond CM. Adipose tissue and the immune system. *Prostaglandins Leukot Essent Fatty Acids*. 2005;73(1):17-30.

53. Hyun CK, Kim ED, Flowers MT, et al. Adipose-specific deletion of stearoyl-CoA desaturase 1 up-regulates the glucose transporter GLUT1 in adipose tissue. *Biochem Biophys Res Commun.* 2010;399(4):480-486.
54. Vijayakumar A, Aryal P, Wen J, et al. Absence of Carbohydrate Response Element Binding Protein in Adipocytes Causes Systemic Insulin Resistance and Impairs Glucose Transport. *Cell Rep.* 2017;21(4):1021-1035.
55. Mao J, Yang T, Gu Z, et al. aP2-Cre-mediated inactivation of acetyl-CoA carboxylase 1 causes growth retardation and reduced lipid accumulation in adipose tissues. *Proc Natl Acad Sci U S A.* 2009;106(41):17576-17581.
56. Guilherme A, Pedersen DJ, Henchey E, et al. Adipocyte lipid synthesis coupled to neuronal control of thermogenic programming. *Mol Metab.* 2017;6(8):781-796.